Investigating Early Lesion Formation Following Papillomavirus Infection Using a Mouse Model and Cell Culture

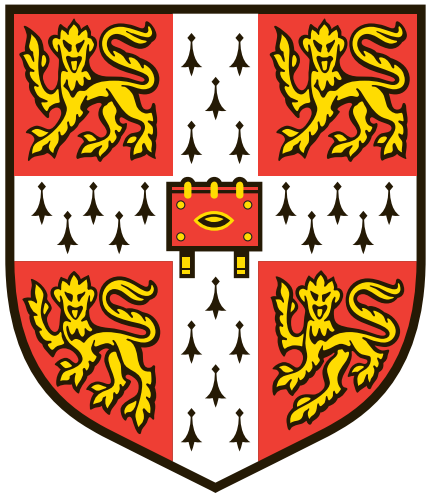

Taylor Saunders-Wood

Department of Pathology

University of Cambridge

This dissertation is submitted for the degree of

Doctor of Philosophy

Jesus College

September 2019

Declaration

This thesis is the result of my own work and includes nothing which is the outcome of work done in collaboration except as declared in the Preface and specified in the text. It is not substantially the same as any that I have submitted, or, is being concurrently submitted for a degree or diploma or other qualification at the University of Cambridge or any other University or similar institution except as declared in the Preface and specified in the text. I further state that no substantial part of my dissertation has already been submitted, or, is being concurrently submitted for any such degree, diploma or other qualification at the University of Cambridge or any other University or similar institution except as declared in the Preface and specified in the text. It does not exceed the prescribed word limit for the relevant Degree Committee.

Taylor Saunders-Wood
September 2019

Abstract

Investigating Early Lesion Formation Following Papillomavirus Infection Using a Mouse Model and Cell Culture

Taylor Saunders-Wood

Papillomaviruses (PV) are small non-enveloped double-stranded DNA tumour viruses, which are able to infect more than 80 different host species. They are a diverse group with over 400 types discovered, of which almost half infect humans. Human papillomaviruses have been linked to a myriad of diseases, including multiple cancers, recurrent respiratory papillomatosis, and genital warts. The disease burden of HPV-related conditions is severe, and there is currently no treatment that can guarantee eradication of viral infection. All PV types characterised so far have a similar genomic structure, and contain the so called 'core ORFs' – E1, E2, L1 and L2 which are essential for viral genome replication and packaging into infectious virions. PV evolution and diversification appears to have been impacted by the availability of certain epithelial niches, with co-evolution and niche adaptation allowing PVs to develop a remarkable species and tissue specificity. Consequently, the function of the PV early proteins can vary between different PV species and types, but as a group they share important organisational similarities that reflect their common requirement to infect and persist in the epithelium following infection. This has allowed the use of animal models to gain insight into the basic virus/host interactions that are targeted by this group of viruses as a whole. The mechanisms by which HPV establishes a lesion, particularly in low-risk types, are not fully understood. However, the recently identified mouse model of PV infection is a useful biological tool to study this period of PV infection *in vivo*.

This body of work aims to expand current knowledge of early events in the PV life cycle. To further understand the mechanisms of cell persistence during PV infection, immunodeficient mouse tail samples inoculated with MmuPV1 were examined to investigate early lesion formation. Five discrete stages of lesion formation were characterised in the immunodeficient animals. In parallel studies, microlesions were rarely observed in immunocompetent C57BL/6J mice, reaching stage three of lesion formation. In-depth tissue analysis suggested a modulation of basal cell density in infected epithelium, and a delay in normal differentiation commitment in E6/E7 expressing cells. Whole genome cell culture experiments were attempted in parallel with human high-risk types, which showed a post-confluent effect of

high concentration EGF on cell growth and genome copy number in cells containing HPV16 genomes. A role for MmuPV1 E6 in growth of cell populations to significantly higher densities was shown through experimentation with cells exogenously expressing viral proteins. Differentiation was also delayed in the cells expressing MmuPV1 E6, demonstrating a recapitulation of events characterised in *in vivo* infections. Novel use of fluorescent cell lines in tandem with confocal microscopy allowed innovative analysis of a high-density monolayer cell culture model. These experiments revealed that MmuPV1 E6 expression resulted in preferential persistence of cells in the lower layer over cells expressing control vector only. Disruption of MmuPV1 E6 binding with MAML1 protein abrogated this phenotype, suggesting that this interaction was necessary for the lower layer persistence phenotype shown by MmuPV1 E6 expressing cells.

Overall, the findings of this thesis suggest that expression of MmuPV1 E6 confers a competitive advantage on infected cells in the basal layer of the epithelium, allowing expansion of the reservoir of infection. Patterns of virus gene expression suggest a related but distinct life cycle phenotype for MmuPV1, a pi papillomavirus type, when compared to alpha papillomaviruses. Wherein, amplification begins immediately upon basal layer exit as opposed to the exit and reentry phenotype suggested in high-risk lesions. Further characterisation of these phenotypes will likely provide important information on key mechanisms in early lesion formation, and it is reasonable to consider that pi papillomaviruses may serve as a better model for beta papillomaviruses than alpha types.

Acknowledgements

First of all, I'd like to thank Professor John Doorbar for the opportunity to take up this PhD position; it has been incredible to work in such an esteemed lab, and I have learned so much about scientific resilience and thinking critically about my own work. I am grateful for all of his feedback and support throughout this PhD. I would also like to thank the members of the Doorbar Lab for providing a friendly and stimulating work environment, and for helping me with different experiments along the way. In particular, I would like to thank Dr Nagayasu Egawa, who was a role model and a mentor to me these past four years. He played a large part in the structuring and development of my project, whilst simultaneously managing his own work as well as the work of other students. Without his patience, good humour, and creativity, I wouldn't have made it to where I am today.

Similarly, the support of such a wealth of friends has been a huge part of my life, and I am so fortunate that they are too many to mention everyone here by name. Having friends in the department made the PhD feel more possible; seeing people succeed ahead of and alongside me made it seem a less insurmountable task. Being a member of Jesus College shaped my whole experience whilst in Cambridge, so some special thanks is owed to the College and all of its staff for welcoming me, supporting me, and providing a home away from home. It has truly been a blessing to meet so many spectacular people at Jesus College, and I know that some of these friendships are for life. Thank you!

Finally, to my mum and dad, all of this is because of you. You've never pushed me, you've only shared in my excitement in learning, and encouraged my insatiable curiosity at any and every opportunity. Extra thanks are needed for my mum for counting thousands of cells by hand and for my dad for proofreading my first full draft! When I found out I had been offered the place to study my PhD here, I was most excited to share the news with you both; I always love to make you proud, as it is the best thanks I can give for everything you've given me.

Table of Contents

List of Figures

List of Tables

Abbreviations

BPV	bovine papillomavirus
BrdU	bromodeoxyuridine
COPV	canine oral papillomavirus
CRPV	cottontail rabbit papillomavirus
CSL	CBF1-Su(H)-LAG1
Ct	cycle threshold
DNA	deoxyribonucleic acid
dsDNA	double-stranded DNA
ECM	extracellular matrix
EGF(R)	epidermal growth factor receptor
EV	epidermodysplasia verruciformis
FISH	fluorescent *in-situ* hybridisation
Fucci	fluorescent ubiquitination-based cell cycle indicator
H&E	haematoxylin and eosin
HES	hairy and enhancer of split
HDACs	histone deacetylases
HSPGs	heparan sulphate proteoglycans
HPV	human papillomavirus
IF	immunofluorescent
IHC	immunohistochemistry
IFN	interferon
K1	keratin 1
K10	keratin 10
K17	keratin 17
LTR	long terminal repeat
MAML	mastermind-like protein
MCS	multiple cloning site
mg	milligram
ml	millilitre
MnPV	Mastomys natalensis papillomavirus
mRNA	messenger RNA
NIKS	normal immortalised keratinocytes
NICD	notch intracellular domain
NLS	nuclear localisation signal

ORF	open reading frame
PV	papillomavirus
PBM	PDZ-binding motif
PCR	polymerase chain reaction
pRB	retinoblastoma protein
qPCR	quantitative polymerase chain reaction
ROPV	rabbit oral papillomavirus
RRP	recurrent respiratory papillomatosis
RE	restriction enzyme
RNA	Ribonucleic Acid
RT	room temperature
cSCC	cutaneous squamous cell carcinoma
SV40	simian virus 40
UV	ultra-violet
UVR	ultraviolet radiation
URR	upstream regulatory region
VGE	virus genome equivalent
VLP	virus-like particle
wt	wild-type
ZZ	double Z shaped

1.0 Introduction

1.1 Classification of Papillomaviruses

Papillomaviruses (PVs) are double-stranded DNA (dsDNA) tumour viruses that exclusively infect mucosal and cutaneous epithelium. They are a diverse family of viruses, with more than 405 reference genomes currently listed in the Papillomavirus Episteme (https://pave.niaid.nih.gov/). Recent research showed that ancestral anamniotes of the Palaeozoic era were infected with ancestral PV hundreds of millions of years ago, with the most recent common ancestor of amniotes estimated to have existed 184 million years ago. Examination of virus evolution suggested that three key evolutionary events have occurred since then: the primary evolutionary lineages were established following an initial radiation event, a second radiation of virus evolution in parallel with host evolution increased variation, and a final radiation specific to types within a genus of PVs termed *Alphapapillomavirus* occurred after emergence of the E5 protein (Willemsen and Bravo 2019).

PV types characterised thus far all contain the so-called 'core' open reading frames (ORFs) – E1, E2, L1 and L2, which are essential for viral genome replication and subsequent packaging into infectious virions (Canuti, Munro et al. 2019). The diversification of PVs was impacted by the emergence of specific epithelial niches in their hosts, with parallel niche adaptation and evolution allowing PVs to develop a remarkable species and tissue specificity (Van Doorslaer 2013). Consequently, the early proteins of different PVs can vary in terms of their precise functions, but overall, PVs share crucial similarities in their genome organisation that reflect their common life cycle requirement to infect and persist in the epithelium upon entering the cell. PVs are broadly organised into genera based on differences in the sequence of the L1 ORF, which is highly conserved. If a difference of more than 60% exists between L1 ORF sequences, this is considered to be a different or new PV genus (Bernard, Chan et al. 1994). PVs can be further classified by species, which are determined to be discrete if more than a 40% difference in the aforementioned L1 ORF sequence exists. A PV is considered to be a unique type if the L1 nucleotide sequence differs from that of other PV types by more than 10%. PVs with differences of 2-10% in L1 sequence are considered to be subtypes. Finally, if differences of less than 2% in homology between one type and another exist, these are classified as a variants (de Villiers, Fauquet et al. 2004). In rare cases, unique viruses that are difficult to classify have been discovered, such as bandicoot papillomatosis carcinomatosis virus type 1 (BPCV1). This novel virus exhibits both the ORFs of the L1 and L2 protein

alongside ORFs encoding the large T and small t antigens commonly found in viruses of the *Polyomaviridae* (Woolford, Rector et al. 2007). This virus could be the result of ancient recombination events between members from each of the two virus families.

1.2 Virus structure and genome organisation

Despite differences in sequence, PVs have basic similarities. PV particles are around 50-60nm in diameter, are non-enveloped and icosahedral in structure (Buck, Thompson et al. 2005). Genomes are dsDNA episomes of approximately 8000 base pairs, although this size varies somewhat between types. The circular DNA genomes encode around 8 or 9 ORFs, (as shown in Figure 1.1, adapted from McBride 2017) however the number of proteins a PV can encode varies further due to the presence of multiple promoters and implementation of complex splicing patterns. ORFs are termed 'early' when expressed from the early promoter, located in the viral non-coding region (also referred to as the long coding region or the upstream regulatory region), prior to the productive stage of the life cycle. 'Late' proteins are expressed from the downstream late promoter during the synthesis of virus particles (Fehrmann and Laimins 2003). The activity of both the early and late promoters is regulated by differentiation, with early promoter activity in basal cells, and a differentiation-dependent increase in activity of the late promoter following virus DNA replication (Wang, Liu et al. 2017). Aside from promoter activity, numerous splicing events can occur in viral transcripts, some of which are also regulated by differentiation. In high-risk human papillomavirus (HPV) types, E6 and E7 are transcribed together as bicistronic messenger RNA (mRNA). It has been shown that the majority of E7 proteins are translational products of mRNAs of a particular splice variant of E6, known as E6*I (Tang, Tao et al. 2006). In contrast to high-risk HPVs, other PV types transcribe E6 and E7 separately using two different promoters (Xue, Majerciak et al. 2017). As mentioned above, all PVs possess 'core' proteins: E1 and E2, which are involved in virus genome replication, and L1 and L2, which are crucial for proper packaging and release of the virus from the host (Zheng and Baker 2006). Variation between types is more apparent when considering the presence of further genes, E6, E7, E4 and E5. There is no E3 ORF due to an initial error in sequencing made in the analysis of bovine papillomavirus (BPV)1 genome (Lambert, Spalholz et al. 1987).

E1 encodes a DNA helicase which is vital for the replication of PV genomes (Wilson, West et al. 2002). However, in depth studies have suggested that E1 is dispensable for maintenance replication of virus genomes, and may only be required for establishment and amplification

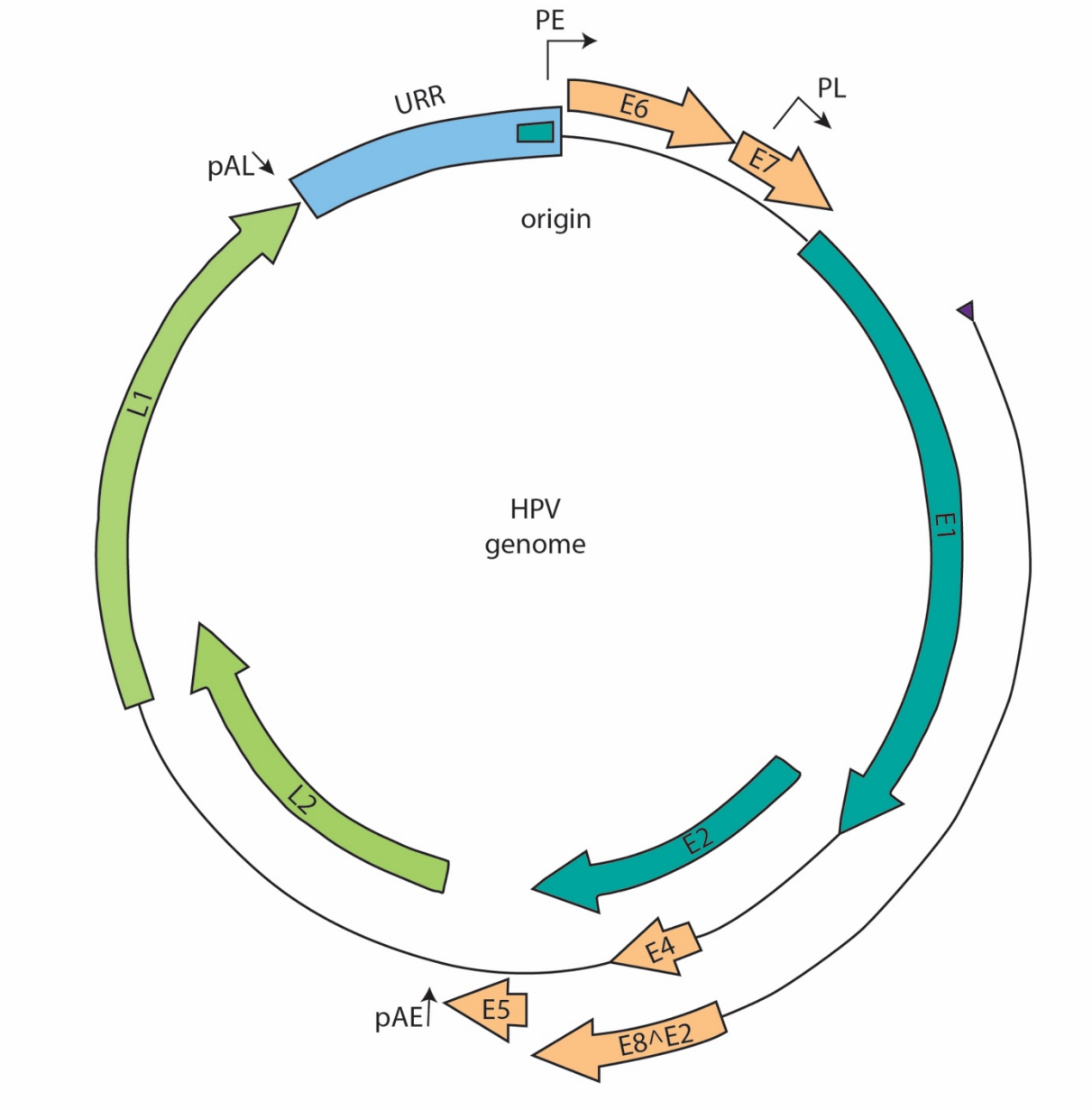

Figure 1.1 The structure of the human papillomavirus genome
Diagram shows the circular double-stranded DNA genome structure of an alpha type human papillomavirus. Core proteins required for replication, E1 and E2, are shown in blue. Core proteins L1 and L2 required for packaging and structure of virus are shown in green. URR – upstream regulatory region. PE and PL show the location of the early and late promoter respectively. pAE and pAL show the location of the early and late polyadenylation sites. The origin of replication is shown. Adapted from (McBride 2017).

stages of the virus life cycle (Kim and Lambert 2002) (Egawa, Nakahara et al. 2012). Research has indicated that E1 interaction with the E2 protein is also fundamental in the establishment replication of genomes *in vivo* (Berg and Stenlund 1997). These stages are discussed in more detail in Section 1.7. E2 is multi-functional, with roles observed in genome partitioning, viral transcription, and replication of virus DNA, in various PV types (Lehman and Botchan 1998) (Skiadopoulos and McBride 1998) (McBride 2013). Despite its classification as an early ORF, a role for E4 in the later stages of the virus life cycle has been demonstrated due to it appearing as virus propagation begins, and it has been shown to be possibly involved in ameliorating virus exit from the surface of the epithelium (Doorbar 2013). E5 is a protein that is sometimes termed oncogenic and is uniquely found in certain alpha PV types. E5 protein is believed to have a role in both immune evasion, and in improving the efficiency of genome amplification (de Freitas, de Oliveira et al. 2017). E6 and E7 are often termed as 'oncogenic' due to their effects frequently resulting in malignant phenotypes in the infected cell. One important difference between HPV types is that in low-risk HPVs, E6 and E7 proteins are rarely seen to stimulate proliferation of the infected basal and parabasal cells, whereas in high-risk types interference with cell cycle entry and proliferative mechanisms is more common (Egawa and Doorbar 2017). The function of many of these proteins differs greatly between types, and even within different genera, resulting in a wide variety in the propensity of different HPV types to cause disease. This will be discussed in more depth in Section 1.8.

1.3 Human Papillomaviruses

To date, more than 200 distinctly characterised PVs have been shown to infect humans (Van Doorslaer and Dillner 2019) most of which cause asymptomatic infection (Dunne and Markowitz 2006). Early studies examined HPV isolated from plantar warts, and compared the PV particles with polyomavirus particles. While both were shown to be dsDNA viruses, differences in size of particles were noted following examination by electron microscopy (Crawford and Crawford 1963). Although the first HPV to be characterised was isolated from human warts (verrucae vulgaris and verrucae plantares) (Gissmann, Pfister et al. 1977), HPV is most well-known for its discovery as an infectious agent causative of cervical cancer in the 1970s (zur Hausen 2009). The tissue specificity of individual HPVs is made further apparent when the sites of infection of different types are considered. For example, HPV6 commonly infects genital sites, and various studies show that it is detectable in 69-90% of genital wart samples while the closely related HPV11 was shown to be present in only 16-32% (Ball,

Winder et al. 2011) (Aubin, Pretet et al. 2008). HPV11 more commonly infects oral sites (Egawa, Egawa et al. 2015). For example, one study showed that HPV11 was present in 84% of the HPV-positive oral cavity samples analysed (Durzynska, Pacholska-Bogalska et al. 2011). HPVs are classified into five broad genera: *Alphapapillomavirus*, *Betapapillomavirus*, *Gammapapillomavirus*, *Mupapillomavirus* and *Nupapillomavirus* (Bernard, Burk et al. 2010), with *Gammapapillomavirus* being the largest group of around 100 types, followed by *Alphapapillomavirus* and then *Betapapillomavirus* (Gheit 2019). The propensity to cause any disease or symptoms in humans differs considerably between these genera.

1.4 High-risk HPV related disease and vaccination

Alpha PVs encompass types of HPV that are known to cause a broad array of disease in humans. Different types of PVs preferentially infect either mucosal or cutaneous tissue, and symptomatic types can be further divided into so-called "low-risk" and "high-risk" types, with the latter having the ability to cause neoplastic changes in infected tissue that can progress to cancer. Conversely, low-risk types cause warts or benign epithelial proliferations (Doorbar, Egawa et al. 2015, Egawa and Doorbar 2017). Low-risk alpha PV types HPV6 and 11 are perhaps most known as causative agents of genital warts and recurrent respiratory papillomatosis (RRP). A recent study found that 100% of the samples analysed contained at least one or both of these types (Omland, Lie et al. 2014). Whilst not life-threatening, genital warts are unpleasant for the sufferer, and repeated treatments are extremely costly to healthcare providers around the world (Raymakers, Sadatsafavi et al. 2012). RRP is a chronic disease that presents in both adults and children. In patients suffering from this condition, benign squamous cell papillomas proliferate within the aerodigestive tract. RRP usually occurs within the larynx, but it is possible for the condition to spread to the lungs, and the infection can even undergo malignant conversion in some instances (Derkay and Wiatrak 2008). In extreme cases RRP can prove fatal due to severe obstruction of the airways, however the only method of treatment currently available is the ablation of warty papillomas from the inside of the respiratory tract, which then often recur. Consequently, this condition also poses an unpleasant and costly treatment regime for the sufferer (Ivancic, Iqbal et al. 2018).

High-risk HPV types cause a variety of cancers, including anal, oropharyngeal, penile, vulvar, vaginal and cervical cancers (Gillison, Chaturvedi et al. 2008) (zur Hausen, de Villiers et al. 1981). Of all cervical cancer cases, more than 99% are associated with HPV infection, and

over 90% of squamous intra-epithelial lesions also contain HPV DNA (Walboomers, Jacobs et al. 1999). Prior to the introduction of a vaccine, HPV16 and HPV18 were found to be associated with roughly 70% of all cases of invasive cervical cancer worldwide, with some slight variation across different geographies (Smith, Lindsay et al. 2007, Li, Franceschi et al. 2011). However following the introduction of a vaccine, rates of HPV16 and HPV18 infection have fallen by 68% in some countries with greater than 50% vaccine coverage (Drolet, Bénard et al. 2015). The first vaccine to be introduced was the quadrivalent vaccine Gardasil (Merck & Co., Inc., Kenilworth, NJ, USA), which protected against the high-risk types HPV16 and HPV18, as well as the most common low-risk types causative of genital warts, HPV6 and HPV11 (McLemore 2006). Cervarix (GlaxoSmithKline), a bivalent vaccine, protective against HPV16 and 18 only (Harper, Franco et al. 2004) was introduced shortly after. In recent years, the Gardasil vaccine has been further improved upon to also protect against HPV31, HPV33, HPV45, HPV52 and HPV58 in the nonavalent vaccine Gardasil-9 (Merck & Co., Inc., Kenilworth, NJ, USA). These HPV types are most commonly associated with cervical cancers globally after types 16 and 18 (Table 1.1). Therefore, it is estimated that this vaccine could protect against roughly 90% of cervical cancers worldwide, as well as offering protection against other HPV-related cancers (Garland, Pitisuttithum et al. 2018).

Table 1.1 Type-specific HPV prevalence in women with invasive cervical cancer

HPV type	Number Tested	HPV Prevalence % (95% CI)
16	58,796	55.2 (54.8-55.6)
18	58,380	14.2 (13.9-14.4)
31	52,417	3.5 (3.4-3.7)
33	53,804	4.2 (4.0-4.3)
35	47,634	1.7 (1.6-1.8)
39	46,420	1.5 (1.3-1.6)
45	47,048	5.0 (4.8-5.2)
51	44,674	1.0 (0.9-1.1)
52	49,978	3.5 (3.3-3.6)
56	46,019	1.0 (0.9-1.1)
58	50,814	3.9 (3.8-4.1)
59	46,703	1.4 (1.3-1.5)

Reproduced from HPV and Related Diseases Summary Report (Bruni, Albero et al. 2019)

All of the vaccines discussed above are made up of self-assembled pentamers of an L1 capsid protein, and are prophylactic. Administration of the vaccine is protective, as it induces the production of antibodies against the L1 protein, preventing future infection from occurring. However, this means that the vaccine is most effective when administered prior to sexual debut; the vaccine is in no way therapeutic and must be given before exposure to the virus to be protective (Mariani and Venuti 2010). Current vaccination uptake varies globally, and while countries with high uptake such as Australia have demonstrated a considerable impact on HPV-related diseases, countries struggling with vaccine hesitancy such as Japan have seen little to no changes in the incidence rates of cervical cancer (Patel, Brotherton et al. 2018, Utada, Chernyavskiy et al. 2019).

In recent years, mounting evidence has suggested that universal vaccination is required to ensure that males are also protected; it is estimated that a vaccination rate of around 80% in women would be sufficient to successfully have herd immunity in the population, which means men are often left unprotected against HPV-related disease (Prue, Baker et al. 2018). For example, a study in South Korea found that following implementation of the vaccine, overall rates of anogenital warts in women declined, however they continued to rise in men over the same time period, demonstrating a need for the protection of men and surveillance of HPV-related disease in both sexes (Park, Kim et al. 2018). Males are already vaccinated in Australia, and recently the United Kingdom brought boys into the vaccination programme (Kirby 2012, Kmietowicz 2018). Despite issues with vaccine hesitancy, the overall reception for the HPV vaccines has been positive, and is already showing effects on rates of HPV-related disease in the years since its introduction.

Disease burden of cervical cancer is still high, predicted as the fourth most common cause of cancer death in women, behind breast cancer, colorectal cancer and lung cancer. Importantly, cervical cancer is the second most common cause of cancer death in countries with a lower human development index, emphasising the impact that economic and social inequalities have on the burden of this disease. Incidence of cervical cancer and mortality rates of the disease are shown in Figure 1.2. From the data generated it is clear to see that the burden of disease is disproportionately high in South-eastern Asia and Sub-Saharan Africa, emphasising the importance of overcoming barriers to screening and vaccination in these countries. Barriers to screening are numerous, and include poor government investment into effective screening programmes, limited access to healthcare resources, and the social stigma attached to a sexually transmitted disease (Ports, Reddy et al. 2013) (Mishra 2010). Without tackling these

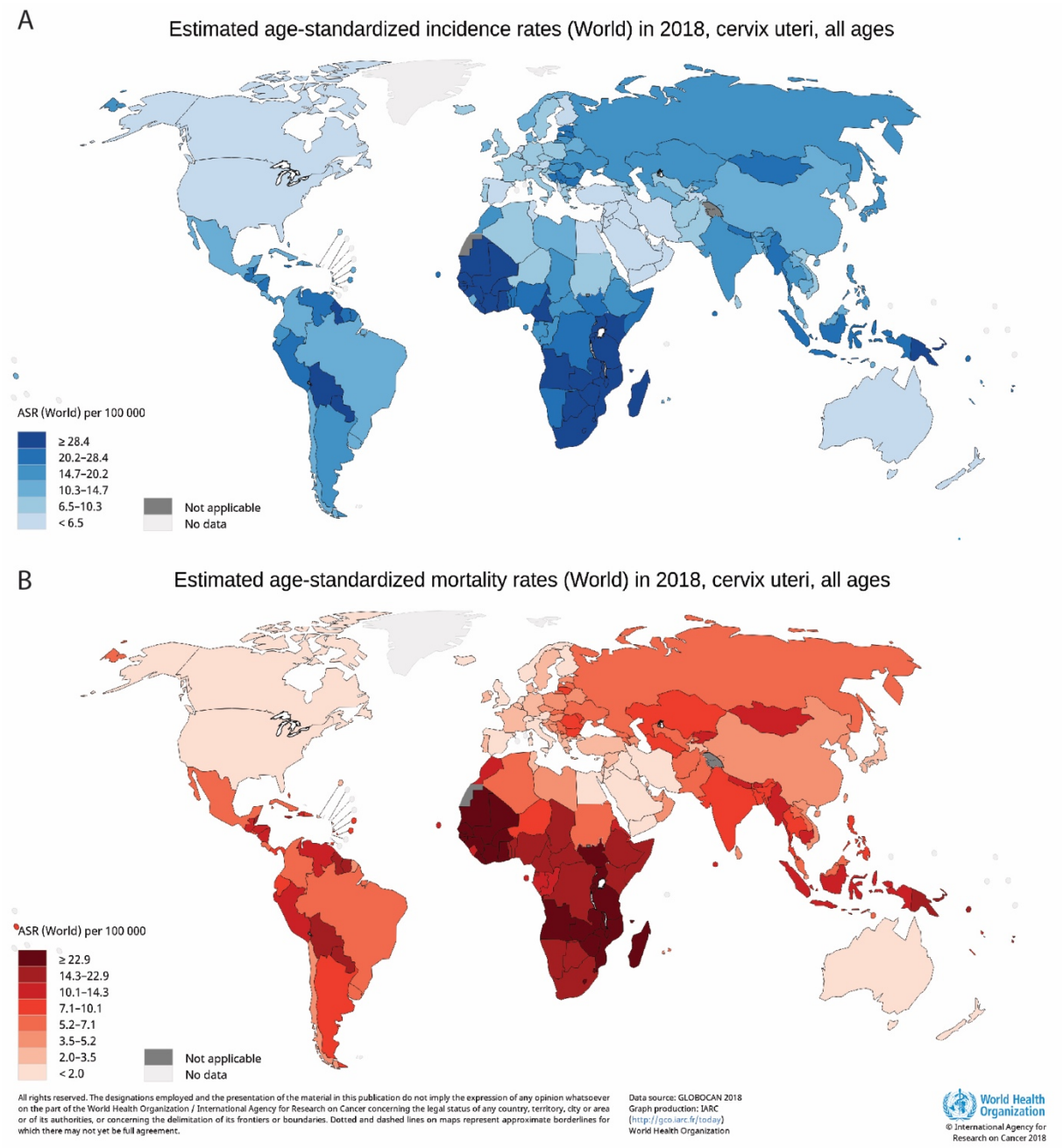

Figure 1.2 Graphic of global maps presenting the disease burden of cervical cancer
A; Estimated age-standardised incidence rates of cervical cancer worldwide in 2018. B; Estimated age-standardised mortality rates of cervical cancer worldwide in 2018. Rates are shown as ASR per 100,000 people, as indicated by the key shown in the bottom left of each map. ASR – Age standardised rates. Source – GLOBOCAN 2018.

issues, incidence and mortality rates of cervical cancer will remain high in these countries with considerable HPV-associated burden of disease (Vaccarella, Laversanne et al. 2017). In 2018 cervical cancer was estimated to cause 311,000 deaths worldwide (Bray, Ferlay et al. 2018).

1.5 Disease association of other papillomavirus genera

Aside from the alpha types, causation of disease is less common in HPVs of other genera. Beta PVs are found so commonly at various sites, it has been suggested that they should be considered to be part of commensal flora in humans. Though most types cause inapparent infection, risk of more insidious disease development rises in immunocompromised patients, or when co-factors such as UV irradiation are involved (Sichero, Rollison et al. 2019). For example, beta PV types HPV5 and HPV8 have been shown to increase the risk of developing cutaneous squamous cell carcinoma (cSCC) in patients suffering from Epidermodysplasia verruciformis (EV) (Jablonska, Dabrowski et al. 1972). EV is a rare hereditary skin disease wherein keratosis-like lesions can develop anywhere on the body, especially on those parts exposed to the sun. The WHO has termed HPV5 and HPV8 as possible etiological agents of cSCC in immunocompromised patients (Bouvard, Baan et al. 2009). Sequencing of HPV L1 DNA can help with diagnosis of this condition, emphasising the involvement of HPV in this disease (Bushara, Miller et al. 2019).

Recent research has shown further evidence that functionality of the host immunity may affect HPV infection. Beta and gamma PV infections are substantially higher in men who are also infected with HIV compared to those who are HIV negative (Smelov, Muwonge et al. 2018). Similar trends were also seen in studies concerning alpha, beta and gamma HPVs, wherein African men suffering from HIV were shown to be at a higher risk of HPV infection when compared with HIV-uninfected men (Meiring, Mbulawa et al. 2017). It is therefore likely that the general immunosuppression caused by HIV infection (Elfaki 2014) makes the microenvironment more amenable to infection with HPV due to the depleted immune response. Analysis of HPV prevalence in SCCs of transplant patients compared with non-immunosuppressed patients showed that HPV DNA was detected much more frequently in SCCs of transplant patients, and that the HPV types found most frequently were beta types, indicating the importance of immune control in modulating infection with types of this genus (Meyer, Arndt et al. 2003). Despite these differences seen in human disease, all PVs share a broad life cycle strategy wherein infection of basal epithelial cells eventually progresses to a productive infection, tightly linked to the process of terminal differentiation (Stubenrauch and Laimins 1999).

1.6 Terminal differentiation of the epithelium

All PVs are known to infect basal cell keratinocytes to establish an infection, and their life cycle is completed alongside terminal differentiation of the infected cells. The structure of human epithelium can be seen in Figure 1.3. Basal cells make up the mitotically active lowest layer of the epidermis, and are responsible for the maintenance and replenishment of all layers of the skin. Recent mathematical modelling of basal homeostasis has suggested that there are three possible outcomes following basal cell division: two differentiated basal cells, two proliferative basal cells, or one of each type (Clayton, Doupe et al. 2007) (Doupe, Klein et al. 2010). When a cell detaches from the basement membrane and exits the basal layer, it moves upwards towards the surface of the epithelium in the process of terminal differentiation, where it is eventually shed from the surface (Jones, Simons et al. 2007). In this way, the epithelium is maintained as a protective physical barrier.

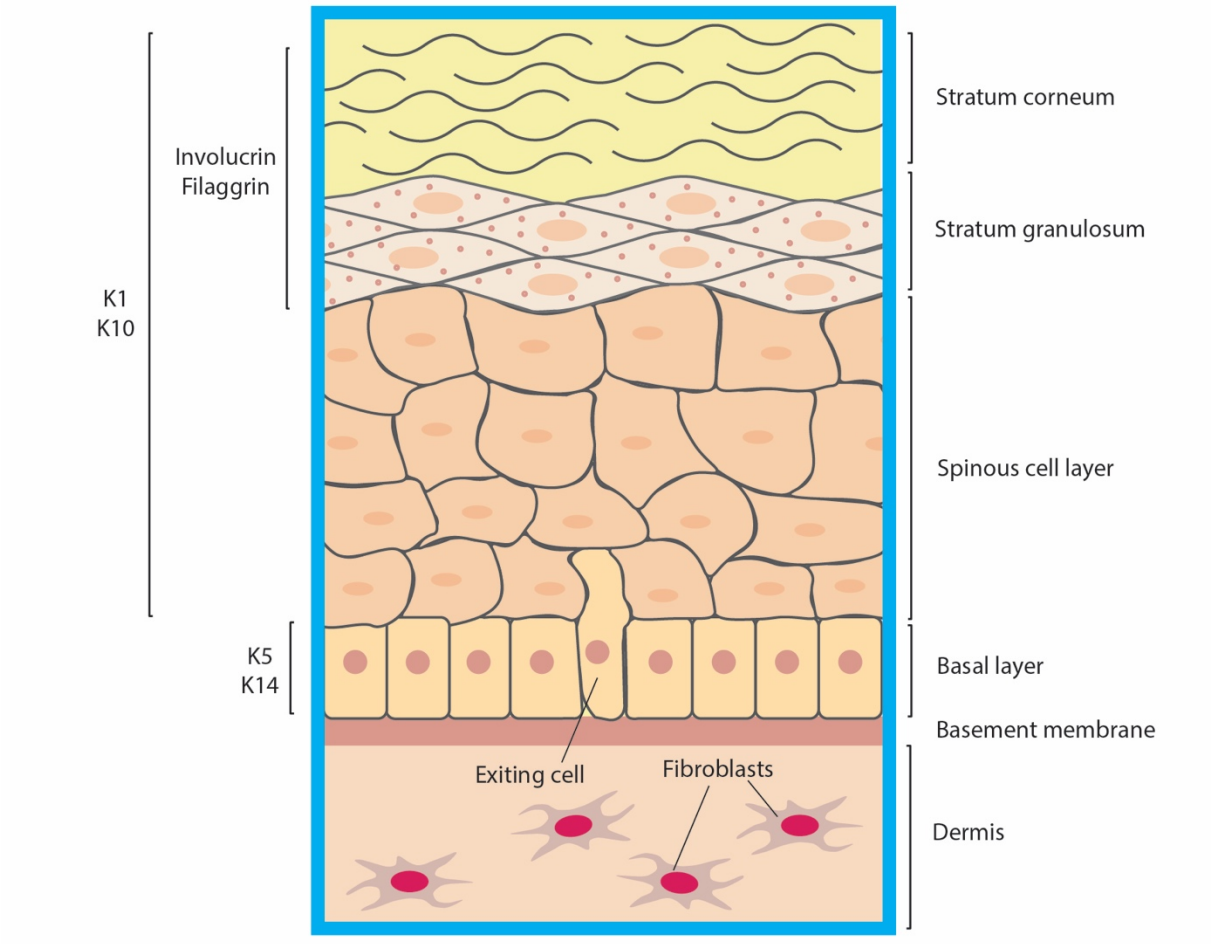

Figure 1.3 The structure of the skin
Human skin has a thick epidermis with multiple cell layers. All layers of the skin are shown in the diagram. The basal layer, spinous cell layer, granular cell layer, and stratified cell layer together make up the epidermis. Differentiation markers are shown to the left of the diagram, Adapted from (Porter and Lane 2003, Pasparakis, Haase et al. 2014).

Expression of different keratins at progressive stages throughout the differentiation process allows discrete layers to be discerned. In the human epithelium, there are four layers of the cutaneous epidermis: the basal layer, the spinous layer, the granular layer, and the cornified layer. Basal cells exclusively express keratin 5 and keratin 14, whilst expression of keratin 1 (K1) and keratin 10 (K10) is seen in the spinous layers as differentiation begins (Fuchs and Green 1980). Expression of the early stage differentiation keratins K1 and K10 is then downregulated in the granular layer. Involucrin and filaggrin are precursors for late stage differentiation transcripts, which are upregulated in the cornified envelope (Zhu, Oh et al. 1999). In mouse tissue similar patterns are seen, however the skin of a mouse is generally much thinner than that of a human, with only 2-3 layers that are 25 μm thickness or less as opposed to 5-10 layers that are 100 μm thickness or greater in human skin (Zomer and Trentin 2018). PV life cycles are tightly linked to this process of terminal differentiation.

Mounting evidence suggests that one way in which healthy tissue is maintained is by the elimination of 'unfit' cells through competition. Recent research has demonstrated that this competitive removal of unfit cells is required to allow maintenance of heathy tissue, both in development and in adults (Merino, Rhiner et al. 2015). These studies with *Drosophila* showed that expression of a gene called *azot* led to the elimination of unfit cells from the population, while knockout of this gene lead to an increase in mutation rates. Research has shown that similar mechanisms exist in mammals, wherein transformed epithelial cells are apically extruded from a population only in the presence of normal epithelial cells, which suggests a method by which 'unfit' cells are lost by direct competition with other cells. For example, in co-culture of normal cells with cells that have knockdown of Scribble, a tumour suppressor gene, mutant cells were apically extruded from the epithelium and underwent apoptosis (Norman, Wisniewska et al. 2012). Similarly, cell culture and *ex vivo* models showed that mutant p53 cells underwent programmed necrosis when co-cultured with normal epithelial cells and were basally extruded from epithelial monolayer (Watanabe, Ishibashi et al. 2018). However, this extrusion and necroptosis did not occur when p53 mutant cells also contained a mutation in the *RasV12* gene, commonly in malignancy. This suggests that cells can overcome normal competition to persist in the epithelium. Current thinking terms this process 'super-competition', which can occur in cells with mutations that allow them to outcompete wild type (wt) cells. These mutations often occur in pathways that have been shown to be important for elimination of 'unfit' cells from the population, including p53, which is targeted by high-risk HPV protein E6 (Bowling, Lawlor et al. 2019). Altering the competitive 'fitness' of the infected cell could be one important part of the PV life cycle.

1.7 THE LIFE CYCLE STRATEGIES OF PAPILLOMAVIRUSES

1.7.1 VIRUS ATTACHMENT AND ENTRY

It is understood that HPV infection can only occur following a microwound or abrasion that exposes the basal lamina, allowing virus particles access to the basal cells (Stanley 2012). Research suggests that virus particles bind to the basement membrane first via heparan sulphate proteoglycans (HSPGs) (Giroglou, Florin et al. 2001). Research carried out with fluorescently labelled HPV16 pseudovirions suggests that viruses then subsequently infect basal cells by transferring to the migratory wound healing keratinocytes and 'surfing' towards the cell body (Schelhaas, Ewers et al. 2008). Virus particles are then internalised by a receptor that is likely specific to keratinocytes, however the identity of this specific receptor is not known. Secretion of an extracellular matrix (ECM) component exclusive to keratinocytes has been demonstrated, which was shown to colocalise with laminin-5, a keratinocyte ECM marker. Adsorption of HPV particles onto these keratinocyte-specific receptors suggested that intermediate association of the virions with these receptors following initial binding to the basement membrane via HSPGs might be the mechanism by which PVs preferentially infect keratinocytes during wound healing (Culp, Budgeon et al. 2006). This provides one reasonable candidate for the specific receptor involved in HPV particle internalisation. Recent research implementing Crispr-Cas9 also discovered potential candidates for this keratinocyte specific receptor, including solute carrier family 35 (adenosine 3'-phospho 5'-phosphosulfate transporter) member B2 (SLC35B2), which is involved in the sulphation of HSPGs (Fu, Tao et al. 2016). This research has not yet been followed up in subsequent publications, however another publication found that inactivation of the *SLC35B2* gene did not affect binding of Zika virus to cells. Conversely, attachment of Dengue virus to the *SLC35B2* deficient cells was decreased when compared with attachment to normal cells (Gao, Lin et al. 2019). Further investigation is required to investigate whether SLC35B2 has a role in attachment of PV to cells.

1.7.2 ESTABLISHMENT PHASE

After trafficking to the nucleus, the virus genome must initially be amplified to a low copy number to establish a reservoir of infection in the basal layer. Copy numbers were found to be 50-100 copies per cell of rabbit oral papillomavirus (ROPV) genomes in the epithelial basal layer of benign oral papillomas in rabbits (Maglennon, McIntosh et al. 2011), and based on research carried out in episomal cell lines the copies per cell in HPVs are estimated to be around 200 copies per cell (De Geest, Turyk et al. 1993) (Stanley, Browne et al. 1989).

Research using inhibitors of different cell cycle stages has shown that inhibition of CDK1, which phosphorylates components of the nuclear envelope during prophase, inhibited HPV infection in a dose-dependent manner. However, inhibition of the formation of the mitotic spindle, which occurs in late prophase and metaphase, did not affect HPV infection of HaCaT cells. This research suggests that host cells must at least enter the early prophase segment of mitosis for virus gene transcription to take place (Pyeon, Pearce et al. 2009). This requirement could be one reason why PVs must infect basal cells; this is the only layer of the epithelium in which cells are mitotically active (Watt, Lo Celso et al. 2006).

E1 and E2 are required for initiation of the establishment phase, and consequently are crucial for successful infection (Ustav and Stenlund 1991) (Ustav, Ustav et al. 1991). E1 binds to the origin of replication in cooperation with the E2 protein, and unwinds the PV DNA (Sedman, Sedman et al. 1997). This process is tightly regulated in a variety of ways, including post-translational modifications of E1 to control localisation. E1 has been shown to directly interact with importins via its nuclear localisation signal (NLS) sequence, and pseudophosphorylation within this site prevents *in vitro* interaction of E1 with importin. Further, the use of a GFP tagged pseudophosphorylation mutant of E1 showed that nuclear localisation of E1 protein is disrupted *in vivo* as a result of pseudophosphorylation of two NLS residues (Bian, Rosas-Acosta et al. 2007). This is supported by research from another group, which showed that phosphorylation of Ser283 is required for shuttling of E1 between the nucleus and the cytoplasm in HeLa cells (Hsu, Mechali et al. 2007). The interference of cellular factors also plays a role in control of E1-dependent replication. For example, human TATA-binding protein has been shown to interfere with HPV11 E1-E2 protein complexes forming at the origin of replication. Similarly, transcription factor protein YY1 has been shown to prevent viral origin-specific replication of HPV18 by interacting with the E2 protein (Hartley and Alexander 2002) (Lee, Broker et al. 1998).

1.7.3 Maintenance phase

Following initial establishment of infection, viral episomes must then be stably maintained within infected cells to provide the reservoir of infection. This maintenance stage takes place in mitosis-capable basal cells that have not yet begun the process of terminal differentiation, and might be able to occur in the absence of E1 and E2. It is likely that this replication occurs once per S phase of the infected cell, and may be mediated by E2 (Murakami, Egawa et al. 2019). Replication of PV genomes has also been shown to occur by random replication as

well as once per S phase. This depends on the level of E1 and E2 proteins present in the host cell and on the identity of the host cell itself (Hoffmann, Hirt et al. 2006).

1.7.4 Amplification phase

To successfully produce infectious virions, a final stage of genome amplification must occur. Two major promoters control HPV transcription: an early promoter located in the long coding region (LCR) termed p97 in HPV16, and a downstream late promoter termed p670 in the HPV16 genome. Levels of expression from these promoters are regulated by differentiation, and an increase in transcription from the late promoter has been shown to be dependent on differentiation (Wang, Liu et al. 2017). In some high-risk PV types such as HPV16, amplification occurs in cells in the mid to upper layers of the epithelium, prior to packaging into virions for release from the surface. The thickness of this proliferative layer increased in relation to the severity of cancer progression in HPV16 positive lesions (Middleton, Peh et al. 2003). Increased levels of E1 and E2 are observed during this phase, allowing increase of viral copy numbers as a result of cell-cycle independent genome replication (Ozbun and Meyers 1998). As infected cells exit the spinous layer, gene expression is massively upregulated and the genome copy number can increase to thousands of copies per cell (Flores and Lambert 1997) (Doorbar 2007) (Chow, Broker et al. 2010). Differences are observed in different types of PVs during this stage of the life cycle. For example, in high-risk HPV types, the proliferating cell phenotype persists into the upper layers. Virus amplification continues as these cells enter a G2 phase state, following S-like phase of growth. Conversely, cells infected with low-risk HPV types appear to undergo a re-entry into an S-phase like state as they enter the mid to upper layers of the epithelium. Genome amplification of low-risk HPV genomes is thought to coincide with this cell cycle reactivation (Doorbar, Quint et al. 2012). There are wide ranging differences between the functions of E6 and E7 in different types of PVs, and in high-risk types the collateral effect these proteins have on the cell can eventually lead to cancer. These mechanisms will be discussed in detail in Section 1.8.

1.7.5 Release of virus particles

For packaging of virus genomes prior to release, the structural proteins L1 and L2 are required, which are also transcribed from the late promoter in the uppermost layers of the epithelium in the final stages of the life cycle (Ozbun and Meyers 1998). These proteins are typically only observed in cells that are positive for E1^E4 transcripts (Middleton, Peh et al. 2003) and it is thought that the process of virus shedding may be aided by structural

alterations in the cornified cell layer caused by E1^E4 (Bryan and Brown 2000). The icosahedral capsids of PV particles are made up of 360 copies of L1 proteins and an estimated 12 L2 protein copies (Modis, Trus et al. 2002). Genomes are packaged within these particles. Fully formed virus particles are shed from the skin during desquamation, wherein terminally differentiated keratinocytes are lost from the uppermost epithelial layer (Bryan and Brown 2001). The release of virus within these desquamed cells may even improve virus survival or transmission (Egawa, N, personal communication). Although there are many differences in the function of different proteins between PV types, this general life cycle allows PVs to successfully infect and persist in basal cells of the epithelium, as shown in Figure 1.4.

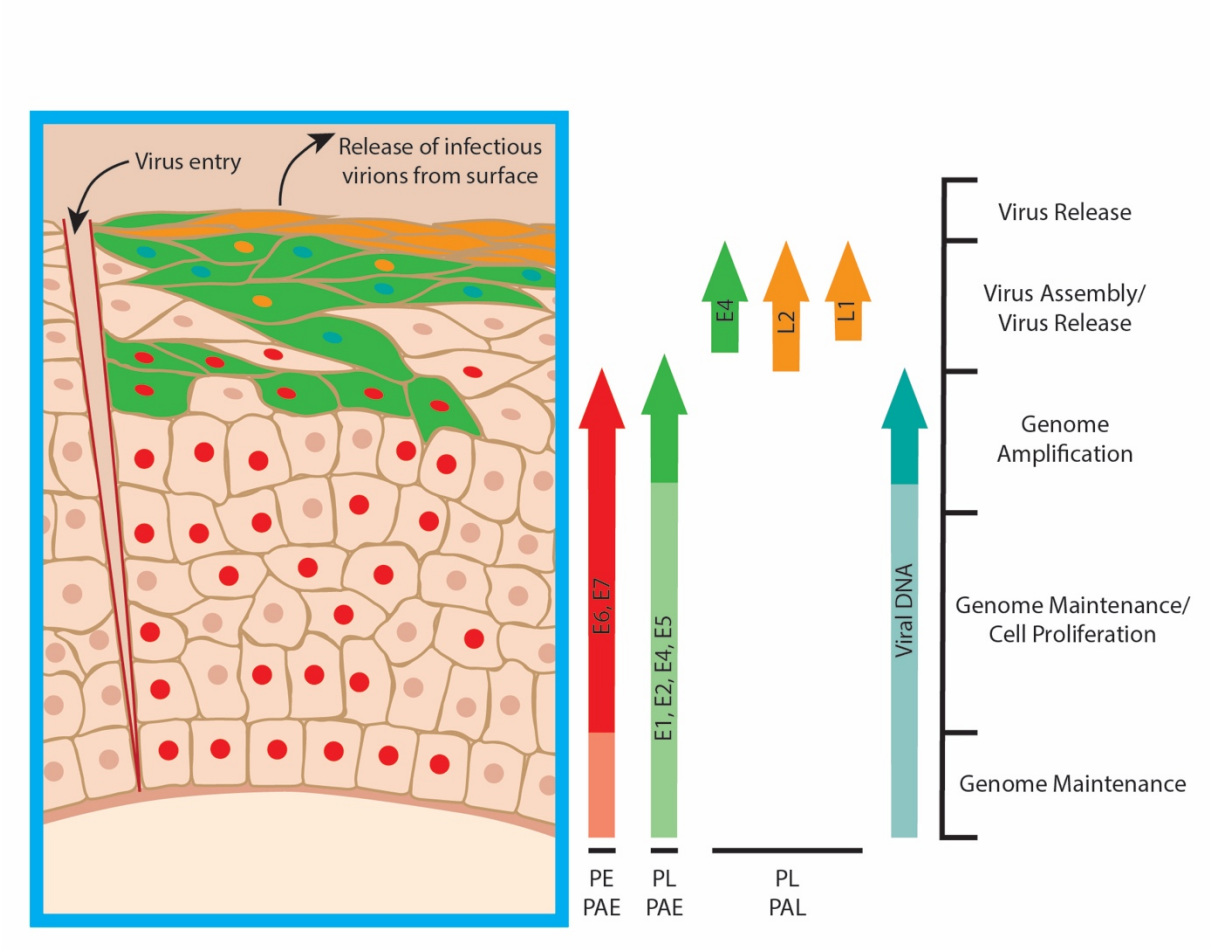

Figure 1.4 Generic life cycle of high-risk HPV
Annotations to right of the diagram indicate initiation of viral gene expression and key stages of the life cycle. In lower layers, viral proteins E6 and E7 are expressed and drive the infected cells through the cell cycle (red coloured nuclei indicate cycling cells). In mid layers of the epithelium, proteins required for genome amplification are increased in infected cells. These cells also express viral E4 protein, and are often in the G2/S phase of the cell cycle despite having exited the basal layer (green colour of cells shows presence of E4, red nuclei show the cell is in the G2 or S phase). In upper layers of the epithelium, cells exit the cell cycle, and viral packaging proteins L2 and L1 are produced in some E4-containing cells. Virus genome is packaged in these cells. Virus particles are shed from the surface. PE – early promoter; PL – late promoter; PAE – early polyadenylation site; PAL – late polyadenylation site. Adapted from (Frazer 2004, Doorbar 2007).

1.8 E6 AND E7 FUNCTIONS IN DIFFERENT PAPILLOMAVIRUS TYPES

1.8.1 ONCOGENIC FUNCTIONS OF HIGH-RISK HPV E6 AND E7

As mentioned in the previous section, the abilities of different PV proteins can vary a great deal depending on the type. High-risk HPVs are mucosal types primarily found in the alpha genus that are associated with many anogenital cancers (Muñoz, Bosch et al. 2003). Due to the established link between certain cancers and high-risk types, and the transforming activity of E6 and E7 demonstrated in rodent and human cell lines, these proteins have been studied expansively (Bedell, Jones et al. 1987, Munger, Phelps et al. 1989). Carcinogenesis of high-risk HPV-associated cancers is tightly linked to the expression and resulting oncogenic activity of their E6 and E7 proteins (Vande Pol and Klingelhutz 2013) (Roman and Munger 2013). One well-known mechanism of E7 is its binding to retinoblastoma family proteins, which results in unscheduled passage of the infected cell through the G1/S cell cycle checkpoint due to the resulting release of E2F transcription factors (Münger, Werness et al. 1989) (Dyson, Howley et al. 1989). E2F is then able to stimulate G1/S transition by activating transcription of genes involved in the cell cycle, such as cyclin A and E (Dyson 1998). Proliferation is also stimulated by E7 inhibition of $p21^{WAF1/CIP1}$ and $p27^{KIP1}$, which are inhibitors of CDK (Zerfass-Thome, Zwerschke et al. 1996) (Jones, Alani et al. 1997). E7 has also been shown to stabilise p53, a tumour suppressor that induces cell growth arrest or apoptosis in response to cellular stress (Demers, Halbert et al. 1994) (Haupt, Berger et al. 2003). Therefore, E6 directed degradation of p53 allows infected cells to avoid the apoptotic cell death that would usually be triggered. High-risk HPV E6 binds to E6AP, a cellular ubiquitin ligase. Subsequent recruitment and degradation of p53 then takes place. p53 cannot be bound and degraded by either E6 or E6AP separately (Huibregtse, Scheffner et al. 1993) (Scheffner, Werness et al. 1990). The E6 protein of some high-risk HPV types has also been shown to abrogate the function of p53 by binding to histone acetyltransferase CBP/p300, a transcriptional coactivator of p53, and consequently downregulating p53 activity (Zimmermann, Degenkolbe et al. 1999). Finally, E6 binding to p53 alone can lead to inactivation of the p53 protein due to the resulting conformational changes (Lechner and Laimins 1994).

An important function of high-risk HPV E6 is its ability to recognise and bind to PDZ-domain containing substrates via a short PDZ-binding domain found at the C-terminus of the protein (Kiyono, Hiraiwa et al. 1997) (Lee, Weiss et al. 1997). Indeed, research suggests that an intact PDZ domain-binding motif (PDM) is significant in pathogenicity of early high-risk infection,

particularly for the amplification of genome copy numbers (Lee and Laimins 2004). Past research has shown that high-risk E6 is able to direct the degradation of multiple PDZ-domain containing substrates, including Scribble, MAGI-1 and MAGI-3 (Massimi, Shai et al. 2008). A number of the PDZ proteins that have been shown to be targeted for degradation following interaction with high-risk E6 are involved in cell polarity, tight junction formation, and adhesion. Measurement of ZO-1, a tight junction component that colocalises with hSrib, demonstrated that expression of high-risk HPV E6 in Madin-Darby canine kidney (MDCK) cells resulted in a decrease in tight junction integrity (Nakagawa and Huibregtse 2000). MAG-1 is also associated with tight junctions, and restoration of MAG-1 levels by inducing expression of MAG-1 resistant to E6 PDZ-mediated degradation resulted in increased tight junction assembly within HPV18 positive cancer cells. An effect on cell proliferation and regulation of apoptosis was also shown, demonstrating the involvement of this PDM interaction by E6 on the integrity of cell junctional structures as well as proliferation and cell survival (Kranjec, Massimi et al. 2014).

1.8.2 Genomic instability caused by high-risk HPV E6 and E7

Aside from these well-known functions, both high-risk E6 and E7 have also been shown to trigger genomic instability in infected cells. Long-term dysregulation of various cell processes in these ways results in the oncogenic transformation of cells infected with HPV. For example, E6 has been shown to dysregulate cdc2-associated histone H1 kinase activity leading to disruption of mitotic checkpoints, and E6 inhibition of p53 also results in induction of tetraploidy of cells (Thompson, Belinksky et al. 1997) (Incassati, Patel et al. 2006). E7 also contributes to genomic instability by abrogating the cell cycle checkpoint that occurs at the formation of the mitotic spindle. This process occurs independently of E6, perhaps through elevation of MDM2, which is an important negative regulator of p53 (Thomas and Laimins 1998). Similar modulation of cell cycle regulatory proteins has also been shown in HPV58, which is highly associated with cervical cancers in Eastern Asia, suggesting important oncogenic consequences of the downregulation of retinoblastoma protein (pRB) and p130 (Zhang, Li et al. 2010).

1.8.3 Impact of high-risk HPV E6 and E7 on differentiation

Dysregulation of differentiation has also been shown to be a fundamental aspect in HPV positive tumours when compared to HPV negative tumours (Mendelsohn, Lai et al. 2010) (Hatterschide, Bohidar et al. 2019). As expected, high-risk HPV E6 and E7 have been shown

to affect differentiation in multiple ways. Raft culture of human keratinocyte cells expressing high-risk HPV E6 and E7 resulted in a decrease in differentiation observed throughout the layers of cells, which became more pronounced when cells of a later passage were used (Hudson, Bedell et al. 1990). Retroviral transduction to express coding sequences of E6 and E7 from a variety of high-risk mucosal HPV types also demonstrated an effect on differentiation when raft culture of these cells was attempted (Schutze, Snijders et al. 2014). Similar effects were observed in studies utilising mutant whole genomes of HPV16 in raft culture, further demonstrating the impact of E6 and E7 expression on normal cell differentiation (Bergner, Halec et al. 2016).

The effect that high-risk HPV E6 and E7 can have on differentiation can also be shown with transcriptional studies comparing control cells with cells retrovirally transduced to express HPV16 E6 and E7. Results showed that the expression of several keratinocyte differentiation genes was downregulated by HPV16 E6 and/or E7 in primary human keratinocytes (Gyöngyösi, Szalmás et al. 2015). Earlier analysis of transcriptional differences was carried out using cDNA arrays. Results showed that in differentiating cultures, significant differences in expression of over 100 cellular genes were observed between control cells and experimental cells retrovirally transduced to express HPV16 E6 and E7. This suggests that E6 and E7 are likely to impact upon gene expression to alter normal differentiation (Nees, Geoghegan et al. 2000). More recently, research has shown that HPV16 can inhibit the cleavage of NOTCH, a receptor known to be involved in the pathway of differentiation. In combination with p53 degradation this lead to promotion of proliferation in cell culture, and a reduced commitment to differentiation, which could result in higher persistence of infected cells in the basal layer of infected tissue when compared to non-infected cells (Kranjec, Holleywood et al. 2017).

1.8.4 HIGH-RISK HPV E6 AND E7 IMPACT UPON THE IMMUNE SYSTEM

In addition to these other functions, E6 and E7 of high-risk HPVs have also been shown to have some effect on the immune system, which may be necessary for success of the virus in the host tissue. Early micro-array analyses demonstrated that, amongst other genes involved in regulation of cell growth, cells containing the HPV31 genome had a significant downregulation of several genes involved in the normal response to interferon (IFN). Of particular note, Stat-1 was shown to be downregulated. Given the significant role that Stat-1 plays in IFN response, this suppression likely results in poor IFN responsiveness *in vivo*, and

may contribute to the evasion of the immune system by infected cells (Chang and Laimins 2000). Similar results were seen in cDNA micro-arrays of cells expressing HPV16 E6 and E7. Whilst E7 showed a modest effect, co-expression of E6 and E7 or E6 alone resulted in notably decreased expression of genes responsive to IFN signalling and genes regulating cell cycle entry, and a significant induction of DNA binding activity for NF-κB (Nees, Geoghegan et al. 2001). NF-κB is a transcription factor involved in regulation of many immune functions, and has been shown to protect keratinocytes from apoptosis (Chaturvedi, Qin et al. 1999). Conversely, high-risk HPV infected keratinocytes were shown to impair the acetylation of NF-κB/RelA K310 through upregulation of the epidermal growth factor receptor (EGFR) to drive expression of cellular protein IFN-related developmental regulator 1 (IFRD1), which was shown to be instrumental in the acetylation process. This resulted in a decrease in production of pro-inflammatory cytokines and a subsequent decrease in immune cell attraction (Tummers, Goedemans et al. 2015). Another study has also shown that HPV16 E6 could inhibit NF-κB by competitively binding to CBP, a co-activator of NF-κB. HPV16 E7 protein binding to p300/CBP-associated factor (PCAF) also inhibited NF-κB, which resulted in a downregulation of IL-8, an important chemoattractant for T cells and lymphocytes (Huang and McCance 2002).

1.8.5 Impact of other E6 and E7 proteins

Given the difficulties in maintenance of other PV types in culture and their less prominent role in the causation of disease, the effects of E6 and E7 proteins of PV types aside from those high-risk types are less well studied. The E6 proteins of some beta papillomaviruses are able to bind p53, however they cannot target the protein for degradation (White, Kramer et al. 2012). Beta papillomavirus types HPV5 and HPV8 E6 proteins are also able to bind to CBP/p300, however the mechanistic process behind the inactivation of function is different to that seen with the alpha types; beta type E6 prevents the phosphorylation of p300 required for protein stabilisation by AKT, which results in a reduced level of p300 in the cell. This was also shown to attenuate expression of some markers of differentiation, including K1 and K10 (Howie, Koop et al. 2011). Studies also suggest that low-risk E7 is less able to induce hyperplasia and impair differentiation when compared to high-risk E7 (Ueno, Sasaki et al. 2006). In particular, low-risk alpha type HPV6 E7 has been shown to destabilise p130, a member of the pRb family, and a decrease in expression of involucrin was observed in HPV6 E7 expressing HFKs, suggesting a differentiation delay (Zhang, Chen et al. 2006).

More recently, proteomic approaches revealed that cutaneous E6 proteins of beta papillomavirus type HPV8, BPV1 (a delta type), and mu papillomavirus HPV1 were all shown to bind to mastermind-like protein 1 (MAML1), a transcriptional co-activator involved in Notch signalling. Binding of E6 proteins resulted in repression of transactivation of Notch in all cases (Brimer, Lyons et al. 2012). Similar results were seen in another proteomic screen of BPV1 E6 along with the E6 proteins of a more expansive group of beta papillomavirus types (8, 25, 98, 17a, 38,76, and 92) (Tan, White et al. 2012). Additionally, the E6 protein of a recently discovered pi papillomavirus type has also been shown to bind to MAML1 and SMAD2/3, leading to inhibition of both downstream pathways (Meyers, Uberoi et al. 2017). Large scale analysis of binding capabilities of 45 different E6 proteins demonstrated that PVs can be clustered based on their binding to E6-AP or MAML1. In the PV types investigated, types from all genera apart from the alpha genus preferentially bound to MAML1 over E6-AP. Out of the animal types tested, E6 proteins from some pigs (SsPV1) and cetacean PVs were able to bind E6AP and subsequently target its degradation. Conversely, beta papillomavirus E6 proteins were shown to bind to MAML1, along with PVs from several other genera, including Delta, Pi, Gamma, and Mu. No E6 proteins were found to be capable of binding and interacting with both E6AP and MAML1, suggesting a key evolutionary split may have taken place (Brimer, Drews et al. 2017). While the function of proteins varies a great deal between PV types, this data suggests that the Notch signalling pathway is important in PV infection.

1.9 The Notch Signalling Pathway

Both *in vivo* and *in vitro*, Notch signalling has been shown to act as a key determinant in the coordination of keratinocyte transition from proliferation to early stage differentiation phenotypes (Rangarajan, Talora et al. 2001). Generally, the Notch pathway is highly conserved, and has multiple roles in the modulation of cell fate in different tissues (McElhinny, Li et al. 2008). A summary of this pathway adapted from a review by Ranganathan and colleagues is shown in Figure 1.5 (Ranganathan, Weaver et al. 2011). The Notch receptor and its ligands (Delta and Jagged) are large transmembrane proteins consisting of EGF-like repeats. There are two classes of ligands in humans and mice: the delta-like proteins (including DLL1, DLL3, and DLL4) and the Serrate homologues (including Jagged1 and Jagged2) (Kopan and Ilagan 2009). Two proteolytic cleavage events within the Notch receptor itself must occur before successful signalling. First, a furin-like convertase cleavage occurs, which results in the splitting of Notch into two segments: one is comprised of most of

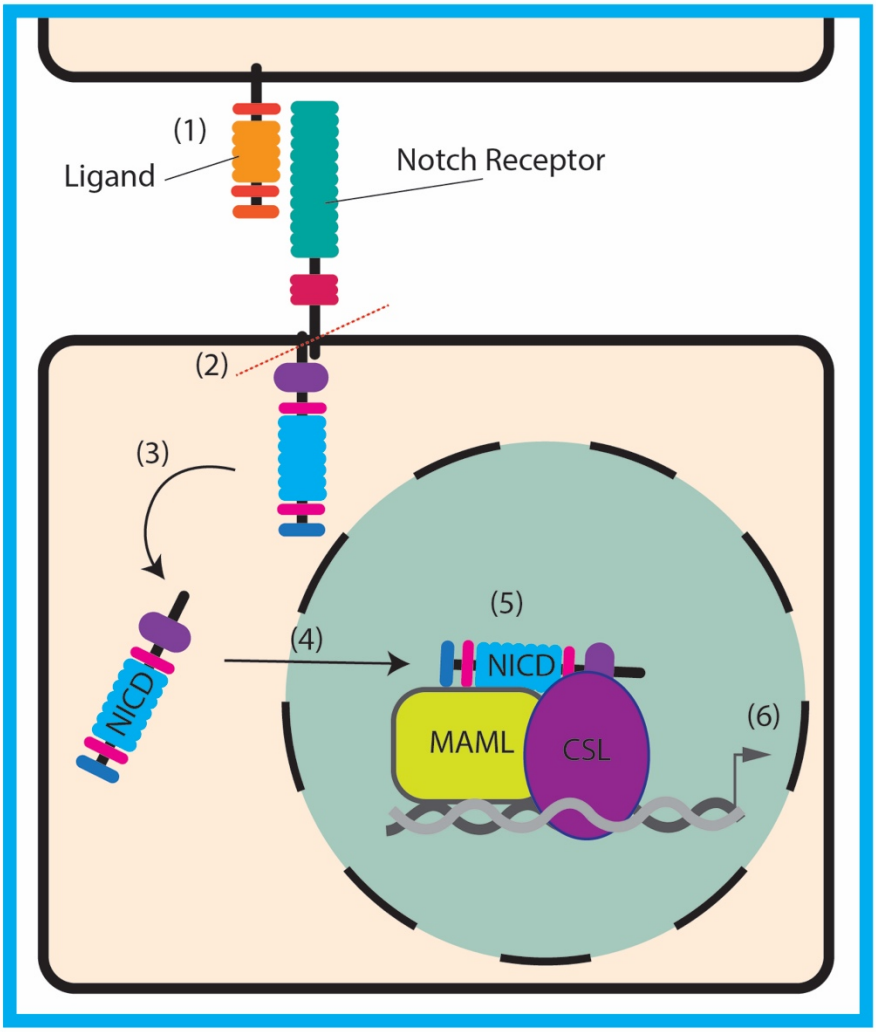

Figure 1.5 The Notch signalling pathway
Diagram showing the canonical Notch signalling pathway. 1; Activation of the Notch Signalling Pathway requires binding of a ligand, such as DLL1, or DLL4. 2; Binding of a ligand causes a conformational change in the notch receptor, which allows S2 cleavage by a metalloprotease tumour necrosis factor-α-converting enzyme. 3; Notch intracellular domain (NICD) is released from the plasma membrane after cleavage of the receptor mediated by the presenilin-γ-complex. 4; NICD is translocated to the nucleus. 5; When NICD enters the nucleus, it forms part of a transcriptional activator complex with MAML1 and CBF1-Su(H)-LAG1 (CSL). 6; Downstream transcription of target genes occurs, such as hairy enhancers of split (HES) family transcriptional repressors. Adapted from (Ranganathan, Weaver et al. 2011).

the extracellular domain, and the second comprises the rest of the Notch receptor structure (Logeat, Bessia et al. 1998). After a ligand binds to the receptor, the ligand is further processed, facilitated by a membrane metalloprotease ADAM-10. This protease causes proteolysis at the S2 site of the Notch receptor, which then allows further cleavage at sites within the membrane spanning region (S3 and S4) by the aspartyl protease γ-secretase (Bray 2006). The Notch intra-cellular domain (NICD) can then be translocated to the nucleus, where

it forms part of a transcriptional complex with the CSL DNA binding protein (CSL: CBF1/RBP-Jκ in mammals, Su(H) in Drosophila, and Lag-1 in Caenorhabditis elegans) (Contreras-Cornejo, Saucedo-Correa et al. 2016) (Mumm and Kopan 2000).

When NICD is absent, transcription is repressed by CSL association with histone deacetylases (HDACs) and ubiquitous co-repressor proteins. However, when NICD is present, it forms a complex with CSL, which could trigger a conformational change that allows transcriptional repressors to displace. A tri-protein complex is then formed with NICD, CSL, and Mastermind (MAML1 in humans and mice), which allows downstream transcriptional activation of target promoters (Ilagan and Kopan 2007). Interaction with MAML1 is necessary for signalling from all four of the Notch receptors (Wu, Aster et al. 2000). In keratinocytes, Notch activation has been shown to negatively target p63. p63, a member of the p53 gene family, has also been shown to negatively regulate Notch-dependent transcription, with Hes-1 being one of its direct negative targets (Nguyen, Lefort et al. 2006). Research has demonstrated that p63 can regulate adhesion and cell survival in keratinocytes; down regulation or upregulation of p63 resulted in corresponding changes in adhesion molecules in mammary cells (Carroll, Carroll et al. 2006). A role in the regulation of proliferation and differentiation of mature keratinocytes has also been demonstrated by using small interfering RNAs against p63 in rafts of primary keratinocyte cells (Truong, Kretz et al. 2006). Impairment of adhesion generally has been shown to also lead to increased differentiation, which emphasises the intrinsic role of p63 in mediating the control of keratinocyte differentiation (Grose, Hutter et al. 2002).

Inactivation studies have clearly demonstrated the role of Notch signalling in regulation of late stage differentiation in keratinocytes (Lin, Kao et al. 2011). Localisation studies have shown that Notch receptors are mainly found in the suprabasal cells, while ligands such as Dll1 have been found mostly in the epithelial basal layer (Watt, Estrach et al. 2008). *In vivo* experiments have shown that NICD complexes with CSL act at the juncture of the basal and suprabasal layer to induce spinous cell layers and downregulate basal fate in the cells. When *RBP-J* was first knocked out, the spinous layer could not form. In contrast, overexpression from Notch1 receptors resulted in expansion of the spinous layer. Expression levels of Hes-1 downstream of the canonical Notch pathway were also shown to be related to stimulation or depression of signalling via this pathway (Blanpain, Lowry et al. 2006). Hes-1 itself was shown to be involved in the repression of spinous layer genes, but was not involved in basal cell marker repression. Overall, it is clear that Notch signalling plays a vital role in successful

maintenance of keratinocytes in a normal epithelium. Given the previously discussed ability of PVs to interact with this pathway, it is clear that this is likely implicated in PV modulation of the cell to successfully infect and persist in hosts.

1.10 *IN VITRO* MODELS OF PAPILLOMAVIRUS INFECTION

1.10.1 CELL CULTURE MODELS

Over the past three decades, PVs have been predominantly researched in recombinant retrovirus models and transfection models in both primary and immortalised cells. Serial passaging of primary epidermal keratinocytes was first described in 1975 (Rheinwald and Green 1975). This was successful due to the introduction of an irradiated mouse fibroblast 'feeder' layer, which provided important tissue factors to the keratinocytes. To study the virus life cycle, cells must be able to stably maintain extrachromosomal HPV DNA (Frattini, Lim et al. 1996). One of the most commonly used cell lines in HPV research is the W12 cell line, derived originally from a CIN1 lesion, that contains around 100 episomal copies per cell of the HPV16 genome (Stanley, Browne et al. 1989). When transplanted into immunodeficient mice, these cells can successfully differentiate and even generate infectious virus (Sterling, Stanley et al. 1990), which makes this a useful cell line to model behaviour of HPV-infected cells in monolayer. However, careful consideration must be given to the passage number of the cells; it has been shown that episomal DNA is lost over time, as cells with integrated HPV DNA dominate the culture population, which can impact experimentation (Alazawi, Pett et al. 2002) (Pett, Alazawi et al. 2004). Therefore, comparison between experiments carried out at different passages can be difficult. Another cell line isolated from a low-grade cervical lesion is the CIN-612 cell line, which contains a mixed population of cells infected with HPV31b. Two sub-clones have been further isolated from this cell-line: the 9E cell line, which stably maintains episomal HV31b DNA, and the 6E cell line, which contains integrated viral DNA (Bedell, Hudson et al. 1991) (Hummel, Hudson et al. 1992).

Use of immortalised keratinocyte cell lines to study HPV is also possible, although one drawback is that any cellular abnormality that caused immortalisation of the cell could have also disrupted important cellular processes, and may therefore affect the PV life cycle. N-Tert cells are derived from a population of primary keratinocytes that were purposefully immortalised by transduction of the telomerase catalytic subunit hTERT gene, and were later able to spontaneously bypass normal senescence as a result of a mutation in the gene $p16^{INK4A}$ (Dickson, Hahn et al. 2000) (Rheinwald, Hahn et al. 2002). This cell line has been used in PV

research, however its mutation in the p16 pathway can be problematic for investigation of oncogenic PV life cycles. Normal Immortalised Keratinocytes (NIKS) are sometimes used in PV research due to their being the natural host of HPV. These genetically stable cells were established spontaneously from a foreskin keratinocyte cell line, and are 'normal' aside from the presence of an extra isochromosome of the long arm of chromosome 8, which was shown to have no visible effect on the normal differentiation process of the cell (Allen-Hoffmann, Schlosser et al. 2000). Study of PVs in this cell line is useful because it allows investigation of low-risk PVs that are unable to immortalise infected cells, or HPV mutants generated to be defective in immortalisation of cells. Research demonstrated that stable maintenance of HPV genomes is possible in this cell line, and that it can also support the virus life cycle (Flores, Allen-Hoffmann et al. 1999). These cells have been used to study a wide range of PV biology, including immune evasion, genome maintenance, and the role of oncogenes in the virus life cycle (Cicchini, Blumhagen et al. 2017) (Lorenz, Rivera Cardona et al. 2013) (Murakami, Egawa et al. 2019) (Flores, Allen-Hoffmann et al. 2000) (Genther, Sterling et al. 2003).

Recently, a novel method of cell culture has been established, which successfully infected primary keratinocytes with HPV16 quasivirions and pseudovirions by first allowing binding of particles to an ECM mimic. Generation of ECM-like depositions was achieved by first culturing HaCaT cells in the culture dishes prior to addition of HPV16 virus particles and subsequent seeding of the primary keratinocyte cells. This method aimed to more closely mimic real-life infection, and successfully showed completion of the virus life cycle in 3D culture of cells in organotypic rafts (Bienkowska-Haba, Luszczek et al. 2018).

1.10.2 Organotypic rafts

Cultivation of keratinocytes on a collagen surface when lifted to an air-liquid interface has been shown to allow culture of stratified epithelium in the form of organotypic rafts, as differentiation is triggered in keratinocytes when they are grown in this way (Fusenig, Amer et al. 1978). A diagram to show the methodology of this system is shown in Figure 1.6 (adapted from (Anacker and Moody 2012). By growing keratinocytes positive for HPV in these raft systems, production of infectious virions in culture is possible, which is an incredibly useful and important system for the study of PVs (Meyers, Frattini et al. 1992). Recapitulation of a productive virus life cycle in N-Tert cells containing HPV11 episomes led to the production of infectious virus particles, showing the utility of this model for low-risk types as well as high risk (Fang, Meyers et al. 2006). Previous reports have also demonstrated

efficient infection of primary keratinocytes with HPV18 to consequently produce high titres of infectious virus in organotypic raft culture (Chow, Duffy et al. 2009) (Wang, Duffy et al. 2009). Use of rafts has allowed important investigation of the virus life cycle in a model that closely resembles stratified epithelium. However closely this model mimics the epithelium, it is not as robust as use of an animal model of infection.

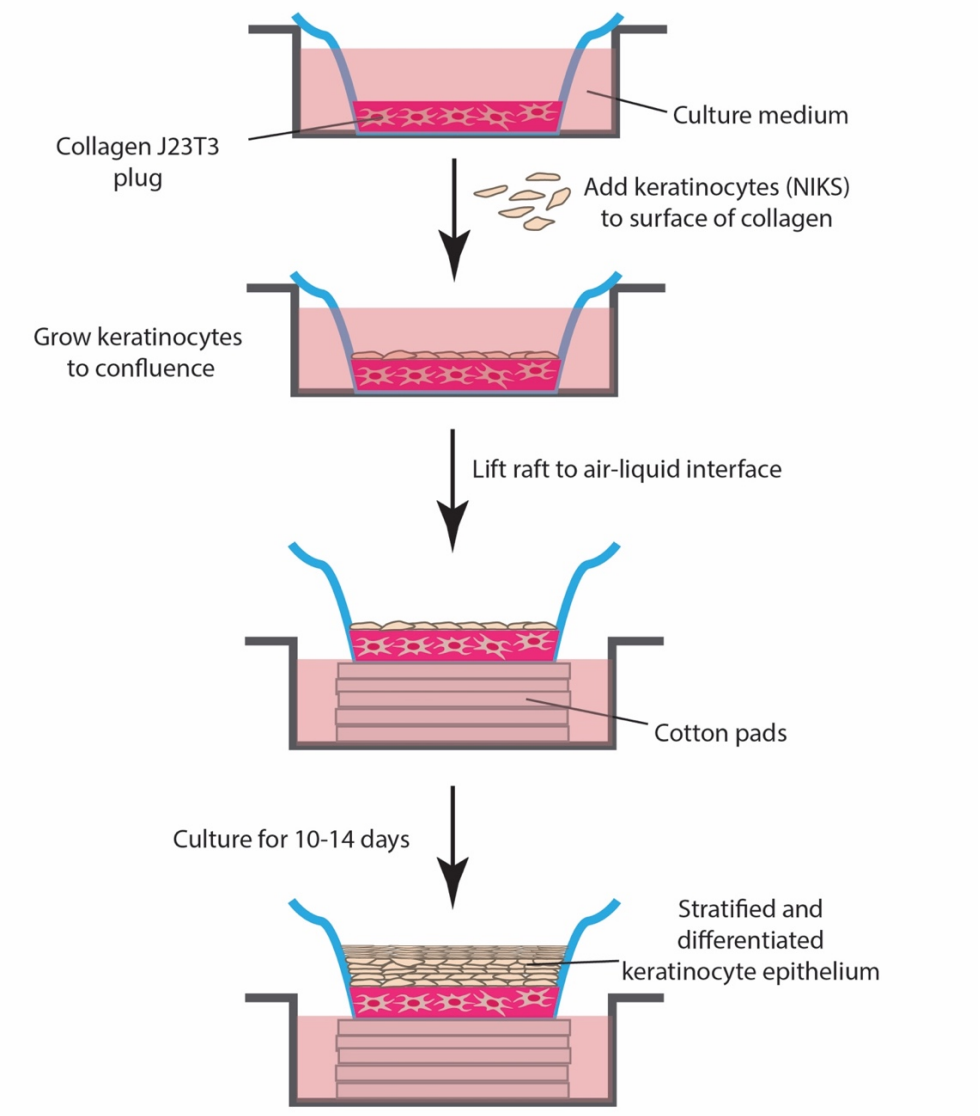

Figure 1.6 Organotypic raft culture
Diagram showing the methodology of organotypic raft preparation from Normal Immortalised Keratinocytes Adapted from (Anacker and Moody, 2012).

1.11 Animal papillomaviruses and models of infection

While much of the current knowledge of PVs concerns human types, the number of non-HPVs to be discovered has been increasing. Most of the PVs discovered thus far are in mammals, and it was originally thought that PV infection was restricted to amniotes (Rector and Van Ranst 2013). To date, nine non-mammal PV hosts have been discovered, including sea turtles (Herbst, Lenz et al. 2009), Adélie penguins (Varsani, Kraberger et al. 2014), and other species of bird (Terai, DeSalle et al. 2002) (Tachezy, Rector et al. 2002) (Gaynor, Fish et al. 2015). Almost all PVs are considered to be within the sub-family *Firstpapillomavirinae*, except for one PV type encoding only E1, E2, L1 and L2. Sparus aurata papillomavirus 1 is the only member of the *Secondpapillomavirinae,* associated with skin lesions of the gilt-head (sea) bream (Lopez-Bueno, Mavian et al. 2016) (Van Doorslaer, Chen et al. 2018).

Historically, it has been understood that PVs exhibit extreme species specificity due to co-evolving tightly with their hosts acquisition of new ecological niches over millions of years (Brooks and Ferrao 2005). In animal PVs, association with cancer is extremely rare, and has only been described in a few limited cases. For example, PV type RrpPV1 was isolated from a nasolabial tumour found in a free-ranging chamois (Mengual-Chulia, Domenis et al. 2014). Another study suggested that EcPV2 could have a causative role in genital tumour pathogenesis in horses; EcPV2 DNA was found exclusively in genital tumour samples (Scase, Brandt et al. 2010). A link between cattle cancer and papillomavirus infection was first suggested in 1978 (Jarrett, McNeil et al. 1978) and in 1986, a paper reported that BPV4 was the etiological agent causative of upper digestive tract papillomas, which could become cancerous if the animal fed on a specific bracken fern pasture (*Pteridium aquilinum*) (Campo and Jarrett 1986). Infection of the oesophagus with BPV4 subsequently provided a useful animal model of PV. While it is interesting to note the oncogenic potential of non-human PV types, these animals are not so conducive to a laboratory research environment. Although some evidence suggests that species specificity may be less strict among hosts that are genetically similar (Gottschling, Stamatakis et al. 2007), there has still been the need for more amenable animal models of PV infection in research. Due to the strict host specificity of PVs, no animal model that can be infected with HPV exists, however use of animal PVs to study general principles of infection is possible. A phylogenic tree recently generated by Doorslaer and McBride is shown in the below figure (Figure 1.7) (Van Doorslaer and McBride 2016). The locations of a high-risk and a low-risk HPV type in relation to different key animal types commonly used to model infection are shown, to demonstrate evolutionary distances between these types.

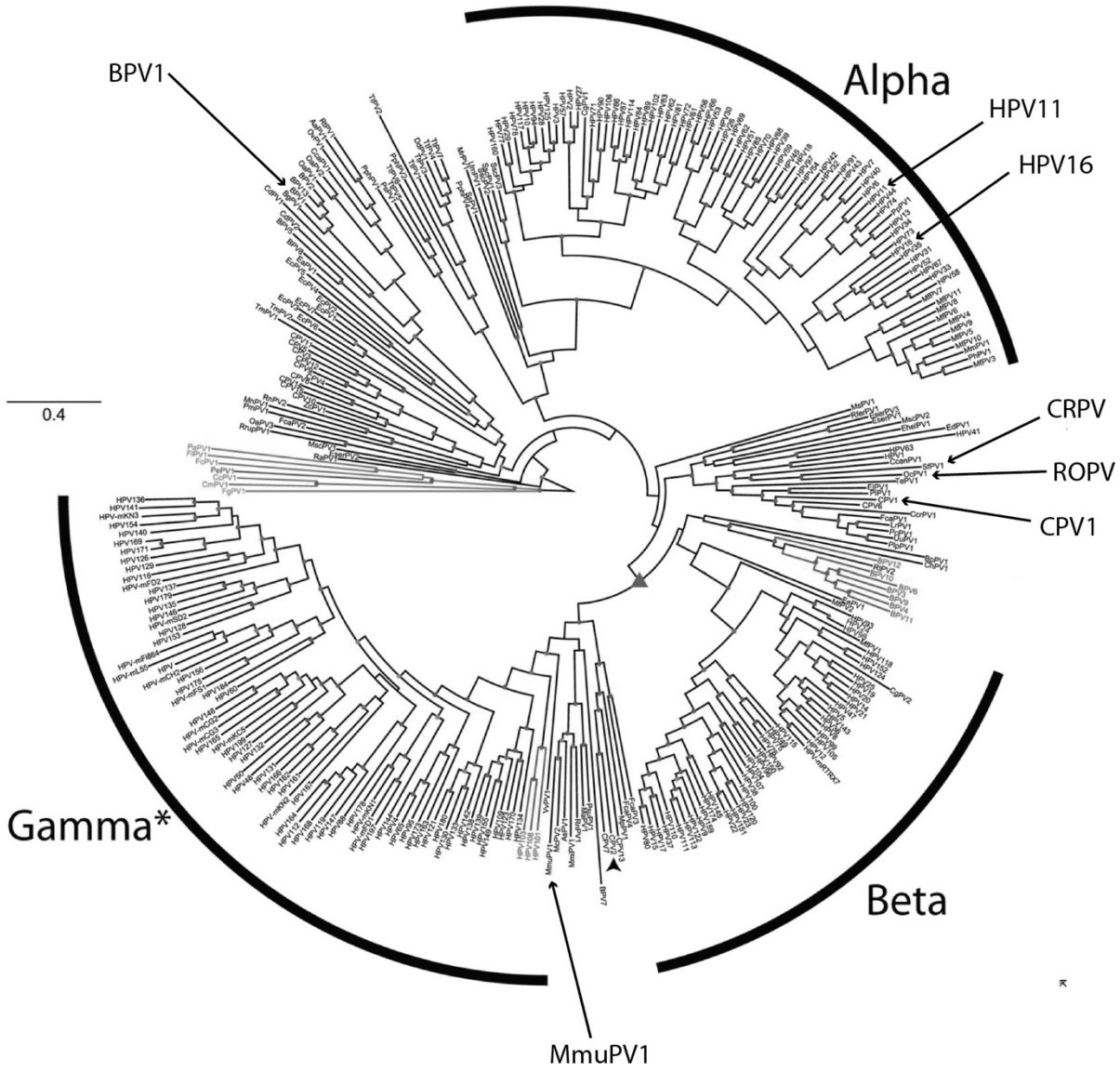

Figure 1.7 Maximum likelihood evolutionary tree of *Papillomaviridae*
Diagram shows an evolutionary tree. Tree was generated using a portioned supermatrix generated from the E1, E2, L1 and L2 core nucleotide sequences. Some members of the Gamma genus have yet to be officially recognised as so, as demonstrated by the asterisk. Selected types have been labelled with black arrows to show their relative locations within the tree. The black arrowhead distinguishes CPV2, which is the root of the phylogenic tree shown. Classification was based on Bernard et al, 2010 and de Villiers et al, 2004. Adapted from (Van Doorslaer and McBride 2016).

1.11.1 RABBIT PAPILLOMAVIRUSES

First described in 1933 (Shope 1933), research using rabbit PV infection was further established when use of a DNA clone of cottontail rabbit papillomavirus (CRPV) was shown to produce infectious papillomas in cottontail rabbit skin, providing a model of cutaneous infection (Brandsma and Xiao 1993). This type is officially termed SfPV1 in the Papillomavirus Episteme (http://pave.niaid.nih.gov), and can also be used to infect domestic rabbits, making experimentation more practicable (Syverton 1952). This model was useful because manageable lesions would grow at the site of infection and subsequently regress, allowing modelling of regression and even latency. Importantly, lesions were of sufficient size to provide a considerable quantity of material for molecular and histological analysis (Stanley and Nicholls 1997). Additionally, approximately 60-75% of infected sites persist and develop into squamous cell carcinomas, meaning this PV could be suitable for modelling high-risk disease (Reuter, Gomez et al. 2001). Early investigations into latency with this model showed infection of sites with low titres of virus did not result in visible papillomas. Despite the lack of visible infection, DNA was detected at the site up to 18 weeks later, and mechanical irritation of the infection site resulted in reactivation of infection, supporting the concept of latent infection (Amella, Lofgren et al. 1994). Further, studies demonstrated that protective immunisation of rabbits was possible using a L1 virus-like particle (VLP) based vaccine (Christensen, Reed et al. 1996).

However, this type of PV cannot infect mucosal tissue. Conversely, another type of PV that infects domestic rabbits is ROPV, which has a tropism for oral mucosal tissue (Parsons and Kidd 1943). This type is officially termed OcPV1 in the Papillomavirus Episteme (http://pave.niaid.nih.gov). In terms of genomic structure and timings of the life cycle, ROPV infection is a reasonable mimic of low-risk infection of mucosal tissue by HPV6 and HPV11 (Peh, Middleton et al. 2002). Over the years, this model has been used to investigate various aspects of PV biology, and has also been used to test therapeutic agents. In terms of latency, while DNA was not visible at the site of infection using *in situ* hybridisation visualisation, polymerase chain reaction (PCR) based methods were able to demonstrate presence of PV DNA following regression of lesions, providing further support for the theory that PVs can still persist following immune-modulated regression of infection (Maglennon, McIntosh et al. 2011). Similar experiments have been carried out with canine models of PV infection.

1.11.2 Canine papillomaviruses

The transmissible nature of warts in dogs was first noted more than 100 years ago (Penberthy 1898). Since then, this model has been used in a multitude of experiments that have furthered knowledge of PV biology immensely. As a mucosal PV, canine oral papillomavirus (COPV) (also called CPV1) has been widely used despite its high purchase and maintenance costs, and in particular has been of paramount importance in the study of immune involvement in PV infection (Nicholls and Stanley 1999). Immune modulation of PV infection was demonstrated in multiple experiments showing regression of lesions and later immunity to reinfection (Chambers, Evans et al. 1960) (Konishi, Tokita et al. 1972). Experiments in passive transfer of serum from previously infected immune dogs to naïve uninfected dogs showed that introduction of neutralising antibody to these dogs prior to infection was protective, however serum transfer to already infected dogs had no effect on lesion regression. This showed that humoral immunity was not involved in the clearance of infection (Suzich, Ghim et al. 1995). Further experiments into adaptive immune responses showed that T lymphocyte infiltration occurred alongside regression of lesions, and the canine model of PV infection was further used to demonstrate the excellent efficacy of formalin-attenuated virus as a vaccine (Bell, Sundberg et al. 1994). Such experiments were important in developing the concept of pre-emptive protection against PV infection in humans. Although the use of canine PVs to model infection has greatly diminished due to availability of other animal models, recent retrospective analyses have emphasised the increasing incidence of viral papillomas with malignant transformation in dogs over the past decade (Thaiwong, Sledge et al. 2018). Investigation into the possible reasons behind this observation may prove useful.

1.11.3 Bovine papillomaviruses

Although the least practically manageable of the animal models, BPV research has also been important. Early research demonstrated that BPV was an infectious agent causative of epithelial hyperplasia (Cheville and Olson 1964). In fact, BPV1 was the first PV genome to be fully sequenced (Chen, Howley et al. 1982). Since then, research with BPV has been incredibly useful for furthering the understanding of PVs despite dissimilarities in disease and mechanism (Munday 2014). Of the known BPV types, 12 have been shown to cause warts in cattle (Rector and Van Ranst 2013). Subgroups have been proposed, one for those types that cause epithelial warts, and one for those that cause fibropapillomas, which present with a considerable proliferative dermal component to the papilloma (Campo and Jarrett 1986). However, recent studies have demonstrated that multiple types of BPV can be detected within

the same lesion, therefore it is somewhat unclear which of the types might actually be asymptomatic (Schmitt, Fiedler et al. 2010). Following cloning and characterisation of BPV genomes (Campo and Coggins 1982), studies have been carried out in monolayer culture to investigate molecular biology and gene function (Jareborg, Alderborn et al. 1992) (Lentz, Pak et al. 1993). Interestingly, BPV1 and BPV2 have been shown to infect species other than cattle, such as horses (Potocki, Lewinska et al. 2012). Despite the useful research done with this model, high costs and complex husbandry requirements mean that a smaller, more manageable host for study is desirable.

1.11.4 Rodent papillomaviruses

The animal most commonly used in research is the mouse but until 2011 no PV capable of infecting a laboratory mouse was known. However, PVs had been isolated from a range of other rodents, including hamsters, rats, and other types of mouse (Iwasaki, Maeda et al. 1997) (Kocjan, Hosnjak et al. 2014) (Schulz, Gottschling et al. 2012) (Van Doorslaer, Rector et al. 2007). Histological analysis of samples taken from European harvest mice demonstrated the presence of a variety of skin lesions associated with the presence of PV (Sundberg, O'Banion et al. 1988). Research with rat PVs added to the case for latent disease, in that mechanical irritation of sites of latent Mastomys natalensis papillomavirus (MnPV) infection in the southern multimammate rat led to an increase in viral load at the site and earlier onset of MnPV-producing skin tumours (Siegsmund, Wayss et al. 1991). Some evaluation of therapeutic approaches to treat MnPV1-induced papillomas has also been carried out in more recent years. Use of a L1-based VLP vaccine proved effective in in the prevention of MnPV1 induced skin lesions in *M. coucha*, whether the infection was natural or experimental, under both immunocompetent and immunocompromised conditions (Vinzón, Braspenning-Wesch et al. 2014). However, given the lack of detailed knowledge regarding how similar the immune system of *M. coucha* is to the human immune system, use of a laboratory mouse model is perhaps more relevant.

In 2011, a strain of PV was discovered spontaneously in a closed colony of NMRI-*Foxn1*^{nu}/*Foxn1*^{nu} mice. Excitingly, this was shown to be transmissible to immunocompetent mice, opening a new area of research in the PV field (Ingle, Ghim et al. 2011). Analysis showed that the genome was 7510bp in length, containing at least 7 ORFs: E1, E2, E4, E6, E7, L1, and L2. MmuPV1 was designated to the *Pipapillomavirus* genus, along with four other rodent types (Joh, Jenson et al. 2011). Shortly after this a variant of MmuPV1 was

discovered, along with three PVs discovered in Norwegian rats (Schulz, Gottschling et al. 2012). Examination of the expression patterns of MmuPV1 L1 and L2 proteins demonstrated that prior to expression of L2, L1 sometimes localised to the cytoplasm in the lower layers of the epithelium, and expression was nuclear only in the presence of L2. Conversely, L2 was only observed in the upper layers (Handisurya, Day et al. 2013). Whilst different from the expression patterns of high-risk types, wherein neither L1 nor L2 are expressed in the lower layers (Florin, Sapp et al. 2002), this pattern of expression is comparable to that of HPV1 (Egawa, Iftner et al. 2000). Given the ease of manipulation of this animal model, this is a valuable system with which to study PV infection, and in particular, the earliest stages of lesion formation. A diagram to show a comparison between the genome of MmuPV1, HPV8, HPV11, and HPV16 is shown in Figure 1.8, to demonstrate important similarities and differences. As shown, all four types possess the "core" proteins E1, E2, L1 and L2, as well as the "accessory" proteins E6 and E7. Notably, only the alpha types contain the E5 protein.

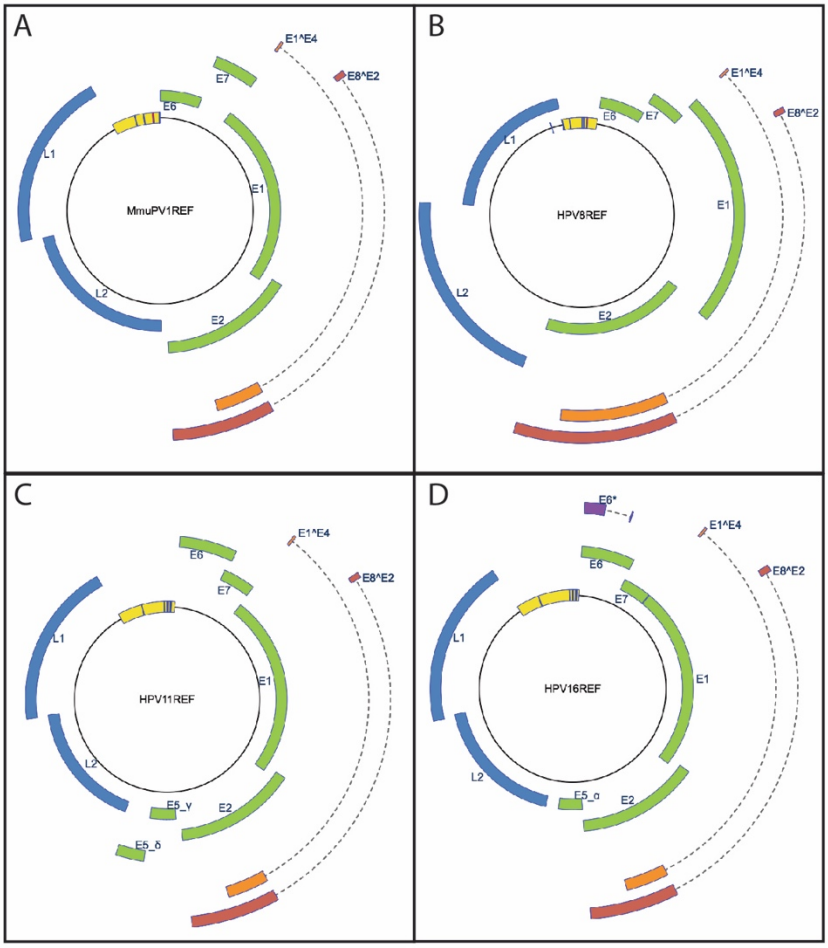

Figure 1.8 Comparison of MmuPV1 genome with selected human types
A; MmuPV1 genome. B; HPV8 genome. C; HPV11 genome. D; HPV16 genome. Early proteins are shown in green. Late proteins are shown in blue. Splice variants are shown in red and orange. The URR is shown in yellow. Genome graphics generated from **pave.niaid.nih.gov.** Adapted from (Van Doorslaer, Li et al. 2017).

Initial research with the MmuPV1 PV model suggested that virus was only capable of infecting cutaneous tissue, and various groups have shown that development of lesions occurs on the muzzle, tail, ears, and back in immunosuppressed mice (Ingle, Ghim et al. 2011) (Handisurya, Day et al. 2013) (Uberoi, Yoshida et al. 2016). However, later research showed that MmuPV1 virus could also infect oral, anal and vaginal sites, and demonstrated that viral copies could be detected in lavage samples as early as 6 weeks following initial infection (Hu, Budgeon et al. 2015). This study also showed that wounding promoted infection and resulted in a higher viral DNA load being detected in subsequent sampling. Another study similarly demonstrated the development of vaginal papillomas in immunocompromised mice following MmuPV1 infection (Joh, Ghim et al. 2016) and showed that passive transfer of hyperimmune sera from C57BL/6 immunocompetent mice to immunodeficient mice prevented lesion development in the experimental mice. Infection with MmuPV1 at cutaneous sites can lead to development of secondary infection at mucosal sites, which further establishes the MmuPV1 model as useful for *in vivo* study of PV disease (Cladel, Budgeon et al. 2013).

As MmuPV1 was originally isolated from florid muzzle papillomas of immunocompromised mice (Ingle, Ghim et al. 2011), it was considered whether this PV type could successfully infect other mouse strains. An investigation into the effect of host strain background on infection was carried out by Sundberg and colleagues, which demonstrated a clear T-cell deficiency requirement in successful infection (Sundberg, Stearns et al. 2014). No lesions formed following infection of immunocompetent C57BL/6J wt mice, however this strain became susceptible to infection when mutated to lack B cells and T cells. Mutation to cause B cell deficiency alone was insufficient to allow MmuPV1 infection, showing that T cells are important in modulating infection. A similar investigation into the effect of immune status of the host on infection showed comparable results (Handisurya, Day et al. 2014). More recent work has highlighted two immunocompetent strains that support infection with MmuPV1 at mucosal sites whilst conversely managing to control disease at cutaneous sites (Cladel, Budgeon et al. 2017). These were mice of strains NU/J and Hsd: NU, both heterozygous for the *nu* mutation. Infected sites progressed to carcinoma *in situ* in NU/J infected mice, which suggests that the mouse model of PV infection could also be useful for the study of malignant progression of infection in an immunocompetent background. Research has shown that MmuPV1 infection can also occur in other strains if the immune system is sufficiently suppressed, for example, by ultraviolet irradiation (UVR) (Uberoi, Yoshida et al. 2016) or cyclosporine A immunosuppression (Handisurya, Day et al. 2014). Overall MmuPV1 can be used to model various aspects of PV infection in a tractable, commonly used lab animal.

1.12 Aims of the thesis

PV warts are understood to be clonal in origin, expanding from a single infected cell (Alizon, Murall et al. 2017). As current treatment methods cannot ensure removal of all infected cells, there is no way to guarantee total eradication of infection during each treatment (Lipke 2006). Persistence is therefore problematic for effective treatment of certain conditions linked to HPV infection. Understanding what competitive advantages an infected cell must have to develop into a lesion is important; establishing the way in which single infected cells compete with their neighbours to successfully develop lesions could reveal significant mechanisms of infection. Such mechanisms may also explain how certain types of HPV are able to form productive lesions without the pro-proliferative capabilities of their high-risk counterparts.

This thesis aims to study the homeostatic characteristics of infected cells with a view to understand how infections form and persist, by examining and modelling the generic characteristics of PV infection using the mouse model of PV infection, and subsequent cell culture systems. Three main avenues were explored:

1. **Investigation and improvement of the mouse model of PV infection to further understanding of early lesion formation.** Initial mouse experiments were carried out in collaboration with Dr Nagayasu Egawa. Immunodeficient mice were predominantly used to examine a wide range of time points, however brief experimentation with immunocompetent mice was also carried out.

2. **Exploration of mouse PV protein function in a cell-based assay to investigate the effects of individual proteins on keratinocytes.** The main aim of these experiments was to recapitulate phenotypes observed and investigated in the mouse model of PV lesion formation, and to understand the role of individual proteins in the context of 2D and 3D cell culture.

3. **To establish a cell line stably expressing mouse PV genome to compare maintenance and amplification of genomes with HPV types.** NIKS cell lines were established that could stably express HPV16 genomes, and investigations into genome maintenance and impact on growth were carried out.

2.0 Materials and Methods

2.1 Buffers and reagents

Table 2.1 Buffers and reagents

Name	Constituents
LB Agar	LB medium plus 2 % Bacto agar
LB Media	1 % tryptone, 0.5 % yeast extract, 1 % NaCl
50X TAE	242 g Tris base, 57.1 mL glacial acetic acid, 18.6 g EDTA
PBS	1 % NaCl, 0.025 % KCl, 0.14 % Na_2HPO, 0.025 % KH_2PO_4
PBS EDTA	PBS and 0.5mM EDTA
FBS DMSO	FBS and 5% DMSO
Trypsin	0.8 % NaCl, 0.02 % KCl, 0.12 % Na_2HPO_4, 0.02 % KH_2PO_4, 0.01% EDTA, 0.13 % trypsin, 0.001% phenol red.
Blocking Buffer A	0.3 M Tris, 20% Methanol, 0.02% SDS
Blocking Buffer B	25 mM Tris, 20% Methanol, 0.02% SDS
Blocking Buffer C	25 mM Tris, 20% Methanol, 6-amino-caproic acid, 0.02% SDS

2.2 Keratinocyte and fibroblast monolayer cell culture

2.2.1 Cell lines

2.2.1.1 J2-3T3 mouse fibroblasts

The murine J2-3T3 cells are a cell line of immortalised fibroblast cells established from embryos of Swiss albino mice (Todara 1963). A blastocidin resistance plasmid, pcDNA6-bsd (Invitrogen), was transfected into these cells and then selected for to establish blastocidin resistant J2-3T3 cells. These cells are irradiated and widely used to form monolayers of 'feeder cells' to support NIKS cell growth.

2.2.1.2 Normal Immortalised Keratinocytes (NIKS)

NIKS are a cell line derived from spontaneously immortalised HPV-negative human foreskin keratinocytes. These cells are often used for experiments with HPV genomes. The cells originate from a neonatal foreskin cell line, BC-1-Ep, and spontaneously immortalised over serial passages (Allen-Hoffmann, Schlosser et al. 2000).

2.2.1.3 NIKS containing HPV16, HPV11 or MmuPV1 genomes

NIKS were transfected with both recircularised replication competent HPV16 genomes (W12), HPV11 genomes, or MmuPV1 genomes, and a Blasticidin resistance gene contained within a pcDNA6 vector to allow for selection of successfully transfected cell lines. While a mouse cell line was considered for use with MmuPV1, NIKS cells were chosen to allow direct comparison across the different genomes in the available time-frame. Following the establishment of individual colonies, cells were expanded over time to make stocks.

2.2.1.4 EF-1F Human Foreskin Fibroblasts

EF-IF foreskin cells have been maintained as a primary cell line, and were first isolated from human foreskin tissues. EF-IF cells have been utilised to create dermal equivalent in organotypic raft culture.

2.2.1.5 293TT cells

HEK-293 cells were generated originally by treatment with sheared adenovirus type 5 DNA. This cell line was then treated with simian virus-40 DNA, which led to establishment of 293T cell lines. 293TT cells were generated by stable transfection of an SV40 Large T Antigen cDNA expression cassette in the 293T cells. These cells are widely used in the PV field for the production of PV-based reporter vectors and the production of recombinant proteins in mammalian cells.

2.2.2 Media and supplements

2.2.2.1 Cell culture media

Table 2.2 Cell culture media

Media	Components
FI	375 mL F12-Hams (Gibco; UK), 125 mL high glucose DMEM (Gibco; UK). Supplements: 5 mL (100x stocks) of adenine, cholera toxin, hydrocortisone, insulin and pen/strep, 5 % (v/v) FBS
FC	500 mL FI media with 500 µl 1000x EGF
FC100	500 mL FI media with 5000 µl 1000x EGF
FC500	500 mL FI media with 25000 µl 1000x EGF
DMEM	500 mL DMEM (Sigma), 50 mL FBS and 5mL pen/strep
Freeze media	45 mL FBS and 5mL DMSO

2.2.2.2 Supplements

Media supplements were prepared as follows, with filtration sterilisation to minimise contamination risk.

100x adenine – 121 mg of adenine (Sigma, UK) was dissolved in 25 ml of HCl (0.005M, 247.4 μL concentrated HCl in 500 ml of water)

100x cholera toxin – 1 mg of cholera toxin (Sigma, UK) was dissolved in 1.2 ml of sterile water to make up a 10 μM solution.

Epidermal growth factor – 100 μg of EGF (R&D Systems, USA) was dissolved in 10 ml of sterile water. 90 ml of HBES containing 0.1% bovine serum albumin was added. Solution was filter sterilised and stored at -20°C.

Foetal bovine serum – (labtech.com, UK)

100x hydrocortisone – 25 mg of hydrocortisone (Calbiochem) was dissolved in 5 ml of cold 100% ethanol to make a 5 ml/ml solution. 0.8 ml of this solution was added to 100 ml HBES and 5% (v,v) Foetal Bovine Serum (FBS) (Hyclone, UK).

100x insulin – 12.5 mg of insulin (Sigma, UK) was dissolved in 25 ml of HCl (0.005M, 247.4 μL concentrated HCl in 500 ml of water). Before adding to the insulin stock, 2 ml of FBS was passed through a 2 μm filter.

Penicillin/Streptomycin – (Gibco, UK)

2.2.3 MONOLAYER CELL CULTURE METHODOLOGY

2.2.3.1 JT-3T3

JT-3T3 cells were seeded into a T-75 flask at $1x10^6$ concentration in 10 ml of DMEM and stored at 37°C. Cells were passaged when they reached around 90% confluence. To harvest cells, media was first aspirated from the flask. Following this, cells were washed with 2 ml PBS and incubated in 1ml of trypsin at 37°C until cells detached in single cell suspension. To passage, trypsinised cells were resuspended in DMEM and from this suspension a new flask of J2-3T3 cells was cultured. Media was changed every two days. For long term storage at -80°C, cells were harvested, and spun down at 1500 rpm for five minutes using a benchtop centrifuge (Sigma, US). Cells were then resuspended in 500 μl freeze media and frozen at -80°C.

2.2.3.2 NIKS, NIKS exogenously expressing virus proteins, and PV-containing NIKS culture methods

NIKS were cultured in 10 ml of FC media on a monolayer of irradiated J2-3T3 feeder cells. J2-3T3 cells were irradiated for 14 minutes and 14 seconds (220kV, 14mA; resulting dosage was 60Gy). In routine experimentation, a monolayer of 1 x 10^6 irradiated J2-3T3 cells was seeded in a T-75 flask in 10 ml of DMEM or FC media and left for at least two hours to allow cell attachment. NIKS were cultured to around 80% before passage. To harvest the NIKS, media was aspirated and cells were washed in 2 ml PBS. Next, cells were incubated for five minutes in 0.5mM EDTA PBS at room temperature (RT) to detach feeder cells. Following aspiration of 0.5mM EDTA PBS, cells were washed twice in 2 ml of PBS. Finally, cells were incubated in 1.5 ml trypsin for 15 minutes to detach the NIKS in single cell suspension. Cells were then resuspended in 8.5 ml of FC media. Cells were reseeded at 1x10^6 concentration in 10 ml of FC in a 75 ml flask seeded with irradiated J2-3T3 cells and stored at 37°C. FC media was changed every two days. For storage long term, cell suspension was spun down at 1500 rpm for five minutes and resuspended in 500 µl freeze media at 4 x 10^6 concentrations.

2.2.3.3 Cell counting of NIKS cell lines

Where necessary, all counting of cells was carried out with the Beckman Z1 coulter particle counter. To count the cells, 200 µl of each cell suspension was added to 9.8 ml of isoton (1:50 dilution), which was counted.

2.2.3.4 Monolayer growth assays of NIKS cell lines

Growth assay experiments were carried out to assess the cell proliferation in culture over a period of nine days. Cells were counted in triplicate over the nine-day period. Around 1x10^5 irradiated JT-3T3 cells were seeded into each well of a six-well plate in FI media and left to attach for at least two hours before seeding of 1x10^5 experimental or control NIKS cells into each well. Plates were left overnight at 37°C and on the following day media was changed to experimental media, which was changed every two days. To harvest cells for counting, each well was washed with 1 ml of PBS, after which cells were incubated in 1 ml of 0.5mM EDTA PBS to detach feeder cells. After this time, plates were tapped firmly to stimulate full detachment of feeders. Each well was washed twice with 1 ml of PBS and then 0.5 ml of trypsin was added to each well. Plates were then incubated at 37°C for at most 20 minutes, up until the cells had completely detached from the plate surface. To create single cell suspension for counting, 3.5 ml of FI media was added to each well and total volume of solution was pipetted up and down, before adding the contents of each well to a 15 ml falcon tube. Cells were counted as described above (2.2.3.3).

2.2.3.5 High-density competition assay

For high-density competition assays, cells were seeded at a high density on 4 chamber polystyrene vessel tissue culture treated glass slides (Fisher Scientific, UK). To each chamber, $4x10^4$ irradiated J2-3T3 cells were added to provide a favourable growth environment. Immediately after this, $4x10^5$ experimental cells were seeded at a 1:1 ratio of mCherry expressing cells versus EGFP expressing cells ($2x10^5$ cells of each group). Cells were cultured in FC media for up to 10 days. Media was changed the day after seeding and every other day.

2.2.3.6 Genome copy number monolayer growth assay

T-25 flasks were seeded with PV-containing NIKS at a $3.3x10^5$ concentration in 4 ml of media (FI media). The day on which cells are seeded was marked as day 0. Samples were collected on days one, two, three, four and seven. To collect samples, cells were handled as described above for NIKS cells, up to resuspension in FC media. Cell suspension was transferred to a 15 ml tube, spun down at 5,000 rpm for five minutes, washed in PBS and spun down. Pellet was resuspended in 200 µl PBS and frozen at -80°C. The media in remaining flasks was changed to experiment media concentration –FC, FC100 or FC500. Media in the flasks was changed every two days. To analyse samples, DNA extraction kit (Qiagen, UK) or DNA/RNA/Protein Minikit (Qiagen, UK) was used to extract DNA, then Syber green qPCR kit protocol followed).

2.2.3.7 EF-1F human foreskin fibroblasts

EF-1F fibroblasts were grown in T-75 flasks in 10 ml of DMEM until around 80% confluent. To harvest, cells were gently washed in 2 ml of PBS. After removing PBS, cells were incubated at 37°C 5% CO_2 in 1 ml of trypsin for 5-10 minutes. Following cells detachment from the flask, 9 ml of DMEM was added to the flask. The mixture was then transferred to a 10 ml falcon tube. Mixture could be split between T-75 flasks for expansion of EF1Fs, or spun down at 2000 rpm for 5 minutes to stock. Cell pellet was resuspended in an appropriate volume of freeze media.

2.2.3.8 293TT cells

293TT cells were grown in T-75 flasks in 10 ml of DMEM until around 90% confluent. To harvest, cells were carefully washed in 2 ml of PBS. After removing PBS, cells were incubated at 37°C 5% CO_2 in 1 ml of trypsin for 5 minutes. Following cells detachment from the flask, 9 ml of DMEM was added to the flask. The cell suspension was then added to a 10 ml falcon tube. Mixture was split between T-75 flasks for expansion of 293TTs or spun down

at 1500 rpm for 5 minutes to stock. Supernatant was removed and the cell pellet was resuspended in a volume of freeze media appropriate for the number of cells collected.

2.2.3.9 Virus infection of HaCaT cells

Wells of an 8-well slide chamber were coated with collagen prior to the seeding of cells. Collagen mix (as described in section 2.3.2), was diluted 1/1000 in DMEM. Diluted collagen mix was then left to solidify for 1 hour at RT prior to the seeding of cells. HaCaT cells were seeded at a density of 2 x 10^4 cells per well. Cells were cultured in DMEM for 24 hours prior to infection. Serial dilutions of virus genome equivalent (VGE)s were added to wells to calculate the approximate number of infectious units per VGE. VGE represents the estimated quantity of genomes to which plasmid DNA in a serially diluted sample compares. Media was changed 24 hours following infection, and cells were fixed a further 24 hours after this media change.

2.3 Organotypic raft culture of keratinocyte cell lines

Rafts were cultured in a level one containment hood, until collection of samples.

2.3.1 Media and reagents for raft culture

The table below shows the media required for the culturing of organotypic rafts.

Table 2.3 Raft medias

Media	Components
FI media	375 mL F12-Hams (Gibco; UK), 125 mL high glucose DMEM (Gibco; UK). Supplements: 5 mL (100x stocks) of adenine, cholera toxin, hydrocortisone, insulin and pen/strep, 5 % (v/v) FBS
Cornification media	500 ml FI media with 5% (v/v) FBS, 610 µl $CaCl_2$ (final concentration 1.88mM). Add fresh N 1,2-dioctanoyl-sn-glycerol (C8:0) (Sigma, UK) to a final concentration of 10 µM.

2.3.2 Preparation of dermal equivalents

Preparation of dermal equivalents was carried out entirely on ice, to ensure collagen did not solidify. First, 20 ml of rat-tail collagen was resuspended with 2.5 ml 10X DMEM, 460 µl 10N NaOH, 250 µL of Pen/Strep (100x) and 2.5 ml FBS. Approximately 1 ml of this

suspension was added to each individual transwell insert (Costar, UK), which was already placed within a deep 6-well plate (BD Biosciences; UK). This was left to solidify for 5 minutes. EF-1F fibroblasts (600 µl of a 7.5 x 10^6 cells/ml suspension) were then added to the remaining collagen mixture, and once the 1 ml of collagen had set, 2.6 ml of this was added to the individual transwell inserts. The collagen was then left to harden for 30 minutes at 37°C 5% CO_2 until the dermal equivalent had solidified completely. Dermal equivalents were then left submerged in DMEM for 1-7 days.

2.3.3 Seeding and differentiation of keratinocyte cell lines

NIKS cells or NIKS cells exogenously expressing experimental proteins were trypsinised, counted and resuspended as described above. Cells were resuspended in FI media at 2 x 10^7 concentration of cells/ml. Medium was removed from the inserts and 50 µl of the cell suspension (around 1 x 10^6 of cells) was added dropwise to the centre of each dermal equivalent. These inserts were left at 37°C 5% CO_2 for 30 minutes to 2 hours to allow cells to properly attach to the dermal equivalent. After incubation, 12 ml of FI media was added to each well. These were left for 4 days at 37°C 5% CO_2 and media was changed every other day. On the fourth day, the rafts were lifted. Medium was aspirated from each deep well and sterile cotton pads were placed under each insert to allow an air-liquid interface to be established. Raft cultures were subsequently fed with 12 ml of cornification medium from below, which was changed every other day, until harvesting. Rafts were cultured in this manner to allow differentiation for up to 12 days after lifting.

2.3.4 Harvesting and fixation of raft samples

Following differentiation, rafts were removed from their transwells for fixation by cutting off the base of the transwell using a scalpel blade. The raft was then immediately placed into a plastic vial containing 10 ml of 4% PFA. Rafts were fixed for 24 hours at 4°C, after which the raft was placed in PBS until sectioning. For longer periods between fixation and sectioning, rafts were placed in 70% ethanol.

2.3.5 Sectioning of raft samples

Rafts were paraffin embedded by the Addenbrooke's Hospital Tissue Bank facility. Paraffin embedded rafts were then transversely sectioned (sections of 5 µm thickness) on to Superfrost plus slides.

2.4 Mouse Work

2.4.1 Mice

Immunodeficient athymic Hsd:AthymicNude-Foxn1nu mice (purchased from Envigo, UK) and Female C57BL/6J immunocompetent mice (purchased from Charles River, Kent) were maintained under specific pathogen free (SPF) conditions in the Animal House, Department of Pathology, University of Cambridge. All mice were housed in aseptic micro-isolator cages in a category two facility. Animals housed and cared for in the Animal Facility and were handled with appropriate personal protection equipment. Mice used were between 8 and 12 weeks of age. All procedures were performed in accordance with the Animals Scientific Procedures Act (1986) and licensed by the United Kingdom Home Office.

2.4.2 Virus Preparation

Mature papillomas were harvested from the tail of a mouse and disrupted in phosphate buffered saline by homogenisation using an electric rotor stator homogeniser. Cellular debris was then removed by centrifugation at 8000 x g for 10 minutes, leaving the virus particles in the supernatant. To pellet virus particles, resulting supernatant was ultra-centrifuged in a swinging bucket rotor at 130,000 x g. The virus pellet was then resuspended in 10% FBS, and crude virus stocks were stored at -80°C. VGE was estimated by visualising infected HaCaT cells by detecting E6/E7 MmuPV1 transcripts using RNAscope *in situ* hybridisation. The infectious titre was then estimated using Reed-Muench method (Reed and Muench 1938).

2.4.3 Scarification and virus infection

In vivo infection was carried out by scarification of multiple sites along the tail with a 27-gauge needle whilst mice were anesthetised, followed by inoculation with 4 µl of MmuPV1 virus supernatant. MmuPV1 virus supernatant was applied to the tail by pipette. Mock infections were carried out as described with PBS. Tails were harvested and fixed overnight in 4% paraformaldehyde and then stored in PBS until embedding.

2.4.4 Incorporation of Bromodeoxyuridine

Incorporation of Bromodeoxyuridine (BrdU) was analysed to assess replicating cell DNA in tissue. Mice were injected with 200 µl of 10 mg/ml BrdU solution (Sigma Aldrich, UK). Tissue was harvested 24 hours later.

2.4.5 Marking of the wound site

To attempt marking of the wound site, 4 µl of Carboxylate-Modified Microspheres (ThermoFisher Scientific, UK) was applied to the wound site and allowed to dry for five minutes. Alternatively, 4 µl of EZ-Link™ Sulfo-NHS-LC-Biotin (ThermoFisher Scientific, UK) was applied to the site and allowed to dry. When using the EZ-Link™ Sulfo-NHS-LC-Biotin in combination with virus infection, the product was added after the inoculation of virus to the wound site as described above in 2.4.3.

2.4.6 Dissection of tissues for histology

Mice were killed by cervical dislocation. Tissue samples such as lesions or entire tails were removed using sharp scissors. Tissue was immediately inserted into 4% PFA for around 24 hours. Tissues were placed in 70% ethanol after fixation until processing.

2.4.7 Processing of tissues for histology

Tails were cut from end to end using a sharp scalpel blade on the opposite side to the infected sites. Skin was then carefully stripped away from the bone using a scalpel and forceps. Wound sites were cut transversely across the middle of the wound site. These small strips of skin were then placed into a plastic cassette between two pieces of foam, with the wound site edge facing to the right. Tissues were then processed using a Thermo Scientific Shandon Excelsior Tissue Processor on an overnight programme from neutral buffered formalin (10%, 1 hour) through six absolute alcohols (99%, 45mins, 1hr, 1h15min, 1h15min, 1h15min, 1h30min) to xylene (3 solutions; 1hr, 1h15min, 1h30min) to molten paraffin wax (3 solutions; 1h, 1h15min and 1h30min).

2.4.8 Embedding tissues in paraffin

Embedding was performed on a Leica EG1160 embedding centre either by Helen Skelton, a histologist based at the Department of Pathology, or by an Addenbrooke's Hospital Tissue Bank histologist. Molten wax was poured into inox moulds and mouse tail samples were orientated to provide a transverse section of the tail tissue. Wax was allowed to harden around the cassettes to make up the completed block.

2.4.9 Cutting sections and mounting slides

Sections of 5µm thickness were cut using a microtome, floated onto water at 45°C to smooth out any creases and a glass slide was then placed underneath to allow adherence of the paraffin section to the slide as the section was lifted from the water. Slides were then allowed to dry out in an oven at 37°C. Sections were cut and mounted at the Human Research Tissue Bank, by a Research Support Biomedical Scientist. Slides were incubated at 37°C overnight prior to any staining protocol.

2.5 Molecular biology techniques

2.5.1 Plasmids

2.5.1.1 Papillomavirus plasmids

PV full-genome plasmids used were as follows:

Table 2.4 PV full genome plasmids

HPV Type	Size (bp)	Vector and size (bp)	Restriction enzyme	Provided by
HPV11	7931	pBR322 (4361)	*BamHI*, Buffer 3.1 (NEB)	Neil Christensen
HPV16	7906	pTZH (4922)	*BamHI*, Buffer 3.1 (NEB)	Margaret Stanley
MmuPV1	7857	pAsylum (878)	*Xba1* Buffer 2.1 (NEB)	Neil Christensen

2.5.1.2 Construction plasmids

Plasmids for the construction of expression vectors used were as follows:

Table 2.5 Construction plasmids

Vector	Size (bp)	Provider
pLXSN	7931	Clontech (631509)
pQCXIN	7906	Clontech (631514)
pBOB-EF1-FastFUCCI-Puro	12352	Addgene (86849). Gift from Kevin Brindle & Duncan Jodrell (http://n2t.net/addgene:86849; RRID: Addgene_86849). (Koh, Mascalchi et al. 2017)

Further details can be seen in the Appendix (Chapter 8.0).

2.5.2 Transfection of PV genomes into NIKS

For transfection of genomes, NIKS were harvested and plated in 60mm 6-well plates on a layer of $1x10^5$ J2-3T3 irradiated feeder cells at a density of $2x10^5$ cells per well. Cells were then cultured overnight in FI media. Transfections were carried out using the FuGENE® HD Transfection Reagent (Promega; E2311) using the protocol provided. Cells were transfected with up to a total of 1.6μg of circular DNA, purified from bacterial cultures, alongside 0.4μg of a circular blasticidin resistance plasmid for selection. Cells were passaged to T-75 flasks 24 hours after transfection and cultured overnight in FI media. A further 24 hours following passage to the T-75 flasks, selection was started, with cell media being changed to FC media with 6μg/ml blasticidin. Media was replaced 48 hours later. Finally, culture medium was changed to FC a further 48 hours afterwards, completing the transfection procedure.

2.5.3 Transfection of exogenous expression vectors into 293TT cells

Production and subsequent infection of recombinant retroviruses was carried out as described previously (Naviaux, Costanzi et al. 1996). One day prior to transfection, 293TT cells were seeded at $5x10^5$ in a 6 well plate. The following day, 2 μg of maxiprepped plasmid DNA was made up to a total volume 100 μl in opti-MEM™. To check transfection efficiency, 1.5 μg of plasmid along with 500 ng of an EGFP plasmid were used. In a separate Eppendorf, 6 μl of Polyethyleneimine (PEI) was added to 94 μl of opti- MEM™. DNA and PEI mixtures were mixed together and incubated for 30 minutes at RT. During this incubation, media on 293TT cells was changed to fresh DMEM. DNA-PEI mixture was added dropwise to the well and incubated for 24 hours at 37°C 5% CO_2. Media was changed after 24 hours. Upon confluence, 293TT cells were collected, or media was collected and filtered for virus. Cell suspension was spun down at 1500 rpm, washed with 2 ml of PBS, and spun down a second time at 1500 rpm. After a final wash in 2 ml of PBS, cells were spun down at 1500 rpm and then resuspended in RIPA buffer. Pellets were stored at -20°C until protein extraction.

2.5.4 Viral Transduction

NIKS cells were seeded one day in advance of transduction on a bed of γ-irradiated J2-3T3 feeder cells. Transduction was carried out by incubation with retrovirus for 2-6 hours with 4μg/ml of Polybrene (SantaCruz, Texas). Cells were selected in G418 400 ng/μl for 48 hours and expanded through two passages before use in experiments. Expression was confirmed by transient transfection in 293TT cells.

2.5.5 Bacterial transformation

Plasmid DNA was transformed into chemically competent cell line One Shot® TOP10 *E. coli* or One Shot® Stbl3™ Chemically Competent *E. coli* (ThermoFisher Scientific, UK). Manufacturers protocol was followed and the transformed bacterial culture was plated out onto LB agar plates with appropriate selection; ampicillin (100 μg/ml), kanamycin (50 μg/ml). Plates were left at 37°C overnight for around 16 hours to allow growth.

2.5.6 Bacterial plasmid DNA extraction

Before extraction of plasmid DNA from successful colonies, single colonies were isolated using a pipette tip, which was then added to a tube containing 2-3 ml of LB broth (100 μg/ml ampicillin). Cultures were shaken at 220 rpm at 37°C overnight for around 16 hours. Extraction of plasmid DNA from culture was carried out using a Qiagen spin mini-prep kit (Qiagen, UK) with 1.5 ml of the expanded culture. DNA extraction and elution was carried out following the manufacturer protocol and supplied buffers. For large-scale DNA extraction, 250 μl of the expanded culture was added to 250 ml of LB broth containing 100 μg/ml ampicillin, which was then cultured overnight at 37°C with shaking at 220 rpm. Plasmid DNA from resulting expanded culture was extracted with the EndoFree plasmid maxi kit (Qiagen; UK, manufacturer protocol and supplied reagents used).

2.5.7 Extraction of genomic DNA from HPV16 NIKS

To prepare cells for DNA extraction from cell culture, cells were pelleted by centrifuge (1500 rpm for five minutes), resuspended in 500 μl PBS and then pelleted again using a microcentrifuge (1500 rpm for five minutes). Cell pellets were put on ice immediately and stored at -80°C until extraction of DNA. Extraction of total genomic DNA was carried out using QIAamp DNA Blood Mini kit (Qiagen; UK). The complete set of buffers and reagents required were provided within the kit.

2.5.8 Extraction of genomic DNA, RNA and protein

To simultaneously extract total DNA, RNA and protein, cells were harvested, washed in PBS, and stored as a pellet at -20°C. Extraction of DNA, RNA and protein was carried out using an AllPrep DNA/RNA/Protein Mini Kit (Qiagen) and QIAshredder® kit (Qiagen) according to the protocol provided. RNA was stored at -80°C in 2μg aliquots. DNA and protein samples were stored at -20°C.

2.5.9 Quantification of plasmid DNA and RNA

Plasmid DNA and RNA was quantified using a Nanodrop 8000 spectrophotometer.

2.5.10 Reverse transcription

To synthesis cDNA, reverse transcription of RNA was carried out using the SuperScript™ III First-Strand Synthesis Kit (Life Technologies). A volume of approximately 1µg of extracted RNA was added to two tubes, each containing 2 µl of dNTP mix and 2 µl of oligo$(dT)_{20}$ primers. These volumes were then made up to 20 µl using DEPC-treated water. Mixtures were incubated for five minutes at 65°C in a four-bay DNA Engine Tetrad 2 Peltier Thermal Cycler (Bio-Rad, USA), and then placed on ice for a minimum of one minute. Following this, a master mix was added to each tube, the components of which are described in Table 2.6. To the first tube, 2 µl of SuperScript™ III reverse transcriptase was added, while 2 µl of DEPC-treated water was added to the subsequent tube to act as an internal control. Tubes were then incubated for one hour at 50°C, and then incubated for five minutes at 85°C to terminate the reaction. Following this, samples were chilled on ice before collecting the reactions by brief centrifugation. Next, 2 µl of RNAse H was added to each reaction and incubated at 37°C for 20 minutes. cDNA was stored at -20°C ready for use.

Table 2.6 cDNA synthesis mix

cDNA Synthesis Mix (per reaction)	
10X RT Buffer	4 µL
25mM MgCl2	8 µL
0.1M DTT	4 µL
RNaseOUT™ (40 U/µL)	2 µL

2.5.11 Quantitative RT-PCR (qPCR)

Quantitative real-time polymerase chain reaction (qPCR) was carried out to analyse RNA samples utilising cDNA as a template for the reaction. To assess levels of transcripts, forward and reverse primers (Table 2.7) were used (Griffin, H, 2016). GAPDH primers were used as endogenous controls. The qPCR technique was also employed to allow quantification of PV genome copy number per cell by quantifying both PV genome copy number and GAPDH copy number. GAPDH was used as an internal housekeeping gene to quantify the number of cells. Forward and reverse primers for both the PV DNA and GAPDH were designed to target

these sequences. The GAPDH region chosen for amplification was selected based on it being the region with the lowest level of homology to mouse GAPDH DNA. This was to minimize any readout interference as a result of mouse J2-3T3 fibroblast contamination in the sample. Amplification of DNA in the reaction was achieved using a SyberGreen ROX mix reagent containing a hot start DNA polymerase. Samples were run in the reaction in triplicate for each primer set in 96 well plates (ABgene, UK) and an ABI 7000 sequence detector system was used for analysis.

2.5.12 qPCR Primer Design

Table 2.7 qPCR primer design

Primers used for qPCR	
HPV16 E5 **(cDNA)**	Forward: TGTGCTTTTGTGTGTCTGCC Reverse: AAACACCTAAACGCAGAGGCT
HPV16 E6FL **(cDNA)**	Forward: TGGGAATCCATATGCTGTATGTGA Reverse: ACGGTTTGTTGTATTGCTGTTCT
HPV16 E6T **(cDNA)**	Forward: CAGGAGCGACCCAGAAAGTT Reverse: CTGTTGCTTGCAGTACACACA
HPV16 E1 **(cDNA)**	Forward: GGGTGGTTGCAGTCAGTACA Reverse: TGCTAACATTGCTGCCTTTG
HPV16 E7 **(cDNA)**	Forward: CATGGAGATACACCTACATTGC Reverse: AGATCAGTTGTCTCTGGTTGCA
GAPDH **(cDNA)**	Forward: GATTTGGTCGTATTGGGCGC Reverse: TTCCCGTTCTCAGCCTTGAC
HPV-16 E4	Forward: GACTATCCAGCGACCAAGATCAG Reverse: CTGAGTCTCTGTGCAACAACTTAGTG
GAPDH	Forward: CCTCCCGCTTCGCTCTCT Reverse: CTGGCGACGCAAAAGAAGA
HPV-11	Forward: ATCTCGATTTTTGCACGCGCCGTTTGTGT Reverse: ATAGATCTCACAACTTAGTCACTGGGTGTAAC
MmuPV1 E6	Forward: GGTGCTTGTATTGTGTGCCGC Reverse: TGCCAGCCATGCACTCTACC
MmuPV1 E7	Forward: GGTGAGCCTGACCTACCCGA Reverse: CGGAGAACAGTGTCGCAGCA

2.5.13 qPCR REAGENT MASTER MIX

Power SYBR® Green Blue PCR Master-Mix (ThermoFisher Scientific, AB4163A) was used to amplify and detect cDNA or DNA in 364-well PCR plates (ThermoFisher Scientific, 4309849) using an ABI-7500 Real-Time PCR System. Before loading the plate, a new reagent master mix was prepared for each set of primers used. The final volume in each well was 10 µl, and each sample was plated in triplicate. A master mix of reagents was made up each time the experiment was carried out. Primers were first diluted to 1µM working stocks in sterile H_2O. Total volume of master mix made depended on the number of reactions being analysed. After mixing, 32 µl per reaction was added to 2 µl of DNA, which was tapped well to mix. Following this, 10 µl of each 34 µl mixture was plated into triplicate wells.

Table 2.8 qPCR mix

qPCR mix (per reaction)	
Primer mix	3.2 µl
SYBR Green	16 µl
DW	11.8 µl

2.5.14 qPCR PLATING ARRANGEMENT AND REACTION CYCLE SET UP

Plating of samples was carried out in triplicate to ensure statistically significant data collection. Following the qPCR cycles, running of a dissociation programme was also carried out; SYBR green is known to bind to dsDNA products that are non-specific.

Table 2.9 qPCR cycle parameters

	Step	Number of cycles	Time per cycle	Temperature
qPCR cycle parameters	1	1	2 minutes	50°C
	2	1	15 minutes	95°C
	3	45	15 seconds	95°C
	4	1	1 minute	60°C
	Step	**Number of cycles**	**Time per cycle**	**Temperature**
Dissociation parameters	1	1	15 seconds	95°C
	2	1	20 seconds	60°C
	3	1	95 seconds	95°C

2.5.15 qPCR STANDARD CURVES AND CALCULATIONS

For each experiment and each primer set, a standard curve using known quantities of sequence-containing construct was generated. For genome quantification, six ten-fold serial dilutions of a vector containing the appropriate PV sequence were plated out using methods described above in triplicate. To generate a standard equation to determine the number of copies of HPV present in each reaction, concentrations of serially diluted DNA were converted into their corresponding copy numbers. For GAPDH quantification, six ten-fold serial dilutions of a pDrive vector containing the GAPDH ORF were plated out using methods described above in triplicate. Where standard curves were not produced, set standard curves were applied to the data, and these were as follows:

HPV16: $y = -3.332x + 32.335$
GAPDH: $y = -3.4x + 30.339$
HPV11: $y = -3.269 + 28.787$
MmuPV1: $y = -3.167 + 29.019$

These equations fit the format of $y=mx + c$, a linear equation. In this equation, y represented the number of cycles taken to amplify one copy DNA. The value m represented was the efficiency of the primer sets; -3.33 is considered a perfect linear relationship between the cycle threshold (Ct) value and the DNA copy number. This equation was utilised to establish the total copies of virus genome and GAPDH in each reaction. Each triplicate (Ct) of values was averaged. If $y=mx+b$ where y is the Ct value, m is the slope, x is the unknown, and b is the y intercept, solving for $\ln^{-1}x$ should give the total number of copies within a reaction. The GAPDH value was initially divided by four; this would give the total number of cells in each reaction because as well as the two existing sequences, the NIKS genome was found to contain two GAPDH pseudogenes. Following this, the Ct value for the virus genome can be divided by the number of cells to finally give genome copy number per cell.

2.5.16 SITE DIRECTED MUTAGENESIS

Inverse PCR mutagenesis was used to insert additional bases into a known vector to build a new construct. Or, to introduce a protein tag to the protein of interest. Primers were designed to correspond to area of interest in the construct, with additional sequence at the ends of the sequence to allow addition of two restriction enzyme sites or the protein tag.
Primer designs were as described below in Table 2.10.

Table 2.10 Primers for site-directed mutagenesis

Target	Sequence
11full-XhoI	F: atCTCGATttttgcacgcgccgtttgtgt R: atAGATCTcacaacttagtcactgggtgtaac
16full-XhoI	F: atCTCGAGaaactatatttgctacatcctgtttttg R: atAGATCTatatacaatgaataaccacaacaca
MmuPV1-E6-HA	F: GGGGACAAGTTTGTACAAAAAAGCAGGCTgccAccATGTACC CATACGATGTTCCAGATTACGCTgaaatcggcaaaggctacactctcg R: GGGGACCACTTTGTACAAGAAAGCTGGGTtatagtaatggtttgcagaacccgcag
MmuPV1-E7-FLAG	F: GGGGACAAGTTTGTACAAAAAAGCAGGCTgccAccATGcagggcccattaccaacaattgc R: GGGGACCACTTTGTACAAGAAAGCTGGGTtaCTTGTCGTCATCGTCTTTGTAG TCtcgttttccatttctgaggttcacg
MmuPV1-E6-R130A	F: AGGCTACTGCGGGTTCTGC R: GCCCACATGTGGCGCACC

Reaction mixture was as follows:

Table 2.11 PCR reaction mixture

PCR Reaction mixture	
PCR grade water	35 µL
2mM dNTPs	5 µL
Primer A	1.5 µL
Primer B	1.5 µL
Plasmid template DNA (50 ng/µl)	1 µL
KOD-Plus-DNA Polymerase	1 µL

Cycle set up was as follows:

Table 2.12 Site-directed mutagenesis PCR cycle

qPCR cycle parameters	Step	Number of cycles	Time per cycle	Temperature
	1	1	2 minutes	94°C
	2	1	10 seconds	98°C
	3	45	13 minutes	68°C

After the final cycle, temperature was decreased to 4°C and held to complete. The provided manufacturer protocol was used to complete the inverse PCR mutagenesis.

2.5.17 Gateway cloning technology System for vector construction

A gateway cloning kit (ThermoFisher) was used to establish exogenous expression vectors. Following PCR amplification of the desired entry sequence, LR reactions were carried out according to manufacturer's protocols. Reactions were transformed into competent *E. coli* as described above. Following selection and DNA extraction of the donor reaction, BP reactions were carried out according to manufacturer's instructions. Reactions were then transformed into competent *E. coli* and selected once again, before DNA extraction for experimentation.

2.5.18 Agarose gel electrophoresis

TAE buffer (1X) was made up using water and TAE (50X). One gram of agarose powder was measured out using a Sartorius scale set and powder was then added to 100 ml of TAE buffer (1% agarose gel). The solution was microwaved at 70W with periodic swilling of mixture until powder completely dissolved. The gel was left to cool until the temperature was low enough to add to the gel tank and was then allowed to set. Gels were cast and run at a constant voltage of 100V using a Mupid-One Submarine gel electrophoresis system. For staining, the gel was added to TAE buffer containing SybrSafe (1 µl SybrSafe added per 10 ml solution). Gels were visualised using UV.

2.5.19 DNA extraction from agarose gel

DNA was extracted from agarose gel using a Wizard SV Gel and PCR Clean-Up system (Promega, UK) according to manufacturer's instructions.

2.6 Immunocytology and Immunohistochemistry

2.6.1 Immunocytology of monolayer cells

To collect monolayer keratinocytes to carry out immunocytology, cells were seeded on a bed of irradiated J2-3T3 feeder cells ($1x10^4$ cells per well) at a density of $1x10^4$ per well in a four-chamber culture slide (Falcon, 354104). Cells were cultured for three and seven days to provide pre and post-confluent samples. To overcome cell density variation due to plating error, cells were plated in quadruplet at serially increasing densities in 8 well slide chambers (Thermofisher, UK). Cells were plated at $1x10^4$ cells per well or $8x10^4$ cells per well. These cells were then grown for two days, with a media change after 24 hours. After this time, samples were collected, providing pre-confluent and post-confluent data sets.

2.6.1.1 Fixation of cells

Cells were fixed with 5% paraformaldehyde for 30 minutes at RT. Growth medium was first aspirated from the wells, and cells were washed twice with PBS. Following incubation in PFA, cells were washed three more times with PBS and stored at 4°C in PBS.

2.6.1.2 Immunocytology and mounting monolayer slides

All steps were carried out at RT. The PBS solution was aspirated from each well. For permeabilisation, cells were incubated for 30 minutes in PBS added 0.2% Triton X-100 (Promega), then washed in PBS. All cells were blocked in 10% normal goat serum (NGS) (Cell Signalling Technology) in PBS for one hour. For K10 staining, anti-keratin 10 antibody DE-K10 (Neomarkers, mouse monoclonal antibody) diluted in 10% NGS in PBS at a 1:250 dilution was applied to the slides and left for one hour. Next, slides were washed in PBS three times. An anti-mouse Alexa 488-conjugated secondary antibody (1:150 dilution in 10% NGS in PBS) was used to detect the primary antibody; the secondary antibody was left for one hour. DAPI was added alongside the secondary antibody at a 1:1000 dilution as a nuclear counterstain. Subsequently, the slides were rinsed three times in PBS then dried gently. Finally, a drop of Citifluor® reagent was added to each well space and a coverslip was placed across the slide, taking care to avoid air bubbles. Slides were stored at 4 °C.

Table 2.13 Immunocytology antibodies

Antibody	*Target*	Species	Clone	Dilution	Incubation	Supplier
Primary	K10	Mouse	DE-K10	1:100	16 hr. RT	Neomarkers
Secondary	Mouse IgG	Goat	n/a	1:150	1 hr. RT	Invitrogen

2.6.2 Fluorescent Immunohistochemistry of rafts and tissue samples

2.6.2.1 Antibodies and chemical reagents

Table 2.14 Immunohistochemistry antibodies and reagents

Target	*Species*	*Clone*	*Dilution*	*Incubation*	*Supplier*
K10	Mouse	DE-K10	1:100	o/n 4°C	ThermoFisher
K17	Rabbit	ab53707	1:100	o/n 4°C	Abcam
Tenascin C	Rabbit	ab108930	1:100	o/n 4°C	Abcam
BrdU	Rat	ab6326	1:200	o/n 4°C	Abcam
HES-1	Rabbit	D6P2U	1:100	o/n 4°C	Cell Signaling
H3 ps10	Rabbit	06-570	1:500	o/n 4°C	Merck
E4	Rabbit	MusE4	1:200	o/n 4°C	In house
L1	Rabbit	MusL1	1:200	o/n 4°C	In house
Involucrin	Rabbit	sc-28557	1:100	o/n 4°C	Santa Cruz
L1	Mouse	MPV.B9	1:100	o/n 4°C	Neil Christensen
Anti-Mouse	Goat	A32723 A32742 A32728	1:200	1 hr RT	ThermoFisher
Anti-Rabbit	Goat	A-11012 A-11008 A32733	1:200	1 hr RT	ThermoFisher
Anti-Rat	Goat	ab150160	1:1000	1 hr RT	Abcam
Biotin	n/a	S11227	1:200	1 hr RT	ThermoFisher
DAPI	n/a	n/a	1:1000 / 5% NGS	1 hr.	Sigma
Tyramide	n/a	n/a	1:200 Amp. diluent	10 minutes	Perkin Elmer
HCl	n/a	n/a	1M	15 minutes	Fisher Chemical
ImmPRESS HRP kit	Rabbit	MP-7401-50	n/a	1 hour	Vector Laboratories

2.6.2.2 Deparaffinisation and epitope exposure of rafts and tissue

To carry out immunohistochemical analysis on mouse tissue or raft samples, samples embedded in paraffin went through a process of dewaxing and rehydration. To dewax the section, slides were submerged into a container of xylene for 10 minutes, with occasional agitation. They were then placed into a second container of xylene for a further 5 minutes. After the removal of wax, rehydration of tissue sections was achieved by submerging the slides in graded alcohols for 2 minutes at a time (twice in 100% ethanol, followed by once in 80%, 50% and 30% ethanol). Slides were then submerged in dH2O for at least 5 minutes. A bench top oven was then used to carry out the step of epitope exposure. Slides were incubated in DAKO Target Retrieval Reagent (Aligent, USA) for 10 minutes at RT, before being heated to 110°C for 15 minutes in a Decloaking Chamber (Biocare Medical, USA). The sections were then allowed to cool to below 90°C before the pressure cooker was opened. This process took around 1 hour to complete.

2.6.2.3 Application of primary and secondary antibodies to tissue sections.

Immediately following epitope exposure, slides were incubated in PBS for 5 minutes. Sections were then blocked in 10% normal goat serum (NGS) (v/v) in PBS for at least 20 minutes in a humidity chamber at RT. Following the blocking step, primary antibodies were diluted in 10% NGS and applied to the sections overnight at 4°C. Primary antibodies were removed by washing in PBS for five minutes three times at RT. Secondary antibodies diluted in 10% NGS were applied to the sections for 1 hour at RT. In addition to the secondary antibody, DAPI was also applied to slides at this time at a 1/1000 dilution. Secondary antibodies were removed by washing in PBS for five minutes three times at RT. Detailed information for antibodies are described in Table 2.14.

2.6.2.4 Primary antibody amplification

For some antibodies, amplification of the signal was required. In this case, instead of applying an Alexa conjugated secondary, Vector labs amplification reagents described in Table 2.14 were applied to the section following washing. Slides were incubated for 1 hour in a humidity chamber at RT. Following removal of the Impress reagent by washing as described above, tyramide (diluted 1/1000 in amplification diluent) was applied to each section and incubated for 10 minutes in a humidity chamber at RT. The slides were washed again as described above before incubating with 1/1000 DAPI for at least 20 minutes. After a final wash step slides were ready to be mounted.

2.6.2.5 Haematoxylin and eosin staining of rafts and tissue

To examine pathology of raft cultures and tissue sections, staining with haematoxylin and eosin (H&E) reagents was carried out by the Addenbrooke's Hospital Tissue Bank facility.

2.6.2.6 Mounting tissue sample coverslips for microscopy

To prepare samples for microscopic analysis, coverslips were mounted onto the slides. Drops of Citifluor® reagent were applied to each section and a coverslip was carefully placed on top. Light pressure was applied to remove excess reagent and sections were then kept in the dark at 4°C for future analysis. Negative control stains can be seen below in Figure 2.1.

2.6.3 RNAscope in situ hybridisation

The RNAscope 2.5 HD BROWN assay (Advanced Cell Diagnostics, USA) was carried out according to the manufacturer's instructions until visualisation of amplified probes at the step titled "Detect the Signal". At this stage, visualisation was achieved with fluorescein instead of dab as described in the RNAscope® Fluorescent Multiplex Kit User Manual. This was to allow fluorescent immunofluorescent (IF) staining with other molecules of interest. To detect MmuPV1 E6/E7 RNA, the probe used was MusPV-E6-E7 (Cat No. 409771). A probe directly targeting E6 RNA only was designed in collaboration with Advanced Cell Diagnostics (Cat No. 521071). To detect HES1 RNA, the probe used was Mm-Hes1-C2 (Cat No. 417701-C2). More details can be seen in the ACD Target Probe catalogue. Control stains can be seen below in Figure 2.1.

2.7 Microscopy and imaging software

For analysis of H&E stained tissue, samples were scanned using a Panoramic MIDI II (3D Histech, Hungary) following manufacturer's instructions. Images could then be exported as digital files for further analysis. For imaging, fluorescently stained cells and tissues were viewed with a Zeiss A1 microscope equipped with fluorescent filters. A Carl Zeiss Microscopy AxioCam MRm camera was used for image capture and images were viewed using Axiovision software. Confocal images were obtained with a LSM 700 confocal microscope (Zeiss). Acquisition of z-stacks was carried out at X63 magnification. All image analysis was carried out with Zeiss Zen Black software, FIJI and ImageJ.

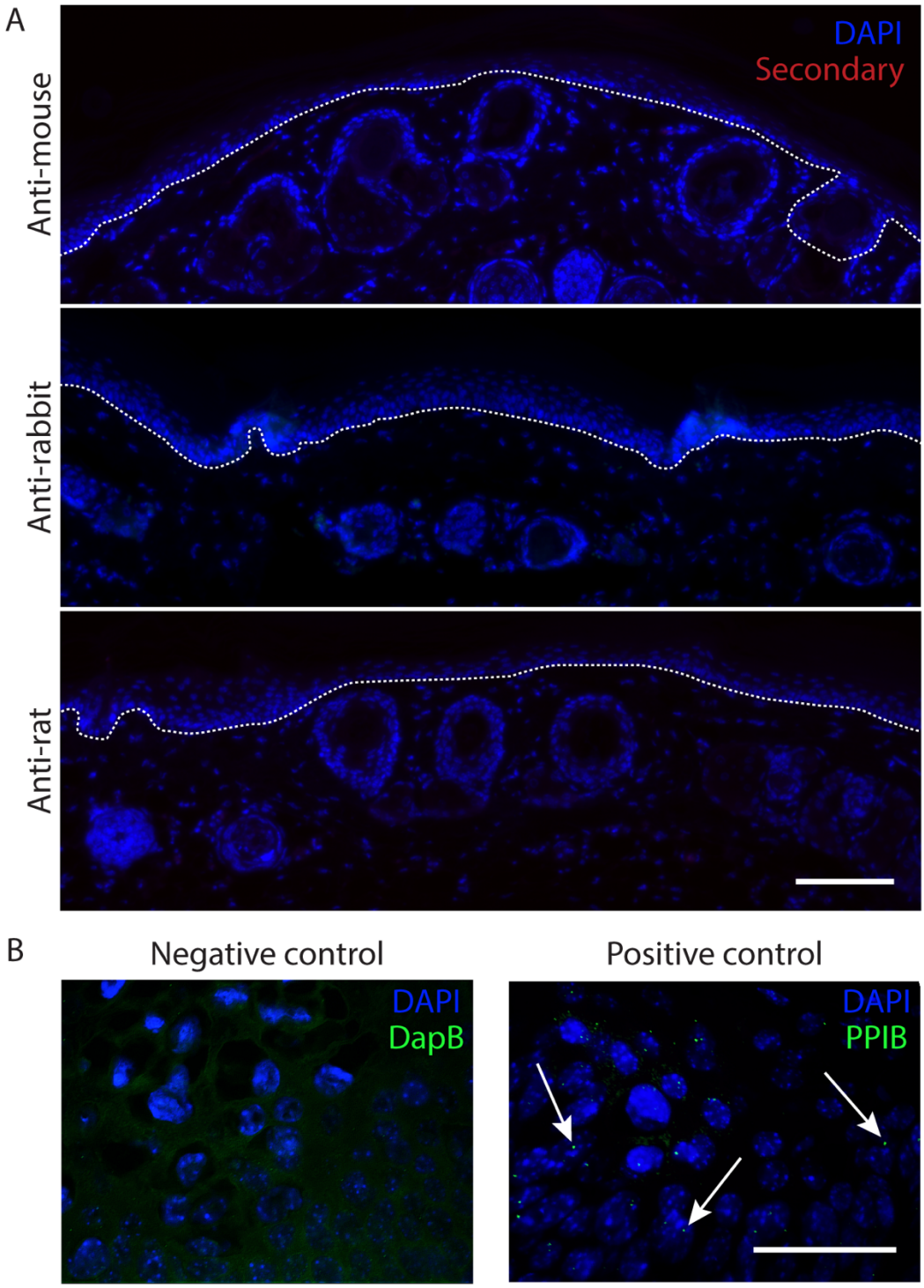

Figure 2.1 Negative control staining for antibody-based immunofluorescence and RNAscope experiments

A. Antibody-based immunofluorescence negative control stains. No primary antibody was added to mouse tail tissue, and slides were then incubated with the secondary antibodies only. Three panels show representative images selected to indicate a lack of tissue autofluorescence or false positive signal from the secondary antibodies. Control staining was carried out as described in Section 2.6.2. Scale bar: 100 μm. B. RNAscope negative and positive control stains. ACD positive control probe Mm Ppib (Cat No. 313911) and negative control probe (Cat No. 310043). Arrows indicate some of the positive signal foci. Scale bar: 50 μm.

2.8 Protein Analysis

2.8.1 Cell lysis for western blot analysis

Cells were grown in appropriate media and collected at desired time point. To collect the cells, RIPA buffer was added directly to cells and agitated to detach cells from the surface. Cells were then pelleted by centrifugation at 2000 rpm and washed twice in PBS before resuspending in 100 µl of lysis buffer. Samples were stored at -20°C until use, or used straight away. Samples were defrosted on ice and pipetted up and down to break cells apart. Samples were then sonicated for ten minutes and spun down at 14,000 rpm for 10 minutes at 4°C. The soluble supernatant was then stored at -20°C for subsequent analysis.

2.8.2 Immunoprecipitation

Immunoprecipitation protocol was carried out on ice. Protein was resuspended in 1 ml of buffer and then sonicated for 10 min. Protein suspension was run through a syringe several times and then spun down at 4°C at max speed (14,800 rpm) for ten minutes. During spin down, 150 µl of either HA or FLAG bead mix was made up to 1 ml in buffer and inverted many times to mix. Solution was spun down at 4°C at 3000 rpm for 2 mins. This wash was repeated three times. Bead mix was then applied to eppendorfs at appropriate volumes (e.g. for three samples, beads were resuspended in 1 ml and split 300 µl per Eppendorf to ensure bead suspension was consistent across samples). Bead suspension was spun down at 4°C at 3000 rpm for 2 mins and the resulting supernatant removed. Then 40 µl of each protein sample supernatant was set aside to act as input (Whole Cell Extract) (stored at -20°C). The remainder of the protein lysate was added to the beads. Samples were then placed in a tube rotator at 4°C for four hours to allow binding. Samples were then spun down, and washed 5 times with buffer after removal of supernatant. Final wash supernatant was removed, and the beads were resuspended in 20 µl of buffer. Samples could then be used in normal western blot protocols as described below.

2.8.3 Protein quantification

Quantification of protein samples was carried out using Pierce BCA assay kit (Thermo Scientific, UK) according to the manufacturer's instructions.

2.8.4 Gel electrophoresis of soluble protein samples

Prior to running on a gel, proteins were denatured. To each sample, the appropriate volume of 4X buffer and β-Mercaptoethanol (must make up 2.5% of total volume) was added and mixed well by flicking. Samples were then boiled for ten minutes at 80°C. For immunoprecipitation, 20 µl of the corresponding input was added to 10 µl 4X buffer 0.25 µl of β-Mercaptoethanol and boiled at 80°C for 10 minutes at the same time as the immunoprecipitated sample. After cooling, soluble proteins were separated using 4–12% gradient polyacrylamide-SDS-Tris-Tricine denaturing gel (Invitrogen, USA). Gels were submerged in 500 ml SDS running buffer in a Bio-Rad gel tank. Protein separation was carried out at 60mA for 50 to 80 minutes depending on the size of the protein.

2.8.5 Membrane transfer of gels for western blot

Polyacrylamide gels were transferred onto PDVF membranes (Bio-Rad, USA). Buffers used in membrane transfers are described in Table 2.1. Membrane was submerged in methanol for ten minutes and then transferred to buffer C. Paper was submerged in each of buffers A, B and C. Gel was incubated in buffer C for ten minutes. Membrane transfer was carried out using a Trans-Blot SD Semi-Dry Transfer Cell (Bio-Rad, USA). Two pieces of buffer A paper were placed, followed by one buffer B. On top of this the membrane was placed, and the gel was placed on top of the membrane. Finally, two pieces of buffer C paper were placed on top of the gel. Transfer was carried out at 120mA for 45 minutes.

2.8.6 Blocking and antibody incubation of western blots

Membranes were incubated in 1% milk/PBS Tween-0.01% (v/v) for one hour at RT after transfer. Membranes were then cut if necessary to allow probing with multiple antibodies. Membranes were next incubated with primary antibodies diluted in 1% milk/PBS Tween-0.01% at 4°C overnight. Antibodies used in Western Blotting are detailed in Table 2.15. Membranes were washed 3 times for five minutes in PBS Tween-0.01% following overnight incubation. They were then incubated with the appropriate secondary antibody for one hour at RT. Secondary antibodies were diluted in 1% milk/PBS Tween-0.01% at 1:5000. After incubation, membranes were washed 5 times for 5 minutes before being allowed to dry between two sheets of paper.

Table 2.15 Antibodies for western blotting

Primary Antibodies for Western Blots			
Target	***Clone***	***Dilution***	***Supplier***
HA	ab130275	1:1000	Abcam
FLAG	M2	1:200	Sigma
MAML1	D3E9	1:500	Cell Signaling
SMAD2	D43B4	1:1000	Cell Signaling
SMAD3	C67H9	1:1000	Cell Signaling
GAPDH	MAB374	1:2000	Millipore

2.8.7 Detection of western blots

Western blots were detected using the LICOR system according to the manufacturer's instructions.

2.9 FACS Analysis

2.9.1 Colour intensity sorting

Cells were sorted for fluorescent intensity with a BD Aria Fusion sorter. A 488nm laser was used to detect GFP positive cells in the 530/30nm channel. A 561nm laser was used to detect mCherry positive cells in the 610/20nm channel. Cells were sorted into four quartiles based on fluorescent intensity, and the highest expressing cells were used in the subsequent colour competition assays.

2.9.2 Flow Cytometry

For analysis of the Fucci expressing NIKS cells, different densities of cells were seeded in 6-well plates ($1x10^5$, $4x10^5$ and $8x10^5$ cells) on a bed of irradiated feeder cells ($5x10^4$). After 24 hours following seeding, media was changed and cells were then collected after a further 48 hours. To collect, samples were washed with 1 ml sterile PBS two times. Feeder cells were then removed by incubation with trypsin at 37°C 5% CO_2 for 2 minutes. Trypsin was then replaced with 1 ml of trypsin-EDTA and remaining cells were incubated for up to 20 minutes at 37°C 5% CO_2. Detached cells were neutralised by adding 2 ml of FC medium. Cells were then pelleted by centrifugation at 1500 rpm for 5 minutes at 4°C. Supernatant was then aspirated, and cell pellets were suspended in 1 ml of FACS running buffer (2% FBS and

0.5mM EDTA in PBS). Samples were kept on ice until analysis was carried out. Prior to FACS analysis, cell suspensions were filtered through a 70mm cell strainer (Corning, USA) to maximise removal of doublet cells. Flow cytometry was carried out using a Cytek® DxP8 machine. For the mAG signal, the filter setting used was F 530/30. For Mko2 signal the setting used was 615/25. For detection of AlexaFluor 647/DRAQ5, the filter setting used was 666/27. Analysis was completed using FlowJo software (Version 10).

2.10 Mathematical Modelling

2.10.1 E6/E7 expression and Cell eccentricity

2.10.1.1 Calculating E6/E7 expression in a region of interest

To quantify RNAscope E6/E7 expression, an equation was generated to evaluate the pixels within each individual cell (region of interest). The intensity of green fluorescence per pixel is represented as a numerical value ranging from 0 (black) to 255 (highest intensity). The equation is shown below where N is the number of pixels in the cell and i is the intensity of fluorescence. Index 1 can be viewed as representing a measure of how much a cell is "turned on" (in terms of the green fluorescence). This index normalises the intensity by taking the cell area into account.

$$Index_1 := \frac{\Sigma_{i=1}^{N=9} I(\rho_i)}{N \cdot 255}$$

$$Index_1 = \frac{\Sigma_{i=1}^{N=9} I(\rho_i)}{N \cdot 255} = \frac{I(\rho_1)+I(\rho_2)+I(\rho_3)+I(\rho_4)+I(\rho_5)+I(\rho_6)+I(\rho_7)+I(\rho_8)+I(\rho_9)}{9 \cdot 255}$$

2.10.1.2 Calculating cell eccentricity

To calculate cell eccentricity, the following principles were applied. The eccentricity *e* of an ellipse is the ratio of the distance *c* between the centre of the ellipse and each focus to the length of the semimajor axis *a*. The eccentricity *e* is such that 0< *e* <=1. The closer the *e* is to 1, the flatter and more elongated the ellipse. The centroid of a cell is its barycentre. The centroid C (cx, cy) is a point in the image with the x-axis coordinate C_x and the y-axis coordinate C_y. This IS calculated as:

$$C_x = \frac{\Sigma C_{ix} A_i}{\Sigma A_i}, C_y = \frac{\Sigma C_{iy} A_i}{\Sigma A_i}$$

where $A_i$is the area of a pixel. For each image, the cells were segmented by hand and the obtained mask was converted into a binary image (cells in white and background in black). The elliptical approximation of each cell was built by making the centroid of each cell coincident with the approximating ellipse. From the centroid of each cell the major and minor axis of the cell were derived and the corresponding approximating ellipse were built.

2.10.2 Spline Interpolation

Spline interpolation was used to most accurately predict unknown time functions in time course experiments by using a sample of generated data points (Hall and Meyer 1976). Spline interpolation is based on a concept that aims to mathematically fit polynomials between known data points. The above concept is applied by minimising the curvature of a curve, $y(t)$ where its curvature can be defined as:

$$\kappa = \frac{\ddot{y}}{(1+\dot{y}^2)^{3/2}}$$

Specifically, cubic splines were used to construct piecewise third-order polynomials $y_i(t)$, since they are known for their accuracy and production of smooth interpolation curves when compared to other types of polynomials, such as quadratic and Lagrange polynomials (Hazelwinkel, 2001).

Each polynomial y is defined as:

$$y_i(t) = a_i + b_i t + c_i t^2 + d_i t^3$$

where a_i, b_i, c_i and d_i are parameters to be estimated by the minimisation algorithm.

To perform cubic spline interpolation, the 'spline' function in the MathWorks MATLAB tool was used.

3.0 Establishing a model of early lesion development

3.1 Introduction

The life cycle of HPV has been widely studied through immunohistochemical analysis of human tissue, as well as tissue collected from various animal models of PV infection. Culturing of keratinocyte cell organotypic rafts has also provided a model *in vitro* system in which to study the life cycle of HPV further in the context of epithelial differentiation (Allen-Hoffmann, Schlosser et al. 2000). PVs are known to exclusively infect epithelial sites, either cutaneous or mucosal. Human biopsy material has provided valuable insight to the life cycle of high-risk PVs in particular, however such samples can be difficult to obtain and are valuable due to associated costs (Ferry-Galow and Chen 2019). Furthermore, biopsy samples can often be quite small, limiting the range of analyses that can be carried out. Therefore, use of animal models of PV infection has helped to bridge the gap between cell culture experiments and human biopsy samples (Campo 2002).

Until relatively recently, no PV type that could infect a laboratory mouse had been discovered. In 2011 MmuPV1 (originally designated MusPV (Ingle, Ghim et al. 2011)) was identified in the *Pipapillomavirus* genus (Joh, Jenson et al. 2011). Although this virus was initially described as being strictly cutaneous, subsequent research has shown it is also able to infect a range of mucosal sites (Cladel, Budgeon et al. 2016) (Hu, Budgeon et al. 2015) (Cladel, Budgeon et al. 2015) (Cladel, Budgeon et al. 2013). More recently, it has been used to attempt to model disease of the female reproductive tract, furthering its relevance as an important model of human disease (Spurgeon, Uberoi et al. 2019). This research into the female reproductive tract model suggested that MmuPV1 is oncogenic, which is surprising given its distant relation to high-risk human disease-causing PV types. Therefore, careful consideration should be given when applying these models. The availability of MmuPV1 provides the opportunity to model PV infection in a convenient animal system, which is amenable to manipulation. Since its discovery, several labs have studied MmuPV1 in order to develop a broader understanding of PV biology, and to develop a better understanding of HPV associated disease (Handisurya, Day et al. 2013, Wang, Jiang et al. 2015, Uberoi, Yoshida et al. 2016, Hu, Cladel et al. 2017, Jiang, Wang et al. 2017).

Recent studies involving MmuPV1 have demonstrated that this PV type was able to bind to the protein MAML1 to affect downstream signalling, similar to HPV8 of the beta genus of PV (Meyers, Uberoi et al. 2017), which is associated with a range of pathologies such as

squamous skin cell carcinoma in humans. Given this shared pathway interaction with a type known to infect humans, the mouse model provides a useful system with which to study aspects of persistence and cell competition *in vivo* by examining the mechanics of basal cell expansion. Overall, this chapter aims to characterise the earliest stages of lesion formation using the recently established mouse model of PV infection.

3.2 Results

3.2.1 Selecting a method of wounding

The mouse model of PV infection has only been introduced within our lab in the past three years. Previously published literature concerning the experimental wounding of mouse tails describes various processes by which to wound the tail site, such as abrasion of the site using a rotary device (Handisurya, Day et al. 2013), or removal of epithelia by scarification of the site with a 27-gauge needle to an extent that does not cause bleeding (Uberoi, Yoshida et al. 2016). Whilst the method of wounding using a needle is well established, and was used initially in our lab, we considered whether a more reproducible method of wounding the tail skin might be beneficial to our model. For instance, reproducibility of early time course experiments might be negatively impacted as a result of erratic wounding by human hand. Consequently, it was decided that two methods of wounding would be attempted and compared to determine which approach was more consistent before initiation of longer experiments.

The first method of wounding selected was the standard scarification of the mouse tail site using a 27-gauge needle to scratch the tail surface until the basal layer was exposed. The alternate method of wounding attempted was to use an Auto Derma Pen Microneedle Stamp Device (Carer, T&B, Guangzhou, China), which is an automated device wherein 12 microneedles of adjustable length are repeatedly pressed superficially into the epidermis. The needles were adjusted to a length of 0.25mm and the mouse tail was then subjected to ten seconds of wounding with the device pressed firmly onto the tail. Mice were wounded either with a 27-gauge needle or with the Auto Derma pen, and tail samples were then collected 1, 4 and 7 days after wounding for analysis. Six mock wound sites were investigated at each time point within each group, and a representative image of H&E stained tissue sections is shown from each cohort in Figure 3.1. Wound sites were preliminarily identified by the presence of scabbing over the recently wounded tissue; this was expected to be visible by light microscope without necessitating further processing or analysis of the tissue. Another

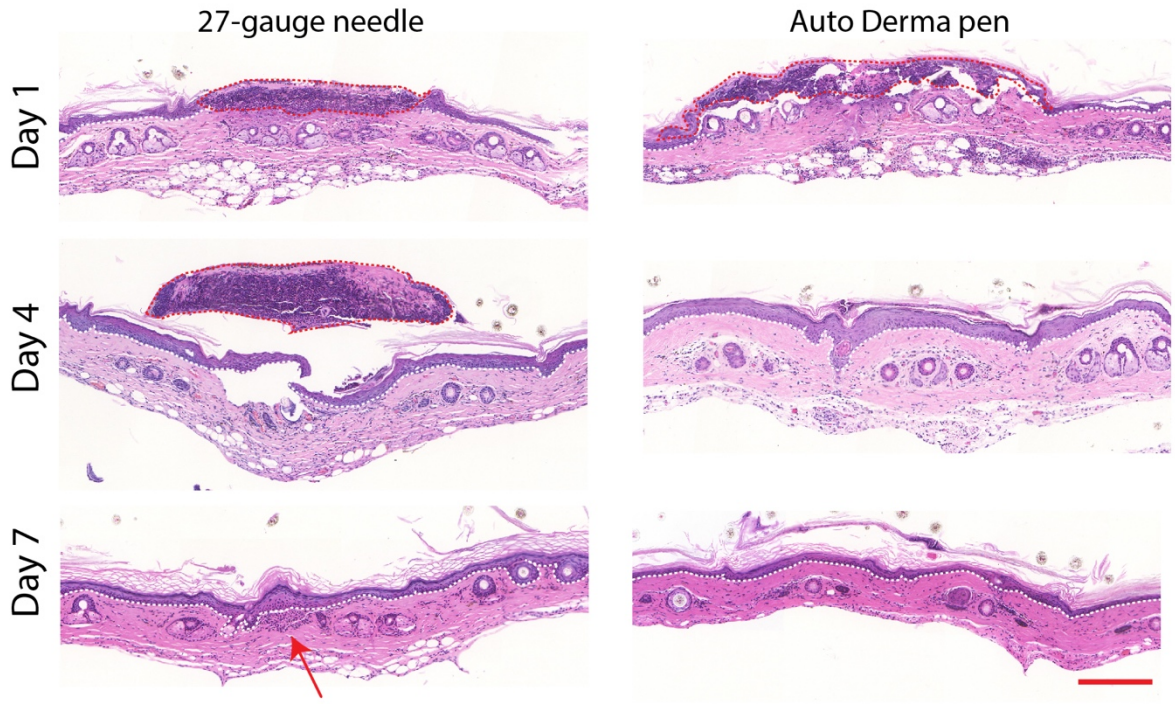

Figure 3.1 Haematoxylin and eosin staining shows cell morphology with two different methods of wounding 1, 4 and 7 days after wounding
Panels show wounding by scratching with a 27-gauge needle and using an Auto Derma pen for each time point. The white dotted lines indicate the position of the basal layer. Scabs are outlined with a red dotted line. Red arrow shows inflammatory cells. Scale bar: 200 μm. Data representative of 2 independent experiments, n=3.

criterion used to identify healing wound sites was the presence of inflammatory cells at the site of infection, which can also be broadly identified with H&E staining alone (Ross and Pawlina, 2006). Some scabbing of the wound was evident at day one in both groups (highlighted with a red dotted line outlining the scabbed area), making the wound site itself reasonably simple to locate. However, whilst the wound site was still easily identifiable by location of the scab at day four in the group wounded with the 27-gauge needle, it proved harder to locate in the samples from those wounded with the Auto Derma pen, and 4 of the 6 sites analysed for this group appeared to not contain wounded tissue. At day 7, the tail samples scarified with a 27-gauge needle were identified by the presence of inflammatory cells observed beneath the epidermis (marked with a red arrow) in each of the six samples. In comparison, inflammatory cells were only located at one of tail sites analysed in the second group wounded with the Auto Derma pen, whereas the other 5 sites contained no inflammatory cells and no scabbing above the epidermis. Consequently, we decided that the needle method of scarification would be the best method to use; despite the somewhat greater scope for the introduction of human error and variability, this method resulted in 100% of the sites collected being wounded sites. In comparison, the sites wounded with the Auto Derma

pen were rarely easy to define as a wound site beyond the day one time-point. Further, the introduction of many small sites in a relatively large area of tissue would result in greater difficulty in locating wounded sites upon in-depth tissue analysis. Since one of the main methods intended for application to subsequent samples was to be RNAscope (ACD, USA), an expensive process, it was important to keep the number of tissue samples required for processing low. Finally, use of this standard method of wounding would allow more straightforward comparison with some of the other work in the field of mouse PV research. Therefore, scarification with a needle was selected as the method of wounding for future experiments.

3.2.2 RNAscope probe design for detection of MmuPV1 gene expression

Previous research in the field has found it difficult to locate low levels of PV DNA *in situ* in the basal layer during the early stages of lesion formation; detection methods such as traditional fluorescent *in-situ* hybridisation (FISH) lack the necessary sensitivity to amplify such small amounts of DNA. While commonly used approaches do exist that can determine the presence of viral DNA in other ways, including various methods utilising PCR quantification of viral DNA (Molijn, Kleter et al. 2005), it was important to be able to locate infected basal cells in tissue samples to allow immunohistochemical analysis of the earliest stages of lesion formation. A previous study in detecting viral DNA in COPV lesions found that DNA was detectable from 4 weeks following wounding onward, and even then, only in some of the samples analysed (Nicholls, Doorbar et al. 2001). Similar studies examining ROPV were also unable to detect DNA in the basal layer using FISH (Maglennon, McIntosh et al. 2011). In analysis of some human samples, it has been impossible to detect viral DNA in the keratinocyte basal layer of established lesions (Egawa, Iftner et al. 2000). To date no studies have successfully shown DNA in the basal layer of infected tissue using *in situ* methods. Therefore, it was decided that RNAscope *in situ* hybridisation technology would be employed to detect expression of E6/E7 RNA.

A brief diagram detailing methodology of RNAscope can be seen in Figure 3.2A. Following permeabilisation of tissue, double Z shaped (ZZ) probes corresponding to RNA target sites bind in tandem in lengths up to 20 ZZ probes long. These probes are then sequentially amplified before labelling of amplified probes allows visualisation with a microscope. E6 and E7 are considered to be early proteins, known to express in infected basal cells (Doorbar 2005). Therefore, a probe directed to E6/E7 was initially selected. However, we considered

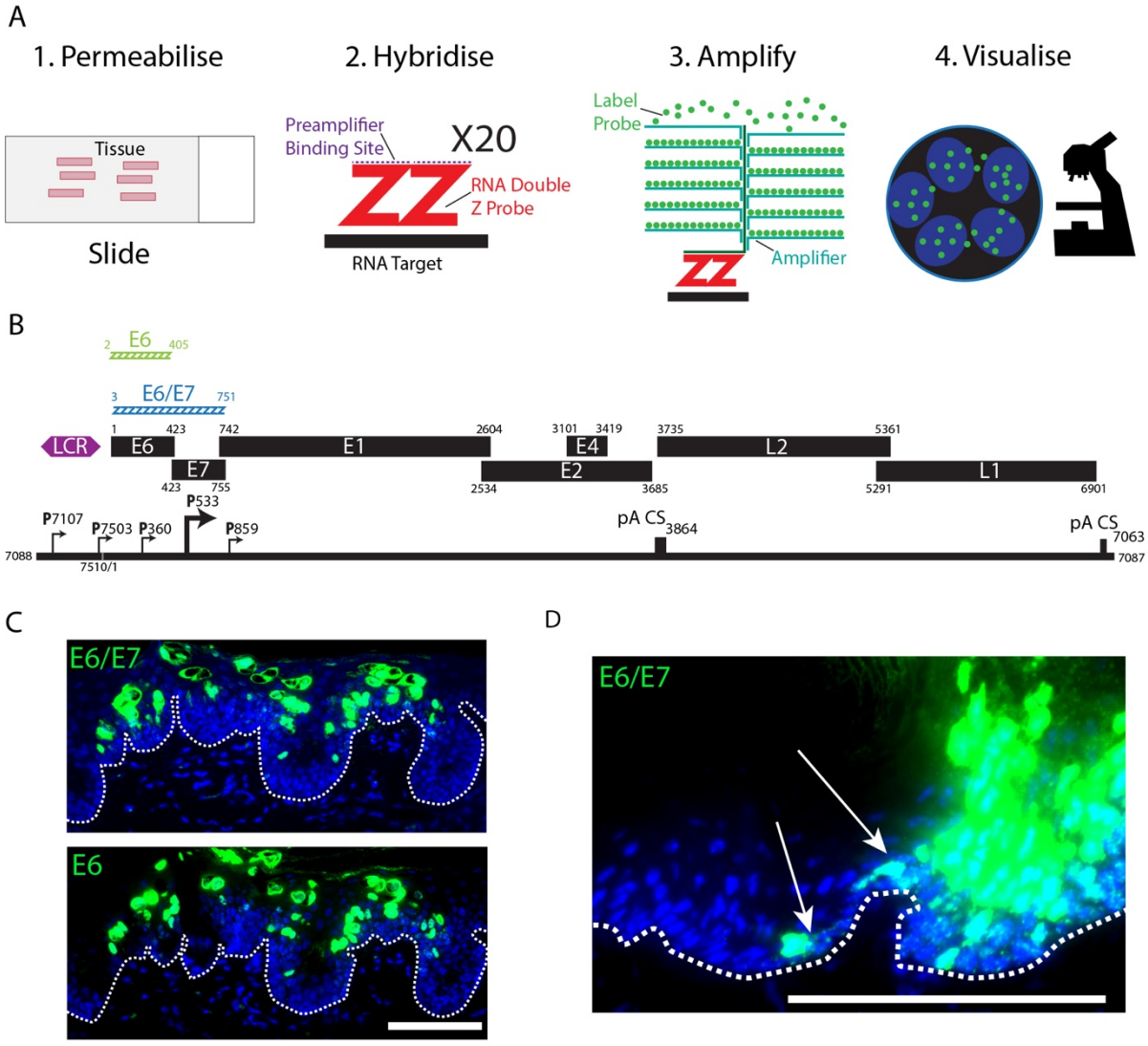

Figure 3.2 Basic principles of RNAscope and double ZZ probe design
A; Graphic representation of RNAscope protocol. Tissue is permeabilised, probes are hybridised to target RNA sequence up to 20 in a row, binding of amplifiers to ZZ probe allows amplification of signal, signal can be visualised using microscopy. B; Schematic diagrams of MmuPV1 ORFs, mapped viral promoters (P), and polyadenylation cleavage sites (pA CS) in the MmuPV1 genome. The numbers shown above each ORF are the first and last nucleotide of the ORF sequence, except for E4 which requires splicing. LCR – long control region. Probes are shown in blue (E6/E7 15 ZZ probe) and green (E6 9 ZZ probe) above their target sequence region. Numbers shown above each probe are the first and last nucleotide of the target of each probe (Adapted from Xue et al, 2017). C; Comparison of expression pattern for both the E6/E7 and the E6 only probe. D; Image taken at X40 magnification to clearly show detection of RNA expression in the basal layer (examples annotated with white arrows). MmuPV1 RNAscope probe signals shown in green. Nuclei were counterstained with DAPI to show host DNA. Dotted white lines indicate the position of the basal layer. Scale bar: 100 µm. Tissue shown 3 weeks post infection.

that a probe targeting E6 or E7 only might also be useful to compare expression levels of each protein. Therefore, a second probe was designed to specifically target E6. The location of both probes is shown in Figure 3.2B alongside a full transcript map of the MmuPV1 genome, to indicate the stretches of RNA that each probe targets. The E6 probe was shorter in length at only 9ZZ probes, compared to the 15ZZ E6/E7 probe. As shown in the example microscope images in Figure 3.2C, it was found that the expression pattern of E6/E7 appeared to be similar to the expression pattern observed with the E6 only probe. It is possible that this is due to the 9ZZ E6 only probe overlapping with the promoter site located at p360, which could lead to additional detection of some transcripts transcribed from this promoter. Or, there may be saturation of signal, making it difficult to discern higher levels of expression. However, it was not possible to investigate this further by designing a shorter probe; probes targeting such a short sequence would be unlikely to function well. A minimum of 6 ZZ probes are required to result in successful amplification of a signal. Therefore, as it was unclear whether the E6 only probe truly only targets E6, RNAscope was carried out for detection of E6/E7 RNA in subsequent experiments. While other methods described above provided plausible alternative methods by which to detect virus DNA, we proceeded with RNAscope because it provided a way to visualise expression of viral RNA, an early event in the virus life cycle and in lesion formation, *in situ*. Importantly, detection of RNA expression in the basal layer of the epithelium was successful, as demonstrated in Figure 3.2D.

3.2.3 Determining the infectious titre of MmuPV1 using RNAscope

Compared to some other viruses, PVs do not form plaques in monolayer culture of cells, and no obvious cytopathic effects can be observed in infected cells to determine which of the population are infected in a rapid manner. The most common method to quantify PV titre is to employ qRT-PCR, usually using E1^E4 as an indirect transcript measure of infection; this is the most abundant viral transcript (Chen, Xue et al. 2014). However, relation of this data to real infectivity is still challenging. To investigate the effect of the amount of virus applied to each site, 8 serial dilutions of virus stock were used to inoculate groups of mice. These mice were then observed over time, and the appearance of a lesion at the site of infection was noted (this experiment was carried out by Dr Nagayasu Egawa). Results shown in Figure 3.3A and B demonstrated that while there was no clear difference between inoculation with 2×10^9 virus genome equivalents (VGE, quantified using qPCR) when compared with 2×10^8 VGE, the remaining titrations showed a strong correlation between decreased virus titre and

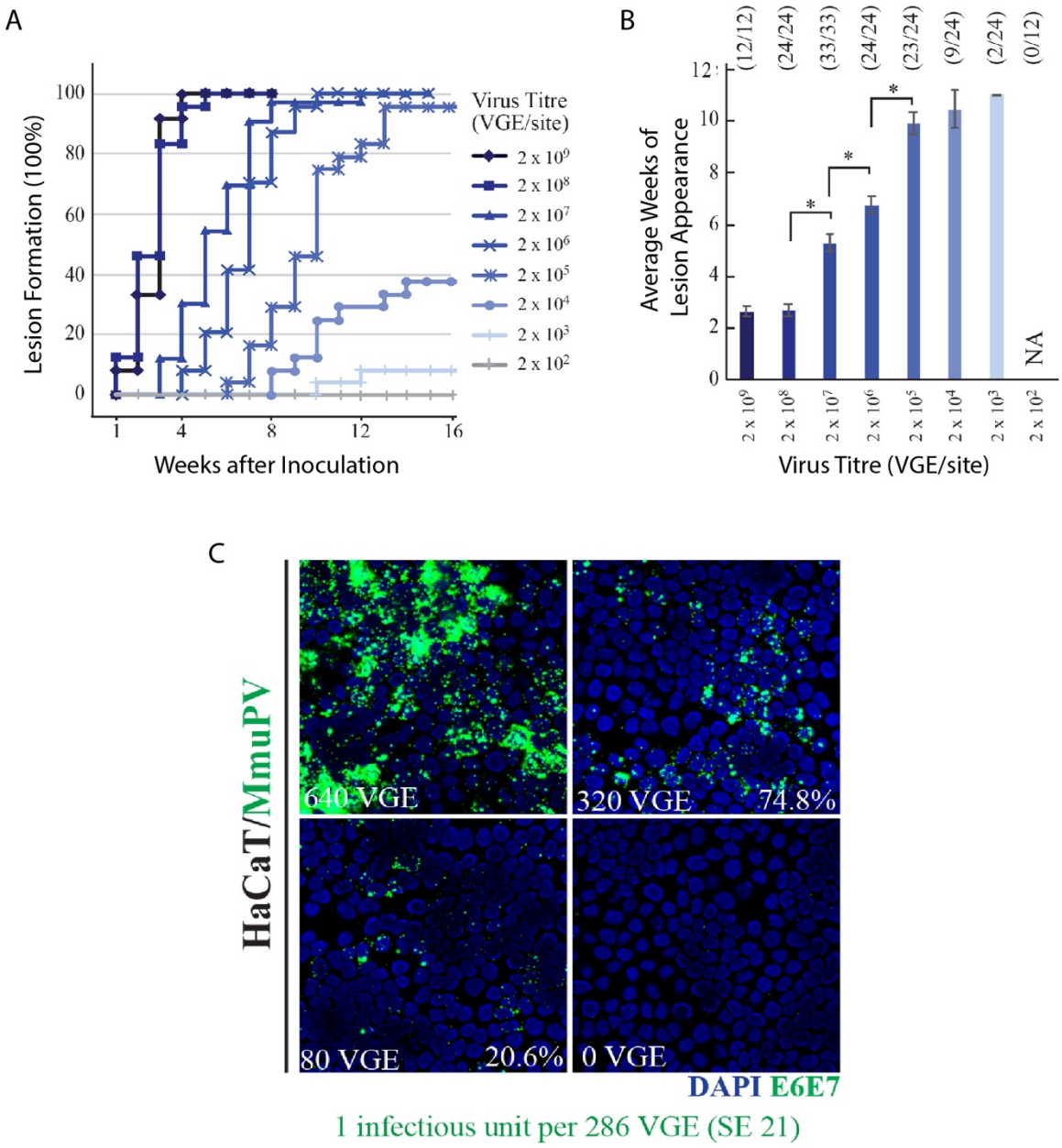

Figure 3.3 Virus titer correlates to lesion formation time and determination of infectious units

A; Mice were inoculated with 8 titrations of virus and the appearance of lesions was monitored over time. B; Average time for a lesion to appear is shown for each virus titration. C; HaCaT cells were infected with different titrations of MmuPV1, and the MmuPV1 E6/E7 positive cells were counted to determine the percentage of infected cells for each titration. Calculations then allowed estimation of the number of infectious units per virus genome equivalents. Representative images shown were taken at 40X magnification. MmuPV1 E6/E7 RNAscope probe signal shown in green. Nuclei were counterstained with DAPI to show host DNA. Two independent experiments, n=12.

increased lesion formation time. To correlate the amount of virus with infectivity, HaCaT cells were infected with different quantities of VGE (as described in 2.2.3.9). The consequent number of infected cells per VGE was quantified by detecting the presence of MmuPV1 in infected cells using RNAscope targeting MmuPV1 E6/E7, as shown in Figure 3.3C. Data suggested that there was approximately one infectious unit per 286 VGE (standard error of 21). Using this data, it is possible to estimate that the number of infectious units applied to each wound site was roughly 69,000 infectious units per site when applying 2 x 10^9 VGE.

3.2.4 Lower virus titre resulted in fewer, smaller lesions forming within a set time

To examine the *in vivo* effect of virus titre in greater detail, mice were inoculated with 2 x 10^9 or 2 x 10^6 VGE (3 inoculation sites per group). When the first mouse of the experimental group began to show macroscopic signs of lesion formation on the tail, all of the animals in that group were collected; this should show the extent of lesion formation in lower titre mice at the same time point. In the mouse inoculated with 2 x 10^9 of virus, 2 of the 5 tissue samples analysed showed evidence of lesion formation (example shown in Figure 3.4A). RNAscope analysis was used to locate areas of infected tissue, whilst staining for E4 protein was also carried out to correlate with RNA expression. In comparison, in the mouse inoculated with 2 x 10^6 VGE (Figure 3.4B), only one site of infection could be located, which was notably smaller than those observed in the highest titre. For quantification, length of infected basal layer in tissue from each group was measured. The total length of infected basal cells spanned 139 μm in the tissue sample taken from the mouse inoculated with 2 x 10^6 VGE, whereas in the tissue sample taken from the mouse inoculated with 2 x 10^9 VGE, the total length spanned by infected basal cells was 1423 μm. The higher titre of virus resulted in a considerably larger lesion forming in the same time span within the centre of the wounded site. These sites of infection were not investigated with great depth; sections were taken from the approximate centre of the wound site only to give an indication of the extent of viral infection present at the chosen time point. Sites analysed also showed multiple foci of infection as opposed to one continuous span of infected cells in the basal layer. This observation gave some credence to the idea that tail lesions might initially form from multiple different infected cells, which will be considered in more detail in Section 3.2.7. These results fit well with the previous data demonstrating that virus titre correlated to lesion formation time. Therefore, for future experiments, it was decided that the highest titre of virus, 2 x 10^9 VGE, would be used to ensure the quickest possible completion of time course experiments.

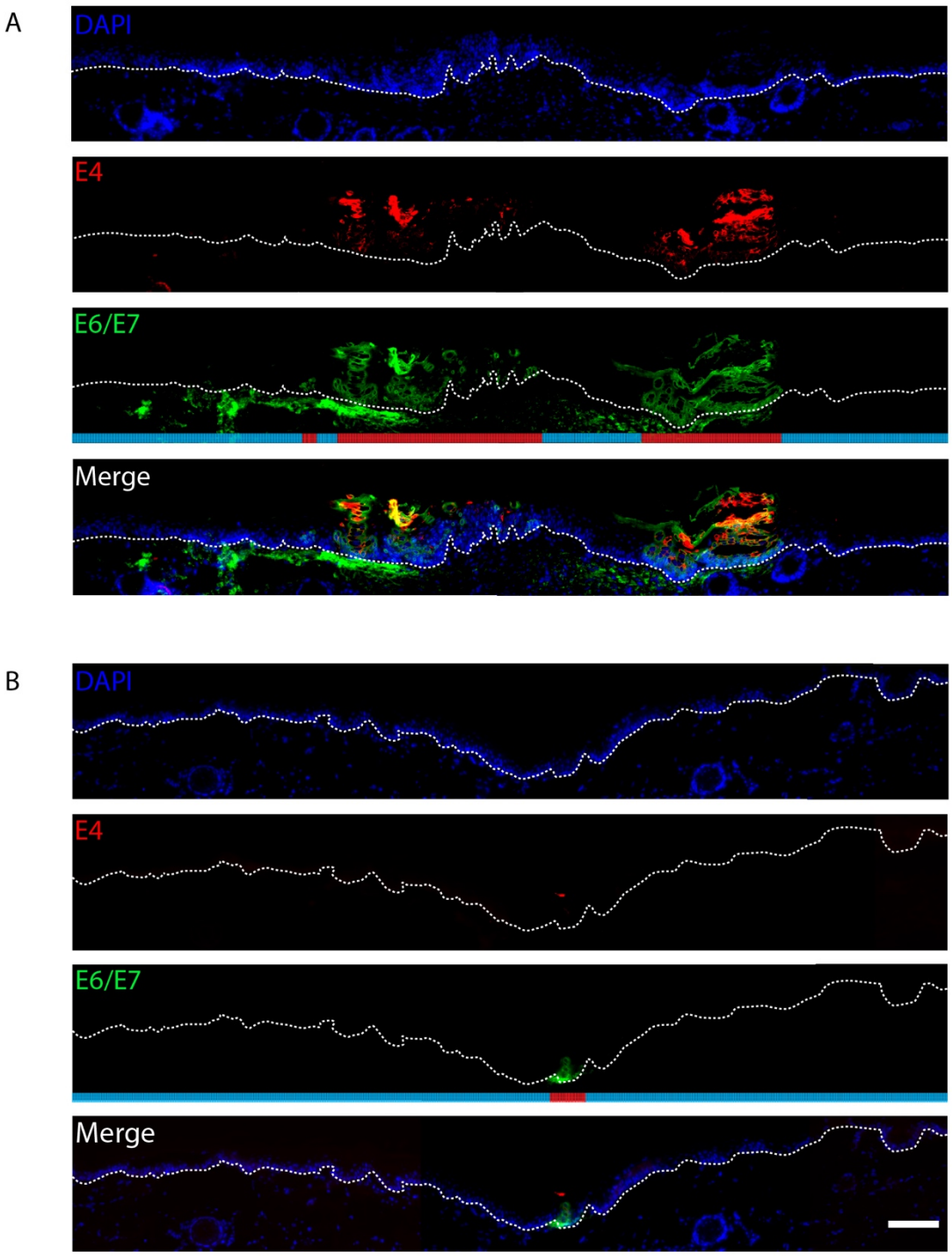

Figure 3.4 Comparison of lesion formation between high and low titre virus infection
Panels show images collected at 5X magnification representing IF detection of viral protein MmuPV1 E4 (red) and RNAscope detection of MmuPV1 E6/E7 (green). Nuclei were counterstained with DAPI to show host DNA. Block coloured lines beneath E6/E7 panels show regions of infection (red) and regions of uninfected epithelium (blue). Dotted white lines indicate the position of the basal layer. Scale bar: 200 μm. A; high titre virus infection (2 x 10^9). B; low titre virus infection (2 x 10^6). Data representative of 2 independent experiments, n=3. Tissue shown 2 weeks post infection.

3.2.5 Characterisation of protein expression in MmuPV1 lesions

To characterise lesions, immunohistochemical analysis was carried out on lesions collected more than 3 weeks after wounding and virus inoculation, termed 'established', in comparison with lesions collected immediately upon becoming macroscopically visible, termed 'early-visible'. These time points were chosen to determine whether the expression pattern of viral proteins changed significantly from when the lesion is first palpable to when lesions have become extremely florid. Examination of the expression of key virus proteins E4, L1, and E6/E7 RNA at these two discrete time points was carried out. IF staining demonstrated that expression of MmuPV1 E4 protein started in the parabasal layer and was continually expressed up to the surface of the epithelium. This pattern of expression was seen in both established and early-visible lesions, as shown in Figure 3.5.

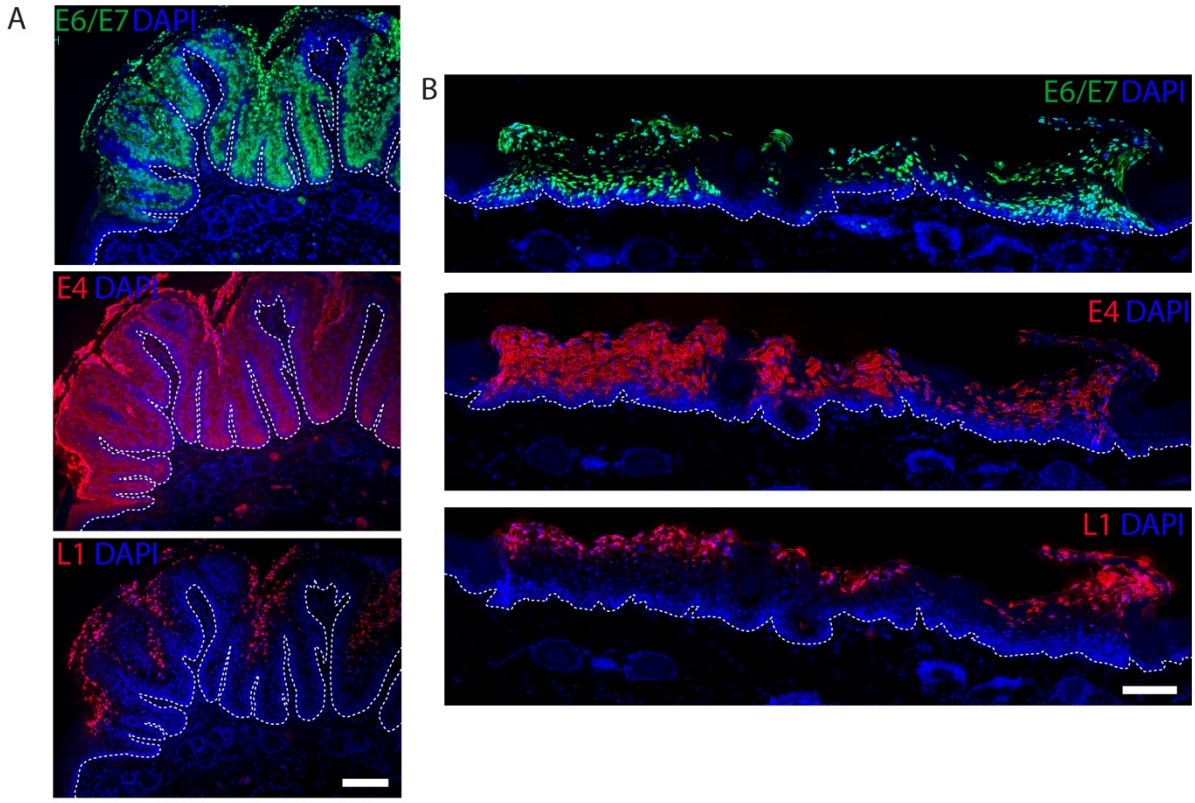

Figure 3.5 Spatial localisation of virus proteins and RNA expression
Panels show images collected representing IF detection of viral protein MmuPV1 E4 (MusE4, in house), L1 (MusL1, in house) and RNAscope detection of MmuPV1 E6/E7 (Cat No. 409771). Nuclei were counterstained with DAPI to show host DNA. Dotted white lines indicate the position of the basal layer. A; Established lesion collected 4 weeks following infection with MmuPV1. Scale bar: 200 μm. B; Early-visible lesion collected at 10 days following infection with MmuPV1. Tissue shown 3 weeks post infection. Scale bar: 100 μm.

Expression of E6/E7 RNA was detectable in the basal layer, and was expressed in much greater amounts from the parabasal layer upwards. This pattern of expression suggested that MmuPV1 may begin the amplification stage of its life cycle immediately after the cell exits from the basal layer. Expression of L1 protein was observed towards the surface of both established and early-visible lesions, demonstrating that these infections are productive. Unlike the staining described by another group previously (Handisurya, Day et al. 2013), no cytoplasmic L1 staining was observed in these samples. The presence of L1 protein also showed that it was possible for a productive lesion to develop only 10 days after initial infection and possibly earlier, as the early-visible lesion shown was collected ten days after wounding and inoculation took place. It was noted that of the two lesion types analysed, established lesions already showed considerable papillomatosis, whereas at ten days following wounding extensive papillomatosis was not yet apparent. To understand the timings of these various events in more detail, a time course experiment was considered.

3.2.6 Identification of six discrete stages of wound healing

As the next set of experiments planned to look at the earliest stages of lesion formation prior to the macroscopic appearance of a wound, and it was clear from the data shown in Figure 3.5 that lesion formation occurred fairly rapidly, the physical process of wound healing in the mouse tail epithelium was examined. Understanding of mock wounded tissue was important as this would be a necessary control in future experiments. By analysing mock wound site tissue, it would be clear what morphological changes were due to normal wound healing, and what might then be attributable to presence of a MmuPV1 virus infection. Three classes of markers were selected to examine the wound sites. These were K10, keratin 17 (K17) and Tenascin C. K10 is a marker of early stage differentiation routinely used in the analysis of keratinocytes, and indicates presence of differentiated epithelium (Schweizner and Winter 1983) (Eichner 1986). K17 is used as a marker for migratory cells, and is known to be upregulated during wounding as reepithelialisation of the wound site takes place (Pastar, Stojadinovic et al. 2014). Tenascin C is an extracellular matrix molecule, important in reformation of the normal epithelium following wounding. Tenascin C was selected as a wound healing marker due to its rapid induction upon injury, and its well documented involvement throughout the entire wound healing period (Midwood and Orend 2009). Using these markers, 6 discrete phases of wound healing were characterised, which are shown alongside unwounded control epithelium staining in Figure 3.6.

i.

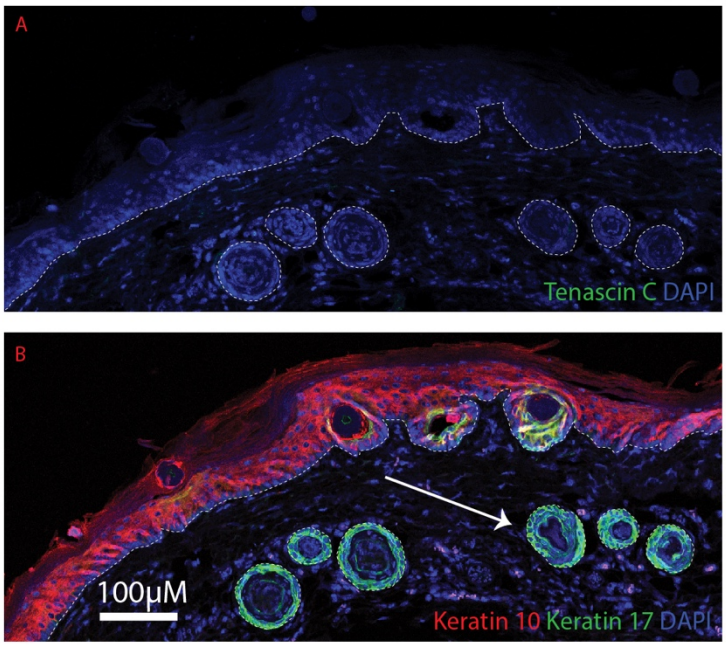
A
Tenascin C DAPI
B
100μM
Keratin 10 Keratin 17 DAPI

ii.

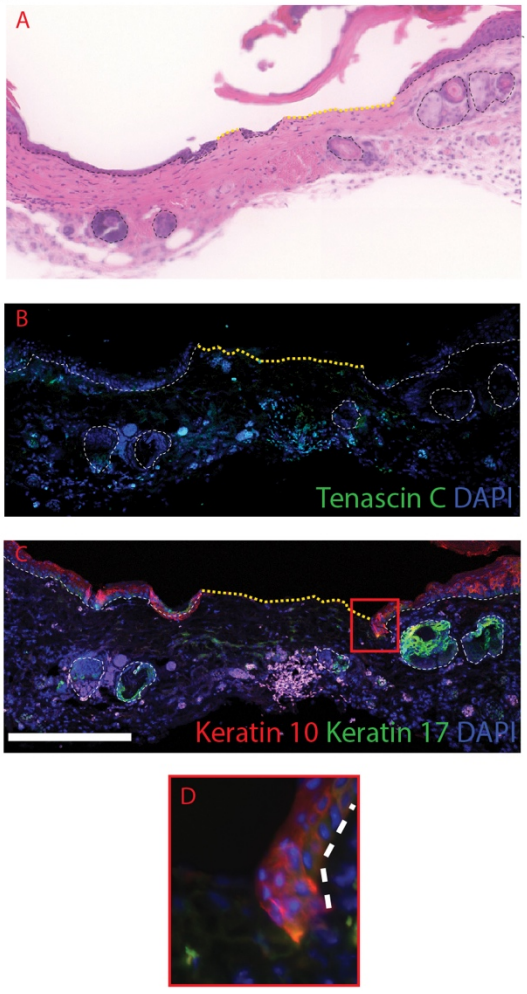
A
B
Tenascin C DAPI
C
Keratin 10 Keratin 17 DAPI
D

iii.

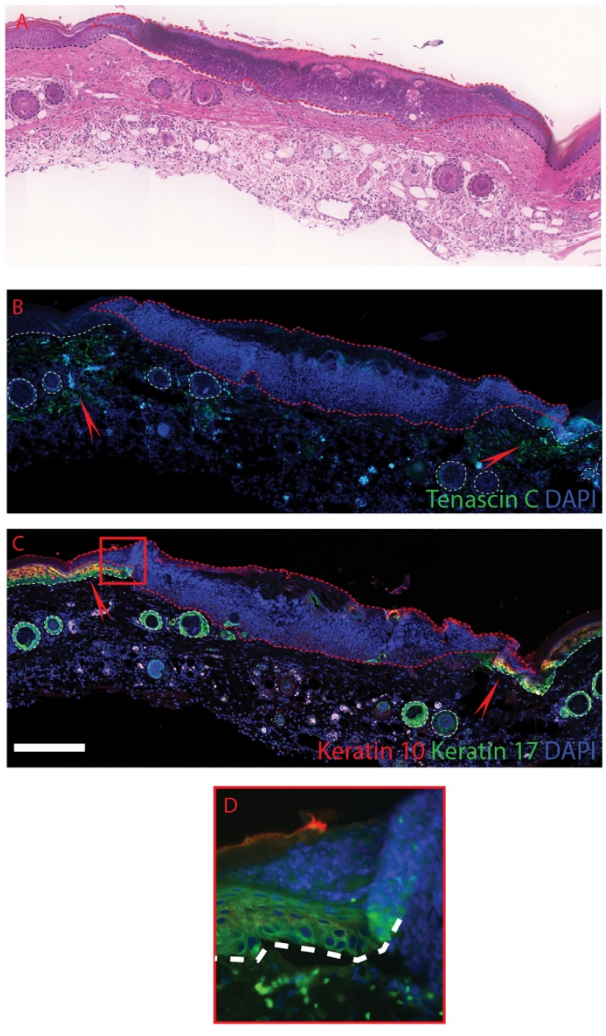
A
B
Tenascin C DAPI
C
Keratin 10 Keratin 17 DAPI
D

iv.

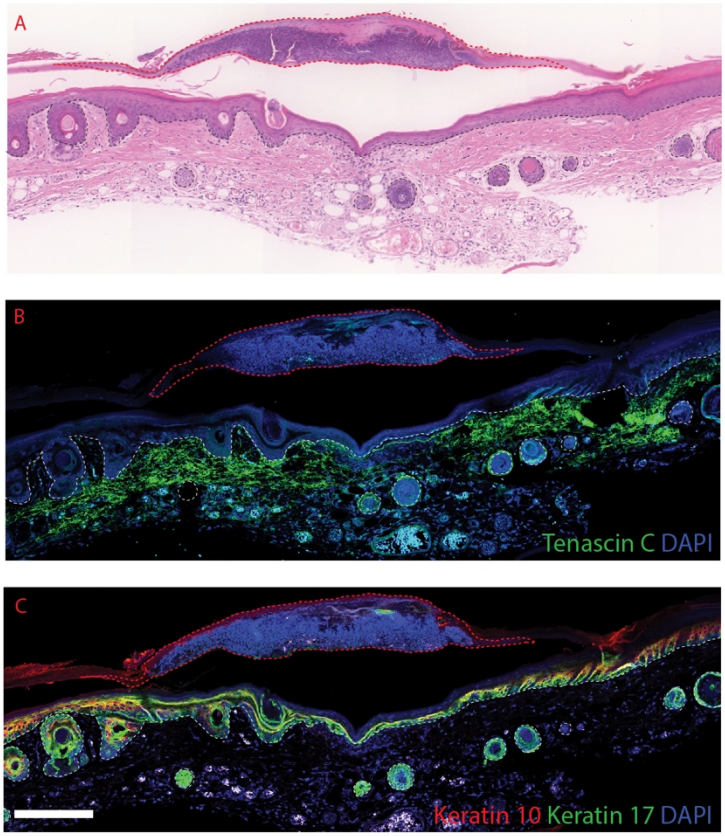
A
B
Tenascin C DAPI
C
Keratin 10 Keratin 17 DAPI

v.

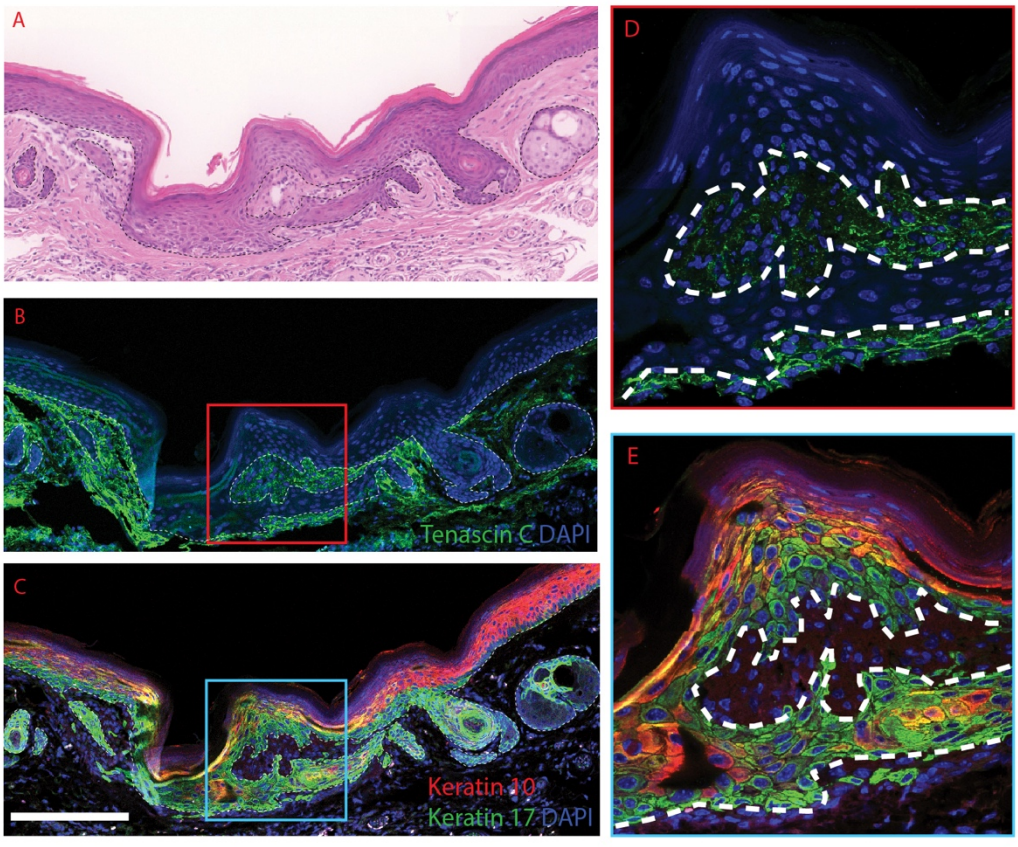
A
B
Tenascin C DAPI
C
Keratin 10
Keratin 17 DAPI
D
E

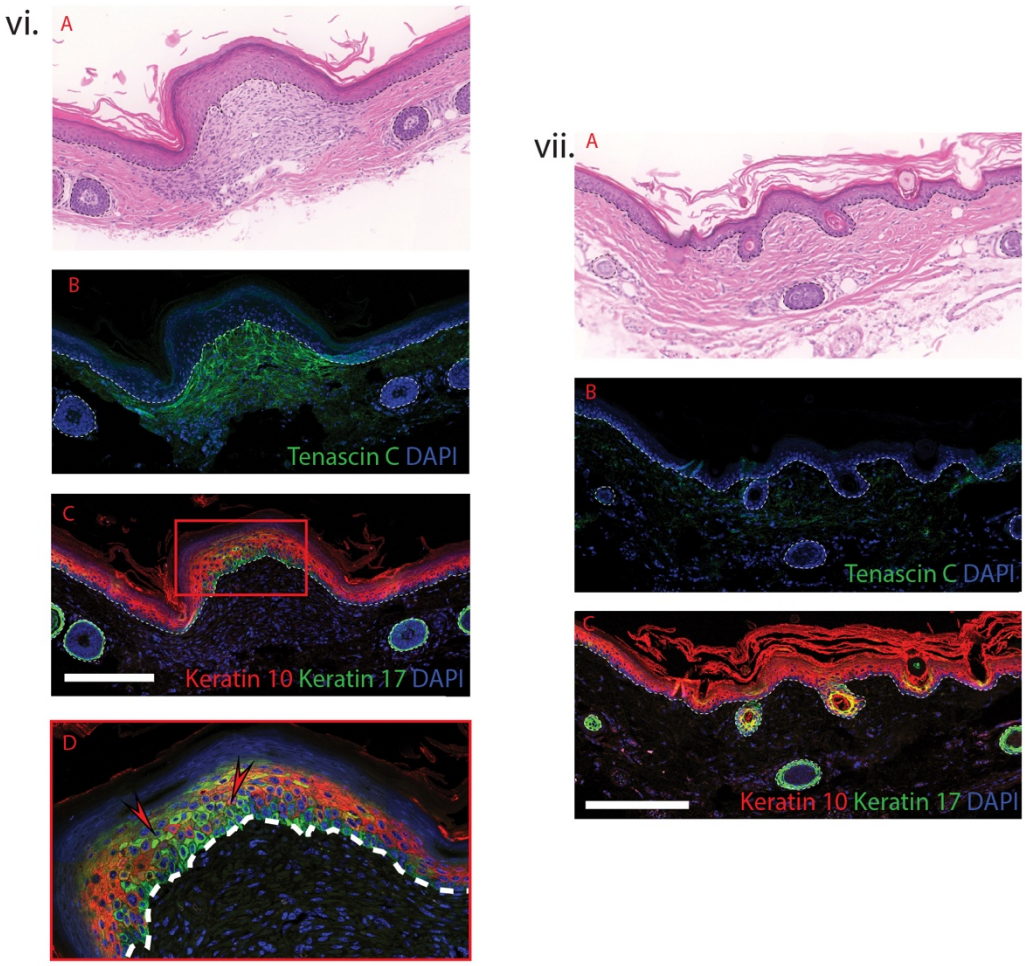

Figure 3.6 Spatial localisation of markers during healing of mouse tail epithelium
Panels show images collected representing Haematoxylin and eosin staining (panel A in each wound healing phase) and corresponding IF detection of Tenascin C (panel B in each wound healing phase), K10 and K17 (panel C in each wound healing phase). Subsequent panels show higher power magnification of selected images taken at 40X magnification. Nuclei were counterstained with DAPI to show host DNA. Dotted yellow line shows denudated epithelium. Dotted white lines show location of the basal epithelium. Scabbing is shown with red dotted lines. Scale bar: 200 μm, unless specified as otherwise. **i**; control IF detection of markers Tenascin C (A), K10, and K17 (B) in unwounded epithelium. Arrow indicates hair follicle. **ii; phase one**, two hours following wounding; no wound healing activation **iii**; **phase two**, 1-3 days following wounding; activation of wound healing at wound periphery **iv**; **phase three**, days 3-4 following wounding, re-epithelialisation under scab of wound **v**; **phase four**, days 5-8 following wounding, reformation of normal basal layer **vi**; **phase five**, days 9-12 following wounding, epidermal bulge corresponds to near completion of wound healing **vii**; **phase six**, two weeks following wounding, wound healing is considered complete. Data representative of 2 independent experiments, n=2.

In normal unwounded epithelium (Figure 3.6i) Tenascin C was largely absent. K10 was restricted to the parabasal layer and above, and K17 staining occurred only sporadically, or in the hair follicles (an example of a hair follicle is indicated with a white arrow). Phase 1 (Figure 3.6ii) shows the wound site two hours after wounding has taken place. The basal layer had been severely disrupted, shown with a yellow dashed line. Presence of a scab is indicated with a red dotted line. Tenascin C staining was negative, and the epithelium at the periphery of the wound site remained normal for K10 and K17 staining; K10 was observed above the basal layer and K17 was only observed in the hair follicles, not in any basal keratinocytes. Phase 2 (Figure 3.6iii) shows the wound site 1-3 days after wounding. Tenascin C induction could be seen at the periphery of the wound site, and K17 activation could be seen in basal cells to either side of the wound site. K10 was still observed in some parabasal cells, however K17 could also be observed in the parabasal layer. Phase 3 (Figure 3.6iv) shows re-epithelialisation of the wound site underneath the scab from 3-4 days following wounding. Reepithelialising cells were all positive for K17, which was expected given the aforementioned involvement of K17 in migration of keratinocytes. Strong induction of Tenascin C was observed beneath the entirety of the wound site. In phase four (Figure 3.6v) reformation of the basement membrane and basal layer was apparent, with distortion of the basal layer evident in all samples examined from days 5-8. K17 expression localised with strong Tenascin C induction, indicating that this area represented the centre of the healing wound. In phase five (Figure 3.6vi) wound healing was seen to be almost complete, and a bulge in the epidermis was seen at the centre of the healing wound. Again, strong induction of Tenascin C localised to the same area as keratinocyte cells that were still positive for K17. At the edges of the healing wound, most keratinocytes had returned to normal patterns of K10/K17 expression. This phase was observed around 9-12 days after wounding had taken place. By two weeks after wounding (Figure 3.6vii) the epithelium had mostly returned to normal expression of all three markers examined, aside from a mild induction of Tenascin C observed at the site. Following this phase, would healing was considered to be complete.

To corroborate with wound healing analysis, and to aid in location of early pre-visible lesions, marking of the wound site was attempted. To do this, use of fluorescent microspheres (Thermofisher Scientific, UK) was first attempted. The beads used are small spheres of only 0.2 μm in diameter made from a type of polystyrene. These commercially available FluoSpheres are loaded with a fluorescent dye to allow visualisation under a fluorescent microscope. The bead mixture was applied to a wound site following scarification, and the sites were subsequently observed 1, 4 and 7 days later as shown in Figure 3.7A and B.

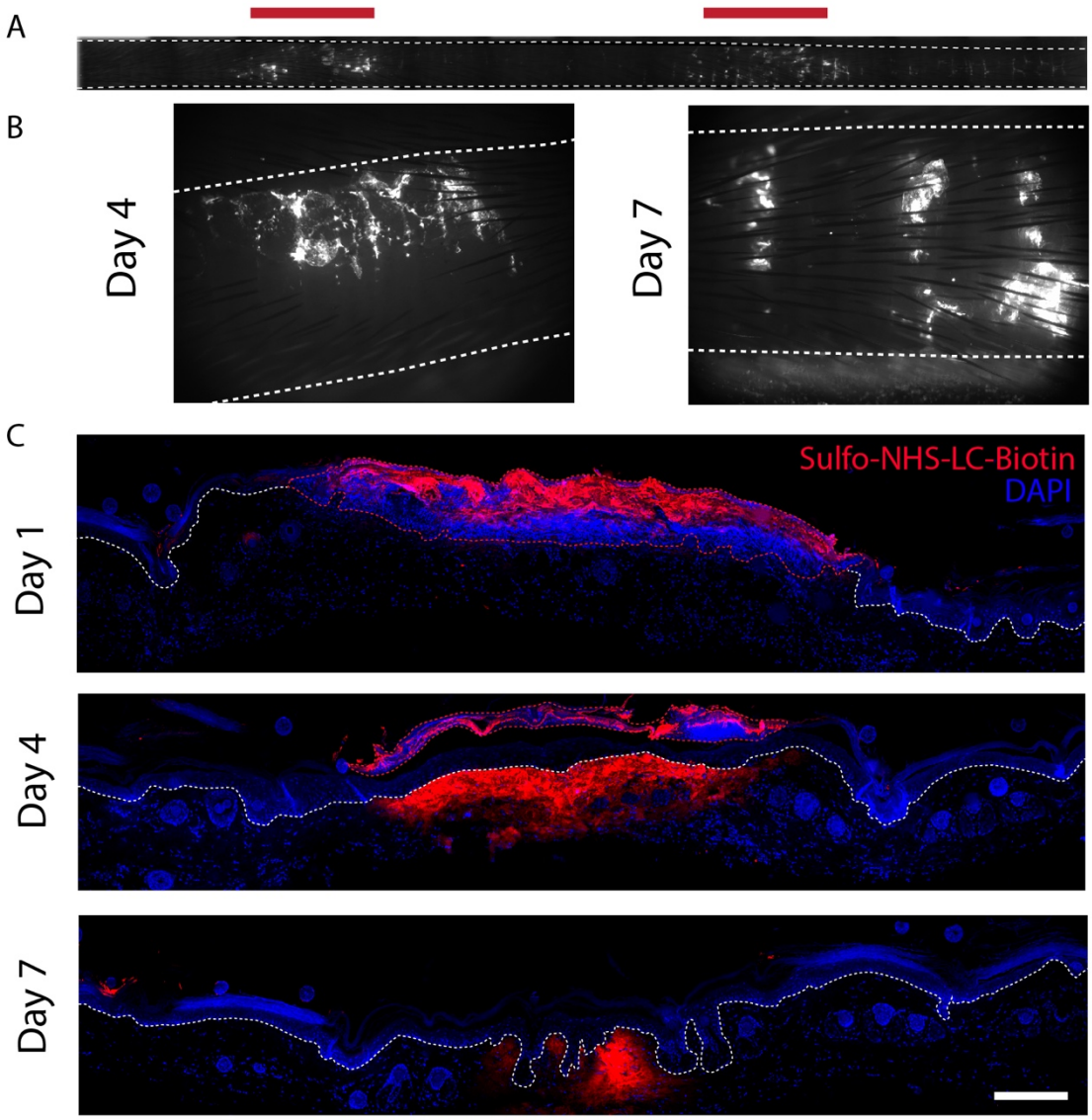

Figure 3.7 Marking of the site of wounding with FluoSpheres or crosslinking reagent
A; Low resolution images of FluoSphere fluorescence visualised with fluorescent microscope prior to tissue processing on the surface of the mouse tail (outlined with white dotted lines). Approximate region scarified on tail is shown above image as red lines. B; Higher magnification images of mouse tissue prior to processing show fluorescence of FluoSpheres on the surface of the tail epithelium 4 and 7 days following wounding and inoculation of the site with FluoSphere suspension. White dotted line indicates edges of the mouse tail tissue. C; Panels show IF imaging of crosslinking reagent Sulfo-NHS-LC-biotin visualised with streptavidin conjugated to Alexa594 (red) on day 1, 4 and day 7 following wounding and inoculation with the crosslinker. Nuclei were counterstained with DAPI to show host DNA. Red dotted lines show presence of a scab above the wound site. Dotted white lines show location of the basal epithelium. Scale bar: 200 μm. Data representative of one independent experiment, n=2.

The sites were marked successfully, with macroscopic visualisation of the beads being possible under a fluorescent microscope. However, no fluorescent signal was observed within the tissue following processing (data not shown), suggesting that the fluorescent signal had been lost from the material during processing for histochemical analysis. A crosslinking reagent EZ-Link™ Sulfo-NHS-LC-Biotin (ThermoFisher, UK) was also examined in parallel experiments. The aim was to apply this compound during wounding so that it would crosslink to surrounding wounded tissue and become assimilated into the site without having great impact on the cell microenvironment. Mice were scarified at three sites along the tail and the crosslinker reagent was applied to the skin surface at each site. Retention of the crosslinker at the wound site was examined over seven days, as shown in Figure 3.7C. On day one and day four, the crosslinker was detected in the scab above the wound site, and was readily detectable from day 2 to 7 under the site of the wound.

It was important to ensure that the crosslinker colocalised beneath the K17 expressing cells, to demonstrate that the site of wounding was being properly marked. It was also necessary to determine whether virus inoculation of the wound site in the presence of the crosslinking reagent would lead to successful lesion formation. As shown in Figure 3.8A, the Sulfo-NHS-LC-Biotin crosslinker colocalised well with the region of K17 positive cells, and MmuPV1 E6/E7 gene expression still occurred at the site of infection (Figure 3.8C). The lesion shown in this figure was macroscopically visible 8 days after wounding, suggesting a similar rate of lesion formation when compared to the early-visible lesions collected previously. However, when lesion sites of mice inoculated with both MmuPV1 and crosslinker were more closely analysed, it was found that the pattern of gene expression had been affected. As shown in Figure 3.8D and E, E6/E7 gene expression in the basal layer of the epidermis was extremely high, and discrete foci could not be discerned. When compared to E6/E7 gene expression in tissue inoculated with MmuPV1 only, the difference in expression was stark (Figure 3.8F). Unfortunately, it was plausible to consider that the crosslinking reagent had also crosslinked to and between virus particles, leading to higher quantities of virus infecting individual cells. We decided that subsequent experimentation should proceed without use of the crosslinking reagent; such high levels of virus gene expression may lead to changes to infection that could be incorrectly attributed to the timing of lesion formation. The colocalisation of the crosslinking reagent with the subset of cells expressing K17 indicated that the use of K17, K10 and Tenascin C was reasonable to locate the centre of a healing wound. Overall, further efforts into optimisation of the FluoSpheres were not made; we decided that use of the set of markers was sufficient to locate a healing wound where necessary.

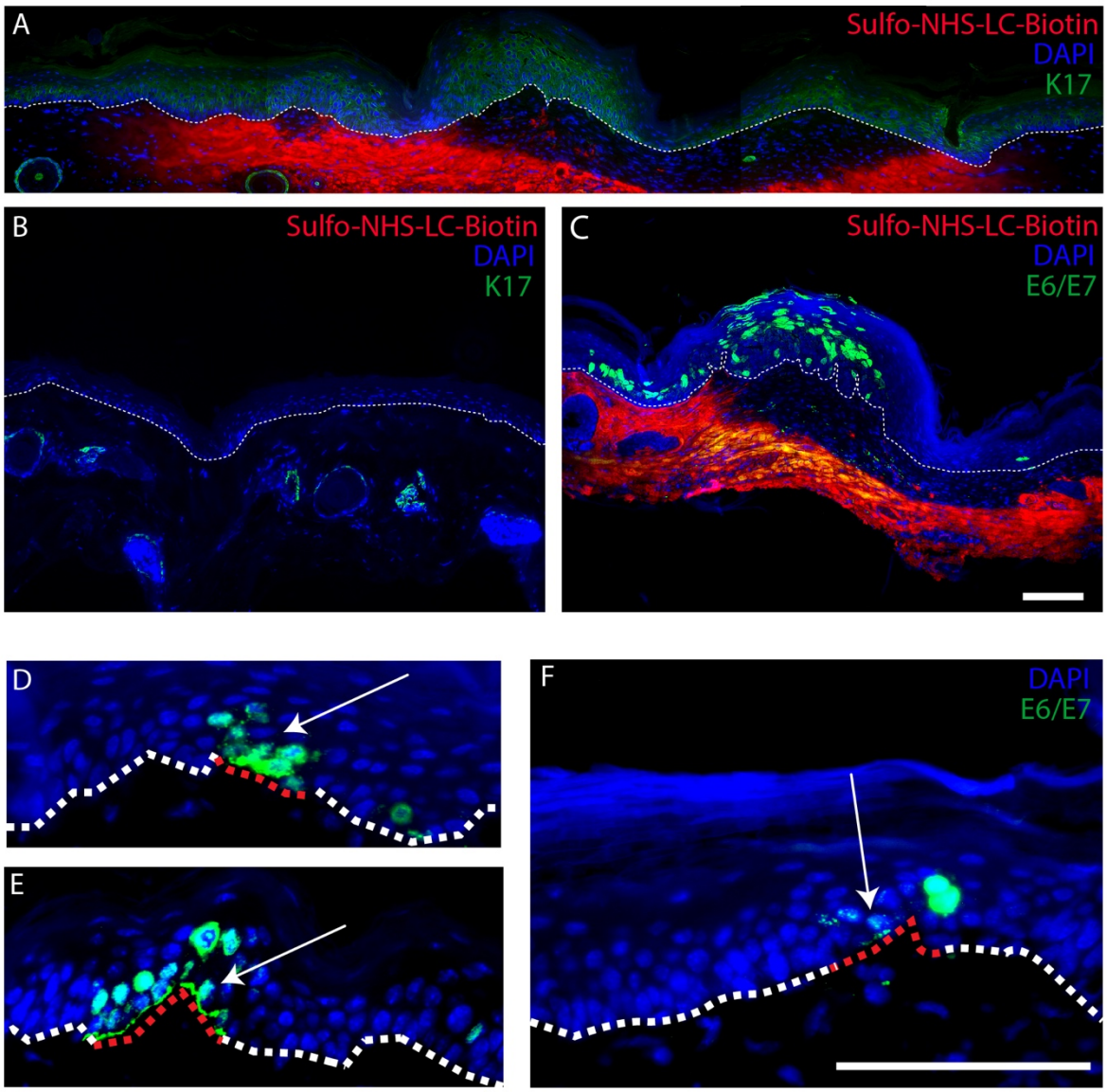

Figure 3.8 Crosslinking reagent colocalises with K17 and interacts with MmuPV1

A; IF detection of K17 (green) and crosslinker reagent Sulfo-NHS-LC-Biotin (red) at site of wounding. B; IF detection of K17 (green) and crosslinker reagent Sulfo-NHS-LC-Biotin (red) at unwounded epithelial site. C; IF detection of E6/E7 RNAscope (green) and crosslinker reagent Sulfo-NHS-LC-Biotin (red). D, E; Images showing E6/E7 RNAscope detection (green) in sites co-inoculated with both crosslinking reagent and MmuPV1, taken at 40X magnification. F; Images showing E6/E7 RNAscope detection (green) in sites inoculated with MmuPV1 only, taken at 40X magnification. White dotted lines indicate location of basal layer. Red dotted lines in D-F show location of E6/E7 positive basal cells. White arrows further highlight location of infected cells. Nuclei were counterstained with DAPI to show host DNA. All tissue shown collected 2 weeks post infection. Scale bar: 100 μm.

3.2.7 Characterisation of the earliest stages of lesion formation

To observe early lesions, athymic nude mice were scarified at three discrete regions along the tail and infected with approximately 69,000 infectious units of MmuPV1 virus at each site. When a lesion first became macroscopically visible at any site (early-visible), the entire tail was collected, allowing collection of "pre-visible" lesions present elsewhere on the same tail. To locate even earlier stages, mouse tails were also collected from day one to five following wounding. Using all of the samples collected, five discrete stages during the formation of an early lesion were characterised, and are shown below in Figure 3.9.

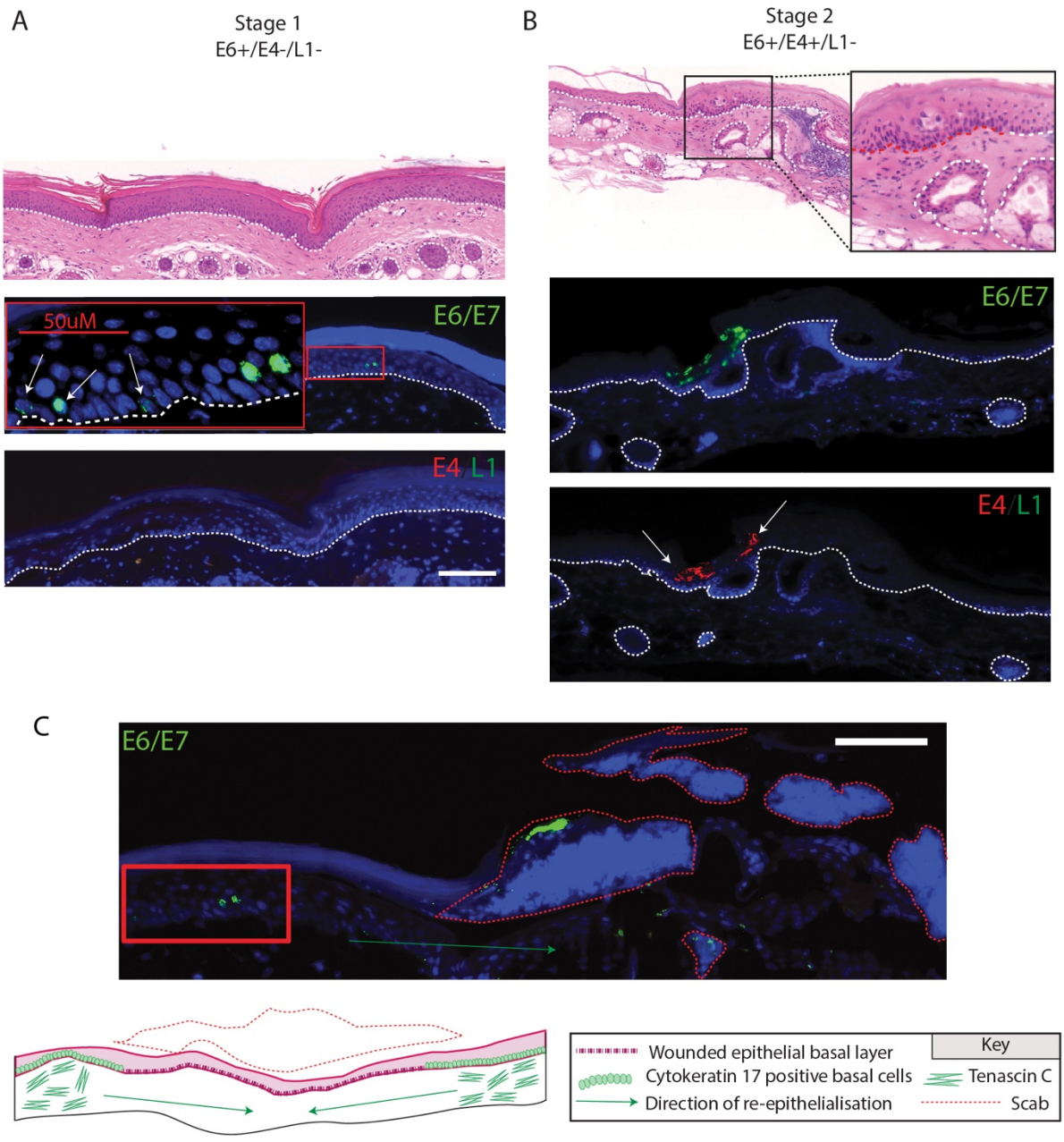

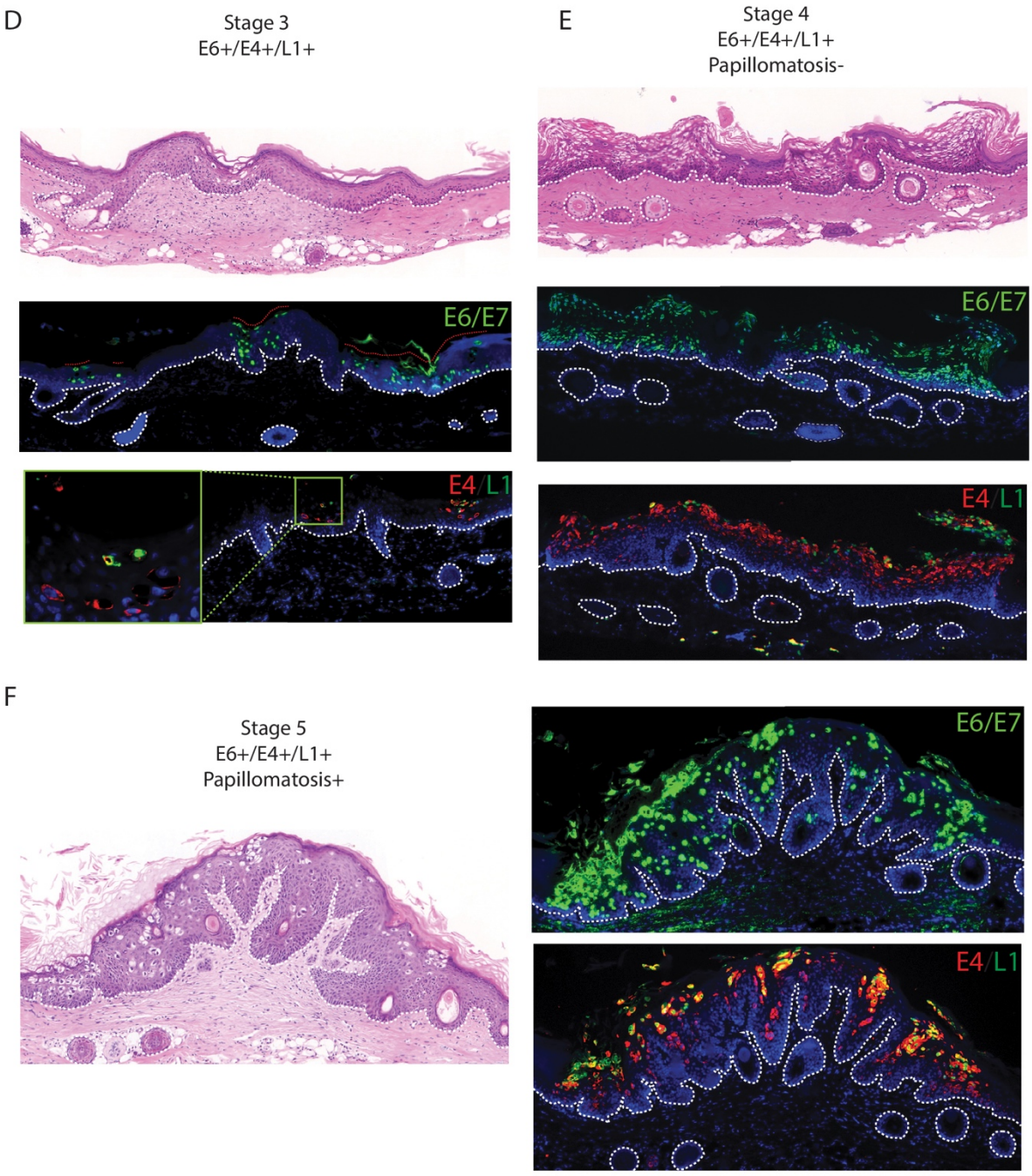

Figure 3.9 Localisation of MmuPV1 E6/E7 expression, E4 and L1 protein in early lesion formation of infected tissues

Time course analysis of early lesion formation of sites infected with MmuPV1 cell-free virus extract. Each set of panels (A-F) shows H&E staining, E6/E7 RNAscope IF (Cat No. 409771, green), and IF detection of E4 (MusE4 – in-house, red) and L1 viral proteins (MPV.B9 – Neil Christensen, green) at a discrete stage of lesion formation. Staining was carried out on adjacent sections. Nuclei were counter-stained with DAPI for host DNA. White dashed lines show the location of the basement membrane. Schematic of early wound healing also shown in C alongside microscopy image showing basal expression of E6/E7 RNA (highlighted in red box) to the right of wound centre. Scab is shown with red dotted line and green arrow shows direction of healing wound. Data collected from two independent experiments, n=5. Tissue collected post-infection - A: D2, B: D5, C: D2, D-F: D10 Scale bar: 100 μm.

Stage one (Figure 3.9A) depicts the earliest lesion formation events detectable. At this stage only E6/E7 RNA is expressed, as shown at 40X magnification in the red box. Expression can be seen in parabasal cells and in a few basal layer cells (shown with white arrows in higher magnification panel). This was observed as early as day two following wounding during analysis. In the 48 samples collected to investigate early stage infection, any early expression of E6/E7 RNA observed was only ever seen in cells where re-epithelialisation had already occurred at that region, suggesting the wound must have healed beyond certain wound healing checkpoints discussed above (Figure 3.6) before viral genes can be expressed. An example of this observation, along with schematic representation of the early stages of wound healing are shown in (Figure 3.9C). MmuPV1 E6/E7 RNA expression can be seen in the left side of the image, while scabbing can be observed to the right side, highlighted with a red dashed line. In stage two, MmuPV1 E4 protein expression (annotated with white arrows) is also present alongside the E6/E7 RNA expression. E6/E7 RNA shows greater levels of expression in the upper layers at this stage. A slight morphological change was barely perceptible in the infected cells, highlighted in a black box (Figure 3.9B). This is underlined in red in the 40X image. Cells appear to be more densely packed than the normal epithelium visible to the left. In the third stage, the first evidence of MmuPV1 virus production is apparent in the uppermost layers (highlighted in a green box, Figure 3.9D), indicating that this is now a productive infection site. Further, discrete foci of infection (shown with red dotted lines) were apparent as the development of a lesion progressed. This phenotype was commonly observed in our model, and suggests that lesions could develop from multiple discrete foci to form one lesion (McBride and Warburton 2017). In the fourth stage, high basal cell density in the lesion site was observed, as can be seen throughout the basal layer of the example lesion shown. One continuous region of infection has developed, compared with the multiple foci of the previous stage. Finally, in the fifth stage of lesion formation induction of papillomatosis was observed in a lesion that was macroscopically visible upon collection (Figure 3.9E). From characterisation of lesions beyond this stage, it is understood that lesions simply continue to grow in an uncontrolled manner from this point onward, into increasingly florid papillomas.

To investigate viral gene expression in an immunocompetent host, C57BL/6J mice were selected due to their established use in the study of immunological responses and well documented genetic background (Song and Hwang 2017). Infection of C57BL/6J immunocompetent mice with MmuPV1 crude virus did not result in the formation of

papillomas at the tail sites, whereas nude mice began to show macroscopically visible lesions within the same time frame (Figure 3.10A). Thorough analysis of tissue samples led to the

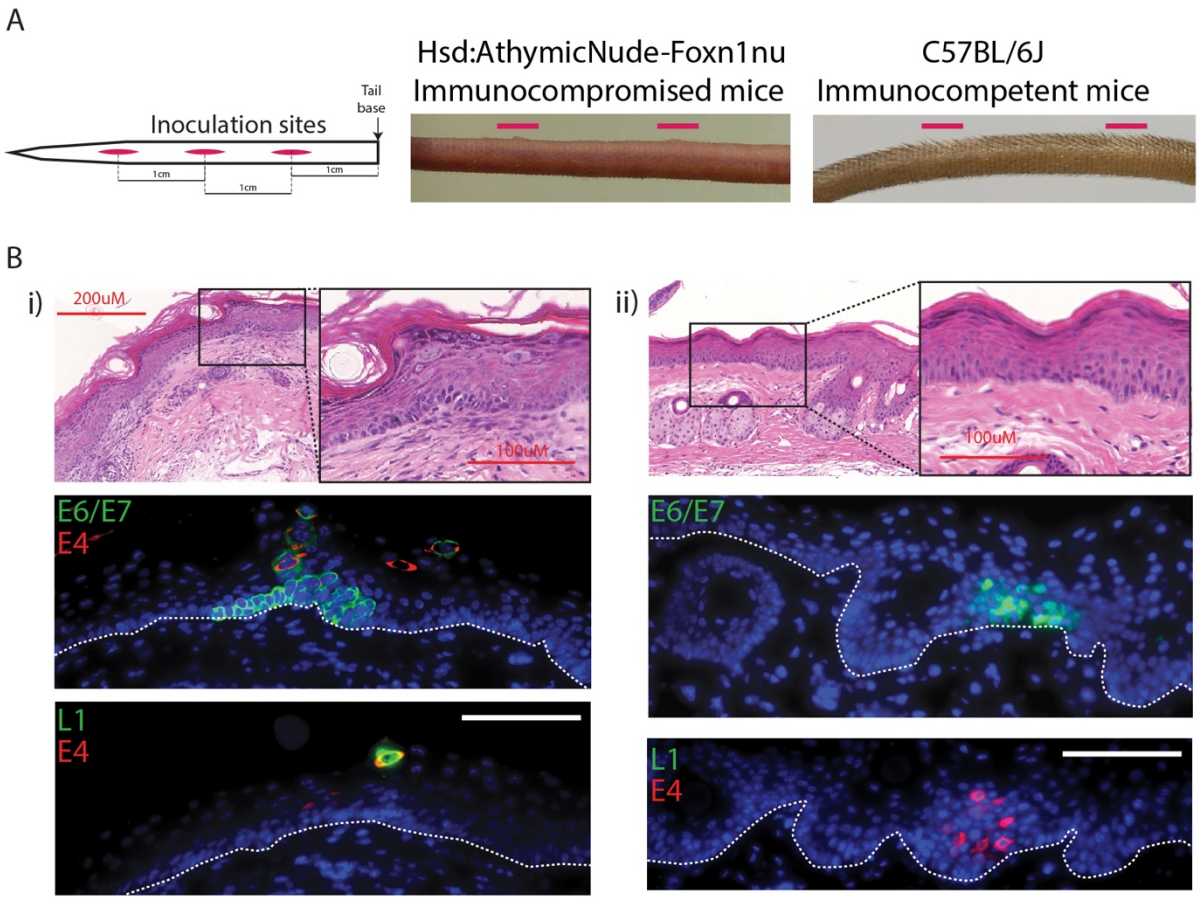

Figure 3.10 Infection in immunocompetent C57BL/6J mice
A; Diagrammatic representation of inoculation sites on mouse tail tissue shown with photographs of immunodeficient and immunocompetent mouse tails following collection. Inoculation sites are shown in red, and the 1cm spaces between the centre of each wound site are annotated. The first wound site is located 1cm down from the base of the tail. Approximate locations of wounding sites are shown with red lines above photographs of tails collected 2 weeks following inoculation with MmuPV1. B; Panels show haematoxylin and eosin staining of two sites of C57BL/6J mouse tail tissue where MmuPV1 microlesions were located, alongside corresponding IF staining of E6/E7 RNA, E4 and L1 viral proteins. Nuclei were counterstained with DAPI to show host DNA. Data collected from two independent experiments, n=14 in experiment one, n=11 in experiment two, due to alteration of the days on which samples were collected. White dotted line shows location of basal layer. Tissue collected post-infection - B: D10, B: D7. Scale bar: 100 μm.

discovery of productive microlesions in C57BL/6J mouse tail tissue at some of the sites of infection. The first microlesion was discovered 9 days following wounding. In this lesion, expression of E6/E7 RNA was evident in the basal cells, and persisted up through the layers of the epidermis to near the skin surface. This strong cytoplasmic expression pattern differs to the less clearly defined basal expression seen in our athymic nude immunodeficient model.

Similarly, E4 protein can be seen colocalising to this area, confirming the presence of a microlesion. Finally, IF staining also indicated presence of small amounts of L1 in the upper layers and at the surface, which supports the claim that this is indeed a productive microlesion (Figure 3.10Bi). A second microlesion was found in tail epithelium collected 7 days following wounding (Figure 3.10Bii). As seen in the first lesion, E6/E7 RNA had much higher cytoplasmic expression when compared to observations in athymic nude mice. E4 protein was found to localise to the same site, indicating presence of a real infection. However, in this microlesion, no L1 expression was detected.

3.2.8 Basal cell density is increased in the early stages of lesion formation

A possible correlation between E6/E7 RNA expression and an increase in basal cell density was observed from stage two of lesion formation onwards. Since this phenotype was seen from a very early stage in lesion formation in the basal layer, an involvement of one of the viral early proteins was suspected in this altered cell behaviour. To examine this further, quantitative analysis was carried out. Uninfected epithelium and mock-infected epithelium were used as control groups. For the early-visible lesion category, lesions that were collected 10 days following wounding (at which point they were confirmed to be macroscopically visible) and were identifiable with RNAscope probes directed to E6/E7 were selected. Mock-infected sites were selected at the same time point of 10 days, using the 3 classes of wound healing markers described above to confirm suitability. For quantification, 40 image sets of DAPI stained tissue at 20X magnification were collected for each category: uninfected epithelium, mock wound sites, early visible lesions and established lesions (mice n=4 per group). The number of basal cells was counted along a stretch of approximately 450 μM in each image (examples of regions counted are shown with red lines beneath the basal layer of tissue shown in each representative image). These counts were then averaged to give a mean cell count per micrometer for each of the categories, as shown in Figure 3.11.

Results showed that basal cell density was significantly increased in the early visible lesions when compared to all other categories, with approximately 0.22 cells per μm (****$p \leq 0.0001$). Basal layer densities in the uninfected epithelium and the mock wound site were quantified at 0.18 and 0.16 cells per μm respectively, and this slight difference in density was also shown to be significant (*$p \leq 0.05$). Interestingly, there appeared to be no significant difference between the mock wound site and that of an established lesion, which was also quantified at approximately 0.16 cells per μm.

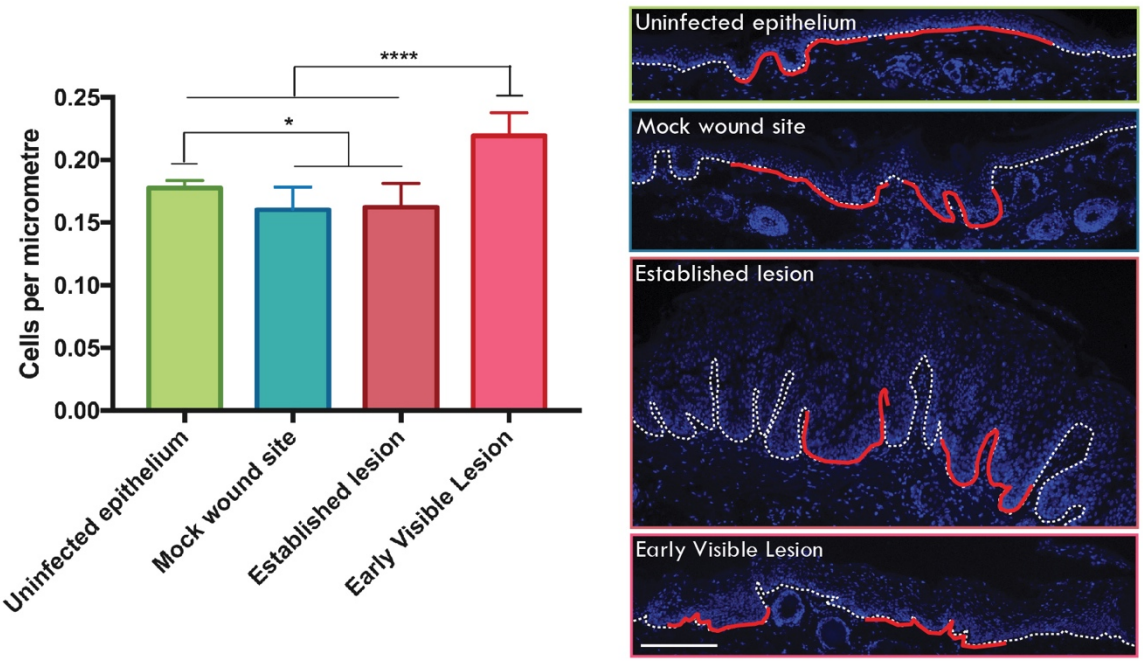

Figure 3.11 Cell density is increased in basal layer of early-visible lesions
Quantitative analysis of basal cell density in four categories of tissue (left panel); uninfected epithelium, mock wound sites, early visible lesions (samples collected at 10 days following wounding and validated using E6/E7 RNAscope), and established lesions (samples collected from florid tail lesions more than 3 weeks following wounding). Basal cell density was quantified by measuring 450 μm stretches of epithelium in 40 image sets taken from different mice (n=4 per category). P-values were calculated with Kruskal-Wallis test with Dunn's correction; * = $P \leq 0.05$, **** = $P \leq 0.0001$. Representative 5X magnification microscopy images are shown (right panel) for each category. Two examples the of measurement method are shown with solid red lines under the basal layer of each microscopy image, with nuclei counterstained with DAPI to show host DNA. These indicate approximate lengths measured in repeats to approximate cell density. White dotted lines indicate location of basement membranes. Data representative of 2 independent experiments, n=4, 10 measurements per site. 16,601 discrete cells counted in total. Uninfected, mock wound, and early visible lesion tissue collected on D10 post-infection; established lesion tissue collected at 3 weeks post-infection. Scale bar: 200 μm.

To consider whether increased cell division was the cause of the increase in cell density, staining for a mitosis-specific marker, phosphorylated histone 3 (H3 ps10), was carried out. There is a strong correlation between early prophase mitotic chromosome organisation and phosphorylation of histone 3 (Veras, Malpica et al. 2009), therefore the use of an antibody specifically targeting phosphorylated histone 3 allows location of mitotic cells. Immunohistochemistry (IHC) was carried out on samples to determine which cells were positive for phosphorylated histone, and these were counted to calculate the percentage of positive cells in each of the four categories (n=5) from the previous analysis: uninfected epithelium, mock wound, early visible lesion, and established lesion. Data is shown below in Figure 3.12. Although on average the percentage of mitotic cells was higher in both the established lesion and the early-visible lesion categories, there was no statistically significant

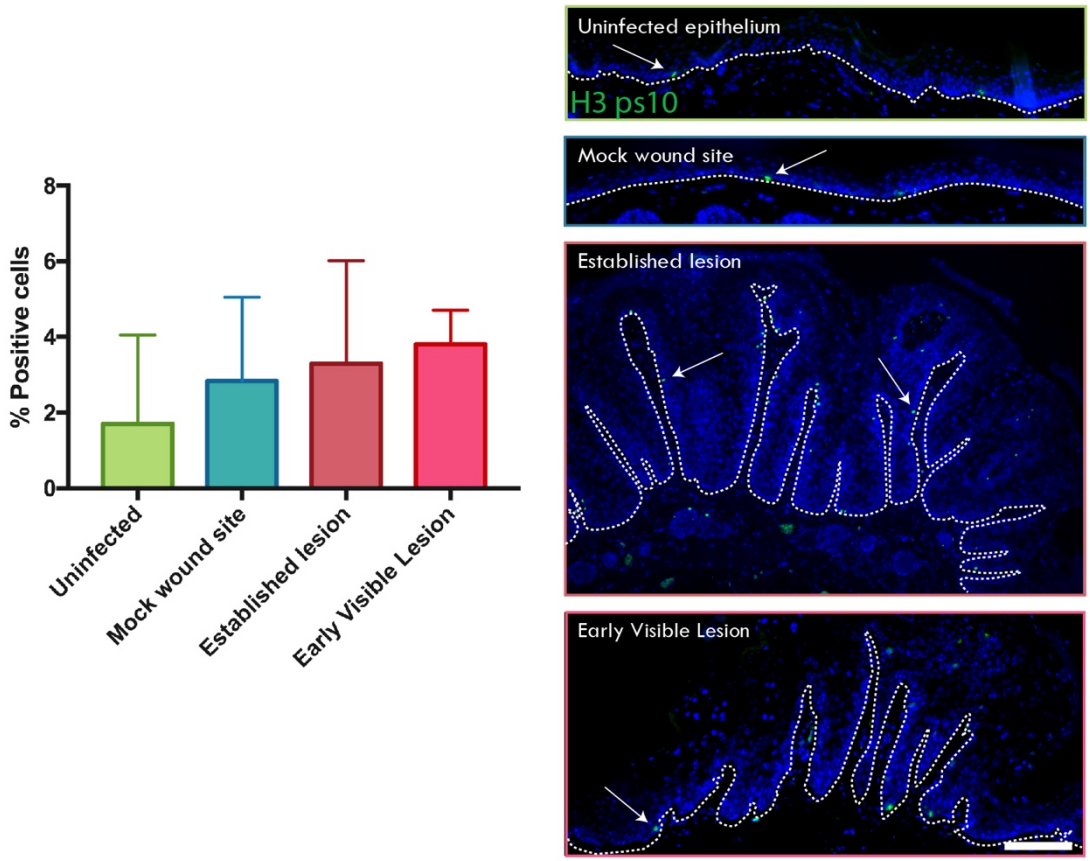

Figure 3.12 Increase in mitotic cells in MmuPV1-infected basal cells

Quantitative analysis of the percentage of H3 ps10 positive cells in the above four categories (one independent experiment, n=3). P-values were calculated with Kruskal-Wallis test with Dunn's correction. Error bars, SD. Representative fluorescent images are shown to the right of the graph. Nuclei were counterstained with DAPI to show host DNA. White dotted lines indicate location of basement membranes. White arrows indicate the location of some of the positive cells. One independent experiment, n=3. Uninfected, mock wound, and early visible lesion tissue collected on D10 post-infection; established lesion tissue collected at 3 weeks post-infection. Scale bar: 200 μm.

difference between the four categories. It was considered that with a greater number of samples to analyse, these differences may become statistically significant, and the observed trend fit with the expectation that cell division might be higher in infected cells. However, it was also postulated that the snapshot in time provided by tissue sample analysis may make it more difficult to analyse the populations of mitotic cells; a high number of samples would have to be processed to remove standard error relating to unusually high or low populations of mitotic cells apparent due to chance timings, and mitotic cells in the epithelial basal layer can be challenging to locate in general (Noske, Stark et al. 2016). Therefore, a different approach was considered.

To investigate this phenomenon in a different way, analysis was carried out to determine if the number of cells driven to replicate their DNA was altered in virus infected basal cells, and whether this differed between early and established lesions. Incorporation of the thymidine analogue BrdU was monitored by collecting tissue samples 24 hours after intraperitoneal injection with the substance. During cell replication, BrdU is incorporated into cellular DNA, which allows tagging of cells that have entered S phase during the period of incubation with the nucleoside analogue (Takagi, McFadden et al. 1993). IHC was carried out on samples to determine which cells within each of the four categories from the previous analysis were BrdU positive. Before quantification, a brief pilot study was carried out to determine the optimal conditions for the visualisation of BrdU in mouse tissue. Incubation with HCl during the normal staining procedure is required to denature DNA and allow binding of the anti-BrdU antibody. Incubation in 1M and 2M HCl for 15 and 30 minutes was attempted, as shown in Figure 3.13A. As incubation in 2M HCl for 30 minutes provided the clearest signal, this was utilised for the subsequent experiment. The number of cells that were BrdU positive was counted to calculate the percentage of positive cells in uninfected epithelium, mock wound, early visible lesion, and established lesion. Results showed a statistically significant increase in the proportion of BrdU positive cells in the basal layer of the early visible lesion when compared to uninfected epithelium (Figure 3.13B).

In uninfected tail epithelium and mock infected tail sites, only 14% and 13% of basal cells were BrdU positive respectively. No significant difference was found between these two groups. In the early visible lesions, 25% of cells in the basal layer were positive for BrdU. There was also no significant difference in percentage of BrdU positive basal cells between early visible lesions and established lesions, in which 24% of basal cells were positive for BrdU. The percentage of BrdU positive cells in early visible and established lesions was significantly higher than in both uninfected epithelium ($*p \leq 0.05$) and mock wounded epithelium ($**p \leq 0.01$). BrdU positive cells in the upper layers of both categories were deemed attributable to virus DNA amplification. Representative images of each group can also be seen in Figure 3.13C. These results suggested that the change in cell density observed as a lesion is first beginning to form is not solely caused by an increase in cell proliferation. The basal cell density in early visible lesions was significantly higher than that of the established lesions, whereas there was no significant difference in DNA synthesis between the two groups. As a result, any disruption of normal basal cell differentiation pathways was the next area investigated.

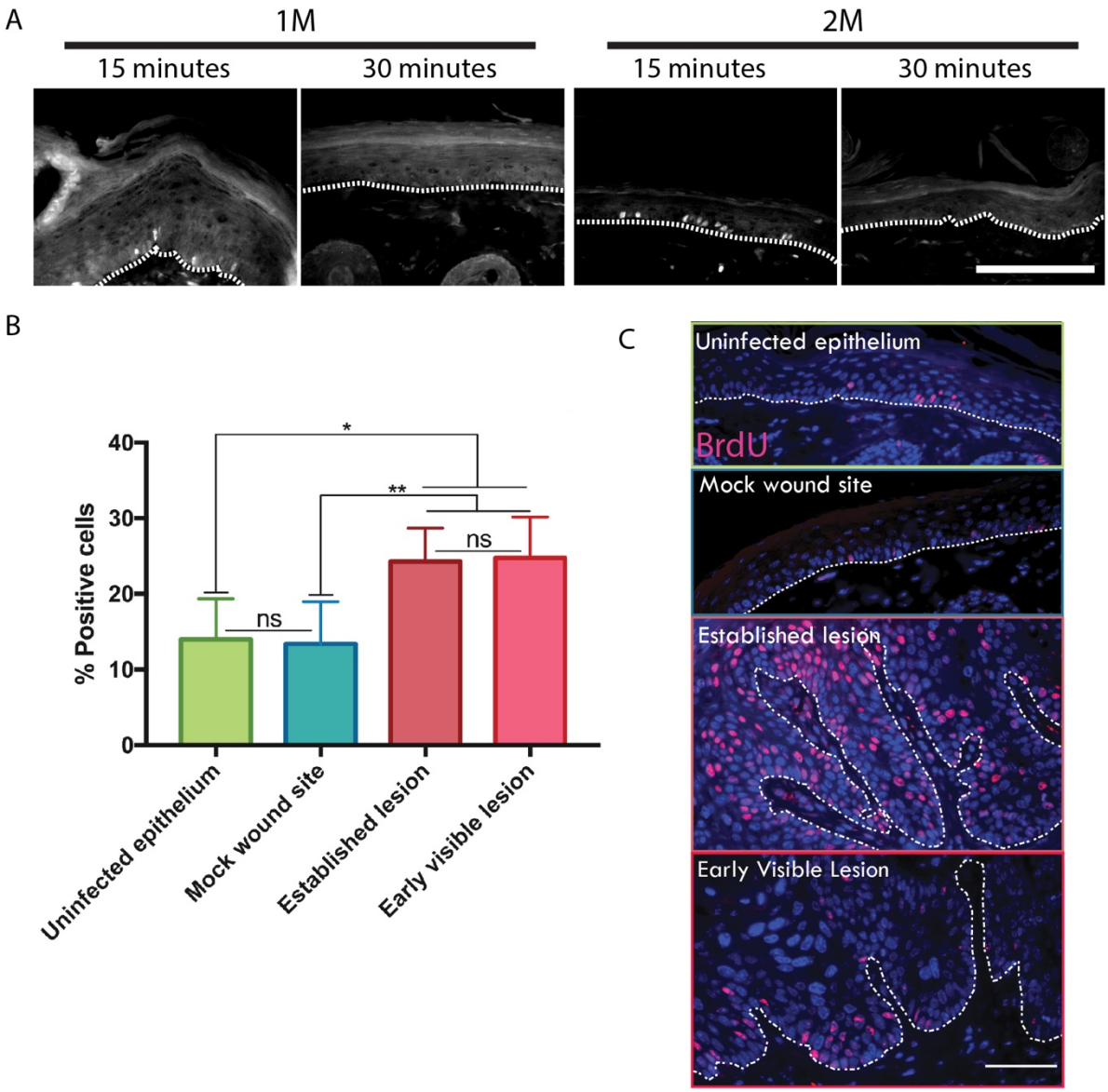

Figure 3.13 Increase in cells entering the cell cycle in MmuPV1-infected basal cells

A; optimisation of anti-BrdU fluorescent staining. Images showing IF detection of BrdU in four different conditions are shown. Scale bar: 100 μm. B; Quantitative analysis of the percentage of BrdU positive cells in the above four categories (n=3). P-values were calculated with Kruskal-Wallis test with Dunn's correction; * = $P \leq 0.05$, ** = $P \leq 0.01$. Error bars, SD. C; Representative images of BrdU staining (red) for each of the four categories. Nuclei were counterstained with DAPI to show host DNA. White dotted lines indicate location of basement membranes. Two independent experiments, n=5. Uninfected, mock wound, and early visible lesion tissue collected on D10 post-infection; established lesion tissue collected at 3 weeks post-infection. Scale bar: 50 μm.

3.2.9 E6/E7 EXPRESSION CORRELATES WITH A DELAY IN NORMAL DIFFERENTIATION IN PARABASAL LAYERS OF DEVELOPING AND ESTABLISHED LESIONS

To examine the involvement of E6/E7 RNA expression in basal cell exit, IHC was carried out for K10, an established early stage marker of cells entering terminal differentiation. Double immunostaining for MmuPV1 E6/E7 RNA and K10 demonstrated that in the presence of the early MmuPV1 E6/E7 RNA, K10 is completely absent (Figure 3.14). To investigate the differentiation pathway further, HES1 RNA expression patterns were visualised using RNAscope ISH. The Notch signalling pathway is generally understood to be involved in the process of differentiation in keratinocytes, and HES1 (hairy and enhancer of split protein 1) is one of its downstream target genes. Therefore, presence of HES1 RNA demonstrates activation of the Notch signalling pathway (Blanpain, Lowry et al. 2006). As shown in Figure 3.14, expression of HES1 was not noticeably delayed and was expressed throughout the basal and parabasal layers. In fact, quantification of HES1 RNA expression per cell in the basal layer of lesions versus uninfected tissue demonstrated a significantly higher level of HES1 RNA expression in the infected basal cells (Figure 3.14B).

This data suggested that the Notch signalling pathway was active. Therefore, it is not total inhibition of the pathway by E6/E7 that leads to the observed delay in differentiation, where cells exited the basal layer without differentiating. The differentiation status of the immunocompetent microlesion shown in Figure 3.15 was also characterised by immunostaining for K10. As seen in the experiments carried out with immunodeficient mice, there is also a decrease observed in K10 staining that correlates with the presence of E6/E7 RNA. Further, it appeared that in this lesion, HES1 RNA expression was also expressing highly in cells that are positive for E6/E7 RNA, which demonstrated that the elevated HES1 phenotype was also present in immunocompetent microlesions. Data indicated that in both immunocompetent and immunosuppressed backgrounds, MmuPV1 infection delayed differentiation commitment in the parabasal layers, which could enhance basal layer persistence of the infected cell, as well as facilitate viral genome copy number rise in the parabasal and suprabasal cell layers. It was noted that the expression of E6/E7 RNA was extremely heterogeneous; even cells immediately adjacent to each other in the same layer of cells could have extremely different levels of expression. Therefore, a more thorough analysis of the expression of E6/E7 RNA was undertaken.

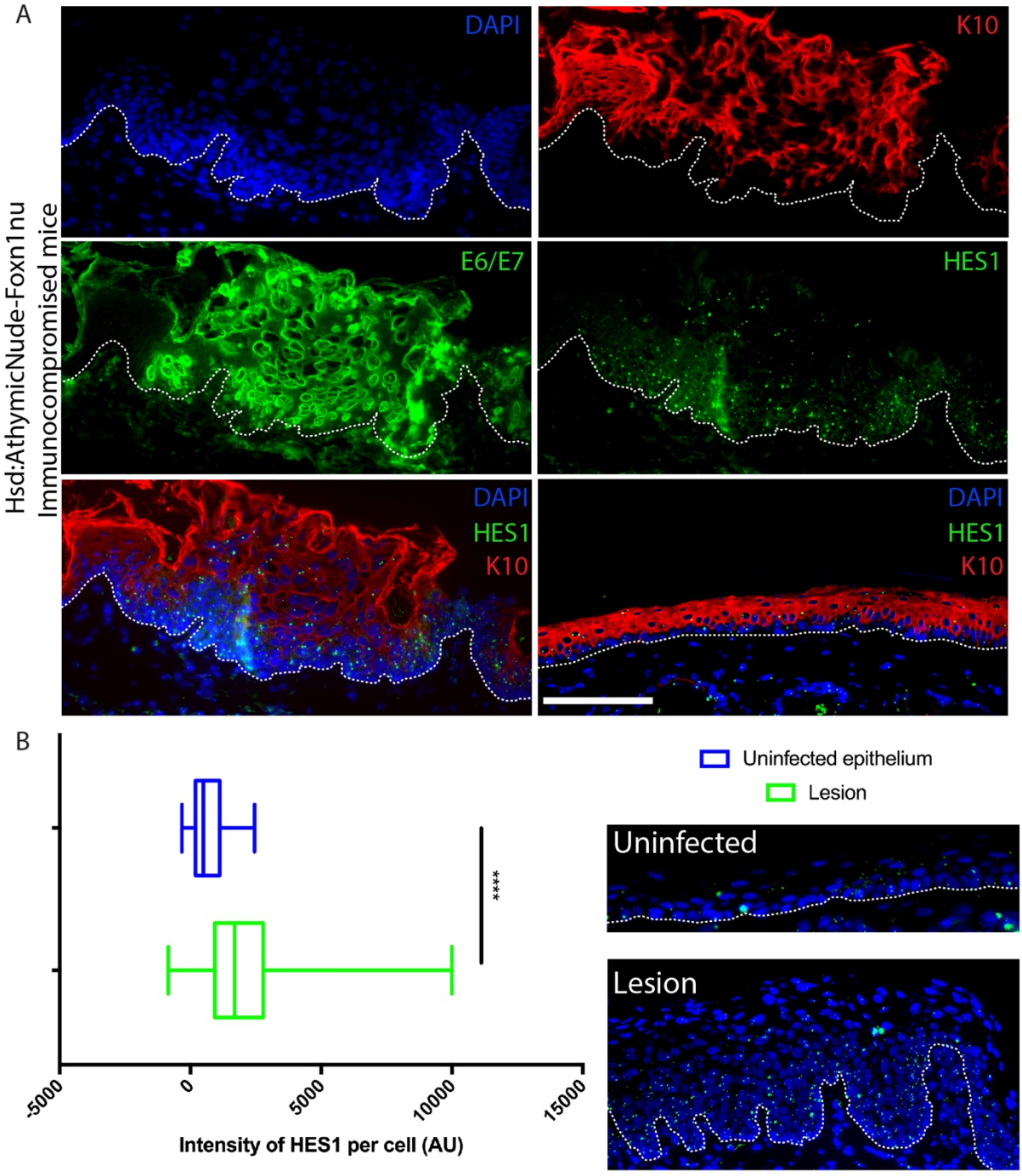

Figure 3.14 Differentiation is delayed in MmuPV1 E6/E7 expressing cells
A; Representative IF analysis of an early visible lesion from an Hsd: AthymicNude-Foxn1nu mouse. Panels show counter-staining of nuclei with DAPI for host DNA (upper left), K10 (upper right), E6/E7 RNAscope (middle left), HES-1 RNAscope (middle right), DAPI HES1 K10 merge (lower left) and DAPI HES1 K10 merge of uninfected epithelium (lower right). Tissue collected 10 days post-infection. Scale bar: 100 μm. B; Box plot to show intensity of HES1 RNA expression in the basal layer of cells of uninfected epithelium in blue (n=10) versus lesion in green (n=10). P-values were calculated with a Kolmogorov-Smirnov t-test; **** = $P \leq 0.0001$. IF images in the panel on the right demonstrate the difference in intensity observed. Two independent experiments, data pooled from these to build histogram dataset, n=5.

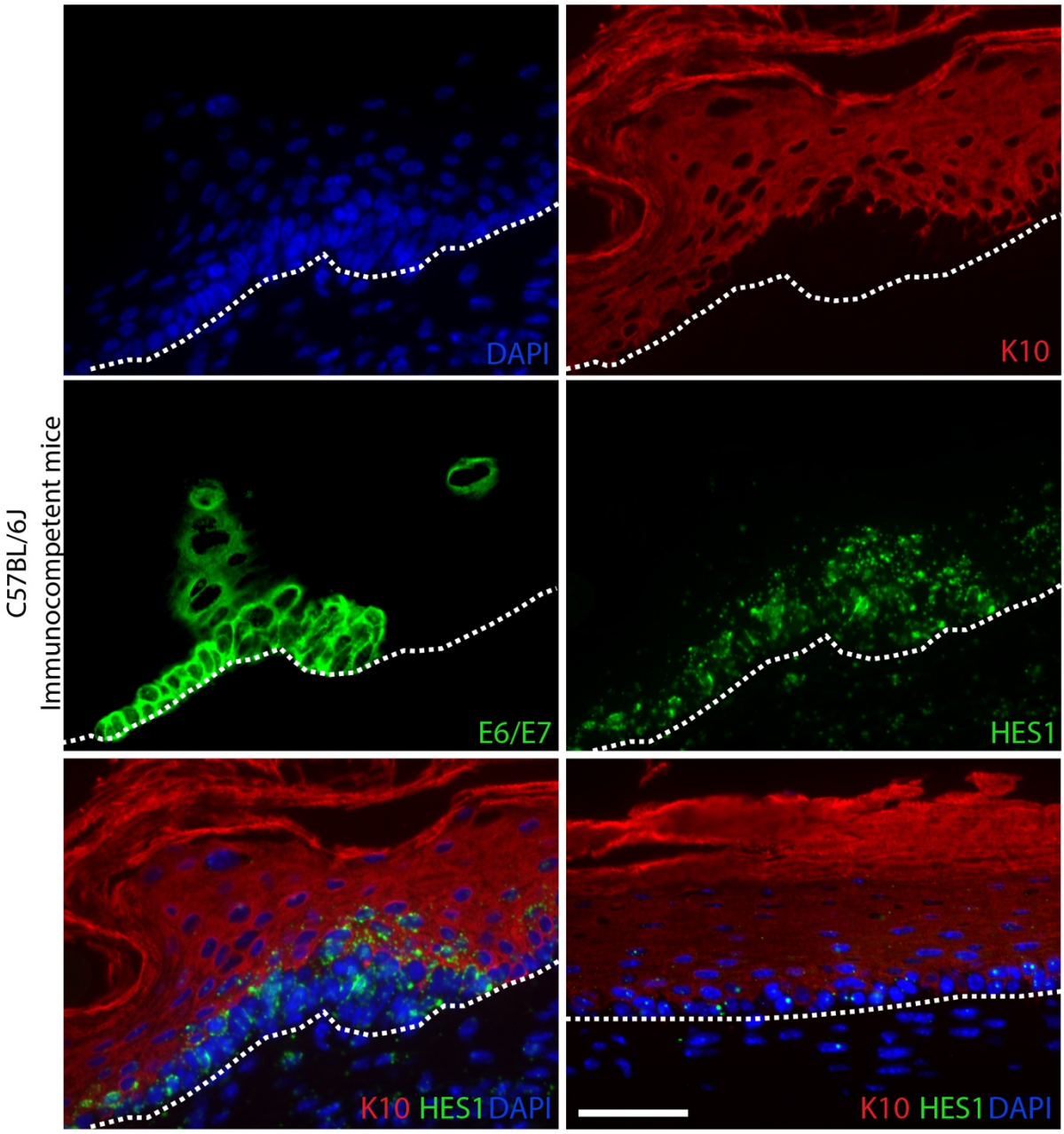

Figure 3.15 Differentiation is delayed in MmuPV1 E6/E7 expressing cells in immunocompetent mice IF analysis of two differentiation markers in a microlesion from a C57BL/6J mouse. Panels show counter-staining of nuclei with DAPI for host DNA (upper left), K10 (upper right), E6/E7 RNAscope (middle left), HES-1 RNAscope (middle right), DAPI HES1 K10 merge (lower left) and DAPI HES1 K10 merge of uninfected epithelium (lower right). Data collected from two independent experiments, n=14 in experiment one, n=11 in experiment two, due to alteration of the days on which samples were collected. Tissue collected 10 days post-infection. Scale bar: 50 μm.

3.2.10 Expression of E6/E7 RNA in the basal layer is heterogeneous and may correlate with basal cell exit

As an increase in basal cell density could not be attributed to increased cell replication alone, it was postulated that MmuPV1 E6/E7 expression may lead to persistence of infected cells in the basal layer by overcoming normal cell density modulation and contact inhibition. To investigate this in tissue, the expression level of E6/E7 RNA in individual cells was scrutinised in greater detail by measuring the E6/E7 RNA fluorescence per cell in the basal cells of 8 randomly selected early visible lesions. To quantify the E6/E7 RNA expression in whole cells, z-stack confocal images of a cell layer thickness were collected and then plotted as maximum intensity images. Figure 3.16A shows an example of one of the images that was analysed in the left panel. To quantify E6/E7 RNA expression, individual DAPI-stained cells were manually selected as regions of interest using only the blue channel of the images (shown with red lines in the middle panel), which were then plotted on to the corresponding green channel that showed E6/E7 RNA expression, as demonstrated in the right panel. This allowed quantification of E6/E7 RNA expression per cell without bias. Following quantitation of E6/E7 RNA expression within these single cells, the spread of data was plotted in a histogram, shown in Figure 3.16B.

Interestingly, a weak bimodality was observed in the expression pattern of the cells, suggesting the presence of two discrete subsets of infected cell; a larger one in which E6/E7 expression occurs at a lower level, and a smaller group of highly expressing cells. Statistical tests of bimodality found that the bimodality of the spread of data was not statistically significant (Hartigan's dip test, $p=0.914$). However, the dataset was also significantly not normal when three different statistical tests for normality were applied to the set (D'Agostino & Pearson normality test, $p=<0.0001$; Shapiro Wilk normality test, $p=<0.0001$; KS normality test, $p=<0.0001$). Further, when attempting to fit curves to the dataset, the sum of Two Lorentzian curves (shown as a red line on the histogram in Figure 3.16B) was found to fit the data extremely well, which could suggest the presence of two discrete groups with wide tails within the dataset.

To expand upon this analysis, examination was carried out on larger datasets using a mathematical model to quantify levels of RNA expression by pixel intensity, shown with a graphic in Figure 3.17A. This algorithm, generated by Dr Alberto Giaretta, measured the intensity of individual pixels within the selected region of interest and attributed each a numerical value based on the intensity of expression. For example, for the mock pixel

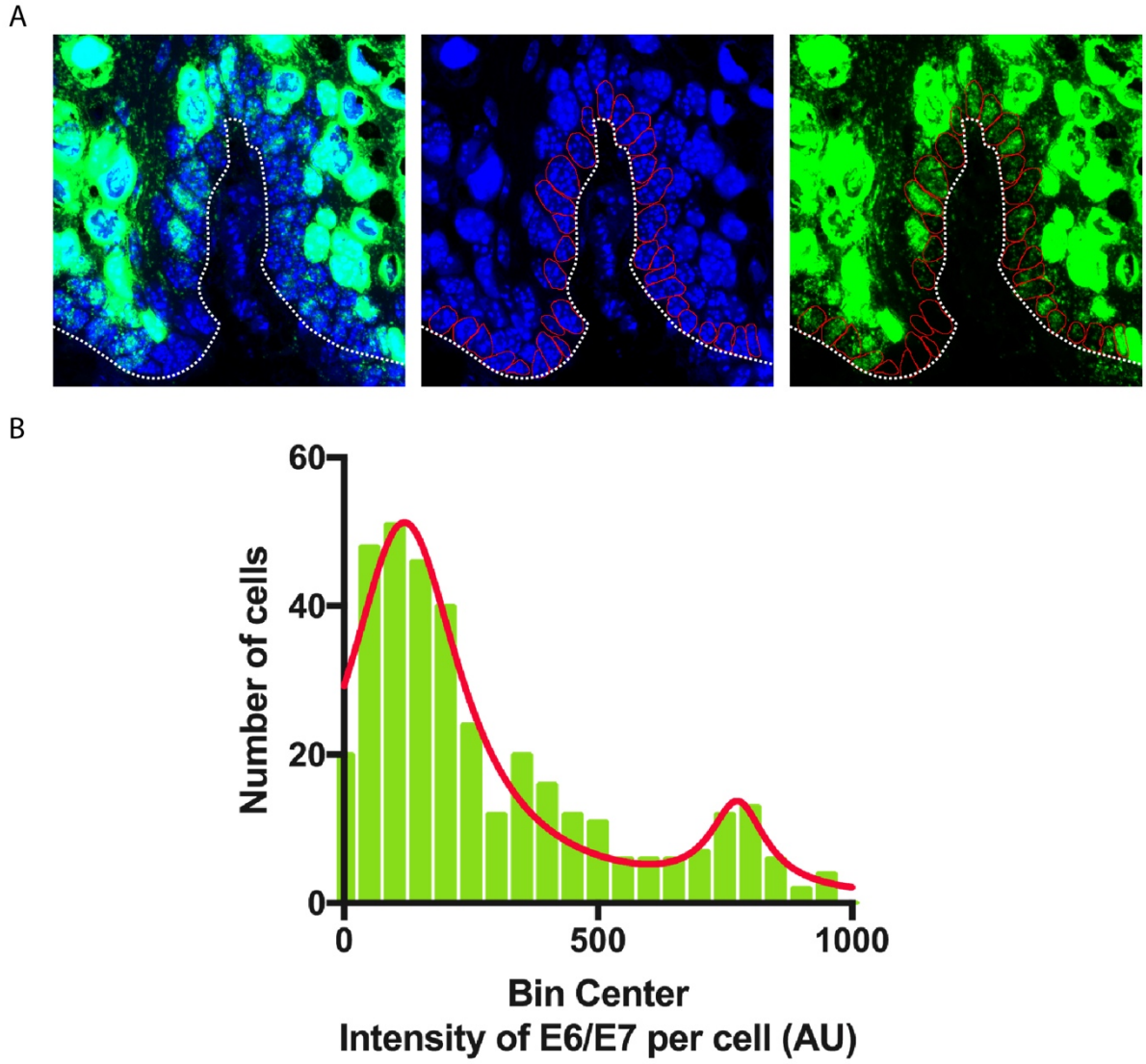

Figure 3.16 Heterogeneous expression of E6/E7 RNA demonstrates potentially bimodal distribution

A; Example of images used in the calculation of E6/E7 RNA expression intensity. Left panel shows maximum intensity merge of confocal z-stack of MmuPV1 infected tissue region (63X magnification). Middle panel shows DAPI channel only, with red selections demonstrating how single cells were isolated as regions of interest. Right panel shows corresponding E6/E7 RNA channel, with previous selection overlaid onto the image. B; Distribution of RNA expression levels in basal cells of early visible lesions (number of cells counted = 458) is shown in a histogram. Intensity of expression per cell (AU) is grouped into bin centres for bimodal analysis. Eight discrete lesions from three different mice, n=5 images analysed per site. Data were pooled from these to build histogram datasets. A Sum of Two Lorentzian distribution line is fit to the data, shown with a red line. Hartigan's dip test, p=0.914. D'Agostino & Pearson normality test, p=<0.0001; Shapiro Wilk normality test, p=<0.0001; KS normality test, p=<0.0001. Tissue collected 10 days post infection.

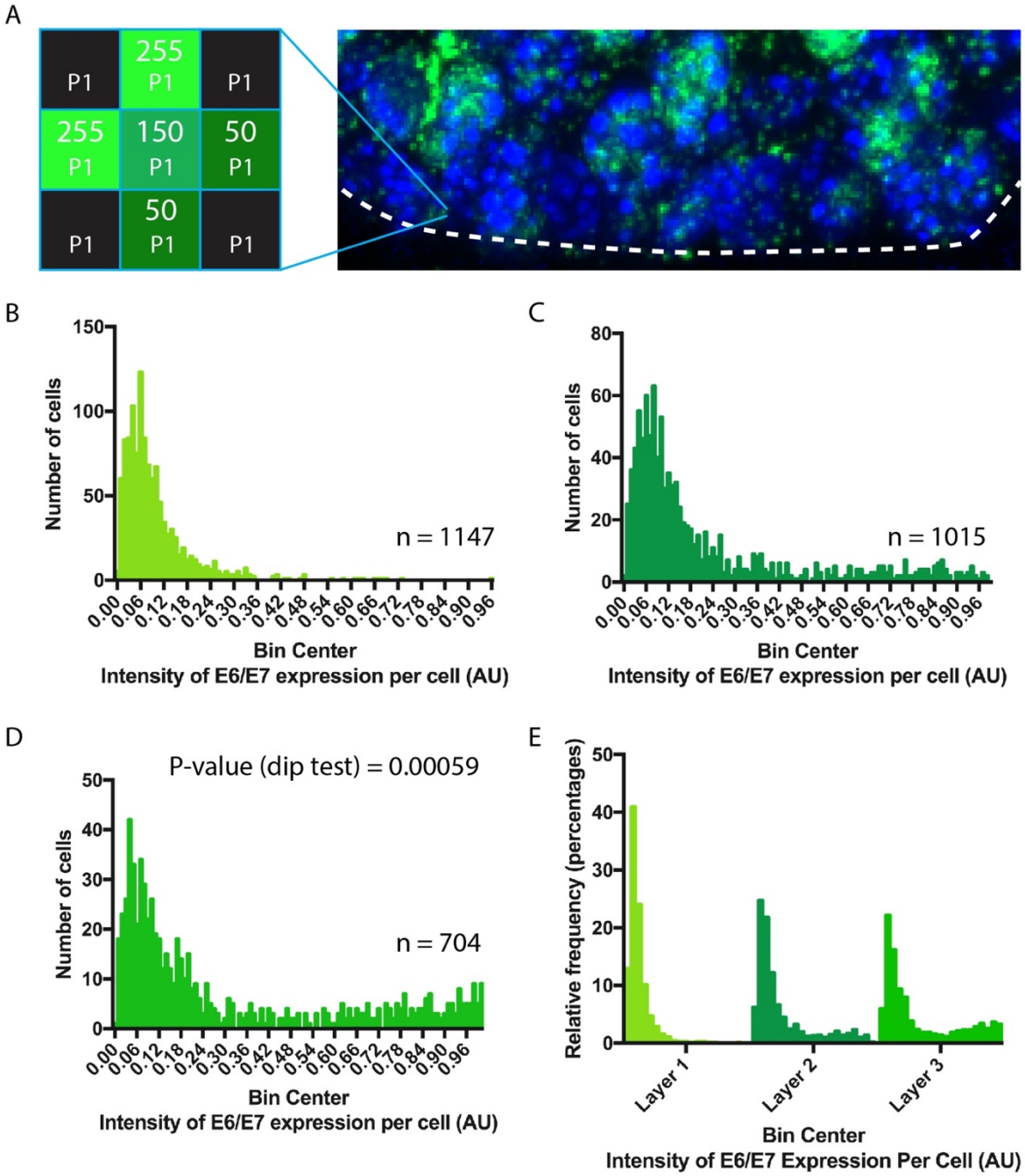

Figure 3.17 Heterogeneous expression of E6/E7 RNA may be linked to basal exit
A; Graphic to demonstrate method of pixel intensity calculation. Each pixel within selected cells is allocated a numerical value based on intensity, negative pixels are given a value of zero. B; Distribution of E6/E7 RNA expression levels in basal cells of early visible lesions calculated by mathematical analysis (n=1147) is shown in a histogram. Intensity of expression per cell (AU) is grouped into bin centres for bimodal analysis. C; Distribution of E6/E7 RNA expression levels in second layer of cells of early visible lesions calculated by mathematical analysis (n=1015) is shown in a histogram. Intensity of expression per cell (AU) is grouped into bin centres for bimodal analysis. D; Distribution of E6/E7 RNA expression levels in third layer of cells of early visible lesions calculated by mathematical analysis (n=704) is shown in a histogram. Intensity of expression per cell (AU) is grouped into bin centres for bimodal analysis. Hartigan's dip test p=0.00059. E; Distribution of E6/E7 RNA expression levels for the first three layers of cells plotted together to show relative frequency. Eight discrete lesions from three different mice, n=5 images analysed per site. Data were pooled from these to build histogram datasets. Tissue collected 10 days post infection.

shown in Figure 3.17A, the black pixels shown in each corner would have a value of 0 whereas green positive pixels could have a range of values as demonstrated. This method of indexing also normalises by the size of the cell, which allowed more precise analysis of fluorescent intensity per cell.

Using this method, larger datasets were analysed by Dr Alberto Giaretta, and the bimodality was not as evident but was still weakly present (Figure 3.17B). It was postulated that the cells expressing higher levels of E6/E7 RNA might be exiting the basal layer. Consequently, the same analysis was carried out on the second and third layers of cells in addition to the first. The bimodality of expression became more apparent in layer 2 (Figure 3.17C), and the bimodality was found to be statistically significant in layer 3, which is shown in Figure 3.17D ($p = 0.00059$). These three layers were then plotted together on the same histogram in relative frequencies to account for the slight differences in the size of the individual groups (Figure 3.17E). The data clearly showed an increase in individual cells expressing greater levels of E6/E7 RNA as the layers are progressed through from the bottom upward. These data also demonstrated that a subset of cells expressing lower levels of E6/E7 RNA are still present in the second and third layers.

It was considered whether further analysis of the data might identify the subset of cells expressing high levels of E6/E7 RNA by considering another variable, such as the morphology of the cell. To look at morphology, 'eccentricity' of the cell was calculated using the centric point of the cell to estimate "roundness". The further from a perfectly round shape the cell was, the more 'eccentric' it was considered to be. The methodology behind this concept is demonstrated in Figure 3.18A. Mathematical calculations of the eccentricity of cells were carried out by Dr Alberto Giaretta. The calculated eccentricity of each cell was plotted against the level of expression of E6/E7 RNA of the same cell. Plotting of these data showed that there was a visible trend between increasing eccentricity and increasing E6/E7 expression, however this was found to be statistically not significant (Figure 3.18B).

While eccentricity gives a crude measurement for the roundness of cells, this is not a perfect correlate with basal exit; our lab considers decreasing contact with the basement membrane to be indicative of detachment and entry into subsequent differentiation programmes, and this link between detachment and differentiation in keratinocytes has been considered in the literature (Grose, Hutter et al. 2002). Therefore, the original datasets for each lesion were reconsidered, and cells were manually selected from the total dataset if their morphological

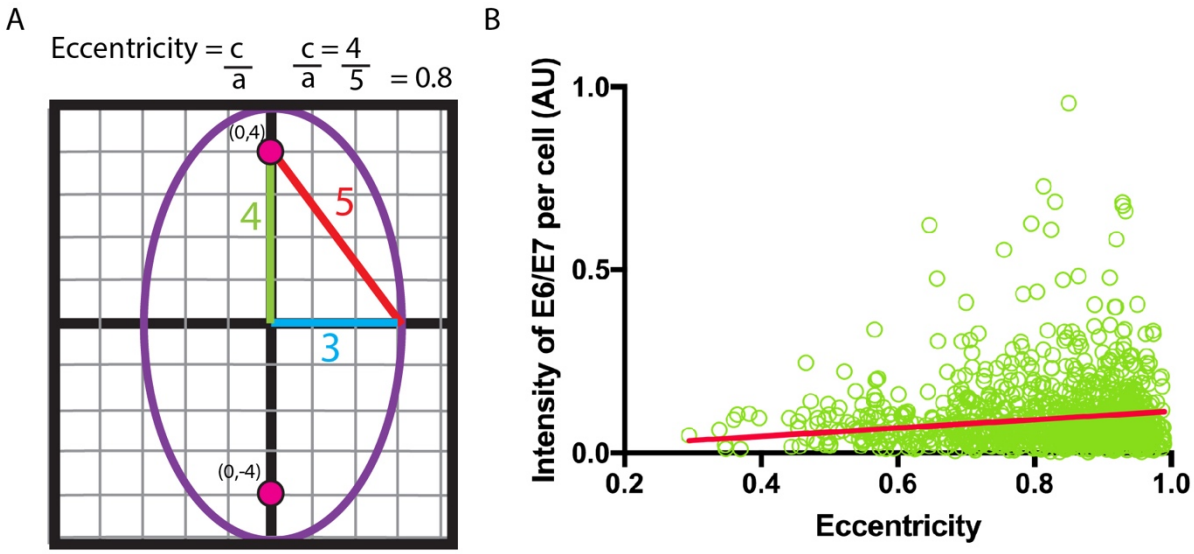

Figure 3.18 Eccentricity of cells correlates with increasing E6/E7 expression intensity
A; Diagram to demonstrate how eccentricity is calculated. Eccentricity is calculated by plotting a right-angled triangle from the centre of the shape to the edge of the shape, and dividing side c by side a, as shown. B; Cell eccentricity is plotted against E6/E7 RNA expression intensity to demonstrate any correlation. Red line plotted is a line of best fit of the data shown. Eight discrete lesions from three different mice, n=5 images analysed per site. Data were pooled from these to build histogram datasets.

appearance suggested they may be exiting the basal layer. For example, if the cell body was thin and considerably longer lengthways than the length of the cell that was attached to the basement membrane, or if the cell shape was notably wide at the top with limited attachment at the basement membrane, these cells were selected. Examples of such cells are shown with yellow dots and white arrows in (Figure 3.19A).

Selection of cells based on morphology was once again carried out using only the DAPI images of the lesion basal cells to allow unbiased selection. Results showed that E6/E7 expression in the selected cells group (n=89) was significantly higher than in the unselected cells group (n=369) (Figure 3.19B). These data suggested that basal exit and increased expression of E6/E7 above a certain threshold might be linked in the MmuPV1 model of PV infection. IHC has the drawback of only being able to examine cells in the snapshot in time at which the tissue was sampled. Consequently, gaining a more in-depth understanding of the mechanics behind the phenotype observed was difficult without substantial time investment and high usage of an expensive process. PVs have long been known to affect commitment to differentiation (McCance, Kopan et al. 1988), therefore it was decided that examination of this phenotype in a cell culture model wherein individual protein functions can be discretely analysed would be carried out.

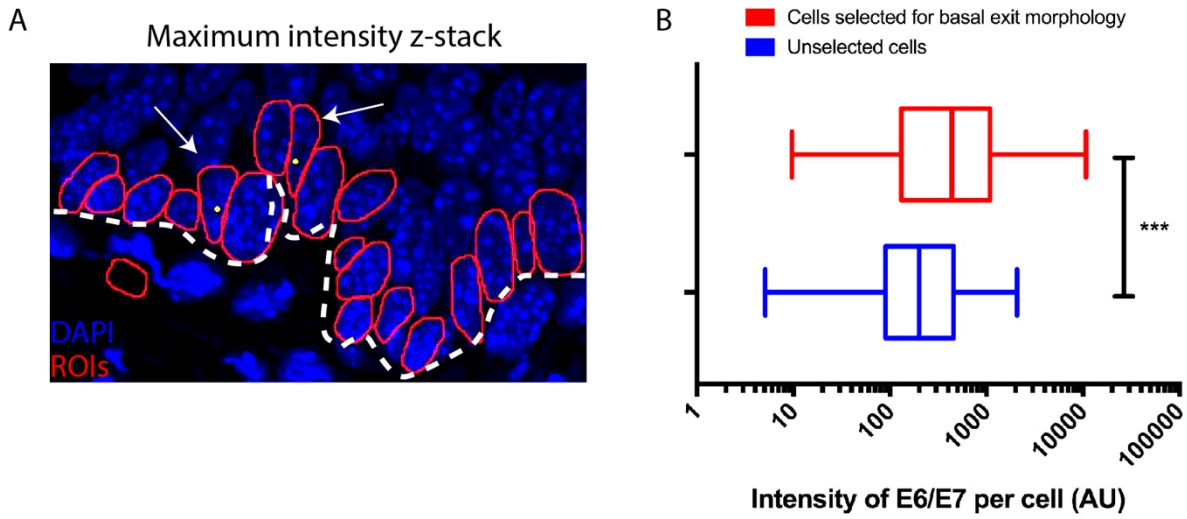

Figure 3.19 Manual selection of cells on the basis of morphology demonstrates that intensity of E6/E7 expression correlates with cell morphology indicative of basal exit
A; DAPI channel image of infected cells to demonstrate cells selected for morphology suggesting basal exit, annotated with white arrows and yellow spots. B; Box plot to show the intensity of E6/E7 RNA expression per cell of two groups. Group 1 (red) contains all cells selected for a morphology suggesting exit from the basal layer (n=89). Group 2 (blue) contains all cells not selected for a basal exit morphology (n=369). P-values were calculated with a Kolmogorov-Smirnov t-test; *** = $P \leq 0.0005$. Eight discrete lesions from three different mice, n=5 images analysed per site. Data were pooled from these to build histogram datasets.

3.3 Discussion

This chapter examined ways in which the MmuPV1 model of PV infection might be improved by more reproducible wounding events, and characterised normal wound healing in the tail epithelium of immunodeficient mice to allow better understanding of the timings around wound healing and the mechanics of the process. There are varied methods of wounding employed by research groups studying mouse PV, including careful scarification of the site using a needle (Sundberg, Stearns et al. 2014) and induction of trauma to the tail site using a Dremel rotary drill (Jiang, Wang et al. 2017). Brief comparison of two such methods determined that scarification with a 27-gauge needle provided a wound site that was most reliable to locate. However, this did mean that issues with reproducibility might be introduced as a result of human error. Research into replicable *in vitro* wounding yielded a novel stamping method to create almost identical wounds across different samples (Lan, Geng et al. 2010) but this was not applicable to *in vivo* studies; the rubber-stamping method described could disrupt cell monolayers but would not be forceful enough to effectively injure the full thickness of mouse tail skin.

The identification of discrete stages of wound healing was useful in understanding the mechanics behind how a wound heals over following injury. From the activation and appearance of K17 positive cells over time, it is clear that keratinocytes with this migratory phenotype are crucial in the healing of a superficial wound to the mouse tail. Superficial wounding to human skin also results in the induction of K17 in keratinocytes (McGowan 1998), suggesting that the mouse epithelium is a reasonable comparison to human in this respect. K17 has also been shown to be upregulated following stimulation of inflammation and proliferation pathways, further validating it as a useful marker of a healing wound (Quigley, Kandyba et al. 2016). Investigation into virus titre and speed of lesion formation using observational studies and RNAscope clearly demonstrated a relationship between the two. Higher virus titres resulted in lesions developing at a quicker pace. In some tissues samples, such as those shown in Figure 3.4, positive E6/E7 RNAscope signal can be seen beneath the basement membrane. However, examination of these samples using a fluorescent microscope found that such RNAscope signal located in the basement membrane was due to surplus tissue debris resulting from sample block cutting, and did not indicate true positive signal within intact cells.

Examination of the earliest possible stages of lesion formation with the immunodeficient athymic Hsd: AthymicNude-Foxn1nu mouse (Envigo, UK) model of PV infection was carried out to elucidate expression patterns as a lesion is first beginning to form. The earliest stage of lesion formation was detected with E6/E7 RNA expression in basal cells just two days following infection, and E4 protein was not yet present in these cells. Similarly, no L1 protein was present. An important observation was that viral gene expression only began once the epithelial denudation had been entirely repaired through re-epithelialisation by K17 positive keratinocytes. A previous experiment observed that, of the different methods examined, only a microwound that retained the basement membrane but removed the entire epithelium resulted in infection of basal epithelial cells (Roberts, Buck et al. 2007). This was because virus was shown to first attach to the basement membrane prior to entry into the basal cells. Such a mechanism might explain the phenotype observed in this experiment; virus could adhere to the basement membrane and then only infect basal cells once migratory keratinocytes have reepithelialised across the wound site containing infectious virus particles. Consolidation of recent research demonstrates that a complicated interplay of factors within the wound environment allows successful infection of basal cells (Ozbun 2019). This complexity should be kept in mind during future analyses.

Observations also suggested that lesions may initially form from multiple foci of infected cells expanding in the basal layer to form one continuous region of infected cells. This is contrary to previous research in the PV field that has suggested that common warts are clonal in origin (Murray, Hobbs et al. 1971). Conversely, analysis of cellular origins in a different wart type, condylomata acuminate, suggested that the genital warts examined were of multicellular origin (Friedman and Fialkow 1976). A consensus on cellular origins of warts has yet to be reached. It is possible that warts are originally multicellular in origin, but that competition between cells, and an increased 'fitness' of one subset of cells compared with another, may eventually lead to elimination of cells of other origins from the wart itself. Such mechanisms have been modelled and described previously (Amoyel and Bach 2014), and could explain disparate results observed within the PV field. In this instance, apparent multiple foci observed within this chapter may also be due to the relatively high titre of virus stock used when compared to natural routes of infection, or may be a mechanism exclusive to the pi types of PV infection. Further consideration is required.

Immunocompetent C57BL/6J mice were infected in parallel with the immunodeficient model. Thorough analysis of 33 discrete wound sites allowed location of two microlesions in these immunocompetent mice. Whilst appearing to be briefly productive at one of these sites, no macroscopic lesions formed on the tail, which was in agreement with previous research (Sundberg, Stearns et al. 2014). It was inferred from their relatively rare occurrence rates when compared to the immunodeficient model, that these microlesions occur transiently before clearance by the immune system. Or, they may occur at such small, controlled sites that they are simply extremely hard to locate. It has been demonstrated that adaptive immune surveillance, importantly by T cells, is the likely way in which MmuPV1 is prevented from forming macroscopic tail lesions in fully immunocompetent C57BL/6J mice (Handisurya, Day et al. 2014). Based on these immune-depletion studies it was shown that depletion of either CD4+ or CD8+ cells was sufficient to allow development of MmuPV1 lesions in SENCAR mice, a strain bred for high susceptibility for chemical carcinogen induction of skin tumours. However, in C57BL/6 mice, depletion of both CD4+ and CD8+ was required for the induction of papillomas at the infection site, demonstrating that the C57BL/6 is more resistant to MmuPV1 infection through T cell-dependent mechanisms. Therefore, it is likely that in our model, development of macroscopically visible papillomas is controlled by T cell infiltration at the site of infection.

Evidence of established virus infection has been demonstrated in immunocompetent mice previously by qPCR, at both cutaneous and mucosal sites in immunocompetent mice (Cladel, Budgeon et al. 2017). Another research group has also shown that immunocompetent FVB/NJ mice became susceptible to MmuPV1 infection and developed papillomas at infected sites following irradiation with UVB (Uberoi, Yoshida et al. 2016). Interestingly, papillomatosis still occurred at the infection site even when the ear inoculated with virus had been protected during UVB exposure of the mouse prior to infection. These data suggested that an indirect systemic immunosuppressive effect of UVB spectra UVR was responsible for the increased susceptibility of the mouse to MmuPV1 infection. Exposure to UVR has been correlated to incidence of cutaneous HPV in both immunocompetent and immunocompromised individuals (Chen, McMillan et al. 2008) (Hampras, Giuliano et al. 2014), demonstrating a role for UVR in ameliorating progression of PV infection in humans. Overall, involvement of the immune system is clearly important in modulating MmuPV1 infection, which is similar to beta PV type infection, suggesting that MmuPV1 is likely to employ similar life cycle mechanisms to those observed in the beta types.

More recently, a model of transmissible genital disease was established using immunocompetent FVB mice (Spurgeon, Uberoi et al. 2019). FVB mice have an unusually high susceptibility to development of chemically induced squamous cell carcinomas (Hennings, Lowry et al. 1993). However, discrete lesions have never been observed in C57BL/6J mice before. It is likely that the microlesions observed were either too early to have been detected and subsequently removed by the adaptive immune system, or were already regressing following immune cell interaction. Such immune modulation is similar to what is observed in infections with HPV of the beta genus. Although infection with this genus is largely asymptomatic, problems often arise with immunosuppression, for example following surgery in kidney transplant recipients (Borgogna, Olivero et al. 2018), or in those suffering with human immunodeficiency virus (HIV) (van der Burg and Palefsky 2009), indicating that presence of a functioning adaptive immune system is what keeps the virus from symptomatic infection. In more recent research with the mouse PV model, similar low-level infection has successfully been shown in NOD/SCID mice (Cladel, Budgeon et al. 2017). These data are promising for the future use of immunocompetent models of PV infection to better understand immune response to PV infection *in vivo* in this easily manageable model.

Following quantitative analysis, a change in cell density in early visible lesion sites analysed was found to be statistically significant, when compared to three control groups. Previous research has indicated that high-risk type HPV16 is also able to modulate basal cell density (Kranjec, Holleywood et al. 2017), therefore MmuPV1 may be able to induce similar phenotypes *in vivo* through the same or alternate mechanisms. It was determined that the likely cause of this increase in density would either be increased drive into DNA replication at the site of infection, or an ability of the infected cell to persist in the basal layer, overcoming normal density restrictions. Quantification of mitotic cells using phosphorylated Histone 3 as a marker proved difficult, however using BrdU allowed visualisation of cells that had undergone DNA synthesis during the time incubated with the thymidine analogue. An increased number of cells undergoing DNA synthesis in the basal layer of both early and established lesions when compared to two control groups suggested that this was not the sole cause of the increase in density. An increase in infected cells undergoing DNA synthesis was similarly shown in a recent paper (Meyers, Uberoi et al. 2017) in what would be termed in this set of experiments as an "established" lesion based on the morphology of the lesion shown.

The next consideration was whether the process of terminal differentiation was occurring normally in virus-infected tissue. Examination of the differentiation status of the lesion revealed a delay in differentiation in all lesion sites examined, from early stage to established lesions. This is in agreement with research recently carried out (Meyers, Uberoi et al. 2017), and it was further demonstrated in our research that this increase in DNA synthesis occurred in early lesions as well as established lesions, and that it was not simply a by-product of wound healing. HES1 RNA expression was visualised, as the paper by Meyers and colleagues had also shown a decrease in HES1 expression in MmuPV1 E6 expressing Tert-immortalised human foreskin keratinocytes (iHFKs). Surprisingly, it was found that HES1 expression in tissue was not downregulated, and was in fact significantly higher in the basal cells of early lesions when compared to uninfected epithelium. From these data, it appeared that the presence of MmuPV1 infection in tissue prevented normal terminal differentiation. Whilst infected cells do eventually detach from the basal layer they do not immediately progress into differentiation, as shown by the delay in K10 staining. In addition, HES1 expression in MmuPV1 E6/E7 positive lesions persists to the upper layers.

Recent research into the Notch signalling pathway has found that discrete ligand activation of the pathway can have distinct downstream effects. Importantly, it was found that Dll1 and

Dll4, two Notch ligands, modulated the Notch receptor in either short frequency-modulated pulses or sustained amplitude modulated signals respectively. Notch pathway activation by Dll1 led to upregulation of Hes1, whilst Dll4 signalling led to upregulation of Hey1 and HeyL (Nandagopal, Santat et al. 2018). Therefore, Hes1 cannot be considered to be directly representative of a Notch-directed differentiation phenotype in tissue; it appears two discrete pathways can be activated through the Notch receptor. Thorough research into the involvement of Notch in epidermal cell fate has distilled three discrete modes of action that Notch signalling activates in spinous cells. Firstly, there can be upregulation of genes required for suprabasal cell differentiation, along with downregulation of genes required expressed in the basal layer. In addition, Notch directs maintenance of a proliferative cell phenotype, but can also direct initiation of terminal differentiation. This research showed that Hes1 may in fact be required for maintenance of a proliferative phenotype, and that promotion of differentiation occurs by a Hes1 independent manner (Moriyama, Durham et al. 2008) An earlier paper also indicated that upregulation of Hes2 and Hey1 was dependent on a p63 mediated downregulation of Hes1, demonstrating p63 modulation of Notch-dependent transcription (Nguyen, Lefort et al. 2006). Overall, it seems that HES1 expression in the tissue is indicative of Notch activation, however this is not necessarily a differentiation phenotype and is much more complex than originally thought. It is likely that the activation of HES1 seen in these data results from stimulation of a proliferative phenotype in the cells that are also positive for E6/E7 RNA expression. Further research into this interplay of pathways in the context of virus infection is required in the future.

A more in-depth analysis of the expression patterns of MmuPV1 E6/E7 RNA in lesions revealed a substantial heterogeneity of expression among infected cells. Initial analysis carried out by hand selecting cells as regions of interest and quantifying intensity of expression per cell found a weak bimodality of expression. While this was not statistically significant, proving bimodality in biological systems is known to be difficult (Jackson, Tucker et al. 1989). To try to further validate this bimodality, a computer-based algorithm was established by a collaborator Dr Alberto Giaretta, wherein pixel intensity was quantified by giving each pixel intensity a relative value and normalising by cell area. Unfortunately, the bimodality was still not statistically significant using this method, and was in fact weaker. This may be due to the fact that an expanded data set was employed for the computer-based quantification. So, either the first groups of cells examined were more bimodal by chance than the larger population, or the tail effect could be impacting the larger dataset. The tail effect is where increasing size of tails in bimodal samples can disguise the bimodality of data

when undergoing statistical testing (Fiorio, Hajivassiliou et al. 2010). Further, the mathematical algorithm accounted for cell density, which could have altered the resulting spread of data.

Additional mathematical examination of bimodality in the next two layers of cells revealed increasingly bimodal populations, with a statistically significant bimodal population of basal cells from the third layer. These data suggested that the heterogeneity of expression seen in the lower layers persists and becomes more extreme as the cells move upwards towards the surface of the epithelium. Therefore, the levels of virus gene expression are partially linked to detachment from the basement membrane, however a switch to the higher expressing subgroup does not occur in all cells. A paper investigating S-phase re-entry in high-risk E7-expressing NIKS cells found that while some post-mitotic cells were able to re-enter the cell cycle after differentiation, a subset of cells instead demonstrated increased levels of accumulating cyclin E and p21cip1 protein in a replication incompetent complex (Noya, Chien et al. 2001). Formation of these distinct cell populations was attributed to an ability of normal cells to overcome unscheduled entry into S phase, and that virus induced cell cycle entry could only occur in cells with low levels of cyclin E and p21cip1. It is possible that a similar interplay of protective mechanisms between normal cells and levels of viral gene expression could be evident in the cells analysed in this experiment, which could explain the heterogeneity of gene expression observed.

Further analysis of heterogeneous E6/E7 expression revealed a possible role of gene expression in basal exit. Leading on from the increase in bimodality observed through the first three layers, linking of intensity of E6/E7 expression to basal cell exit was attempted by plotting eccentricity of the cell (Rangamani, Lipshtat et al. 2013) against the E6/E7 expression of that cell with another mathematical modelling set carried out by Dr Alberto Giaretta. Although a correlation was observed, this was not statistically significant. Following up on this work with further investigation, manual selection of cells revealed that the subset of cells selected for a morphology suggesting basal exit had a statistically significantly higher level of E6/E7 expression compared with the unselected cells. This strengthened the idea that basal cells might exist in two states of expression, and that the higher expression state might trigger or be triggered by exiting from the basal layer, whereas lower level expression is still able to mediate an advantageous environment for the infected basal cells. The discovery of the bi-stability of cells in recent years has given researchers more to consider when investigating the differentiation of cell populations. For example, whilst existing in the same

environment, only a small subset of a population of genetically identical *Bacillus subtilis* cells will differentiate into genetically transformable cells (Lopez and Kolter 2010). The bimodality of cells can sometimes be interpreted as a sort of feedback loop within the cells, self-regulating the expression of certain factors within the population. Given the heterogeneity of HES1 RNA also observed within these cell populations, regulation of the Notch signalling pathway is a likely candidate for how E6/E7 is mediating an effect on the cell population.

The work carried out in this chapter improved the mouse model of PV infection in our lab by furthering the understanding of the healing wound and examining virus gene expression and protein localisation in a range of early lesion formation stages. The observation of novel C57BL/6J mouse tail microlesions supported the current understanding of immune modulation being important in keeping viral infection under tight control in an immunocompetent host. A role for MmuPV1 in resisting normal basal cell density restrictions was also uncovered, and this was potentially linked to MmuPV1 E6/E7 RNA expression in particular. Data suggested that heterogeneous expression of E6/E7 RNA occurs in MmuPV1 cutaneous lesions, and that this may further expose a bimodality in expression linked to the modulation of basal exit and the delay in differentiation observed. To better understand and expand upon the effect of individual MmuPV1 proteins E6 and E7 on cells, establishment of cell lines stably expressing these key proteins was attempted.

4.0 Investigating viral proteins through exogenous expression in NIKS

4.1 Introduction

The mouse PV MmuPV1 provides a useful model of PV infection in a small, manageable lab animal (Hu, Cladel et al. 2017). Previous research has uncovered an involvement of MmuPV1 in delay of differentiation (Meyers, Uberoi et al. 2017). Investigations detailed in Chapter 3.0 confirmed this observation, and further demonstrated that the delay in the differentiation programme and an increase in basal cell density could be seen in the earliest stages of lesion formation alongside E6/E7 RNA expression, suggesting involvement of E6/E7 in the phenotypes observed. However, it was difficult to distil precise mechanisms of these proteins individually in tissue due to the length requirements of the ZZ probes. To properly understand the roles of E6 and E7 in the phenotypes observed *in vivo*, it was important to establish an appropriate cell culture system, which would allow quantification and analysis of the effects of virus proteins on cells. Therefore, in an effort to uncover the individual roles of MmuPV1 E6 and MmuPV1 E7 in modulation of cell density and differentiation delay, NIKS cell lines stably expressing MmuPV1 E6, MmuPV1 E7, or empty LXSN control vector were established. Our lab has previously used cell lines exogenously expressing virus proteins to investigate the interplay between the HPV E6 and E7 accessory proteins and the replicative machinery of the cell (Murakami, Egawa et al. 2019). This approach has been widely used in the field of PV research for many years and has been critical in understanding the roles of individual viral proteins (Eldakhakhny, Zhou et al. 2018) (Kranjec, Holleywood et al. 2017) (An, Hao et al. 2017) (Francis, Schmid et al. 2000, Rozenblatt-Rosen, Deo et al. 2012, Eldakhakhny, Zhou et al. 2018) (Halbert, Demers et al. 1991).

Retroviral vectors can be used to transfer genes into eukaryotic cells in a highly efficient manner (Miller 1992). To generate infectious virus, 293TT cells are co-transfected with plasmids supplying packaging genes viral gag-pol, viral envelope proteins, and the gene of interest flanked by LTRs to ensure integration of the transfer plasmid sequence into the host following infection. A promoter must also be included in the sequence of this plasmid to ensure successful expression following insertion into the host genome. 293TT cells are commonly used during this stage of retrovirus generation because they have high transfection efficiency and grow predictably, resulting in a high yield of infectious virus. These cells are described in Section 2.2.1.5. After co-transfection with these plasmids, virions that contain the desired sequence plasmid are produced from the cells; the retroviral vector containing the gene of interest also contains a retroviral packaging sequence (Ψ+). Infection of target cells

with virus produced in 293TT cells results in stable expression of the desired gene within the host, however no further virus is produced; no gag-pol or env is present within the host recipient cell (Kurian, Watson et al. 2000).

It was decided that two retroviral vectors would be used to generate cell lines exogenously expressing viral proteins: pLXSN and pQCXIN. pLXSN contains wt 5' LTR for control of expression of the gene of interest, a multiple cloning site (MCS) for cloning in of the desired sequence using available restriction sites (Clark, 2005), and an SV40 promoter controlling expression of the neomycin resistance gene. Similar to pLXSN, pQCXIN possesses a MCS and neomycin resistance. Conversely, pQCXIN contains a CMV/MSV promoter and an IRES (internal ribosome entry site) which allows co-translation of the desired gene and the neomycin resistance gene. Although expression from these promoters varies between cell types, CMV has been shown to direct high level expression of genes in 293TT cells (Qin, Zhang et al. 2010). In keratinocytes, expression of genes from a CMV promoter is understood to be relatively higher than expression of genes directed by LTR (Lathion, Schaper et al. 2003). Preparing constructs with both of these vectors would provide the means with which to express the viral proteins at two different levels, one expressing protein at high levels for validation of expression, and another to provide expression levels closer to what are believed to be biological levels within our system.

4.2 Results

4.2.1 Generation of NIKS cells exogenously expressing viral proteins

To investigate how MmuPV1 affects the growth and differentiation of cells in the epithelial basal layer in more detail, NIKS cell lines exogenously expressing MmuPV1 E6 (NIKS/MmuPV1E6-LXSN) or MmuPV1 E7 (NIKS/MmuPV1E7-LXSN) were generated. NIKS were chosen because they are a keratinocyte cell line; HPV requires infection of basal epithelia to initiate infection, and must complete their life cycle in tandem with keratinocyte terminal differentiation, therefore NIKS are an appropriate cell line to choose (Griffin, Cicchini et al. 2014). NIKS also have proven utility in successful expression of PV gene vectors, as described in Section 1.10.1. First, PCR amplification of MmuPV1 E6 and MmuPV1 E7 was carried out. Primers were designed to introduce a HA tag at the 5' end of the E6 sequence, and a FLAG tag at the 3' end of the E7 sequence. Resulting constructs run on a DNA gel are shown in Figure 4.1A (MmuPV1E6) and Figure 4.1B (MmuPV1 E7). Following the confirmation of correct band sizes and extraction of DNA from the gel using a

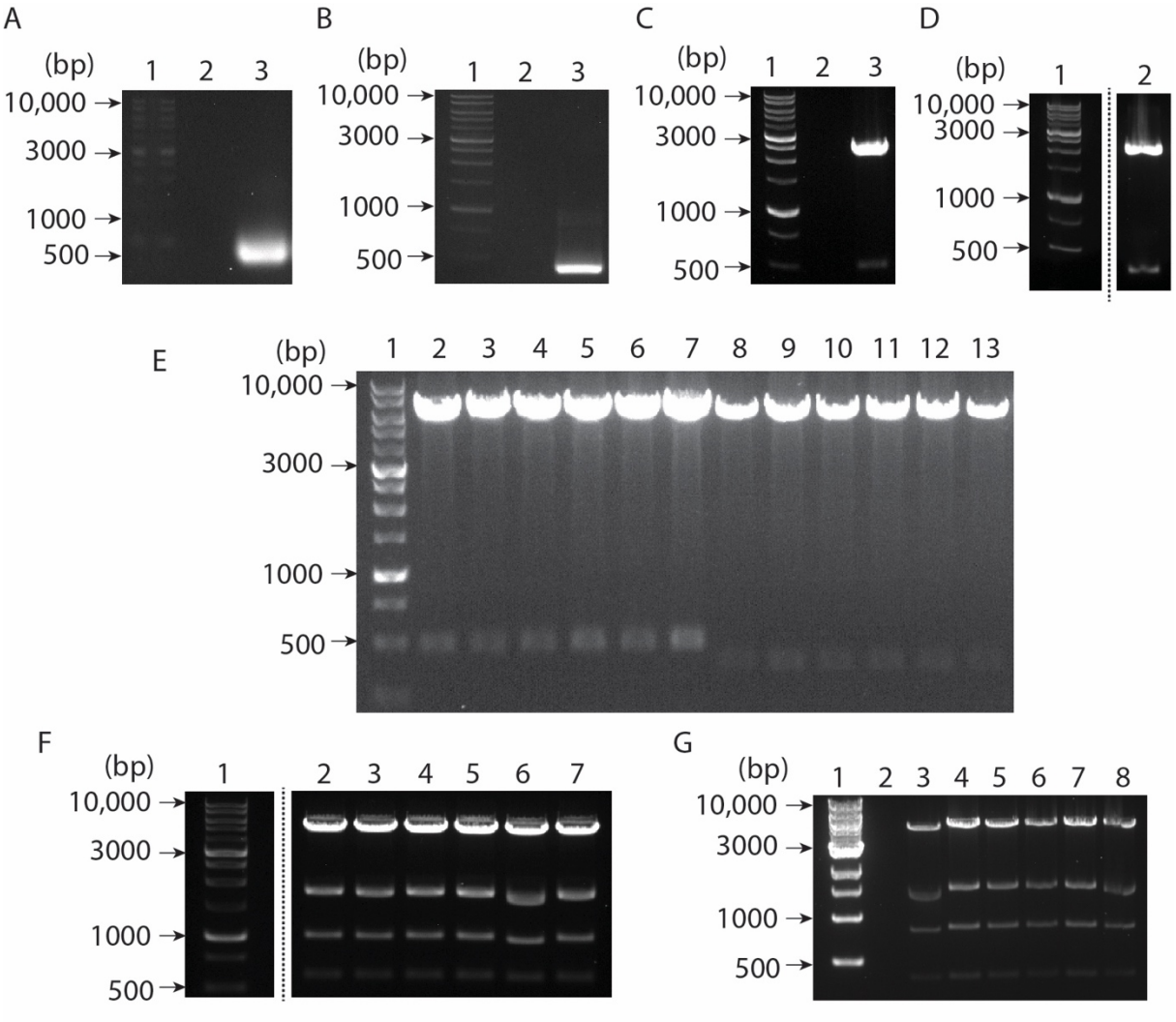

Figure 4.1 Agarose gel electrophoresis to demonstrate stages of vector construction
Ladder is always shown in lane 1. A; PCR amplification of MmuPV1 E6 with HA tag, expected size was around 500bp. Lane 2 – empty, lane 3 shows PCR amplification of E6. B; PCR amplification of MmuPV1 E7 with FLAG tag, expected size was around 400bp. Lane 2 – empty, lane 3 shows PCR amplification of E7. C; BsrG1 RE digest of MmuPV1 E6 after insertion into pDONR221 entry vector. Expected band sizes were around 500bp for the insert and around 2000bp for the remaining backbone. Lane 2 – empty, lane 3 – BsrG1 digest. D; BsrG1 RE digest of MmuPV1 E7 after insertion into pDONR221 entry vector. Expected band sizes following RE digestion were around 400bp for the insert and around 2000bp for the remaining backbone. E; BsrG1 RE digests of MmuPV1 E6 LXSN vector and MmuPV1 E7 LXSN vector. Expected band sizes were around 6000bp for LXSN, 500bp for E6, and 400bp for E7. Lanes 2-7: replicates of MmuPV1 E6 LXSN construct. Lanes 8-13: replicates of MmuPV1 E7 LXSN construct. F; BsrG1 RE digests of MmuPV1 E6 PQCXIN constructs. Expected band sizes following RE digestion were around 5000bp, 1500bp and 1000bp for PQCXIN, and around 500bp for E6. G; BsrG1 RE digests of MmuPV1 E7 PQCXIN constructs. Expected band sizes following RE digestion were around 5000bp, 1500bp and 1000bp for PQCXIN, and around 400bp for E7.

Wizard SV Gel and PCR Clean-Up kit (Promega, UK), gateway cloning technology (ThermoFisher, UK) was then utilised to insert the desired sequences into pDONR221 entry vector plasmids, to generate donor plasmids for the subsequent reaction. Success of this reaction was confirmed by BsrG1 restriction enzyme (RE) digestion of the resulting construct, shown in Figure 4.1C (MmuPV1 E6) and Figure 4.1D (MmuPV1 E7). Entry vector pDONR221 is 4762bp. Band sizes were as expected following digestion with Bsrg1; inserts were around 500bp, and total vector size following successful insert of the desired sequence is around 2000bp. A BP reaction was then carried out to transfer the desired inserts from the pDONR221 entry vector into selected vectors pLXSN and pQCXIN. Following this BP reaction, pLXSN and pQCXIN constructs were once again subjected to BsrG1 RE digestion to check correct insertion of E6 and E7 tagged sequences as shown in Figure 4.1E (MmuPV1 E6 and E7 LXSN), Figure 4.1F (MmuPV1E6 pQCXIN) and Figure 4.1G (MmuPV1 E7 pQCXIN). Band sizes for pLXSN vector RE digests were expected to be around 6000bp, 500bp for E6, and 400bp for E7. BsrG1 RE digests of pQCXIN vectors were expected to show bands with sizes that were around 5000bp, 1500bp and 1000bp for pQCXIN, with 500bp for E6, and 400bp for E7. The expected sizes were observed in all cases, and following Sanger sequencing it was confirmed that the sequences had been correctly inserted into the expression vectors with no base pair mutations (Eurofins, UK).

An HA tag was present in the E6-containing vectors to allow detection of the protein by western blot to confirm expression. Similarly, a FLAG tag was present in the E7-containing vectors to allow detection via western blot. Further, these tags would allow any future use of cell lines in immunoprecipitation (IP) assays. pQCXIN constructs were transiently transfected into 293TT cells to allow detection of expression of E6 and E7 protein via their respective tags, as shown in Figure 4.2A. An HA tagged HPV1 construct designed by another member of the lab (Ke Zheng, 2019 unpublished) was used as a positive control during western blotting. When this experiment was attempted with the proteins expressed in the LXSN vectors, it was not possible to detect the proteins by western blotting, or by IP. Therefore, successful expression in the LXSN constructs was further tested using RT-PCR to confirm the presence of RNA transcripts, as shown in Figure 4.2B. GAPDH primers were used to confirm cells were present and that cDNA synthesis had been successful. MmuPV1 E6 primers were used to detect E6 expression, which were amplified in the NIKS/MmuPV1E6-LXSN and NIKS/MmuPV1E6^{R130A}-LXSN cells, and negative in NIKS/MuPV1E7-LXSN and NIKS/LXSN cells. Similarly, MmuPV1 E7 primers were used to detect E7 expression, which was negative in the NIKS/MmuPV1E6-LXSN, NIKS/MmuPV1E6^{R130A}-LXSN, and

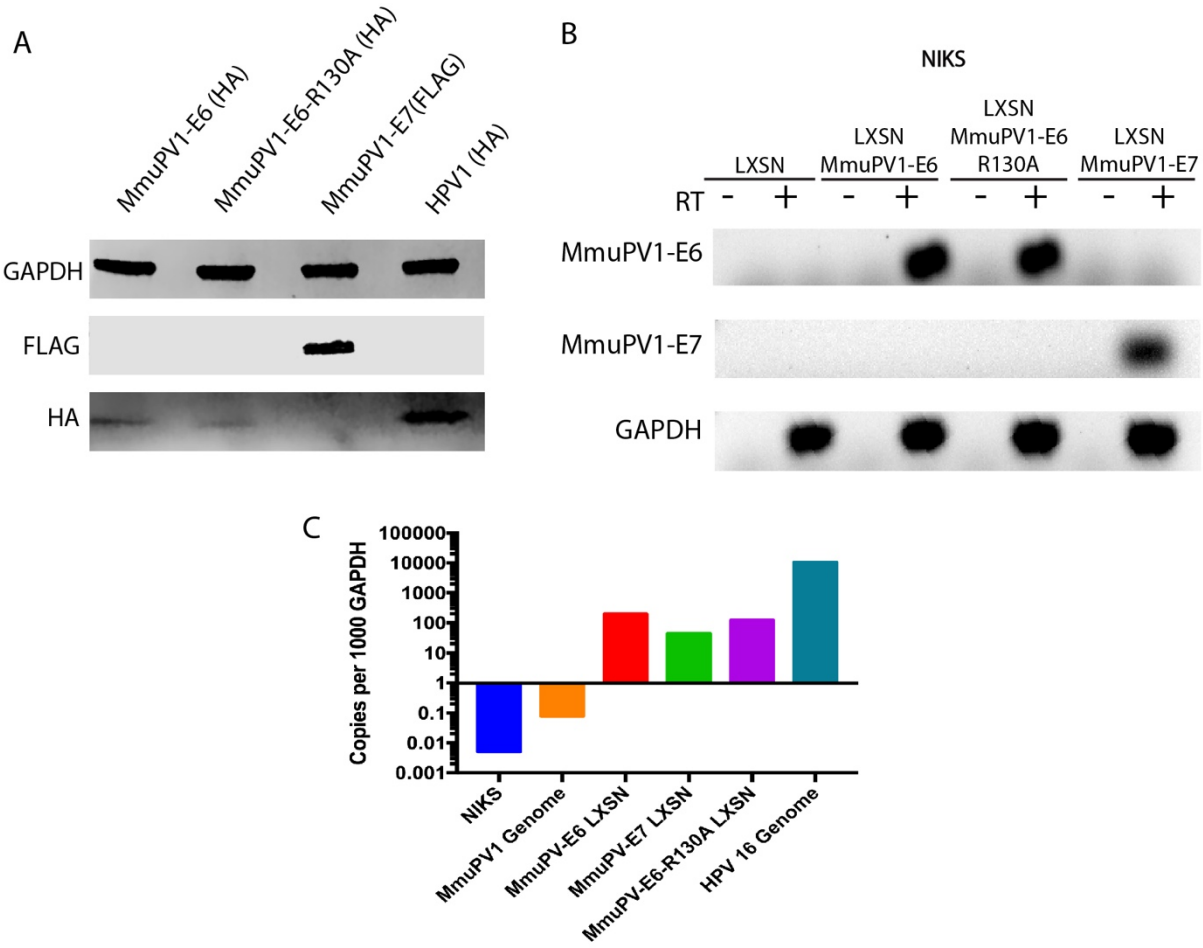

Figure 4.2 Validation of cell lines exogenously expressing key viral proteins
A; Expression of protein in cells was validated by transient transfection of PQCXIN constructs into 293TT cells and Western Blotting of protein samples to show presence of expressed protein. Expression of HA tagged protein can be seen in MmuPV1 E6, MmuPV1 $E6^{R130A}$, and HPV1 E6 samples, but not in MmuPV1 E7. Conversely FLAG tagged protein was only detected in MmuPV1 E7 samples, and not in the other three. B; Expression in LXSN, MmuPV1 E6 LXSN, MmuPV1 $E6^{R130A}$ LXSN, and MmuPV1 E7 LXSN was confirmed at the RNA level following cDNA synthesis from each sample, PCR and gel electrophoresis to check presence of bands for each sample. A reverse transcriptase (RT) negative control was included for each sample (cDNA synthesis was run without addition of RT enzyme). C; Viral transcripts from NIKS, MmuPV1 expressing NIKS, NIKS/MmuPV1E6-LXSN, NIKS/MmuPV1E7-LXSN, NIKS/MmuPV1$E6^{R130A}$-LXSN and HPV16 expressing NIKS grown to sub-confluence were examined following cDNA synthesis and subsequent qPCR analysis. For quantification of MmuPV1-E7 LXSN copies, a MmuPV1 E7-specific qPCR probe was used. For quantification of HPV16 genome copies, a HPV16 E4-specific qPCR probe was used. The remaining samples were quantified using a MmuPV1 E6-specific qPCR probe. Details of qPCR probes used can be found in 2.5.12. Data shows the activity of the early promoter in each case and quantity was normalised to copies per 1000 GAPDH.

NIKS/LXSN cells, and amplified in NIKS/MmuPV1E7-LXSN cells. RT-negative controls were included for each sample to further validate the synthesis of cDNA. qPCR of cDNA transcripts was employed to quantify the relative expression of RNA in the NIKS cell lines versus expression from a cell line transfected with the MmuPV1 genome to estimate early promoter activity. Results showed that levels of expression of target RNA from the LXSN vector were substantially higher than what was observed in cells transfected with MmuPV1 genome, as shown in Figure 4.2C. Previous data from our lab has suggested that NIKS cells may not be able to support high expression of HPV11 E6 and E7; activity of the HPV11 early promoter (p90) was relatively low in NIKS, when compared to that of the HPV16 early promoter (p97) (Murakami, Egawa et al. 2019), which was much higher and is also shown in Figure 4.2C for comparison. These data demonstrated that PV promoter activity in NIKS can vary widely. Therefore, although expression of MmuPV1 E6 and E7 RNA in LXSN cell lines appears to be higher than expression levels from MmuPV1 genome, these levels of expression from LXSN may still be biologically relevant. It is also plausible that other factors could impact upon the levels of protein expression from the promoter. For example, altering codon usage has been previously shown to result in increased mRNA stability and subsequent alterations in L1 protein expression (Collier, Goobar-Larsson et al. 1998). Expression levels of HPV16 genome in NIKS cells is substantially higher, which may reflect that NIKS could be a more appropriate cell host for this high-risk PV type. As such, it was considered reasonable to progress with experiments whilst remaining aware that exogenous levels of protein expression might not be a completely accurate reflection of expression levels *in vivo*. Validation of an E6 mutant (NIKS/MmuPV1E6^{R130A}-LXSN) was also shown in this figure, which will be discussed later.

4.2.2 Cells exogenously expressing MmuPV1 E6 are able to grow to higher densities than both LXSN and MmuPV1 E7 expressing cells

As an increase in cell density and cell proliferation had been quantified *in vivo*, 2D monolayer growth assays were carried out to establish the role of each protein *in vitro,* as shown in Figure 4.3A. From days one to three, before cells had reached confluence, there was no significant difference in the growth of cells across all three groups. At day four, when the cells had just reached confluence, the number of NIKS/MmuPV1E6-LXSN cells was significantly greater than NIKS/MmuPV1E7-LXSN cells (**$p \leq 0.01$) indicating a slight E6-mediated proliferative advantage over the other groups. At day seven there was no significant difference between the number of NIKS/LXSN and NIKS/MmuPV1E7-LXSN cells, which

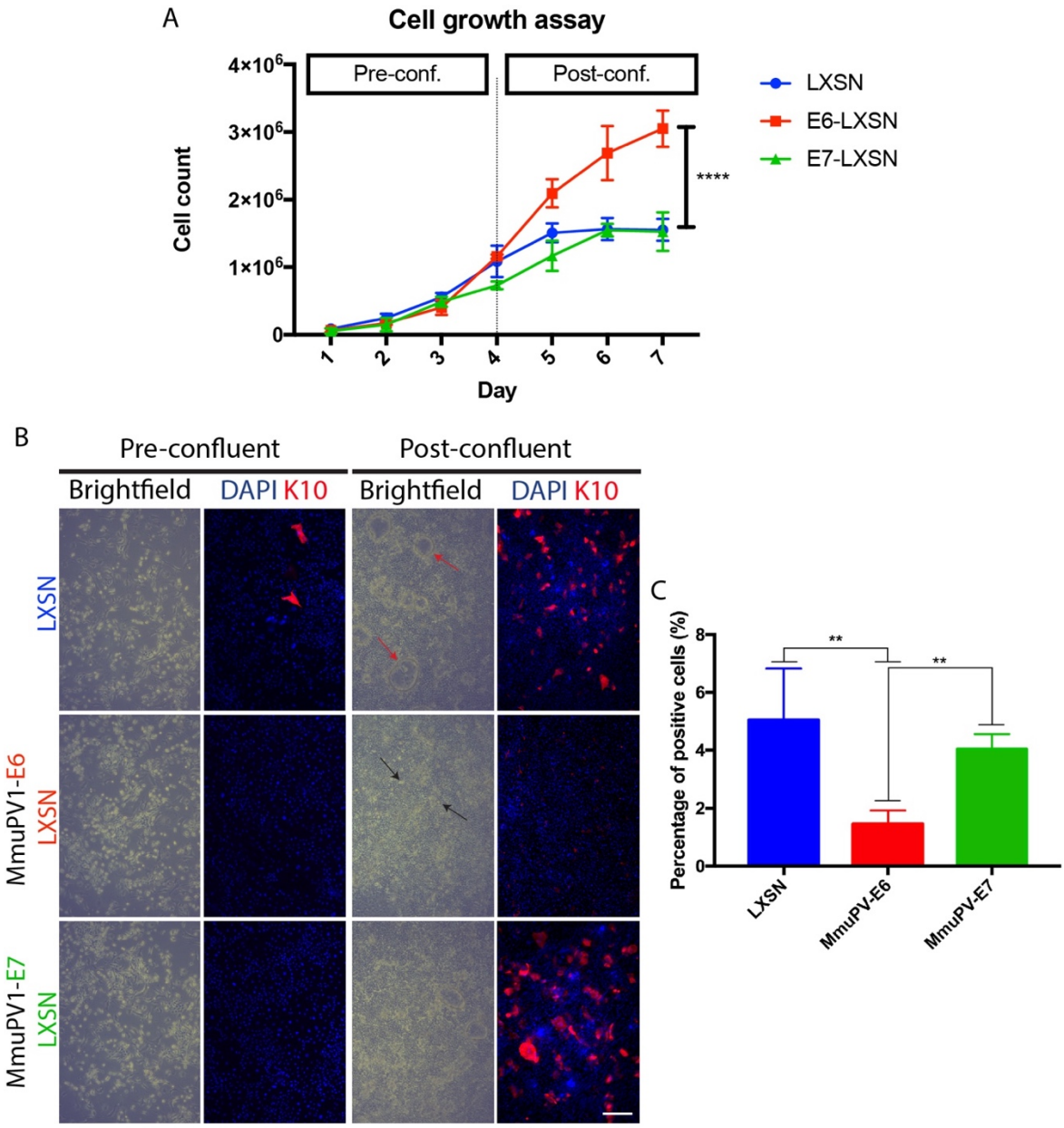

Figure 4.3 Exogenous expression of MmuPV1 E6 LXSN leads to higher cell density and differentiation delay

A; NIKS/LXSN, or NIKS expressing MmuPV1 E6 or E7 were counted in triplicate every day. Cells were pre-confluent at 3 days, confluent at 4 days, and post-confluent by day 5. Three independent experiments, n=3. P-values were calculated with a two-way ANOVA with Tukey's correction; **** = $P \leq 0.0001$. three independent experiments, n=3. B; Cells were stained with K10 (red) at both pre-confluence (day 3) and post-confluence (day 7). Panels show IF detection of K10 at these time points for each cell population. Nuclei were counterstained with DAPI to show host DNA. Scale bar: 100 µm. Light microscope images for each time point are also shown. Red arrows denote presence of ring-like structures in cell monolayer morphology. Black arrows denote the presence of bright, rounded cells. C; Quantification of the number of cells positive for K10 per microscope field at 5X magnification was carried out for each cell population. Number of K10 positive cells was then normalised to number of cells per field in each population to give a percentage of positive cells. Two independent experiments, n=5. P-values were calculated with Kruskal-Wallis test with Dunn's correction; * = $P \leq 0.05$, ** = $P \leq 0.01$. Error bars, SD.

reached $1.55x10^6$ and $1.53x10^6$ cells respectively. In contrast, NIKS/MmuPV1E6-LXSN cells reached $3.1x10^6$ cells, a significantly higher density when compared to the other two groups (****$p \leq 0.0001$). NIKS/MmuPV1E6-LXSN cells are able to grow to much higher cell densities than NIKS/LXSN and NIKS/MmuPV1E7-LXSN cells, demonstrating that MmuPV1 E6 plays an important role in maintaining the proliferative capacity of the cells beyond confluence.

As shown in brightfield images (Figure 4.3B), the morphological appearance of the NIKS/LXSN cells by day 7 was deemed to be highly differentiated due to the ring-like structures often observed within our model in differentiating cultures (shown with red arrows), whereas in NIKS/MmuPV1E6-LXSN cells the small, bright, rounded cells are indicative of cells that are still undergoing replication (denoted with white arrows). Analysis of K10 staining in all three populations indicated that at low densities almost all cells lacked K10. However, at high density, while NIKS/LXSN and NIKS/MmuPV1E7-LXSN cells showed a similar level of K10 expression per field, NIKS/MmuPV1E6-LXSN cells had noticeably lower expression levels of K10. This shows that the effect of MmuPV1 on differentiation seen *in vivo* is also observed in the cell culture model, and that it is reasonable to postulate that MmuPV1 E6 is responsible for this phenotypic change. Quantification analysis of the number of K10 positive cells per field was carried out on randomly selected fields (n = 5) in each category. Analysis showed that when data was normalised by the total number of cells per field to calculate the percentage of positive cells per field, there was a statistically significant decrease in the percentage of K10 positive cells per field (**$p \leq 0.01$) in NIKS/MmuPV1E6-LXSN cells when compared to the other two groups. These results are shown in Figure 4.3C.

4.2.3 Discrete layers of cells exist in monolayer cell culture assays and these can be discerned by using confocal microscopy

During experimentation with K10 staining, it was noted anecdotally that in normal NIKS cells, cells that stained positive for K10 often had noticeably differing morphology, wherein the K10 positive cells appear large and possibly flatter than cells that are K10 negative. As such, a more thorough investigation of this morphology was carried out by staining post-confluent normal NIKS samples for K10, and examining the samples using confocal microscopy. As demonstrated in Figure 4.4, not only do we see that K10 positive cells do indeed have a flatter morphology, it was possible to discern two discrete layers of cells. Cells

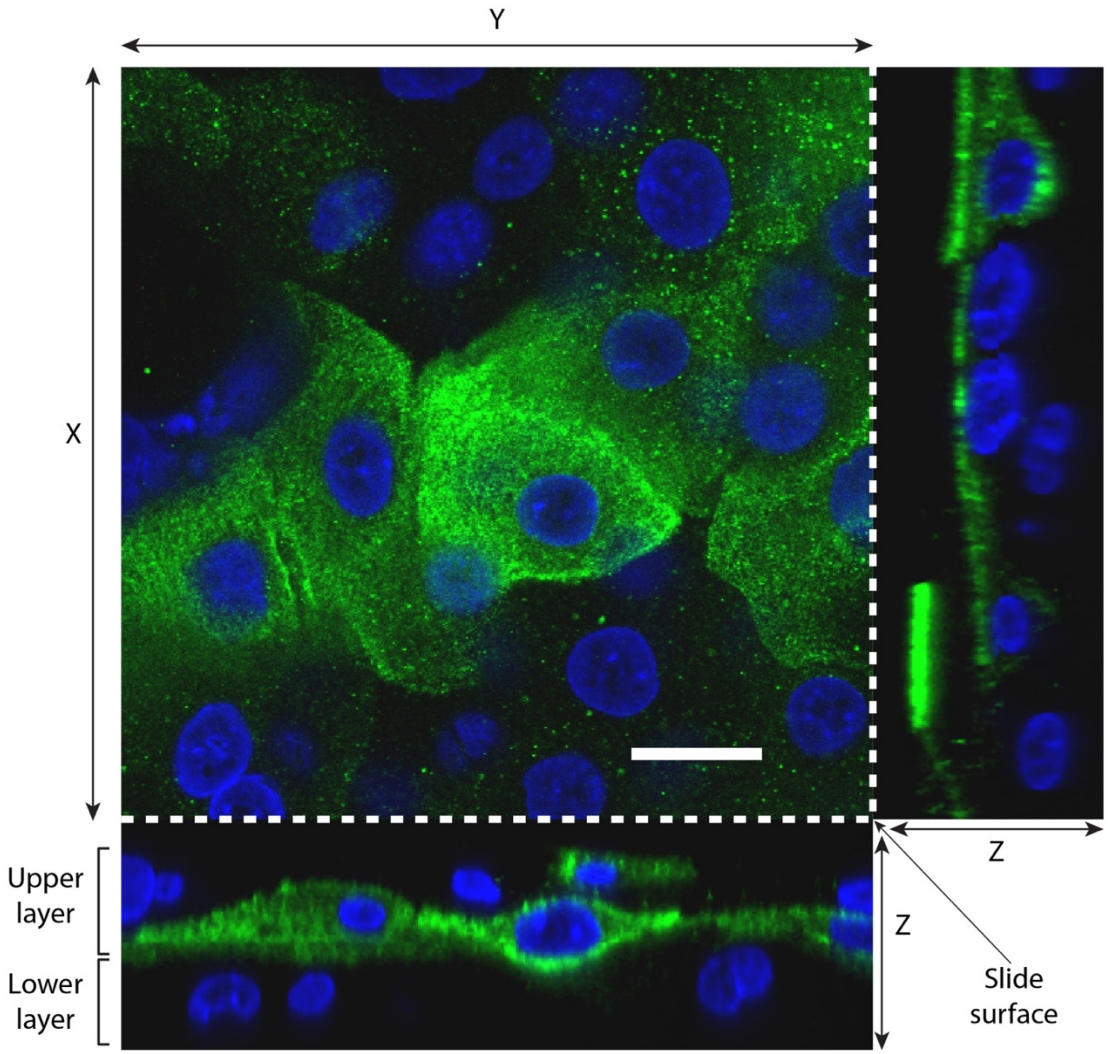

Figure 4.4 Confocal microscopy shows distinct biologically important layering of cells
Confocal microscopy Z-stacked image of NIKS cells at day seven cultured in medium with 10ng/ml EGF. K10 positive cells are shown in green, and nuclei were counterstained with DAPI to show host DNA. Central square image shows surface layer of cells from z stack cross section. Below and to the right of this image, cross sections down both sides of these cells are shown. A layer of K10 negative cells can be seen, forming a lower layer. The cells in the upper layer show some cells staining positive for K10. Scale bar: 20 μm.

in the lower layer were largely negative for K10 staining, whereas cells in the upper layer were predominantly K10 positive. This revealed a critical aspect to our monolayer culture system, demonstrating that cells behaved differently in these discrete layers within monolayer culture. It was postulated that this layering of cells could allow a rough recapitulation of the basal layer and the parabasal layer *in vivo,* and that important protein functions might be discerned through more thorough analysis of cell populations in this manner. As work previously described in Chapter 3 showed that infected cells could be persisting in the basal layer by overcoming normal density restrictions, it was decided that growth characteristics would be observed by generating a set of fluorescent cell lines for competition assay analysis.

4.2.4 Generation of cell lines expressing fluorescent proteins

To investigate the idea of the preferential persistence of infected cells in the basal layer *in vivo* leading to the increased density observed as lesions first begin to form, fluorescent NIKS/LXSN, NIKS/MmuPV1E6-LXSN and NIKS/MmuPV1E7-LXSN cell lines were generated to observe their relative cell growth characteristics over time in a cell competition assay system. Construction of the cell lines is shown diagrammatically in Figure 4.5. First, early passage NIKS cells were cultured in normal conditions until sub-confluent. Cells were then split into two populations. Each population was then transduced to express either EGFP, for a green fluorescent cell line, or mCherry, for a red fluorescent cell line. Next, cells were transduced with appropriate vectors. It was decided that the green cells should act as the control population, and so this population was transduced with LXSN only (NIKS/LXSN EGFP). In tandem, mCherry cells were split into three flasks, to allow a control LXSN mCherry cell line (NIKS/LXSN mCherry), an MmuPV1 E6 cell line (NIKS/MmuPV1E6-LXSN mCherry), and an MmuPV1 E7 cell line (NIKS/MmuPV1E7-LXSN mCherry), to be generated separately. These cells could then be used in subsequent experiments.

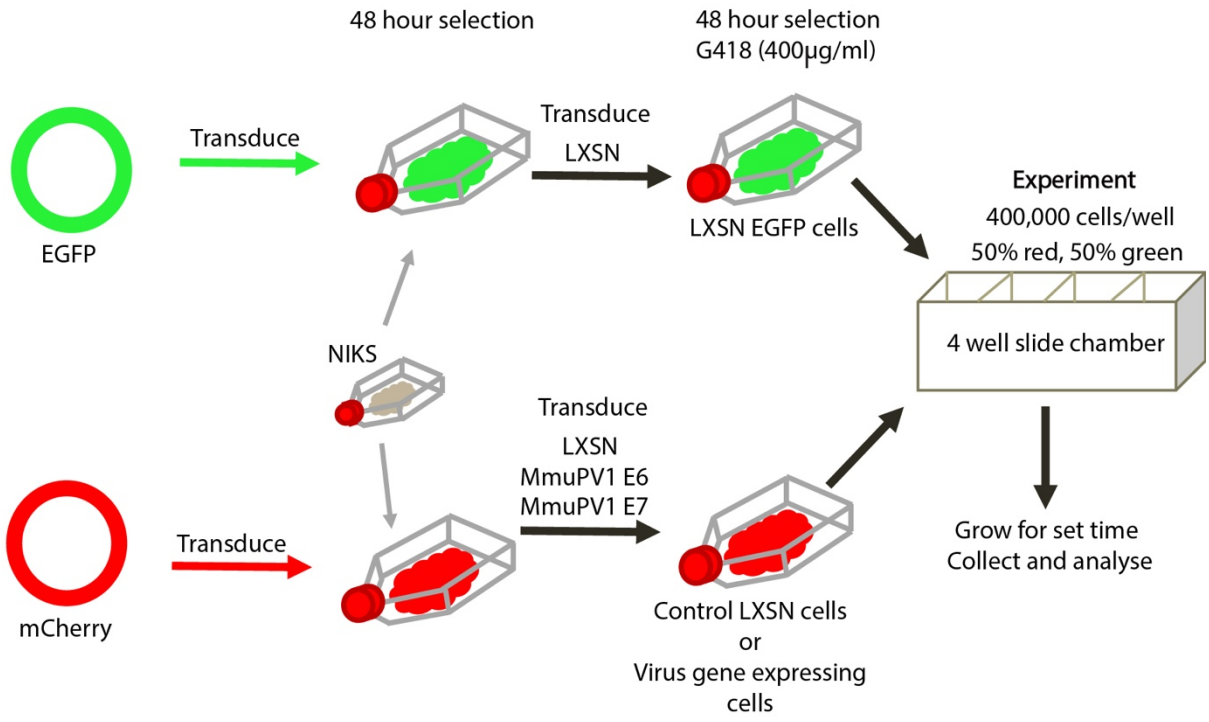

Figure 4.5 Diagram demonstrating generation of fluorescent cell lines
Fluorescence exogenous expression vectors were transduced into normal early passage NIKS cells, which were then subsequently transduced with expression vectors. EGFP cells were transduced with LXSN control vectors only. Different populations of mCherry expressing cells were transduced with LXSN, MmuPV1 E6, or MmuPV1 E7 constructs. Cells were then seeded in competition assays at a 1:1 ratio in 4 well slide chamber.

Before virus transduction to express MmuPV1 virus proteins, cell lines were observed using a fluorescent microscope following transduction to express either EGFP or mCherry. While many cells were expressing successfully, expression levels varied widely within each population, and expression was so low in some cells that it was undetectable at the highest exposures. This could be a result of random integration of the selected genes into the host genome during retroviral transduction, which can result in heterogeneous expression of the desired target gene within the resulting cell population (Bandeira, Tomas et al. 2017). Therefore, I decided that cells should be FACS sorted to allow the sub-population of cells expressing higher levels of the fluorescent proteins to be selected for subsequent experimentation. FACS sorting was carried out by Nika Romashova at the NIHR Cambridge BRC Cell Phenotyping Hub. During FACS sorting, viable cells were first gated for, as shown in Figure 4.6A and Figure 4.7A. Singlets were gated for to ensure only single cells were selected, as shown in in Figure 4.6B and Figure 4.7B. Cells were then split into four sub-populations of cells based on intensity of fluorescence as shown in Figure 4.6C and D, and Figure 4.7C and D. The lowest expressing cells were excluded entirely as cells that would be expressing little or no fluorescent protein. Then four populations comprising of approximately, 10, 20, 30 and 10% of the total population were sorted as low, low-medium, medium, and high expressing cells respectively. IF images of the resulting cell populations are shown in in Figure 4.6E and Figure 4.7E. To minimise unidentifiable cells, the highest expression levels for each group were chosen, and subsequent transduction of vectors was carried out as described above in preparation for experimentation.

4.2.5 Cells exogenously expressing MmuPV1 E6 persist in the 'lower' layer of cells in a high cell density culture environment

To investigate the impact of virus protein on cell growth mechanics and dynamics, cells were seeded at high density in 4-well slide chambers (ThermoFisher, UK), so that the different cell populations were able to grow competitively from confluence onwards. It was important to seed cells at a high density to ensure that no growth advantage conferred prior to confluence could affect the population densities. This guaranteed that any results observed were the result of cell competition within a restricted environment only. For each well, half of the population seeded were NIKS/LXSN EGFP cells, whereas the other half of the population were NIKS/LXSN mCherry, NIKS/MmuPV1E6-LXSN mCherry, or NIKS/MmuPV1E7-LXSN mCherry cells. Cells were then cultured for up to 10 days in this high-density competition assay, with the growth of these mixed cell populations being observed by confocal microscopy after collection and fixation.

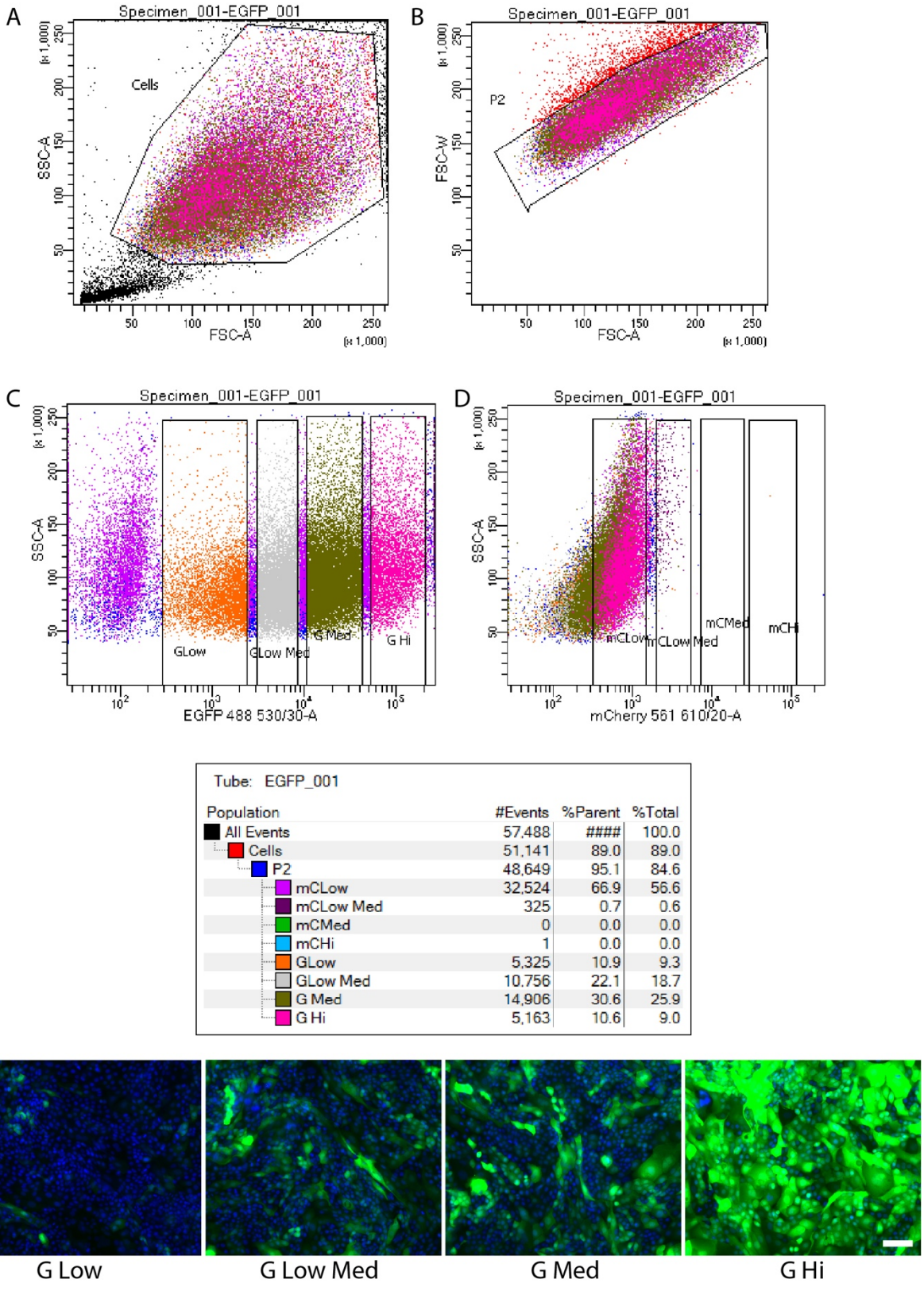

Tube: EGFP_001

Population	#Events	%Parent	%Total
All Events	57,488	####	100.0
Cells	51,141	89.0	89.0
P2	48,649	95.1	84.6
mCLow	32,524	66.9	56.6
mCLow Med	325	0.7	0.6
mCMed	0	0.0	0.0
mCHi	1	0.0	0.0
GLow	5,325	10.9	9.3
GLow Med	10,756	22.1	18.7
G Med	14,906	30.6	25.9
G Hi	5,163	10.6	9.0

Figure 4.6 FACS sorting of EGFP expressing cells
A; Cells were gated to select out any debris within the sample. B; Cells were gated to remove any doublets and to select for single cells only. C; Cells were gated for fluorescence. Both EGFP (left) and mCherry (right) fluorescence was shown. Cells were gated in the EGFP channel into four populations of low (~9%), low-medium (~19%), medium (~26%), and high levels of expression (~9%). B; Microscopy images to show levels of fluorescence in each sub-population of cells in culture following FACS sorting. Scale bar: 100 µm.

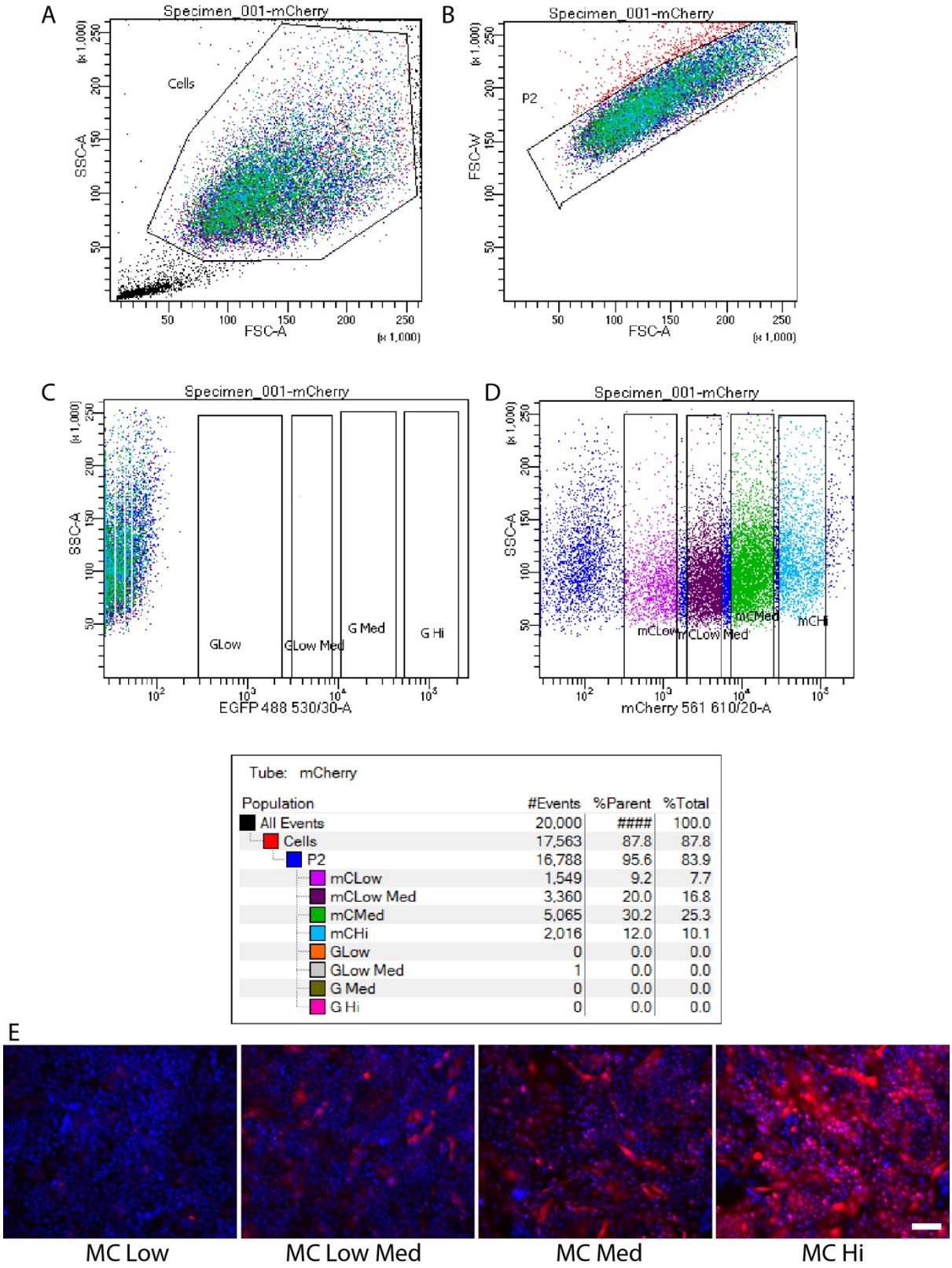

Figure 4.7 FACS sorting of mCherry expressing cells

A; Cells were gated to select out any debris within the sample. B; Cells were gated to remove any doublets and to select for single cells only. C; Cells were gated for fluorescence. Both EGFP (left) and mCherry (right) fluorescence was shown. Cells were gated in the mCherry channel into four populations of low (~8%), low-medium (~17%), medium (~25%), and high levels of expression (~10%). B; Microscopy images to show levels of fluorescence in each sub-population of cells in culture following FACS sorting. Scale bar: 100 µm.

At day one (Figure 4.8A) all three experimental groups had an approximately 50-50 ratio of red versus green cells as was expected. A slight increase in red cells in both the NIKS/LXSN EGFP cells versus NIKS/MmuPV1E6-LXSN mCherry cells (LXSN/MmuPV1E6-LXSN) group and the NIKS/LXSN EGFP cells versus NIKS/MmuPV1E7-LXSN mCherry cells (LXSN/MmuPV1E7-LXSN) group was apparent, and although not statistically significant, this may suggest a slight advantage in cell attachment over control cells. At day ten (Figure B), there were approximately 50% of each cell population occupying both the lower and upper layer of cells in the NIKS/LXSN EGFP versus NIKS/LXSN mCherry (LXSN/LXSN) group and in the LXSN/MmuPV1E7-LXSN group. The lower layer was selected by raising the scanning level of the confocal microscope until the first layer of nuclei were apparent and the focus line was approximately half way through these cells. The upper layer of cells was determined to be at a scanning level approximately 10 μm higher than the first layer; this distance was then kept consistently across all experiments. Conversely within the LXSN/MmuPV1E6-LXSN group, the vast majority of cells occupying the lower layer of cells in culture were NIKS/MmuPV1E6-LXSN mCherry cells (92.59% red cells), whilst the upper layer of cells consisted almost entirely of NIKS/LXSN EGFP cells (94.28% green cells). This suggested that NIKS/MmuPV1E6-LXSN mCherry cells were preferentially persisting in the lower layer of cells.

To observe these phenotypes in 3D, z-stacks of areas of cells manually selected for high density were constructed. Figure 4.9A shows a maximum intensity side view of orthologue plots for each of the cell populations. This again demonstrates that in the LXSN/LXSN and LXSN/MmuPV1E7-LXSN groups, cells expressing EGFP or mCherry can be seen distributed in roughly equal measure in both layers. Conversely, in the LXSN/MmuPV1E6-LXSN group, a lower layer of mCherry expressing cells can clearly be seen, whilst the upper layer consists of almost exclusively EGFP expressing cells. Finally, the pattern of expression of EGFP and mCherry is quantified in Figure 4.9B, shown as the levels of fluorescence intensity against distance from the bottom of the slide. Data shows that in the LXSN/MmuPV1E7-LXSN and LXSN/LXSN groups, there are roughly equal levels of mCherry and EGFP fluorescent intensity in both layers. Conversely, in the LXSN/MmuPV1E6-LXSN group, there is a clear pattern of higher mCherry fluorescent expression in the lower layer, and EGFP fluorescent expression further away from the surface of the slide in the upper layer. Taken together, this data shows that expression of MmuPV1 E6 affords the cell a growth advantage over the control cell population to remain in the lower layer when in direct competition for space. This competitive advantage was not seen in the NIKS cells exogenously expressing MmuPV1 E7.

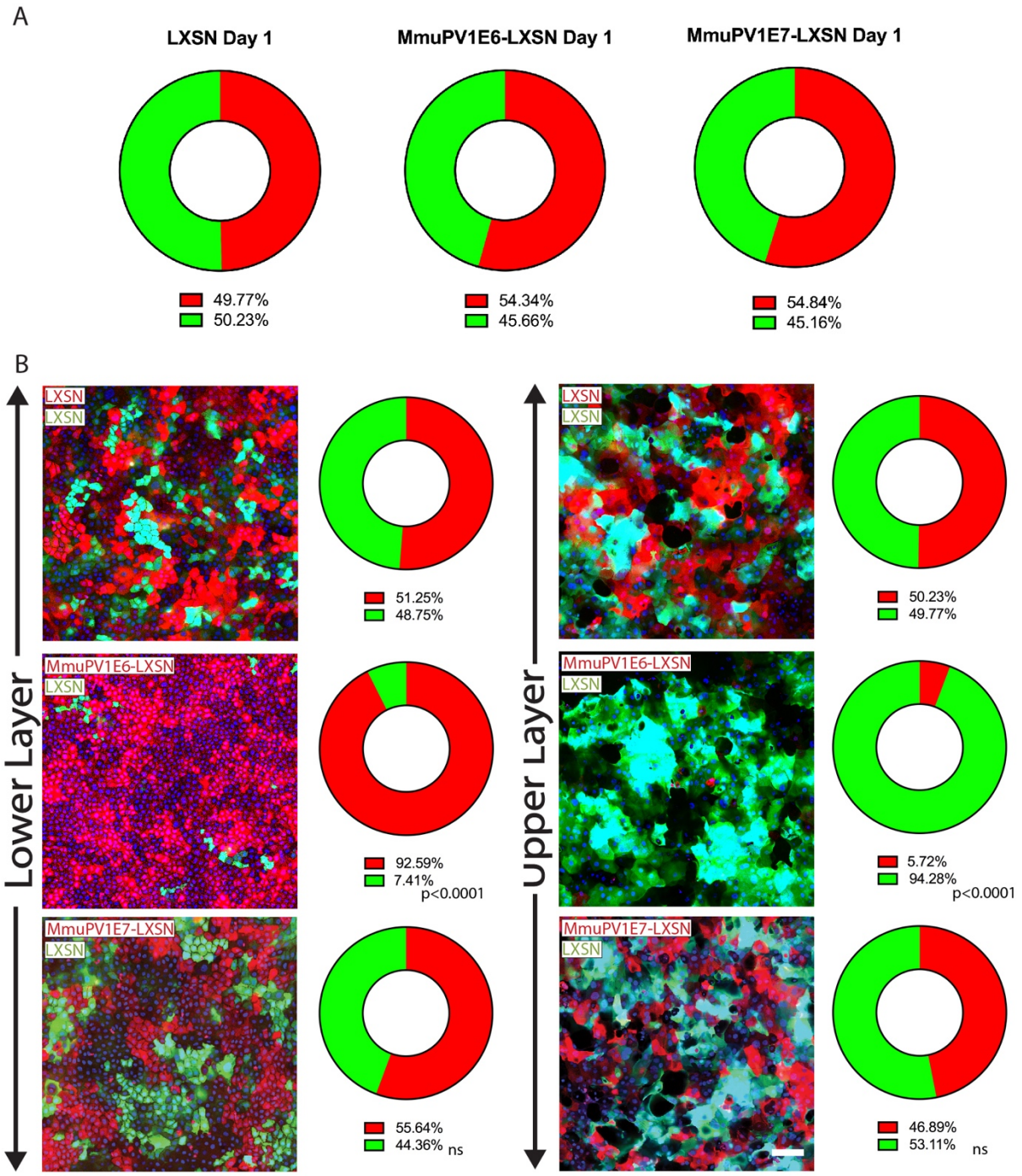

Figure 4.8 NIKS exogenously expressing MmuPV1 E6 preferentially persist in the lower layer of cells in a high-density competition assay

A; Proportions of cells at day 1 are shown with representative parts of a whole graphs. B; IF of LXSN/LXSN, LXSN/MmuPV1E6-LXSN, and LXSN/MmuPV1E7-LXSN. Cell population identity is indicated by colouring of text in the upper left corner of each image. Nuclei were counter-stained with DAPI for host DNA. Lower layer panels are shown to the left, alongside parts of a whole graphs to demonstrate quantitative data. Upper layer panels and accompanying parts of a whole graphs are shown to the right. IF images shown are confocal microscope tile scan images taken at 40X magnification with 5 by 5 fields. Two independent experiments, n=5. Experimental groups were compared with LXSN/LXSN control groups, and P-values were calculated with a two-way ANOVA with Sidak's multiple comparisons test; **** = $P \leq 0.0001$. Scale bar: 100 μm.

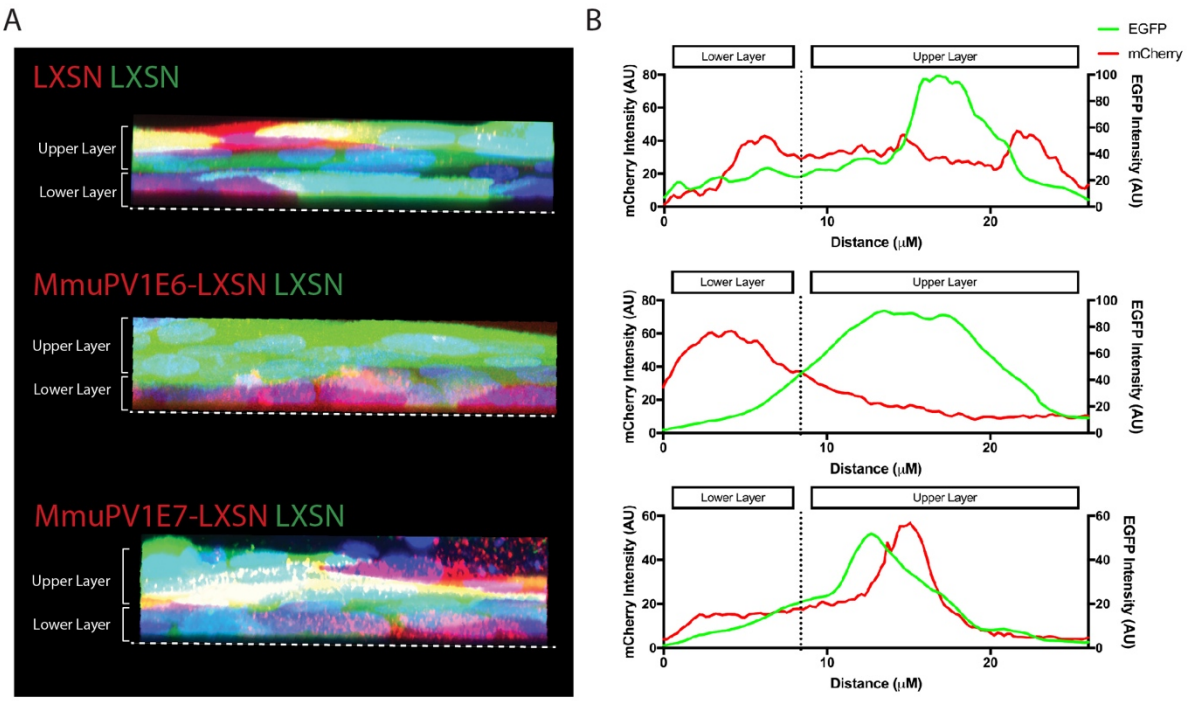

Figure 4.9 3D Maximum intensity plots demonstrate persistence phenotype
A; Maximum intensity 3D plots of z-stacks at 63X magnification are shown for each of the three groups. Annotations show the location of the lower and upper layers. White dotted lines indicate the bottom of the slide glass on which the cells are cultured. The nuclei were counter-stained with DAPI for host DNA. B; The fluorescent intensity of each channel was quantified across 8 different selections of three different z-stack images taken at 63X magnification for each group, and the average intensity has been plotted against distance from the bottom of the slide upward to demonstrate the distribution of fluorescence throughout the z-stack.

4.2.6 Density in the lower layer of MmuPV1 E6 expressing cells is increased

To examine the growth advantage in this lower layer in more detail, NIKS/LXSN, NIKS/MmuPV1E6-LXSN, and NIKS/MmuPV1E7-LXSN cells were cultured to high density in isolation, without competition with another cell population. Quantitative analysis of the lower layer of cells in each of these groups was carried out at day ten, as shown in Figure 4.10A. Data demonstrated that at day ten, NIKS/MmuPV1E6-LXSN mCherry cells reached a significantly higher density in the lower layer of cells when compared to the separately grown NIKS/LXSN mCherry cells and the NIKS/MmuPV1E7-LXSN mCherry cells. Further to our previous result showing an increased density in NIKS/MmuPV1E6-LXSN cell culture, this data indicated that there is an increase in cell density specifically within the lower layer. This quantification of lower layer cell density for all three cell populations was repeated at a day seven time point. When comparing the fold change in lower layer density from day seven to

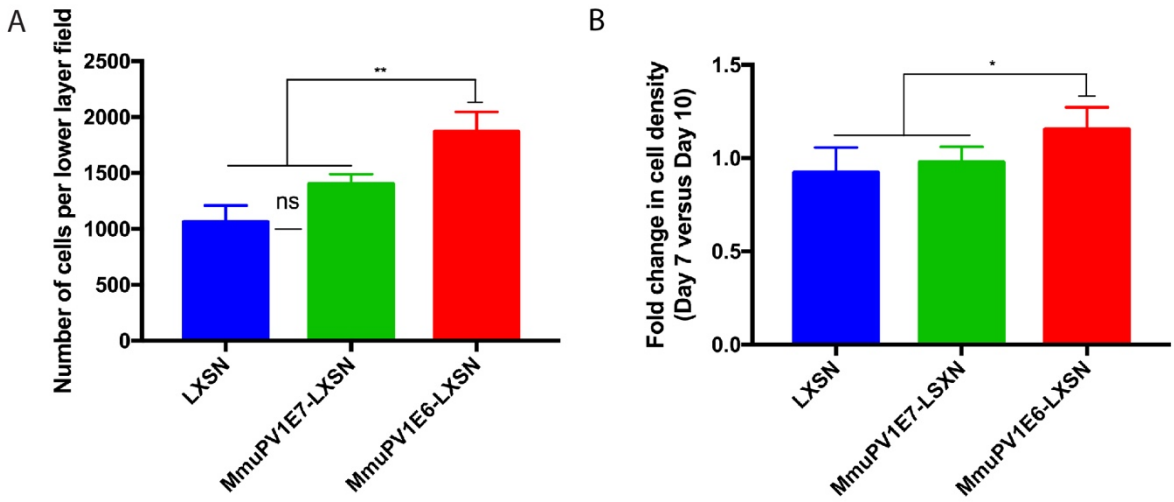

Figure 4.10 Differences in cell density of the 'lower' layer of cells
A; Quantification of the number of cells in the bottom layer of each population (field size: 800.22x800.22 μm). Five random 5 by 5 tile scans were chosen for quantification for each category. Quantification was carried out using the analyse particles function in FIJI image analysis software. B; Samples were analysed in the same manner at a day 7 timepoint. Five random 5 by 5 tile scans were chosen for quantification for each category. Quantification was carried out using the analyse particles function in FIJI image analysis software. Fold change between day 7 and day 10 was calculated. Two independent experiments, n=3. P-values were calculated with Kolmogorov-Smirnov t-tests; ** = $P \leq 0.01$.; * = $P \leq 0.05$.

day ten (Figure 4.10B), NIKS/LXSN mCherry cells and NIKS/MmuPV1E7-LXSN mCherry cells show no significant change in the density of the bottom layer of cells, whereas the fold change in NIKS/MmuPV1E6-LXSN mCherry cell density in the bottom layer of cells is significantly increased. Firstly, these data corroborate earlier results both *in vivo* and *in vitro* that demonstrated that MmuPV1 E6 expressing cells can grow to higher cell densities than control cells. Secondly, these data also suggest that increased basal cell density observed in the early mouse lesions in Chapter 3.0 was due primarily to MmuPV1 E6 expression. In addition, while not significantly denser, MmuPV1 E7 may also confer a mild growth advantage in this bottom layer; the number of cells in the bottom layer of NIKS/MmuPV1E7-LXSN cell culture was higher than the NIKS/LXSN cell population, although not statistically significantly so. Finally, these data could suggest that it is not just the density of cells in the bottom layer affected, but the rate at which cells are exiting this bottom layer. To further understand the molecular pathways involved in directing this particular competitive advantage of MmuPV1 E6-expressing cells, a mutant of MmuPV1 E6 was generated.

4.2.7 Generation of a *MAML1* binding deficient *MmuPV1 E6* mutant

Previously published research into the similarities between MmuPV1 E6 and HPV8 E6 interactions with the Notch pathway confirmed that MmuPV1 E6 was able to bind to MAML1, and that this interaction delayed differentiation in Ca^{2+} treated keratinocytes (Meyers, Uberoi et al. 2017). It was shown that an E6 MAML1 binding mutant could not inhibit Notch signalling and that this mutant was unable to form papillomas *in vivo*. MAML1 is a Notch receptor transcriptional co-activator (Wu, Aster et al. 2000) and Notch is known to be involved in normal terminal differentiation of keratinocytes (Mumm and Kopan 2000). As such, it was postulated that this pathway may be involved in the phenotype observed in the high-density competition assay, and that similar interference with MmuPV1 E6 MAML1 binding in this model could indicate whether the downstream Notch signalling pathway was involved in modulation of the persistence phenotype. Therefore, a MAML1 binding mutant of MmuPV1 E6 was generated. A single point mutation termed R130A was introduced to the MmuPV1 E6 sequence such that binding to the protein was disrupted. Previously published data showed that mutation of this site resulted in disruption of E6 binding to MAML1 (Meyers, Uberoi et al. 2017). Meyers and colleagues chose putative LXXLL contact residues as the site of mutation; interaction with MAML1 by MmuPV1 E6 was shown to occur via these residues. PCR amplification using the existing NIKS/MmuPV1E6-LXSN plasmid was carried out with primers designed to introduce the point mutation at the site of interest. Primers are shown in Chapter 2 (Table 2.10).

RE digestion with BsrG1 was used to isolate the $E6^{R130A}$ fragment, as shown in Figure 4.11A. Gateway cloning technology was then utilised to insert the mutant construct into a pLXSN and pQCXIN vector. RE digestion with BsrG1 confirmed the correct sizes of bands were present when run on an electrophoresis gel, demonstrating that the construct had been successfully inserted into the vector, as shown in Figure 4.11B and Figure 4.11C. Prior to this, $E6^{R130A}$ fragment DNA samples were sequenced, and resulting sequence data was aligned with wt MmuPV1 E6 DNA (Figure 4.11D) utilising data and algorithms of the National Center for Biotechnology Information, by using the Basic Local Alignment Search Tool (https://blast.ncbi.nlm.nih.gov/Blast.cgi) (Mus musculus papillomavirus type 1 viral protein E6 mRNA, complete cds Sequence ID: MF350298.1, Length: 423) (Zhang, Schwartz et al. 2000). Subsequent sequencing alignment data showed that the two sequences were a 99% match, with only 2 mismatches found. As shown with further visualisation of these data

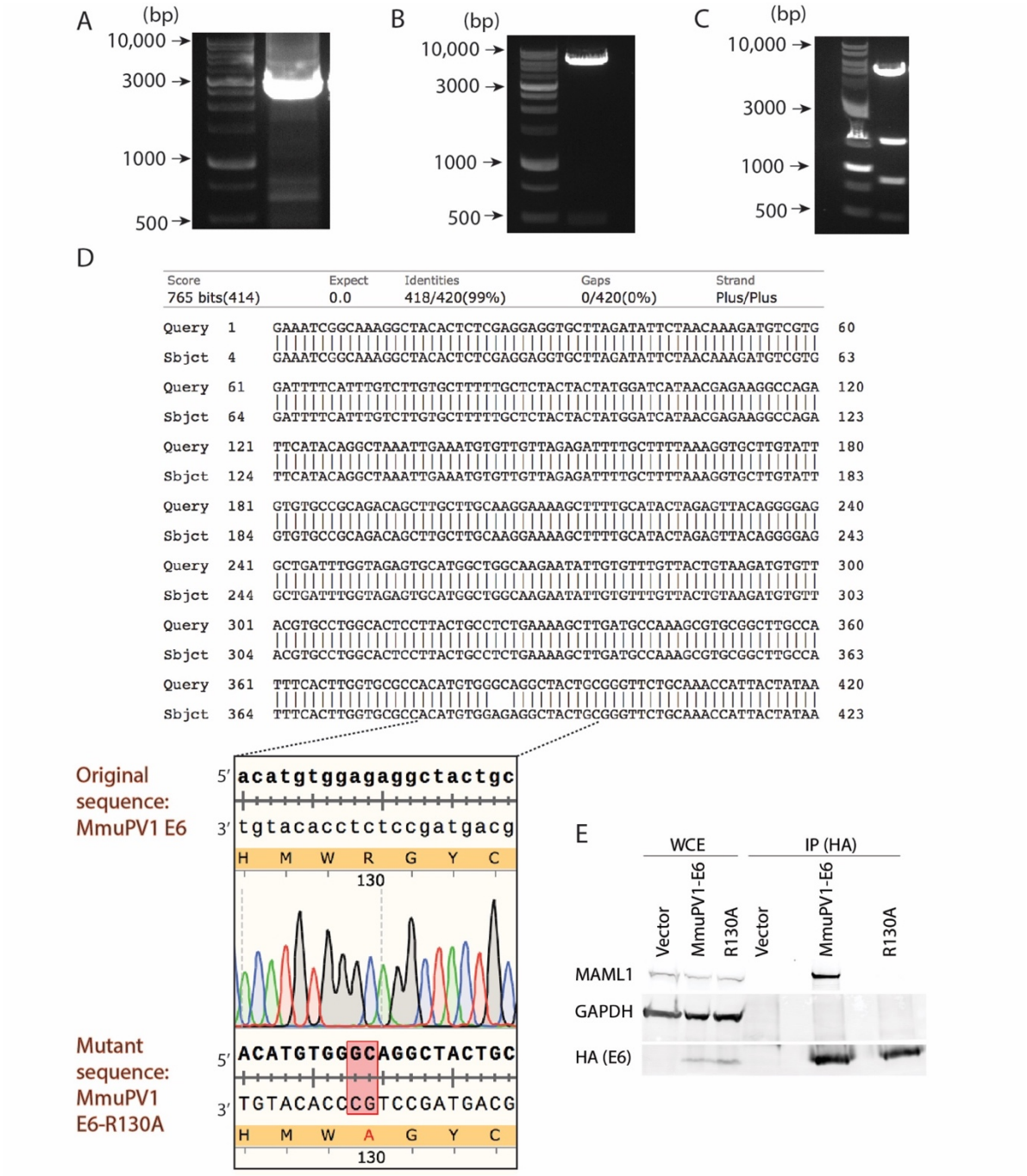

Figure 4.11 Construction of MAML1 binding deficient MmuPV1 E6
Ladder always shown in lane 1. A; PCR amplification of MmuPV1 E6^{R130A} with HA tag from MmuPV1 E6 pDONR construct, expected size of desired band ~ 3000bp. B; BsrG1 RE digests of MmuPV1 E6^{R130A} LXSN vector. Expected band sizes ~ 6000bp for LXSN and 500bp for E6. C; BsrG1 RE digests of MmuPV1 E6^{R130A} PQCXIN vector. Expected band sizes following RE digestion were ~ 5000bp, 1500bp and 1000bp for PQCXIN, and ~ 500bp for E6^{R130A}. D; Sanger sequencing of MmuPV1 E6^{R130A} BLAST alignment with wtE6. Sanger sequencing data of MmuPV1 E6^{R130A} compared with wtE6 sequence is shown. AGA to GCA observed at desired site with DNA of good quality. E; Lysates of 293TT cells expressing HA-tagged wt or mutant MmuPV1 E6 protein were subjected to an HA IP. Immunoprecipitated MmuPV1 E6 and associated MAML1 detected by immunoblotting. Expression levels of proteins were assessed by immunoblotting of whole cell extracts (WCE). GAPDH expression was used as a loading control.

using SnapGene, the two mismatches were base pairs AG of the original sequence being substituted for GC within a AGA codon coding for Arginine. This substitution mutation resulted in Arginine being replaced with Alanine, as intended. The substitution can be seen highlighted in a red rectangle, and the altered amino acid is shown with red text within the sequence. Sequencing data demonstrated the successful introduction of a mutation in the E6 sequence that should diminish the ability of the E6 protein to bind with MAML1 protein. An IP assay was then carried out to determine whether the NIKS/MmuPV1E6^{R130A}-LXSN mutant did have a reduced ability to bind to MAML1, in comparison with wt MmuPV1-E6 and an empty vector control. Results confirmed that the NIKS/MmuPV1E6^{R130A}-LXSN cells had a reduced ability to bind to MAML1 (Figure 4.11E). Presence of an HA-tagged protein was only detected in IP of NIKS/MmuPV1E6-LXSN and NIKS/MmuPV1E6^{R130A}-LXSN cells, and not in the empty vector control. GAPDH demonstrated similar levels of input in the whole cell extract, but was not pulled down in the IP. Validation of successful expression of the E6^{R130A} construct was shown previously in Figure 4.2.

4.2.8 MAML1 BINDING DEFICIENT MMUPV1 E6^{R130A} DOES NOT RETAIN POST-CONFLUENT GROWTH ADVANTAGE, DIFFERENTIATION DELAY, OR ABILITY TO PERSIST IN THE "LOWER" LAYER

NIKS/MmuPV1E6^{R130A}-LXSN cells were established, and a standard growth assay was carried out as shown previously in Figure 4.3. Cells were grown for seven days and sampled every day. Data showed that NIKS/MmuPV1E6^{R130A}-LXSN cells had no significant difference in cell density at day seven when compared to NIKS/LXSN cells, unlike NIKS/MmuPV1E6-LXSN cells, which grew to a significantly higher density (****$p \leq 0.0001$) by this time point (Figure 4.12A). NIKS/MmuPV1E6^{R130A}-LXSN cells also no longer showed a delay in differentiation post-confluence when stained with K10 (Figure 4.12B). Cell morphology was affected; brightfield microscopy revealed that ring-like structures were present in NIKS/MmuPV1E6^{R130A}-LXSN cell populations (shown with red arrows) similar to NIKS/LXSN cells described previously in Figure 4.3B. This suggested that NIKS/MmuPV1E6^{R130A}-LXSN cell populations were more differentiated than the wt NIKS/MmuPV1E6-LXSN cell populations. Quantification of the number of K10 positive cells demonstrated that the percentage of K10 positive cells per field was significantly lower in the population of cells expressing NIKS/MmuPV1E6^{R130A}-LXSN (**$p \leq 0.05$) when compared to the other groups. These data are shown in Figure 4.12C, which clearly demonstrates that the delay in differentiation observed and quantified in NIKS/MmuPV1E6-LXSN cells is lost upon introduction of the E6 R130A MAML1 binding mutation.

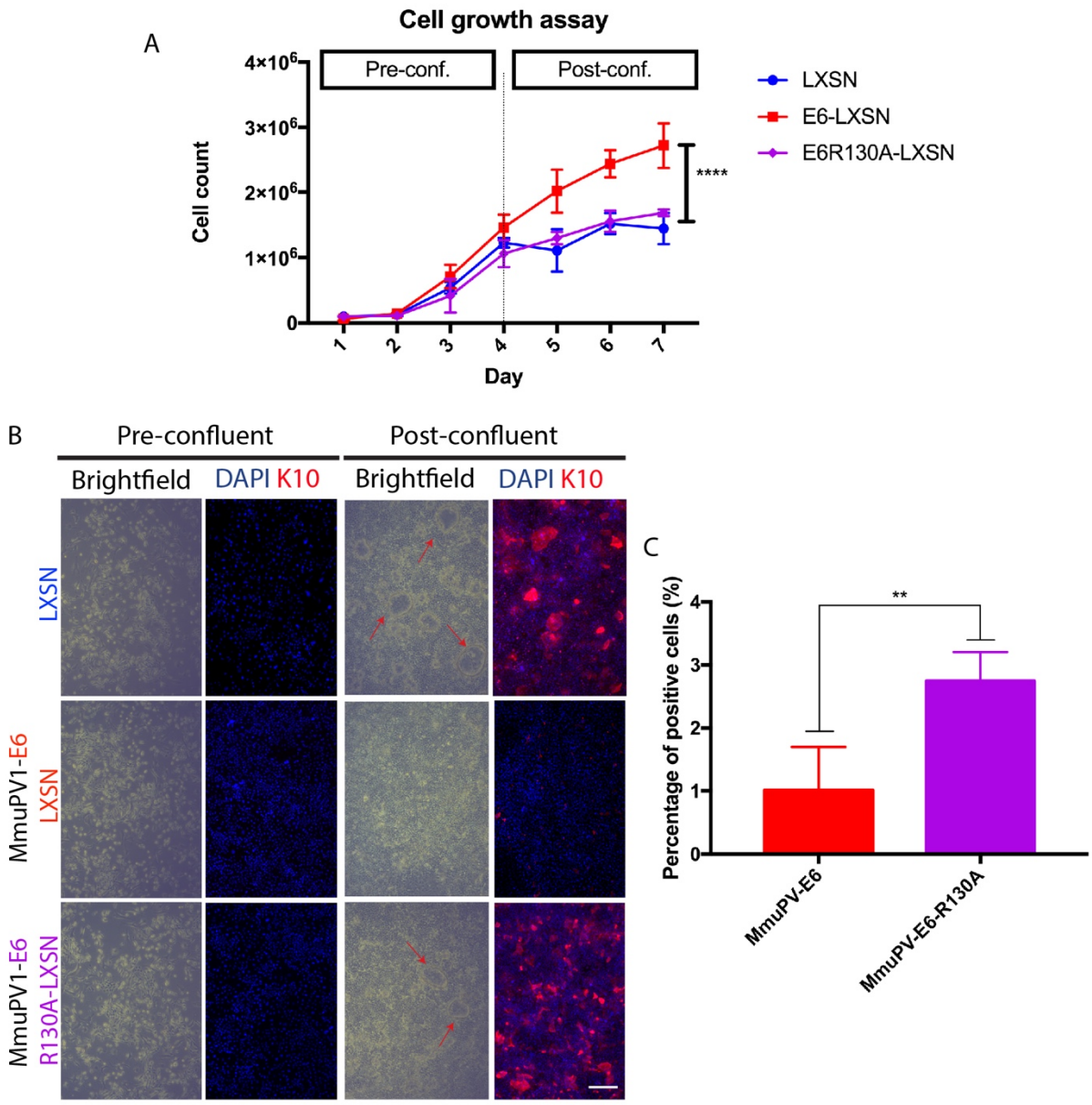

Figure 4.12 MmuPV1 E6 interaction with MAML1 is required for post-confluent density increase and differentiation delay

A; NIKS/LXSN, NIKS/MmuPV1E6^{R130A}-LXSN or NIKS/MmuPV1E6^{R130A}-LXSN cells were counted in triplicate each day. Cells were pre-confluent at 3 days, confluent at 4 days, and post-confluent by day 5. P-values were calculated with a two-way ANOVA with Tukey's correction; **** = $P \leq 0.0001$. Three independent experiments, n=3. B; NIKS/LXSN, NIKS/MmuPV1E6^{R130A}-LXSN or NIKS/MmuPV1E6^{R130A}-LXSN cells were stained with K10 (red) at both pre-confluence (day 3) and post-confluence (day 7). Panels show IF detection of K10 for each cell population. Nuclei were counterstained with DAPI to show host DNA. Scale bar: 100 µm. Light microscope images for each time point are also shown for all three cell populations. Red arrows denote presence of ring-like structures in cell monolayer morphology. C; Quantitation of the number of cells positive for K10 per microscope field at 5X magnification was carried out for each cell population. Number of positive cells was then normalised to quantity of cells per field in each population to give a percentage of positive cells. Two independent experiments, n=5. P-values were calculated with Kruskal-Wallis test with Dunn's correction; * = $P \leq 0.05$, ** = $P \leq 0.01$. Error bars, SD.

Finally, the high-density competition assay was repeated with NIKS/MmuPV1E6^{R130A}-LXSN versus NIKS/LXSN EGFP cells (LXSN/MmuPV1E6^{R130A}-LXSN). LXSN/MmuPV1E6-LXSN was used as a control. Results are shown in Figure 4.13. In LXSN/MmuPV1E6^{R130A}-LXSN groups, there was a statistically significant difference (****$p \leq 0.0001$) between layer occupancy when compared to LXSN/MmuPV1E6-LXSN groups at day 10. While the lower layer occupancy was 89.44% NIKS/MmuPV1E6-LXSN mCherry cells in the wtE6 experiment, this was reduced to 60.75% in the MAML1 binding deficient mutant group with cells expressing NIKS/MmuPV1E6^{R130A}-LXSN mCherry. Similarly, the upper layer of the wtE6 experiment was occupied by 93.15% EGFP positive cells, whereas this was decreased to only 64.52% in the LXSN/MmuPV1E6^{R130A}-LXSN experiment.

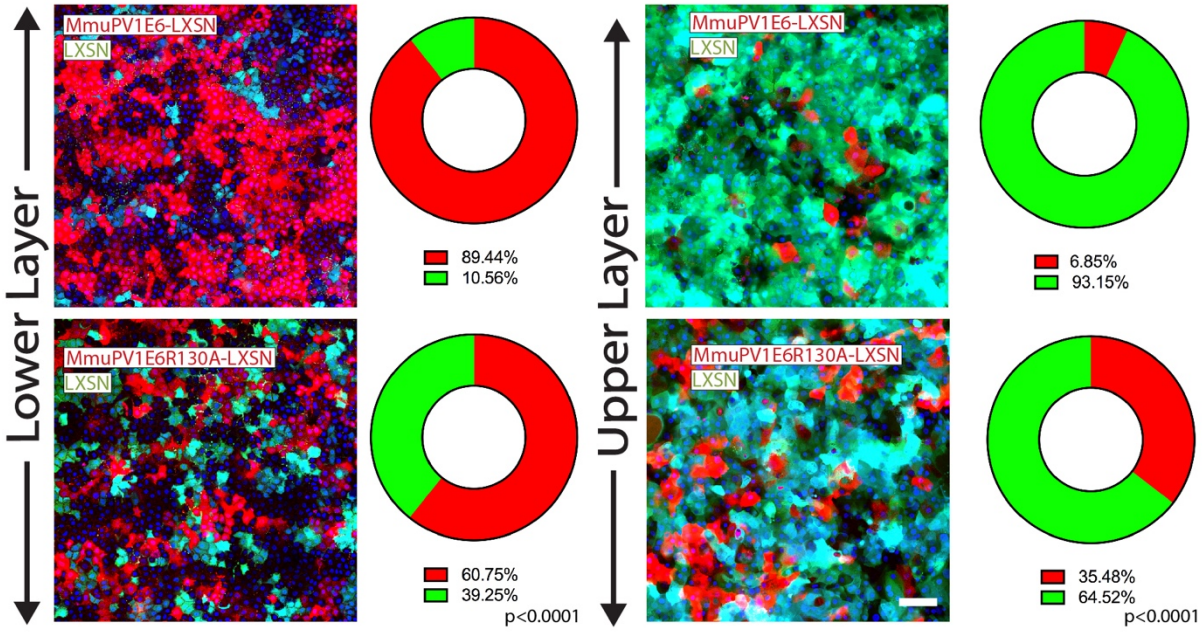

Figure 4.13 MmuPV1 E6 interaction with MAML1 is required for preferential persistence in the lower layer of cells in high-density competition assay
Immunofluorescence of LXSN versus MmuPV1E6-LXSN, and LXSN versus MmuPV1E6^{R130A}-LXSN are shown. Cell population identity is indicated by the colouring of text in the upper left corner of each image. The nuclei were counter-stained with DAPI for host DNA. The lower layer panels are shown to the left, alongside representative parts of a whole graphs to demonstrate quantitative data. The upper layer panels and accompanying parts of a whole graphs are shown to the right. IF images shown are confocal microscope tile scan images taken at 40X magnification with 5 by 5 fields of vision. The lower layer was selected by raising the scanning level until the first layer of nuclei were apparent and the focus line was approximately half way through these cells. The upper layer of cells was determined to be approximately 10 µm scanning level higher; this distance was kept consistently across all experiments. Experimental group MmuPV1E6^{R130A}-LXSN was compared with the LXSN versus LXSN control experiment (no statistically significant difference, not shown) and MmuPV1E6-LXSN group. Two independent experiments, n=5. P-values were calculated with a two-way ANOVA with Sidak's multiple comparisons test; **** = $P \leq 0.0001$. Scale bar: 100 µm.

By using confocal microscopy to analyse patterns of fluorescent expression in 3D, it was further shown that the NIKS/MmuPV1E6^{R130A}-LXSN mutant cell line did not retain the ability of wt E6 to persist preferentially in the lower layer, instead demonstrating a random assortment of EGFP positive and mCherry positive cells in the lower and upper layers (Figure 4.14A). This was also confirmed with quantification of fluorescence against distance from the slide surface. Expression patterns of EGFP versus mCherry in the LXSN/MmuPV1E6^{R130A}-LXSN group were shown to be similar, in contrast to earlier data shown in LXSN/MmuPV1E6-LXSN groups in Figure 4.9 where a strong pattern of mCherry expression in the lower layer was detected.

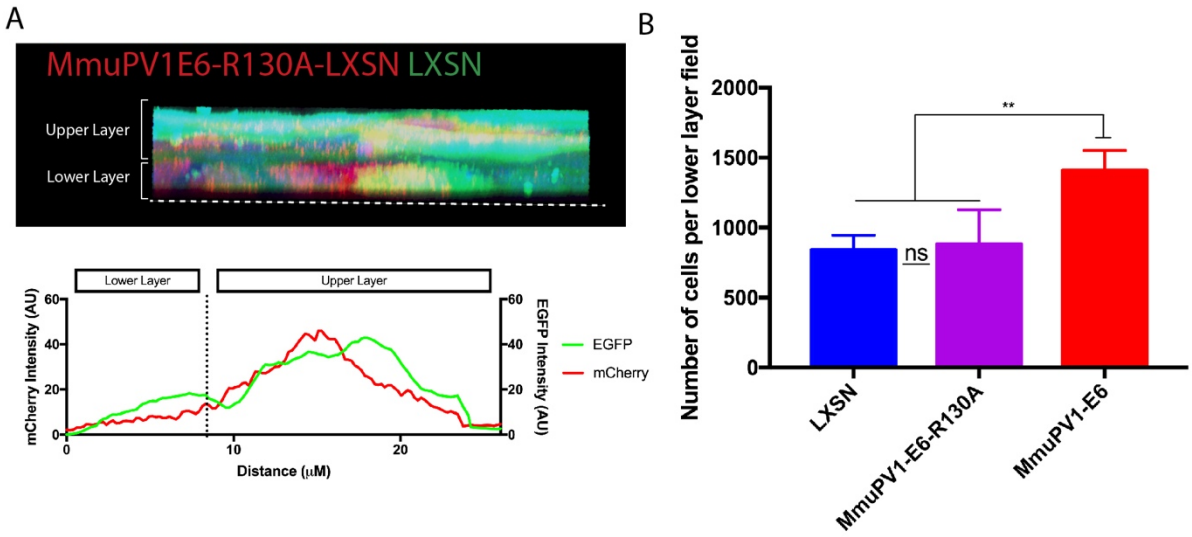

Figure 4.14 3D confocal z-stack analysis demonstrates loss of persistence phenotype in MAML1 binding deficient E6 mutant
A; Maximum intensity 3D plot of z-stacks at 63X magnification is shown (upper panel). Annotations show the location of the lower and upper layers. White dotted line indicates the bottom of the slide glass on which the cells are cultured. The nuclei were counter-stained with DAPI for host DNA. The fluorescent intensity of each channel was quantified across 10 different selections of three different z-stack images taken at 63X magnification for each group, and the average intensity has been plotted against distance from the bottom of the slide upward to demonstrate the distribution of fluorescence throughout the z-stack (lower panel). B; Quantification of the number of cells in the bottom layer of each population (field size: 800.22x800.22 μm). Five random 5 by 5 tile scans were chosen for quantification for each category. Quantification was carried out using the analyse particles function in FIJI image analysis software. Two independent experiments, n=3. P-values were calculated with Kolmogorov-Smirnov t-tests; ** = $P \leq 0.01$.

Finally, quantification of cell density in the lower layer of NIKS/MmuPV1E6^{R130A}-LXSN cells cultured in isolation showed that the increase in lower layer density previously observed in the NIKS/MmuPV1E6-LXSN group was also lost following the disruption of MmuPV1 E6 MAML1 binding, as there was no significant difference between NIKS/MmuPV1E6^{R130A}-LXSN and NIKS/LXSN lower layer cell density at day ten. Data are shown in Figure 4.14B. Conversely there was a significantly higher density of cells at day ten in the NIKS/MmuPV1E6-LXSN population of cells (**$p \leq 0.01$). These data clearly demonstrated that MmuPV1 E6 interference with the Notch pathway via interaction with MAML1 is necessary to allow cells to preferentially persist in the lower layer of cells, and may also mediate the effect of MmuPV1E6 on basal lower cell layer density regulation.

4.2.9 Mathematical modelling of layer occupancy through spline interpolation

To extend our understanding of the dynamics of layer occupancy in the high-density competition assay, three time points were examined, and the percentage occupancy of the lower layer quantified for each. With these data, a spline interpolation was carried out to estimate the growth dynamics of lower layer occupancy over time, without necessitating the immediate in-depth analysis of each category for every time point. Mathematical data are shown below in Figure 4.15, and were generated by Dr Demetris Demetriou. Using spline interpolation to most accurately estimate the curve of the line, the likely progression of lower layer occupancy over time was shown. An error margin of 10% was also plotted to allow for any miscounting of cell populations. Using this method of interpolation, it was shown that NIKS/MmuPV1E6-LXSN cells were predicted to reach 100% occupancy of the lower layer in the LXSN/MmuPV1E6-LXSN high-density competition assay at approximately day 12 of culture. This demonstrates the strong competitive advantage that expression of MmuPV1 E6 confers upon cells over the control cell population. No strong phenotypic trend is apparent in the LXSN/LXSN control group or the LXSN/MmuPV1E7-LXSN group. The LXSN/MmuPV1E6^{R130A}-LXSN group does appear to have a weak trend towards 100% occupancy over time, which is due to the slightly increased mCherry positive cell occupancy of the basal layer observed at day 10. Without observation of this phenotype over a longer time period, it is unclear whether the weak advantage of the NIKS/MmuPV1E6^{R130A}-LXSN cell population would eventually result in 100% occupancy of the lower layer, or whether the weaker phenotype would mean that it was unable to populate the lower layer any further. However, when longer time courses were attempted with this system, all cell populations cultured to day 14 were found to have begun apoptosis (data not shown), suggesting that this

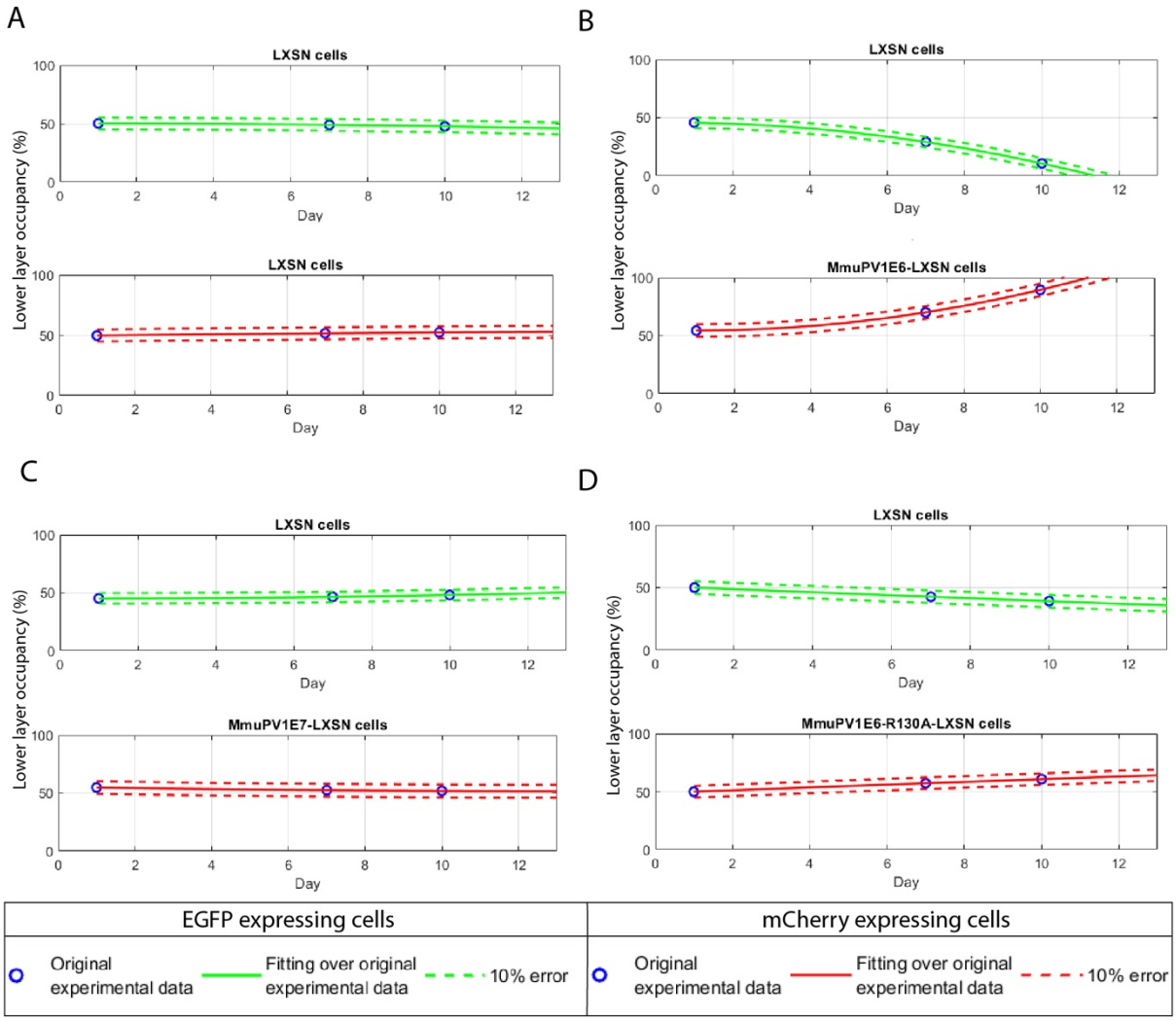

Figure 4.15 Spline interpolation graph demonstrates predictions of lower layer occupancy rates over a 12-day time-course.
Data shown in Figure 4.8 and Figure 4.13 used to generate these graphs. Green line shows occupancy by EGFP expressing LXSN cells. A; LXSN/LXSN spline interpolation graphs. Red line shows occupancy by mCherry expressing LXSN cells. B. LXSN/MmuPV1E6-LXSN spline interpolation graphs. Red line shows occupancy by mCherry expressing MmuPV1E6-LXSN cells. C. LXSN/MmuPV1E7-LXSN spline interpolation graphs. Red line shows occupancy by mCherry expressing MmuPV1E7-LXSN cells. Ten percent error margin is denoted by dashed lines. Blue circles indicate average of original experimental data.

high-density competition assay is unsuited for sustaining long term culture of NIKS. In future experimentation using this model, spline interpolation can provide a useful and mathematically accurate estimation of missing time points to demonstrate predicted lower layer occupancy over time. However, to try and extend the understanding of these phenotypes beyond the ten day time period, organotypic raft culture of cells was attempted.

4.2.10 Differentiation is delayed in 3D culture of cells exogenously expressing MmuPV1 E6

It has been shown previously that the life cycle of HPV can be completed in organotypic raft cultures, making it an attractive quasi- *in vivo* system with which to examine the effects of virus proteins in a mimic of stratified epithelium (Lambert, Ozbun et al. 2005). NIKS/MmuPV1E6-LXSN and NIKS/MmuPV1E6^{R130A}-LXSN rafts were established, along with a control set of normal NIKS rafts which was provided by Kara Zheng. To create the raft epithelium, cells were differentiated on dermal equivalent for up to 14 days at an air-liquid interface. First, H&E staining of rafts was carried out to assess the morphology of the cells in the 3D culture. In normal NIKS, recapitulation of the layers of the normal epithelium was achieved, as shown in Figure 4.16A.

There was no evidence of dysplasia observed in these rafts, and small, uniformly shaped cells can be seen populating the lowest layer. As expected, stratification of cells and normal squamous maturation occurred above the basal layer. Pyknotic nuclei indicative of cellular necrosis or apoptosis were observed in the uppermost cornified layer (Ross and Pawlina, 2006). Similarly, structured stratum corneum could be observed throughout much of the NIKS/MmuPV1E6-LXSN rafts analysed, although there appeared to be an increase in the number of nuclei observed within this layer. Interestingly, the morphology of cells in the basal compartment was noticeably altered in cells exogenously expressing NIKS/MmuPV1E6-LXSN when compared to the normal NIKS rafts. Nuclei were less uniform in their organisation and unstained areas around cells were observed. This morphological change was not evident in the NIKS/MmuPV1E6^{R130A}-LXSN rafts, although a decrease in thickness of the stratum corneum was observed in the samples analysed.

To examine the effect of viral protein expression on terminal differentiation, staining with antibodies targeting K10 was carried out. K10 is usually detected in all layers above the basal layer (Watt and Phil 1983). In normal NIKS rafts, K10 was detected in cells immediately above the bottom layer of cells. These observations suggest that the process of terminal differentiation was occurring normally in the raft system, although occasional K10 positive cells were observed in the lowest layer. Therefore, this model was considered sufficient to investigate the effect of virus protein expression on differentiation. Rafts established with NIKS/MmuPV1E6-LXSN cells were also stained with anti-K10 antibody to allow evaluation of differentiation. In contrast to the normal NIKS cells, induction of K10 was delayed for 2-3

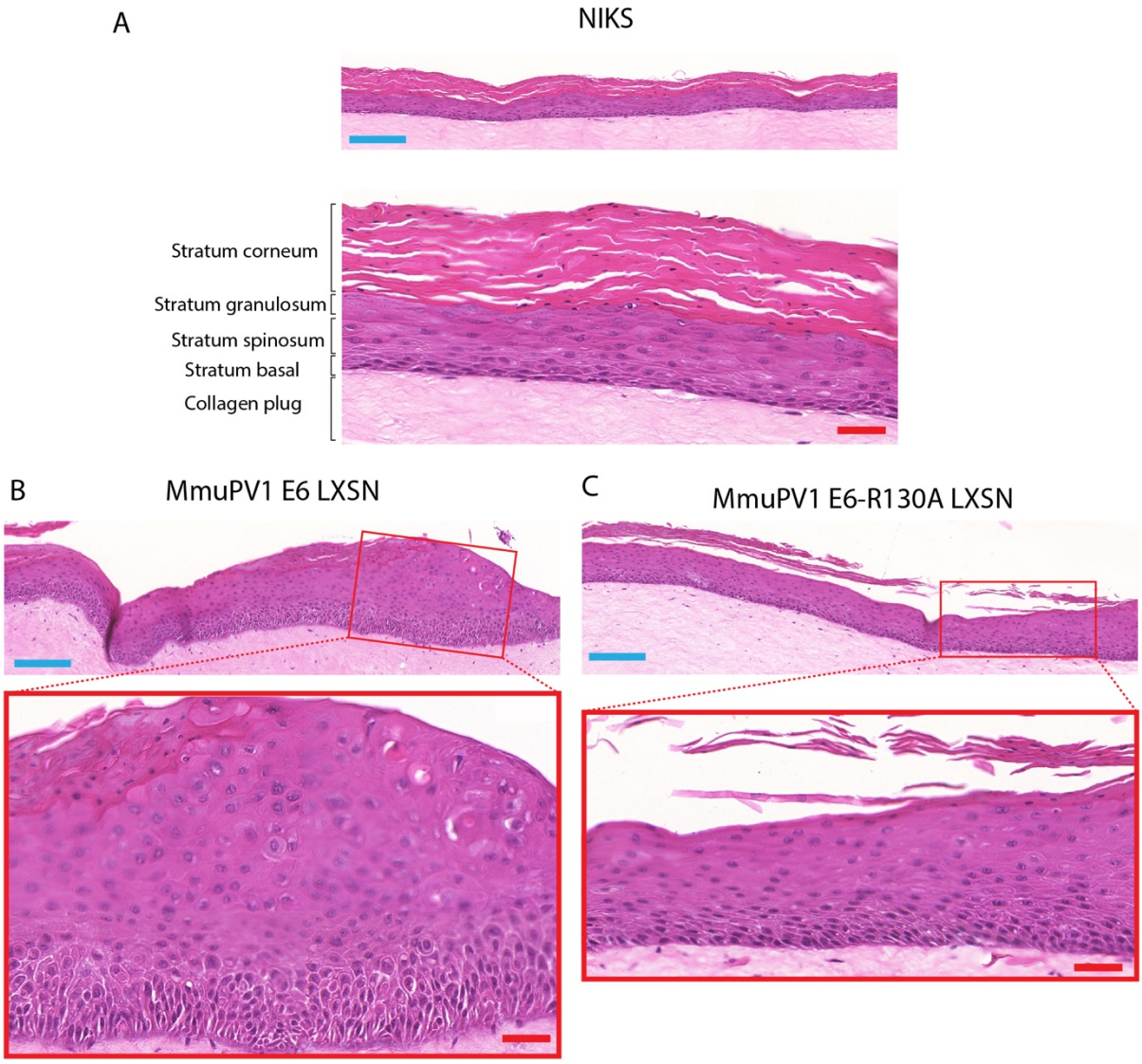

Figure 4.16 Haematoxylin and eosin staining of rafts cultured from normal NIKS compared with NIKS exogenously expressing wt or mutant MmuPV1 E6 viral protein
A; Organotypic raft culture from normal NIKS is shown at 20X magnification and 1:1 magnification. Layers of the stratified epithelium are identified with labelling to the left of the 1:1 image. B; Organotypic raft culture of NIKS exogenously expressing MmuPV1 E6 is shown at 20X and 1:1 magnification. C; Organotypic raft culture of NIKS exogenously expressing MmuPV1 $E6^{R130A}$ is shown at 20X magnification and 1:1 magnification. Scale bar: 200 μm (blue) and 50 μm (red).

layers of cells in the lowest layers. However, when rafts were established with the NIKS/MmuPV1E6^{R130A}-LXSN cells, this delay in differentiation was lost, and instead K10 staining was observed in all cells above the basal layer of the rafts. Therefore, these raft cultures successfully recapitulated the delay in differentiation observed in NIKS/MmuPV1E6-LXSN cells, both in monolayer cell culture and in the *in vivo* mouse model shown in Chapter 3.0. Similarly, this experiment gave further support to previous data that showed a loss of this differentiation delay in NIKS/MmuPV1E6^{R130A}-LXSN cells, indicating that binding of MmuPV1 E6 to MAML1 is required for a delay in differentiation to occur.

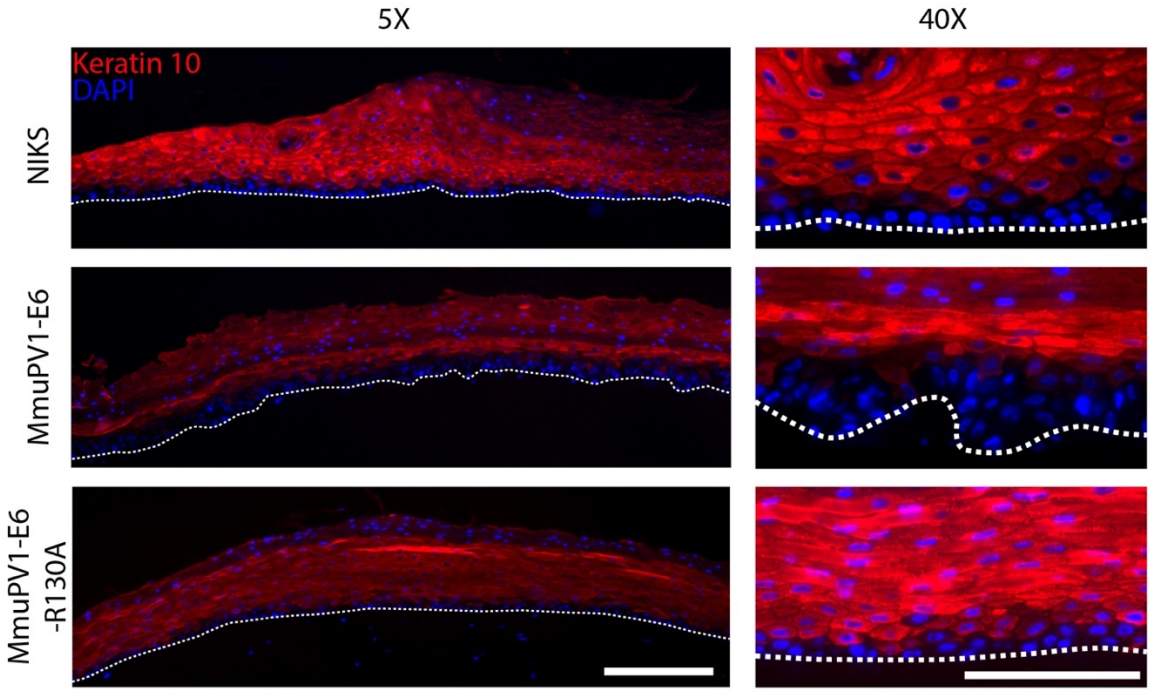

Figure 4.17 Differentiation is delayed in 3D organotypic raft culture of MmuPV1 E6 cells when compared to NIKS only, or cells expressing MmuPV1 E6^{R130A}
Panels show IF detection of K10 (red) in organotypic rafts collected 14 days following seeding for each cell population. Nuclei were counterstained with DAPI to show host DNA. Dotted lines indicate the presence of the basal layer. Scale bar: 200 μm in the 5X magnification image panel, and 100 μm in 40X magnification image panel.

4.2.11 Investigating the persistence phenotype in 3D culture

To further investigation of the ability of NIKS/MmuPV1E6-LXSN cells to competitively persist in the lower layer of cells in cell culture, 3D organotypic raft culture of NIKS/LXSN EGFP cells in co-culture with NIKS/LXSN mCherry, NIKS/MmuPV1E6-LXSN mCherry, or NIKS/MmuPV1E6^{R130A}-LXSN mCherry cells was attempted. Cells were seeded at a 50:50 ratio of NIKS/LXSN EGFP control cells against cells expressing NIKS/MmuPV1E6-LXSN mCherry, NIKS/MmuPV1E6^{R130A}-LXSN mCherry, or NIKS/LXSN mCherry control vector only, similar to the experiments shown in Figure 4.8. Following culture of cells at an air-liquid interface for ten days, rafts were collected, fixed, and stained for EGFP and mCherry; the fluorescent signal was lost during normal processing, however antibodies targeting these proteins were used to visualise locations of the appropriate cells. These rafts are shown below in Figure 4.18.

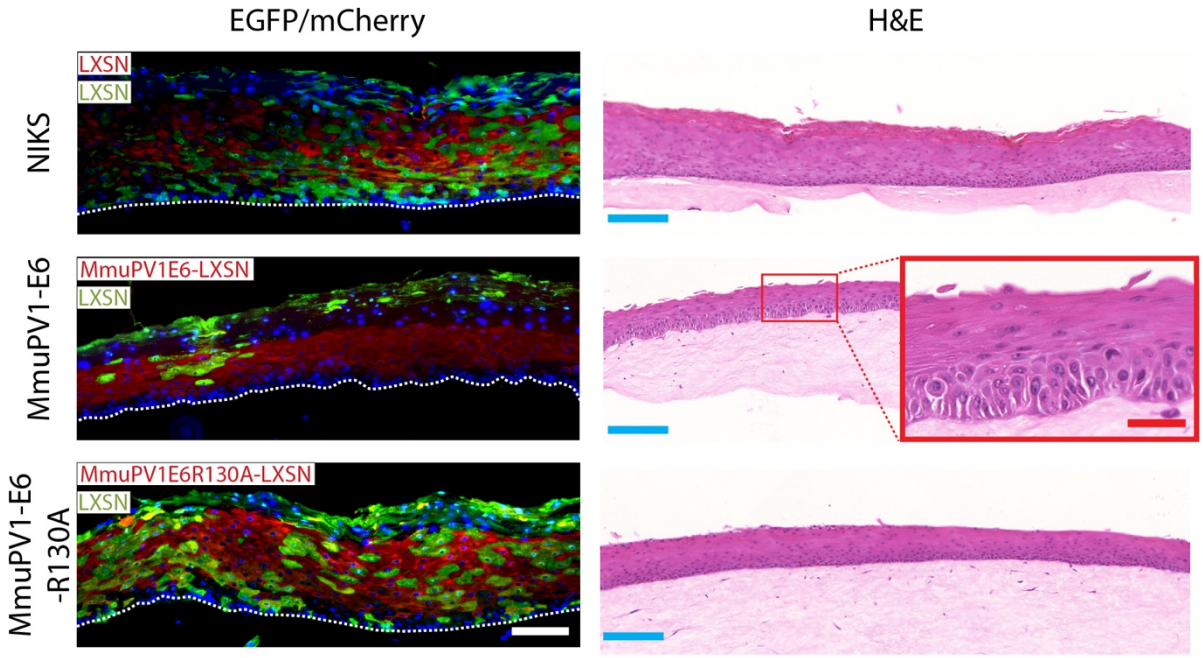

Figure 4.18 NIKS expressing MmuPV1 E6 preferentially populate the lower layers of the raft culture when compared to LXSN/LXSN control or LXSN/MmuPV1E6^{R130A}
Panels on the left show IF detection of mCherry (red) and EGFP (green) in each of the three populations rafted. Identity of cells is shown with coloured labelling at the top left of each image. Nuclei were counterstained with DAPI to show host DNA. Scale bar: 200 μm. Dotted lines indicate the presence of the basal layer. The right panel of images shows haematoxylin and eosin staining of competition assay rafts. Data shown representative of 2 independent experiments, n=2. Scale bar: 200 μm (blue line) and 50 μm (red line) in the higher magnification image, which itself is highlighted in a red box.

In control raft cultures of LXSN/LXSN groups, the distribution of EGFP and mCherry expressing cells appeared to be random, with mCherry and EGFP signal detected throughout the raft layers. However, in rafts established with LXSN/MmuPV1E6-LXSN groups, EGFP positive cells were rarely observed in the lower layers of the raft epithelium, and were most commonly observed in the uppermost layers. Further, H&E staining of rafts showed that the cell morphology observed in the basal layers of the NIKS/MmuPV1E6-LXSN only rafts was also present in the basal layer of the LXSN/MmuPV1E6-LXSN rafts, suggesting that it was cells expressing MmuPV1 E6 populating this lower layer. These results demonstrated that the persistence phenotype observed in the high-density competition assay was replicated in 3D cell culture. To examine the effect of the E6 MAML1 binding mutation in this model, rafts were also established using NIKS/MmuPV1E6^{R130A}-LXSN mCherry cells. As observed in the high-density competition assay, abrogation of the MAML1 binding ability of MmuPV1 E6 resulted in a loss of the ability of cells to persist in the lower layers. Instead, the distribution of EGFP and mCherry positive cells appeared to be random throughout the layers of the organotypic raft, similar to the distribution of cells observed in the LXSN/LXSN raft control.

4.2.12 Cell cycle entry is promoted in virus protein expressing cells at both low and high cell density

Following experiments that investigated the phenotype of lower-layer persistence in cell culture, we wanted to examine the cell cycle activity in these different populations and consider whether an increase in cell cycle entry might correlate with the competitive advantage observed in cells exogenously expressing MmuPV1 E6. A technique recently established in the lab allowed *in vivo* monitoring of cell cycle activity. During G1 phase of the cell cycle, the protein Cdt1 is upregulated to allow licensing of DNA for replication. Cdt1 is directly inhibited by geminin, a DNA replication inhibitor, during S phase, M phase, and G2 phase of the cell cycle. (Wohlschlegel, Dwyer et al. 2000). To investigate any impact of viral proteins on cell cycle entry over time, the Fucci (fluorescent ubiquitination-based cell cycle indicator) cell system was utilised. This system allows visualisation of progression through the cell cycle by the fluorescent tagging of these two discrete proteins, which are reciprocally regulated throughout the cell cycle. Abundance of these proteins is controlled by ubiquitin-mediated proteolysis (Sakaue-Sawano, Kurokawa et al. 2008). The mapping of the cell cycle using these two colours is shown in Figure 4.19A, adapted from (Sakaue-Sawano, Kurokawa et al. 2008).

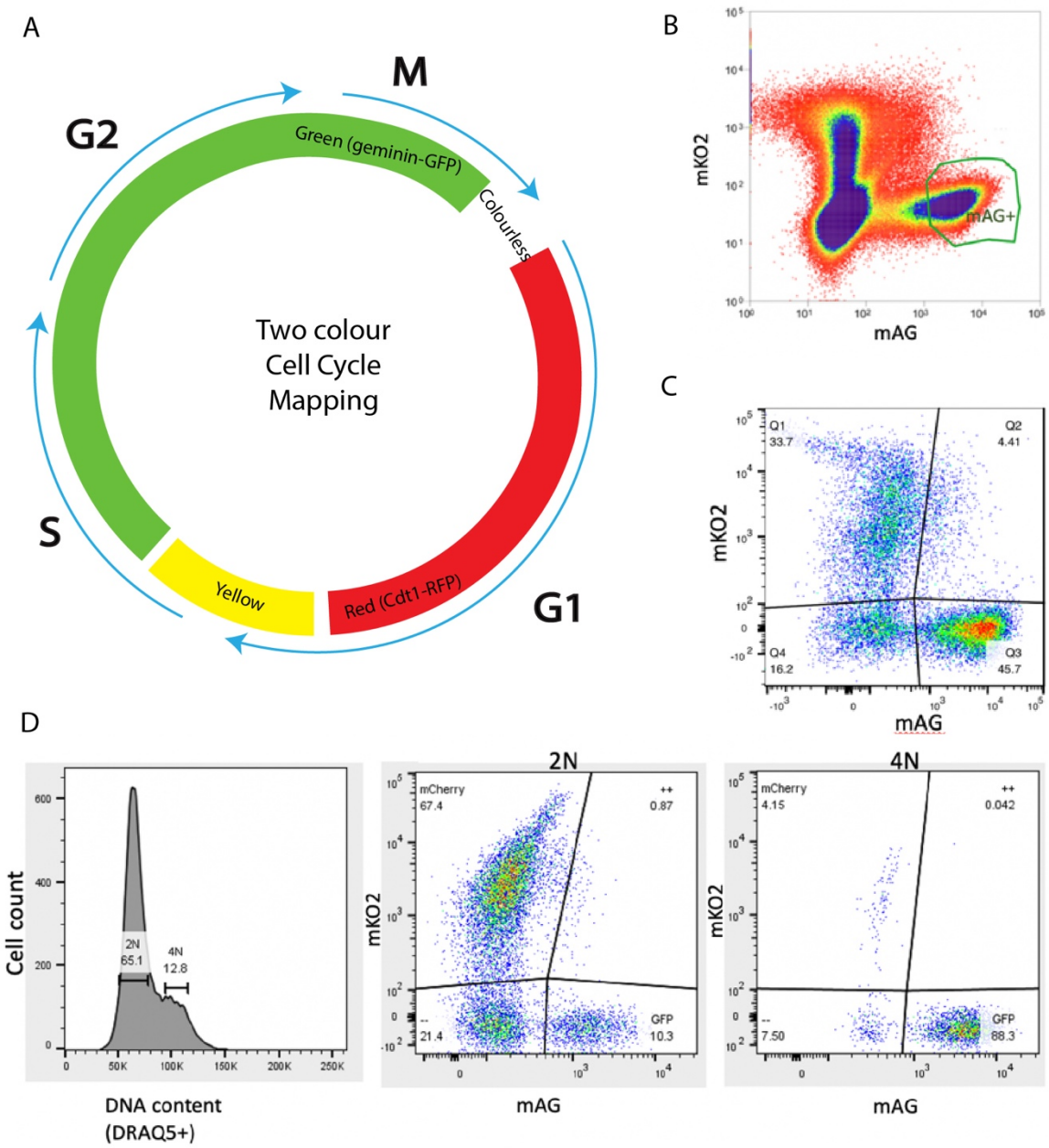

Figure 4.19 The Fucci cell system

A; Fucci expressing cells fluoresce red during the G1 phase of the cycle, yellow during the transition between G1 and S, green during the S, G2, and M phases, and finally are briefly colourless during the division of the cells. Adapted from (Sakaue-Sawano, Kurokawa et al. 2008). B-D shows work carried out by Kara Zheng, who also provided corresponding figures. B; Flow cytometry demonstrating the expression levels of Fucci cell population prior to sorting. Sorted population is shown selected as mAG+, and constituted roughly 10% of the total cells analysed. C; expression levels of Fucci in NIKS following sorting for mAG+ cells. D; DNA content of live cells was stained with DRAQ5. Gating of cells for DNA content was carried out by sorting cells with 2N and 4N. Fucci expression of each of the consequent sorted populations was shown.

Fucci cells were established by viral transduction of a commercially available expression vector with a pBOB backbone (Addgene, UK). However, observation of initial cell populations showed that intensity of fluorescent expression varied a great deal, and a large proportion of the cells were not successfully expressing the fluorescent tags. Therefore, FACS sorting of the population of cells and subsequent functionality checks described in the paragraph below were carried out by Kara Zheng, another member of the research group. First, a population of cells with a high level of expression, denoted as mAG+ in Figure 4.19B, were selected for through FACS, which roughly constituted 10% of the total cell population. Expression levels of the subsequent population of sorted cells is shown in Figure 4.19C. Finally, to check that the Fucci system was working correctly, cells were sorted for DNA content by staining cell nuclei with DRAQ5, a far-red fluorescent dye that is cell permeable. Subsequent sorting by DNA content allowed populations to be split into 2N and 4N, to show G1/S and G2/M phase cells separately. Corresponding expression of red and green fluorescence is quantified by FACS in Figure 4.19D, showing that cells in G1/S phase had high levels of red fluorescence, and cells in G2/M phase had high levels of green fluorescence, as expected. As the system was functioning properly, Fucci expressing cells were then transduced to express MmuPV1 viral proteins to allow investigation of the effect of these proteins on the cell cycle.

NIKS/LXSN-Fucci, NIKS/MmuPV1E6-LXSN-Fucci, NIKS/MmuPV1E7-LXSN-Fucci, and NIKS/MmuPV1E6^{R130A}-LXSN-Fucci cells were seeded at low and high density and cultured for two days before collection for FACS analysis. Data are shown in Figure 4.20. FACS analysis demonstrated that at low density, NIKS/MmuPV1E6-LXSN-Fucci, NIKS/MmuPV1E7-LXSN-Fucci, and NIKS/MmuPV1E6 ^{R130A}-LXSN-Fucci cells all had approximately 1.5 times higher number of cells in G2/M when compared with cells expressing NIKS/LXSN only. At high density, this increase in the proportion of cells in G2/M in all three experimental populations was much greater, as virus protein expressing cells had approximately 8 times higher number of cells in the cell cycle when compared to NIKS/LXSN control cells. Surprisingly, NIKS/MmuPV1E7-LXSN-Fucci and NIKS/MmuPV1E6 ^{R130A}-LXSN-Fucci cells appeared to have a similar cell cycle advantage as NIKS/MmuPV1E6-LXSN-Fucci, despite not demonstrating any statistically significant growth advantage in cell culture. Previous research in our group has shown that E7 affords a more significant growth advantage to cells only when EGF is sparse (Kranjec, Holleywood et al. 2017). Therefore, the Fucci experiment was repeated in FI media, which lacks EGF, to examine any impact of EGF on the cell cycle phenotype. Data are shown in Figure 4.21.

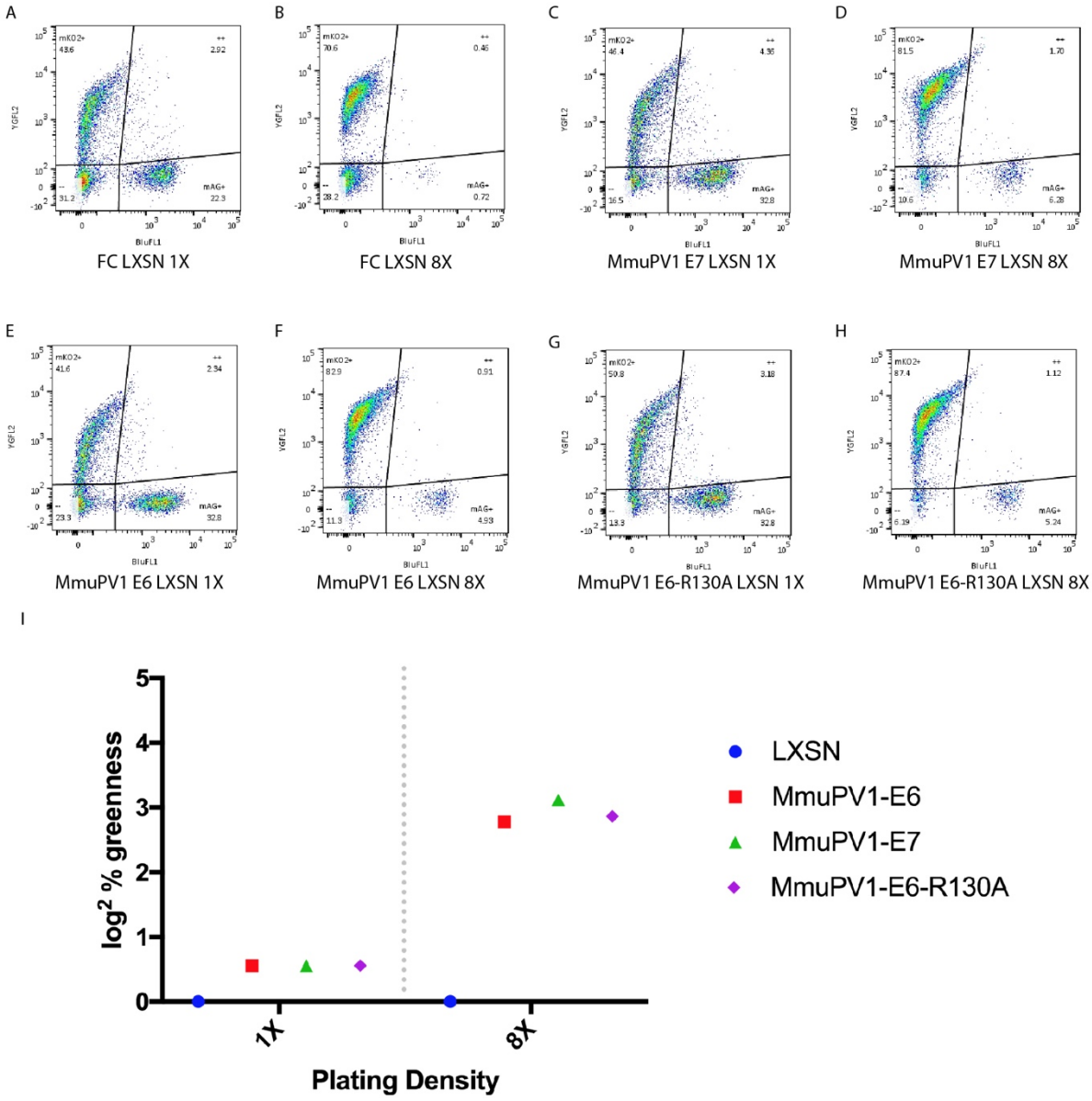

Figure 4.20 FACS analysis of Fucci cells shows increase in cell cycle entry in virus protein expressing cells

A-H; Flow cytometry data from Fucci cells expressing LXSN, MmuPV1 E6, MmuPV1 E7, and Mmu1PV $E6^{R130}$ seeded at 1x and 8x starting cell density. Percentage of cells expressing 'greenness' (mAG+ quadrant) is shown. I; Quantitative comparative analysis of above FACS data to demonstrate fold change in 'green' cells. Raw data was used to calculate the percentage of green cells in LXSN. Data was then normalised to the LXSN control group within each density sub-group. Data are displayed as log^2 of percentage greenness to show fold change. One independent experiment, n=1.

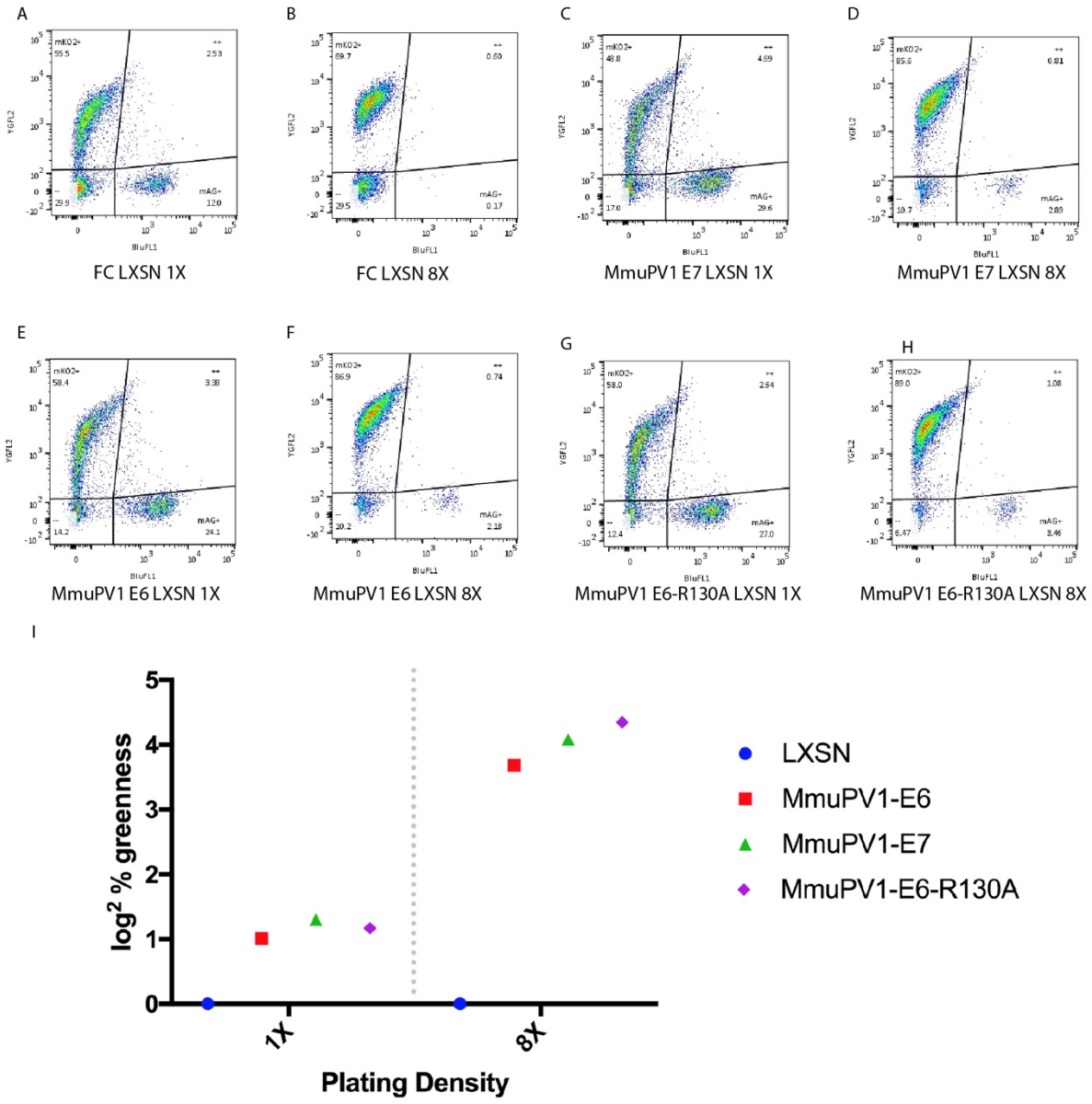

Figure 4.21 FACS analysis of Fucci cells cultured in FI media shows a greater increase in cell cycle entry in virus protein expressing cells when compared with cells cultured in FC media

A-H; Flow cytometry data from Fucci cells expressing LXSN, MmuPV1 E6, MmuPV1 E7, and Mmu1PV E6^{R130} seeded at 1x and 8x starting cell density and cultured in F incomplete media. Percentage of cells expressing 'greenness' (mAG+ quadrant) is shown. I; Quantitative comparative analysis of above FACS data to demonstrate fold change in 'green' cells. Raw data was used to calculate the percentage of green cells in LXSN. Data was then normalised to the LXSN control group within each density sub-group. Data are displayed as $\log^2$ of percentage greenness to show fold change. One independent experiment, n=1.

Growth of these cell populations in FI media increased the growth advantage afforded by virus proteins onto the NIKS; at low density, NIKS/MmuPV1E6-LXSN-Fucci, NIKS/MmuPV1E7-LXSN-Fucci, and NIKS/MmuPV1E6 ^{R130A}-LXSN-Fucci cells all had approximately 2 times higher the numbers of cells in G2/M when compared to NIKS/LXSN control cells. Similarly, the growth advantage seen at high density in FC media was also exaggerated when cells were cultured in FI media, with NIKS/MmuPV1E6-LXSN-Fucci, NIKS/MmuPV1E7-LXSN-Fucci, and NIKS/MmuPV1E6 ^{R130A}-LXSN-Fucci cells showing a roughly 16 times higher number of cells in G2/M when compared with NIKS/LXSN only. From this experimental replicate, it appears that NIKS/MmuPV1E6 ^{R130A}-LXSN-Fucci cells had the most dramatic impact on cell cycle entry in FI media post-confluence, however with repeat experiments these values may balance out with no significant difference in growth advantage between any of the virus proteins. Unfortunately, time did not allow for repetition of these final experiments, however application of this cell culture system in the future will discern more useful information about the virus proteins.

4.3 Discussion

To better understand the involvement of individual virus proteins in the epithelial basal layer, NIKS cell lines exogenously expressing virus proteins MmuPV1 E6 and MmuPV1 E7 were generated. Standard growth assays demonstrated that cells exogenously expressing MmuPV1 E6 had an elevated growth rate post confluence, and that these cells also grew to an increased density in monolayer culture compared with both LXSN expressing control cells and MmuPV1 E7 expressing cells. No statistically significant differences in cell density were seen at pre-confluent time points. Modulation of cell proliferation even at high cell density by high-risk HPV16 E6 has previously been demonstrated (Kranjec, Holleywood et al. 2017), suggesting a common E6 protein function between this high-risk HPV type and MmuPV1, a pi PV. Recent research in our lab suggests that low-risk HPV11 is unable to modulate cell-density post-confluence in the same way as high-risk HPV16 (Murakami, Egawa et al. 2019). Less is known about the gamma papillomavirus E6 protein, however recent proteomic studies have confirmed that gamma HPV196 E6 is able to interact with MAML1 (Grace and Munger 2017) and large scale studies into E6 binding preference confirmed that all beta, gamma, mu and nu genera E6 proteins tested were able to preferentially bind to MAML1 (Brimer, Drews et al. 2017). As the E6 proteins of PV of these genera can bind to MAML1, it is plausible to consider they might be able to confer similar growth advantages on cells as shown with MmuPV1 E6, which would suggest a common conserved function to prevent cell cycle exit as

density increases across PV types. However, this requires further research. Further to this, a clear decrease in K10 positive cells was observed post-confluence in NIKS/MmuPV1E6-LXSN cell populations only. This is similar to phenotypes observed in a recently published paper from our lab, which showed that exogenous expression of both high-risk HPV16 and low-risk HPV11 E6 afforded a growth advantage and differentiation delay to NIKS cells post-confluence (Murakami, Egawa et al. 2019). As discussed extensively in Chapter 1 (Section 1.8), E6 proteins of alpha and beta HPV types have been shown to mediate a delay in normal differentiation. Therefore, these data also demonstrates that the E6 protein of MmuPV1 has a mechanistic effect on keratinocyte cell fate similar to some HPVs that can cause disease in humans, despite their distant evolutionary relation (Uberoi and Lambert 2017).

Utilising confocal microscopy and EGFP/mCherry expressing NIKS cell lines, I was able to examine the growth advantages of cell populations in 3D by isolating discrete layers of cells within the monolayer culture. Data demonstrated a clear phenotype of persistence in the 'lower' layer of cells in populations expressing NIKS/MmuPV1E6-LXSN mCherry when compared with both NIKS/LXSN mCherry control cells and NIKS/MmuPV1E7-LXSN mCherry cells. The phenotype observed in NIKSMmuPV1E7-LXSN mCherry cells was similar to that observed in NIKS/LXSN mCherry control cells, with no statistically significant difference between mCherry-positive cell layer occupancy. The data showed that expression of MmuPV1 E6 in high-density cell culture results in a competitive growth advantage over uninfected cells, wherein normal cells exit the lower layer and E6-expressing cells persist in the lower layer. This competitive advantage may also exist *in vivo*, allowing the reservoir of infected cells to persist in the host by outcompeting their uninfected neighbours. Repetition of the growth, differentiation, and high-density competition assays with a MAML1 binding mutant of MmuPV1 wtE6 (MmuPV1E6^{R130A}) disrupted the phenotypes observed in NIKS/MmuPV1E6-LXSN cell culture experiments, offering strong support for the interference of E6 with Notch signalling being important for the persistence phenotype to occur.

Mathematical and spatial analysis of HPV-induced lesions has given further support to the theory that HPVs are able to modulate the basal dynamics of infected cell populations; modelling of HPV-infected cells as having increased tissue density and decreased exit from the lower layer produced data that correlated with patterns seen in real infection (Orlando, Brown et al. 2013). Recently published work generated a mouse model carrying an inducible dominant negative mutant of Maml1, which would result in inhibition of NICD induced

transcription in the oesophageal keratinocyte cell populations (Alcolea and Jones 2015). Interestingly, results demonstrated that the mutant cells dramatically outcompeted their normal counterparts over time *in vivo.* The persistence of these mutant cells was shown to be due to the MAML1 binding deficient cells not being lost from the basal layer by differentiation, and by their stimulating normal neighbour cells to differentiate. These mutant cell populations also exhibited an increased cell density at confluence of 30%, characterised by a buckling of the epithelium as a result (Alcolea, Greulich et al. 2014). Further, it has recently been shown that high-risk HPV16 E6 interference with the Notch pathway in NIKS cells caused persistence of infected cells in the basal and parabasal layers, along with an associated increase in cell density and differentiation delay (Kranjec, Holleywood et al. 2017). Therefore, it is reasonable to postulate that the impact that MmuPV1 E6 binding with MAML1 has upon Notch signalling would also result in cells having a competitive advantage over normal cells. The observations described in this chapter that show a MAML1 binding-dependent role for MmuPV1 E6 in delaying cell differentiation, increasing cell density, and allowing E6-expressing cells to preferentially persist in the lower layer, fit with this hypothesis.

Research into the binding partners of beta HPV types found that beta genus E6 proteins could bind to MAML1 (Rozenblatt-Rosen, Deo et al. 2012). Further, this binding partner is not shared by high-risk HPV alpha types, demonstrating an alternate mechanism for Notch pathway interaction in this subset of PV types (White, Kramer et al. 2012). BPV has also been shown to bind to MAML1, expanding the types of PV that possess this binding ability. It is possible that these other PV types could manipulate the Notch pathway through MAML1 binding to cause similar cell persistence and differentiation delay *in vivo.* As mentioned in Chapter 1 (Section 1.8.5), large scale analysis of the ability of different PVs to bind to MAML1 or E6AP demonstrated that PV types physically and functionally interacted with one or the other, but not both of these proteins (Brimer, Drews et al. 2017). It is clear that an evolutionary split occurred between PV types that can interact with MAML1 and those PV types that interact with E6AP. All PVs have evolved to survive in their specific epithelial niche over millions of years, and have been shown to employ a variety of mechanisms to achieve the overall unifying goal of completing their life cycle (Doorbar, Quint et al. 2012). The presence of this shared Notch pathway interaction amongst the different PV types, mediated either through E6-AP binding as demonstrated in the high-risk types (Kranjec, Holleywood et al. 2017), or by binding to MAML1 seen in other PV types (Tan, White et al. 2012), suggests that this pathway interaction is important for the successful life cycle of PV in

the host. However, there are PV types that lack a functional E6 protein, therefore these types must successfully establish an infection in the host through other mechanisms, or may not require the competitive advantage that interaction with the Notch pathway can confer upon the infected cell (Van Doorslaer, Chen et al. 2018) (Terai, DeSalle et al. 2002) (Tachezy, Rector et al. 2002).

Growth of the NIKS/MmuPV1E6-LXSN and NIKS/MmuPV1E6^{R130A}-LXSN cell populations in organotypic raft culture demonstrated that the differentiation delay observed in NIKS/MmuPV1E6-LXSN cell culture was maintained in 3D stratified epithelium of these cells, and that interruption of E6 binding to MAML1 disrupted this phenotype. Interestingly, observational analysis of the NIKS/MmuPV1E6-LXSN rafts by H&E staining showed a distinct pattern of unstained areas around cells within the lower layers of the epithelium. These unstained areas could be interpreted as spaces between the cells. It is possible that MmuPV1 E6 is having an effect on junctional proteins between the cells, resulting in spaces being observed between cells following processing and H&E staining. High-risk HPV16 and HPV18 E6 has previously been shown to degrade MAGI-1, a protein involved in tight-junction control, which resulted in disruption of tight-junction integrity in both CaSKi and HeLa cells (Kranjec and Banks 2011). Similar high-risk E6 interactions have been described for other proteins involved in cell to cell contact control, such as PATJ (Storrs and Silverstein 2007) and Par3 (Facciuto, Bugnon Valdano et al. 2014). However, low-risk HPV types are not thought to be able to interact with these proteins due to their lacking a PBM (Pim, Bergant et al. 2012). Research by Pim and colleagues demonstrated that by cloning of a PDZ-binding sequence onto the C-terminus of low-risk HPV E6 proteins to generate chimeras, these proteins could then bind and degrade Dlg protein (Pim, Thomas et al. 2002). However, only mucosal low-risk chimera types could bind to and degrade MAGI-1, whereas cutaneous types could not. This research demonstrates further significant differences between PV types relating to their tissue niches. There is no evidence for PV types lacking a PDZ-binding domain being able to negatively affect cell junctions. However, it may be that MmuPV1 E6 is able to have an effect on cell junctions via an alternative pathway, which would require further investigation in the future. Interestingly, this morphology observed in the rafts of NIKS/MmuPV1E6-LXSN cells is similar to that seen during the rafting of cells expressing a NIKS-HPV16 clone that was shown to express high levels of viral proteins E6 and E7 (Isaacson Wechsler, Wang et al. 2012).

Growth of rafts using EGFP/mCherry expressing NIKS demonstrated that the persistence phenotype of NIKS/MmuPV1E6-LXSN cell lines observed in the high-density competition assay was also observed in 3D organotypic rafts. Similarly, this persistence growth advantage was lost in the rafts of cells expressing NIKS/MmuPV1E6^{R130A}-LXSN, which again demonstrated that an interaction of MmuPV1 E6 with MAML1 protein to disrupt normal Notch pathway signalling was necessary for this persistence to occur. This conclusion could be further validated by generation of a cell line expressing both a dominant negative mutant of MAML1 and normal mCherry protein, which could then be transduced to express wt MmuPV1 E6. This cell line could then be co-cultured with NIKS/EGFP cells to generate rafts, which would establish whether expression of the E6 protein would still confer the persistence phenotype on cells that are lacking normal MAML1 protein. A control group of a cell line expressing only a dominant negative mutant of MAML1 and normal mCherry protein co-cultured with NIKS/mCherry cells would also be necessary to establish whether the loss of MAML1 alone resulted in a persistence phenotype too. Based on research carried out by Alcolea and Jones discussed above, this would be an expected result (Alcolea, Greulich et al. 2014). Use of these cell lines in the high-density competition assay could also further confirm this phenotype.

A recently published paper used mathematical modelling to predict the impact of stochasticity of cell division on the clearance of infection, and declared that much of the clearance of HPV from tissue could be attributed to the randomness of stem cells dividing either symmetrically or asymmetrically (Ryser, Myers et al. 2015). The concept that stochasticity plays a key role in the ability of PV to successfully infect and maintain an infection is certainly important to consider, however this model does not take into account the effect that viral protein molecular mechanisms could have on rates of proliferation. In particular, accounting for PV types that are known to increase cell cycle entry and proliferation within the bounds of this mathematical model would presumably yield data that suggests a more dramatic effect of virus infection on the cell. For example, a more recent paper that generated a mathematical model to examine the impact of low-risk and high-risk E7 protein on the cell cycle showed that G1/S phase transition in basal cells can be altered in response to concentration of E7 protein, presence of various growth factors, and the binding affinity of E7 to pRB (Miller, Munger et al. 2017). Therefore, accounting for the predicted effect of individual viral proteins within mathematical models should be considered.

However, the data shown here demonstrated that MmuPV1 E6 expression can modulate basal cell populations, either by inhibiting the frequency of basal exit in E6 expressing cells, or by stimulating basal exit in other normal cells. Alternatively, E6 may be able to modulate the patterns of symmetrical and asymmetrical division described by Ryser and colleagues in this 'lower' cell population mimic of basal cells, overcoming the negative effect of random chance on the MmuPV1 E6 expressing cell population. Examination of this phenotype within the scope of the high-density competition assay could be attempted by using the EGFP/mCherry fluorescent cell lines in tandem with 3D live-cell imaging, however this has not been possible within the time-frame of this project. In addition to the alteration of cell cycle regulation by viral proteins, and oncogenic effects certain viral proteins have been shown to have on the infected cell, avoidance of immune surveillance by low level expression of viral proteins in the basal layer and HPV modulation of T cell responses are factors that are important for persistence of viral infection, particularly in high risk types (Bodily and Laimins 2011). Whether any HPV types also possess a mechanism of persistence similar to the one shown for MmuPV1 E6 in this chapter has yet to be investigated. Preliminary data (not shown) suggested that HPV11 E6 might also confer phenotypes of persistence on the cells, however further work will be required to validate this initial observation, which forms parts of ongoing research within our lab.

Finally, the Fucci system was used to visualise cell cycle progression in each of the cell lines investigated in this chapter. All three cell lines expressing virus proteins had a greater number of cells entering the cell cycle at both low and high densities when compared to the LXSN control group. As this experiment could only be repeated once due to constraints on time, it is impossible to say whether the slight differences in the number of cycling cells between each of the virus protein expressing cell populations were statistically significant. However, experiments in our lab using the Fucci system with the same FACS-based experimental design have reproducibly shown that other E6 HPV types are also similarly able to drive the cell cycle, and these results were validated further using an alternate quantification approach (Kara Zheng, personal communication). As these data proved to be reproducible, it is reasonable to expect that repeated experimentation with the MmuPV1 Fucci cell lines would also produce consistent data.

High risk HPV E6 and E7 oncoproteins are known to drive cell cycle entry through an array of mechanisms (Pyeon, Newton et al. 2007), and research has demonstrated that some of the beta genus PV E6 proteins are also able to impact the normal response of the cell to DNA

damage by inhibition of p53 target genes such as cell cycle inhibitor p21 (White, Walther et al. 2014). Proteomic studies have shown that some beta genus PV types (HPV38 and HPV92) can even bind to p53 directly, having a posttranslational effect on the protein half-life (White, Kramer et al. 2012). Whether MmuPV1 E6 and E7 proteins drive cell cycle entry in some way is not known for certain, however a recent paper by Meyers and colleagues showed that MmuPV1 E6 could inhibit TGF-β activity by disrupting the transcription complex assembly (Meyers, Uberoi et al. 2017). Inhibition of TGF-β signalling inhibited the induction of keratinocyte growth arrest in this model, which could be the mechanism by which MmuPV1 was shown to drive cell cycle entry in the Fucci system. High-risk HPV16 E7 has also been shown to block TGF-β signalling through interference with the transcription complex (Lee, Kim et al. 2002), an ability which is shared by the E7 protein of low-risk HPV1 E7 (Habig, Smola et al. 2006). These data could suggest a shared mechanism between PVs to interfere with the cell cycle via TGF-β, and it would be plausible to consider whether MmuPV1 E7 possesses such a mechanism. The preliminary data shown in this chapter suggests that MmuPV1 E6 and E7 proteins can also drive cells to enter the cell cycle more often than control cells both pre-confluence and post-confluence. Although the mechanism by which these proteins drive the cell cycle is not known for MmuPV1, it is unlikely that E6 protein utilises MAML1 binding to drive cell cycle entry; disruption of E6 binding to MAML1 did not reduce the proportion of the cell population that had entered the cell cycle.

In conclusion, data presented in this chapter demonstrated that the delay in differentiation and mediation of basal cell density observed in Chapter 3.0 can likely be attributed to MmuPV1 E6, and that the molecular mechanisms behind these phenotypes could involve interference with the Notch signalling pathway; mutation of E6 MAML1 binding abrogated the effect of MmuPV1 E6 on cell density, differentiation delay, and persistence in the lower layer of cells. Importantly, careful analysis of the lower and upper layers of cell culture revealed a mode of persistence conferred upon the cells by MmuPV1E6 only, which is possibly a key mechanism through which PV types that lack so-called ‘oncogenic’ proteins are able to establish and maintain a persistent infection in the basal layer. Both MmuPV1 E6 and MmuPV1 E7 were shown to increase the number of cells entering the cell cycle at both low and high densities, and mutation of E6 MAML1 binding did not appear to affect this phenotype; the MmuPV1E6^{R130A} mutant was shown to result in an increase of cells in the cell cycle that was similar to wt E6 protein. Therefore, it appears that both MmuPV E6 and MmuPV1 E7 have roles in cell cycle entry at low and high densities.

5.0 Cells harbouring papillomavirus genomes

5.1 Introduction

To further investigate the role of E6 in the context of other genes, I attempted to establish a cell line that could stably maintain the MmuPV1 genome. PVs are known to maintain viral episomes in basal cells at a low copy number following initial infection. As E1 has been shown to be possibly dispensable at this stage, it is likely that maintenance replication usually occurs once per S-phase (Egawa, Nakahara et al. 2012). Due to these aspects of the PV life cycle, the study of PVs by transfecting PV genomes into suitable cells to monitor copy number and the effect of the genome on the cell has been used frequently in the field (Chesters and McCance 1989). NIKS cells were chosen for this model as their ability to successfully maintain PV genomes is well established, and keratinocyte cells are known to be naturally infected by PVs (Bedell, Hudson et al. 1991).

Whilst it was thought that experimentation in mouse cell lines may be desirable in the future, we wanted to keep the cell background consistent with the previous chapter (Chapter 4.0). Also, use of NIKS would allow us to compare the effect of MmuPV1 genome with that of HPV11 and HPV16 genomes in the same cell background. While primary keratinocyte cell lines are also often used to study PVs, their heterogeneous nature was less desirable when compared to the homogeneity of NIKS; use of NIKS allows comparison between experiments carried out within a range of passages (Alazawi, Pett et al. 2002). When carrying out comparative analyses in our lab, we find it is useful to keep the cell background constant, particularly when comparing the effect of different mutants or genomes. This allows the examination of subtle differences between cells as a consequence of virus protein or genome expression. While this is also possible in primary cells, the differences in genetic background or passage number may have an effect on the cells. Although NIKS are an immortalised cell line, it has been shown that they respond normally to differentiation signals and contact inhibition, which shows that the features most important to our research are maintained (Allen-Hoffmann, Schlosser et al. 2000).

In the model used in our lab, NIKS cells containing a transfected PV genome are transferred into flasks of culture medium at low density, allowing growth into surrounding empty space. Cells are grown to confluence, which takes approximately four days. This period of growth parallels the time in which keratinocytes would be growing and migrating to fill a space created by a wounding event without differentiating. In wound healing, *in vivo* keratinocyte

cells also proliferate and migrate without differentiating (Paladini, Takahashi et al. 1996). Confluence being reached in monolayer culture initiates early events of keratinocyte differentiation and triggers the productive stage of the life cycle, similar to what is observed during an *in vivo* infection; cell to cell contact inhibits cell proliferation and triggers differentiation (Poumay and Pittelkow 1995). Post-confluence PV-containing NIKS in this culture system are therefore representative of an established PV lesion in that cells have undergone differentiation and are fully confluent. If keratinocyte cells are triggered to differentiate by high density culture, calcium induction, or raft culturing, the culture system is more representative of the later stages of the PV life cycle (Poumay and Pittelkow 1995) (Pillai, Bikle et al. 1990) (Kyo, Klumpp et al. 1997). In this way, the culture model can be used to investigate PVs in representations of different environments. Epidermal keratinocytes have previously been shown to switch between two interconvertible modes of growth dependent on cell density when cultured *in vitro*, therefore careful monitoring of growth pre-confluence and post-confluence allows consideration of these different cell states (Roshan, Murai et al. 2016).

The transfected genome model was chosen to examine the effects of the whole MmuPV1 genome in NIKS cells, to follow up on work carried out with exogenous expression of single proteins as described in the previous chapter. To evaluate the efficacy of the newly established MmuPV1 cell culture model, experiments were attempted in parallel with a 16NIKS cell line, which had previously been successfully carried out in our lab (Murakami, Egawa et al. 2019). In addition, HPV11 NIKS were established, to provide a low-risk HPV comparison (Thomas, Oh et al. 2001). Existing MmuPV1, HPV16, and HPV11 genome vector constructs (shown in Table 2.4) were digested with appropriate restriction enzymes to release the PV genomes, which were subsequently re-ligated to generate circular genomes. Genomes were then transfected into NIKS cells to investigate the effect of the presence of circular MmuPV1 genome on NIKS cells.

5.2 Results

5.2.1 Genome copy number could not be maintained in MmuPV1 NIKS

First, genome copy number was tracked over a period of seven days, to ascertain whether the genomes were successfully maintained in the NIKS cells. The results showed (Figure 5.1) that the 16NIKS cell line was successfully established, with maintenance of genomes from days one to four, and a statistically significant genome amplification post-confluence at day seven.

Conversely, neither the MmuPV1 genomes nor the HPV11 genomes were maintained in their respective cell cultures, and instead the number of copies per cell decreased by roughly 50% each day. These results suggested that during cell doubling, MmuPV1 and HPV11 genomes were not replicating along with the cellular DNA once per S-phase.

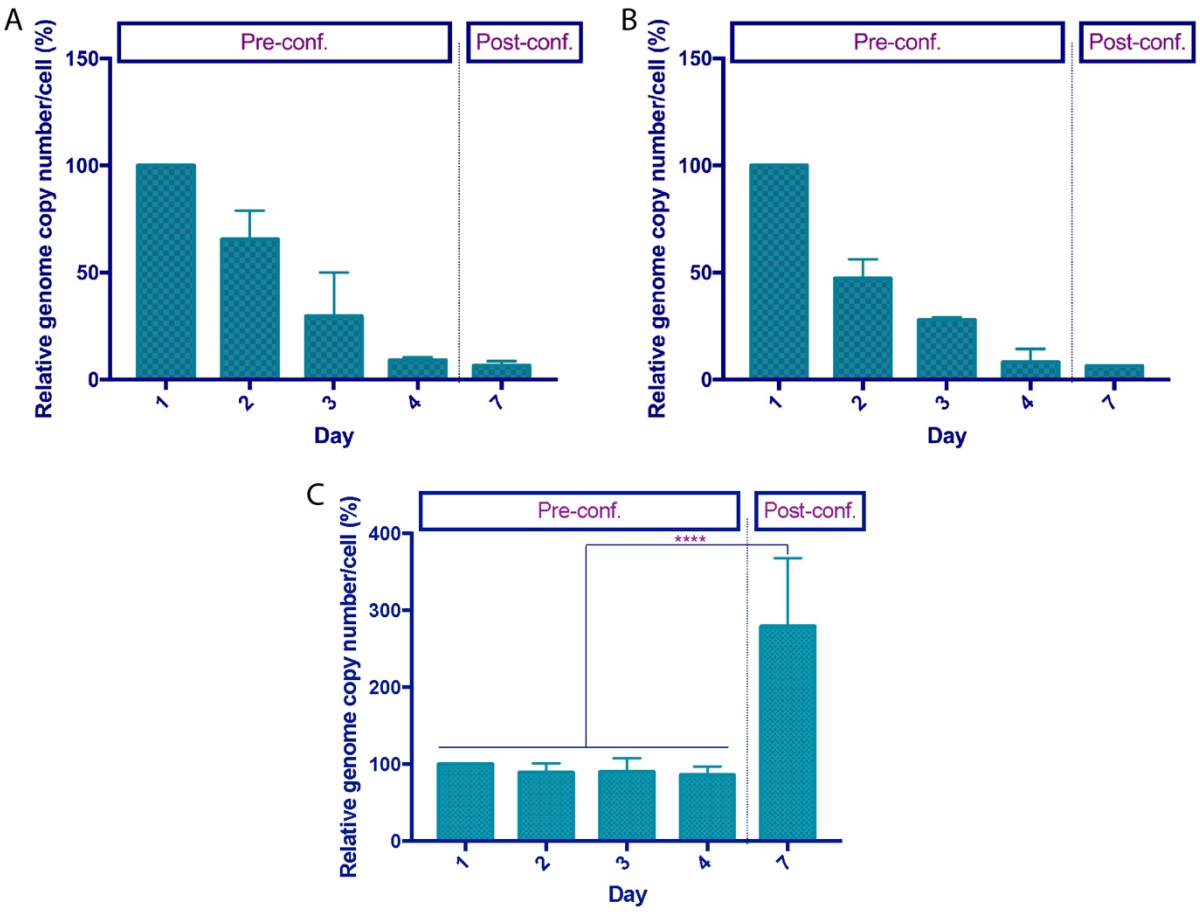

Figure 5.1 Graph to show genome copy number in MmuPV1 NIKS, 11NIKS, and 16NIKS over a period of seven days
The graphs show data from samples collected on days one to four, and day seven. Pre-confluence and post-confluence conditions are indicated with labelling. Bars represent the mean and standard deviations are shown with the error bar plots. Three independent experiments, n=3 for each experiment set (MmuPV1/HPV11/HPV16). P-values were calculated with a two-way ANOVA with Tukey's correction; **** = $P \leq 0.0001$. A; MmuPV1 genome. B; HPV11 genome. C; HPV16 genome.

5.2.2 Effect of EGF concentration on genome maintenance in PV genome harbouring NIKS

Previous work carried out with 16NIKS in our lab has demonstrated that culturing of cells in a higher concentration of EGF media than was usually used in FC media (10 ng/ml EGF) resulted in an increase in genome copy number prior to confluence (Pagliarulo, 2015). Therefore, the genome copy number assay was repeated with cells cultured in FC media with a concentration of 100 ng/ml EGF (termed FC100 media within the text), compared with cells cultured in FC media with the standard EGF concentration of 10 ng/ml EGF (termed FC10 media within the text). Results are shown below in Figure 5.2.

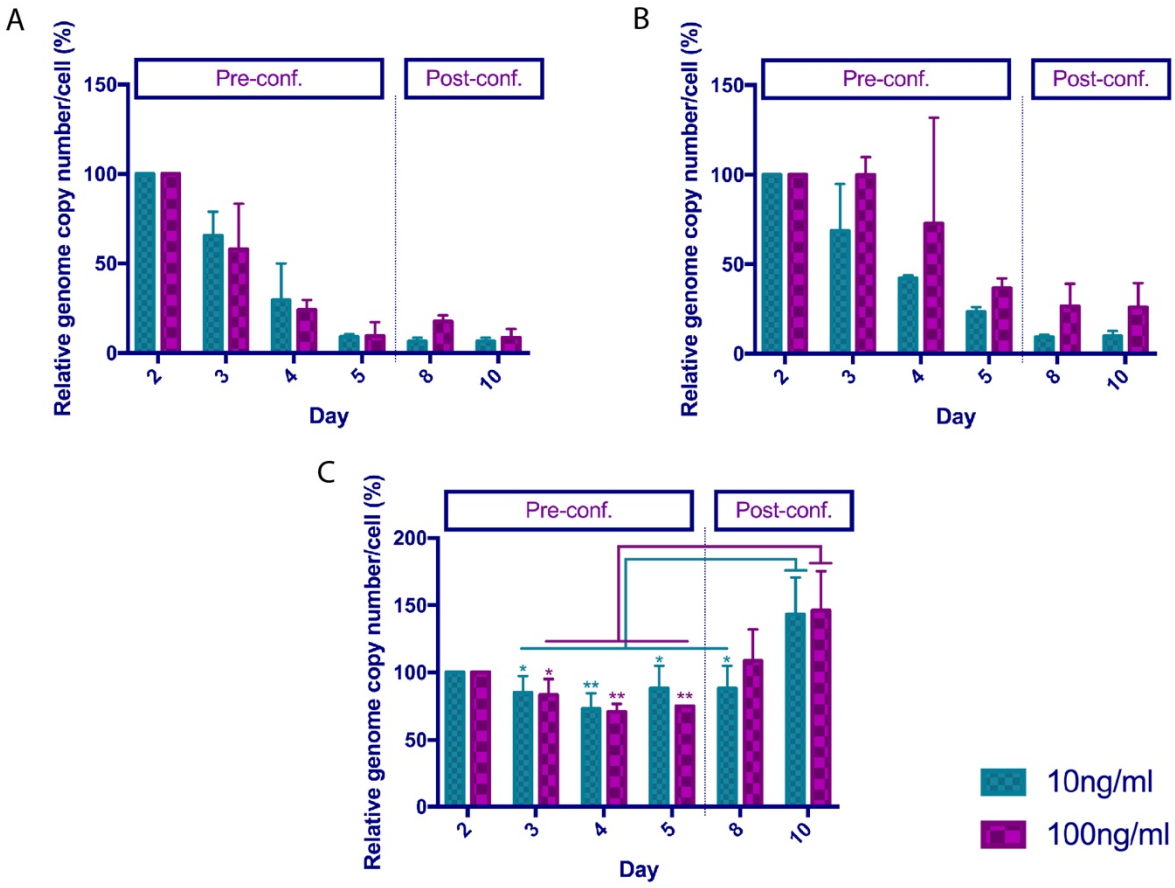

Figure 5.2 Graph to show the effect of EGF concentration on genome copy number in MmuPV1 NIKS, 11NIKS, and 16NIKS over a period of seven days
Two different concentrations of EGF were used: 10 ng/ml and 100 ng/ml. The graphs show data from samples collected on days one to five, day eight, and day ten (day one not shown), at two different EGF concentrations. Pre-confluence and post-confluence conditions are indicated with labelling. Bars are representative of the mean average and standard deviations are shown with the error bar plots. Three independent experiments, n=3 for each experiment set (MmuPV1/HPV11/HPV16). P-values were calculated with a two-way ANOVA with Tukey's correction; * = $P \leq 0.05$, ** = $P \leq 0.01$. A; MmuPV1 genome. Asterisks colour corresponds to the colour of the day 10 comparison. B; HPV11 genome. C; HPV16 genome.

Growth of the cell populations in a higher concentration EGF did not allow successful maintenance of genomes in either the MmuPV1 NIKS or the 11NIKS cell culture systems. Pre-confluence, genome copy number was not maintained over the first four days of culture in either the 11NIKS or the MmuPV1 NIKS when cultured in either FC10 or FC100 media. Interestingly, data showed that EGF concentration may have a mild effect on copy number post-confluence; a slightly higher genome copy number was observed in the FC100 group when compared with the FC10 group in all of the post-confluent time points collected for each group. However, statistical analysis demonstrated that there was no significant difference in genome copy number between cells cultured in FC10 media versus cells cultured in FC100 media.

5.2.3 Impact of EGF concentration on growth of genome-containing NIKS cells

In parallel to the genome copy number experiments, growth assays with cells cultured in both FC10 media and FC100 media were carried out. Cells were cultured for 9 days, and data are shown below (Figure 5.3A). In 11NIKS, 16NIKS, and MmuPV1 NIKS cell lines, the cell populations cultured in FC100 media grew to a higher density than the corresponding FC10 media groups once post-confluent. In contrast, there was no such EGF-mediated difference in cell count prior to confluence being reached at day five. To simplify comparative analysis, all groups at day nine were first compared with normal NIKS cultured in either FC100 or FC10 media as the control group. At day nine, 16NIKS and MmuPV1 NIKS cultured in FC100 media had both reached a density significantly higher than normal NIKS cultured in FC100 media (****$p \leq 0.0001$, **$p \leq 0.01$). Statistically significant higher densities at day nine were also observed in 16NIKS cultured in FC10 media (***$p \leq 0.001$) compared with the appropriate control group (NIKS cultured in FC10 media) (****$p \leq 0.0001$).

It was noted that it may be more relevant to consider the rate of cell growth after reaching confluence at day five, rather than to only consider total cell number at each time point. To analyse the effect of EGF concentration on post-confluent growth rates of each group, the fold change in cell number from day one to day three and day five to day nine was calculated, and plotted into graphs shown in Figure 5.3B and Figure 5.3C respectively. Analysis showed that while there was no significant effect of EGF on rate of growth from day one to day three in any of the groups, both HPV16 NIKS and MmuPV1 NIKS showed a statistically significant response to culture in FC100 media post-confluence from day five to day nine. These data suggests that both MmuPV1 and HPV16 may be able to respond to micro-environmental

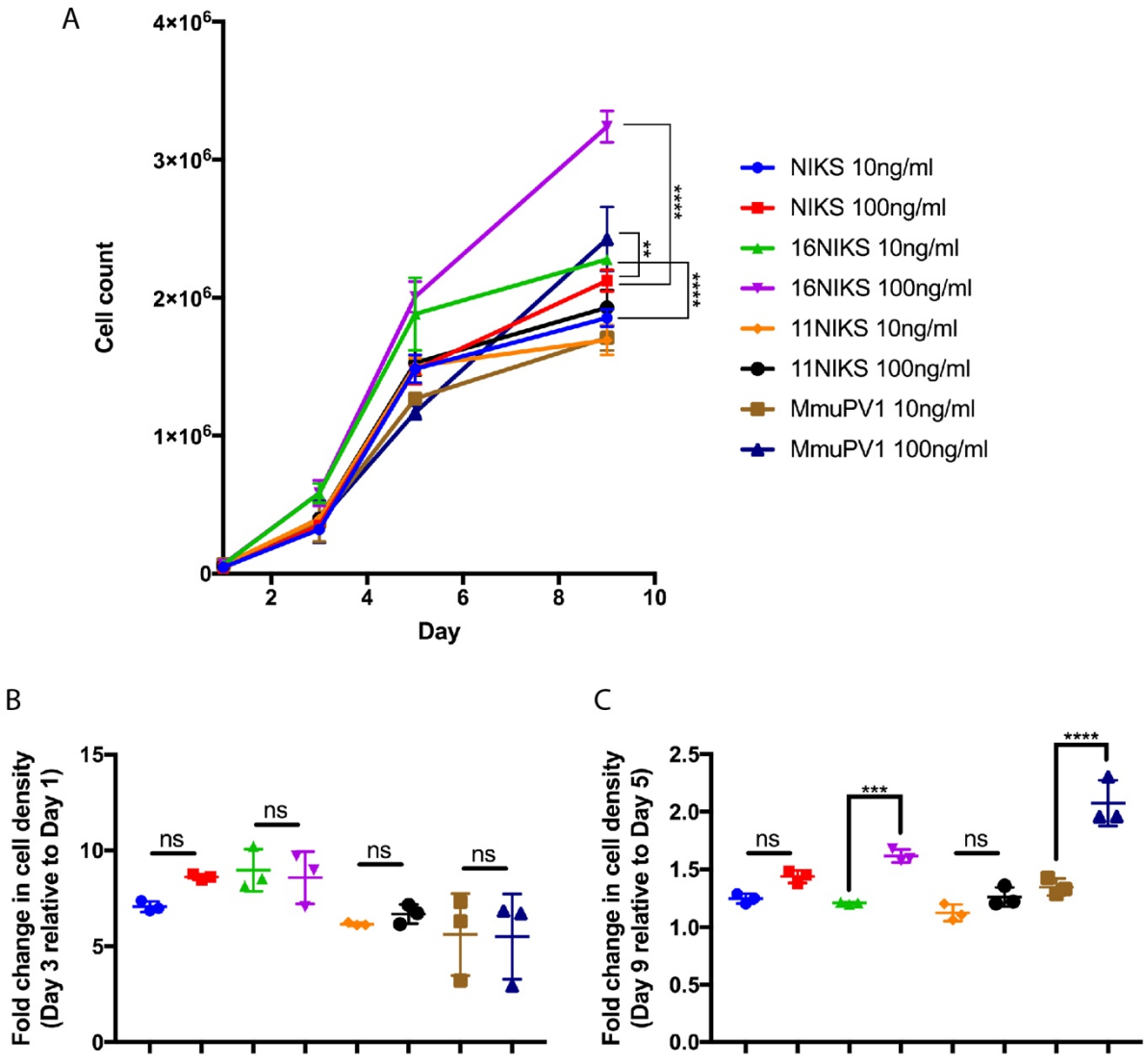

Figure 5.3 Increased EGF concentration has a density-dependent effect on the growth of different cell lines over the course of nine days

Two different concentrations of EGF were used: 10 ng/ml and 100 ng/ml. NIKS, 16NIKS (HPV16 genome), 11NIKS (HPV11 genome) and MmuPV1 NIKS (MmuPV1 genome) were grown in both concentrations of media for comparison of effect of genome, treatment and genome plus treatment. Cell samples were collected on day one, three, five, and nine. A; Data shows the growth of cells over nine days. Each data point represents the mean cell count, and the standard deviations are shown with error bars. Three independent experiments, n=3. P-values were calculated with a two-way ANOVA with Tukey's correction; **** = $P \leq 0.0001$. B; The fold change in cell density was calculated by normalising each replicate for the day three time point by the average cell count for day one in each experimental group. C; The fold change in cell density was calculated by normalising each replicate for the day nine time point by the average cell count for day five in each experimental group. Three independent experiments, n=3. P-values were calculated with a one-way ANOVA with Tukey's correction; **** = $P \leq 0.0001$, *** = $P \leq 0.001$.

changes in EGF concentration to impact cell growth at high cell density with a mechanism that HPV11 lacks. It is also important to consider these data in parallel with previous data which showed that MmuPV1 and HPV11 genomes were not maintained in NIKS cell culture. The effect of EGF could be different if genomes were properly maintained, and the more significant effect on genome copy number observed in 16NIKS cells post-confluence may be due to the amplification of genomes detected at this time point. If this were the case, it may be reasonable to suspect that the MmuPV1 post-confluent response to EGF concentration increase could be even more significant if genomes were successfully maintained. After repeated attempts to stably maintain MmuPV1 and HPV11 genomes in NIKS were unsuccessful, it was decided that work with these cell lines would cease due to time constraints. However, some of the results generated with the 16NIKS cell lines allowed further analysis.

5.2.4 Higher EGF concentration delays differentiation in NIKS and 16NIKS

For 16NIKS in particular, a significant post-confluent impact on cell density was observed in cells cultured in FC100 media. Although not statistically significant, genome copy number was also higher at both post-confluent time points in cells cultured in FC100 media when compared with cells cultured in FC10 media. Therefore, a further experiment was carried out to investigate the effect of culture in FC100 media on the differentiation status of both 16NIKS and normal NIKS cell populations. NIKS and 16NIKS were cultured in 8-well slide chambers (ThermoFisher, UK). Cells were seeded into wells and fixed at day three and day seven after seeding to provide pre-confluent and post-confluent samples for immunostaining analysis. Prior experimentation within our lab has repeatedly shown that K10 staining is present in normal NIKS at day 7 (Murakami, Egawa et al. 2019), so this therefore acted as a positive control. As mentioned in Chapter 3.0, K10 is an early stage marker of differentiation.

Immunostaining data shown below in Figure 5.4 showed that there was no positive K10 staining detected at day 3 in either NIKS or 16NIKS cells cultured in either FC10 media or FC100 media, confirming that cells had not begun to differentiate at this pre-confluent time point irrespective of EGF concentration. Immunostaining results also confirmed that at day seven of the tissue culture model, normal NIKS demonstrated high positivity for K10 staining as expected. Cell culture in FC100 media was shown to notably decrease K10 staining in NIKS cells, whilst in 16NIKS cells cultured in FC100 media, K10 was almost entirely absent. Quantification of signal intensity was carried out using ImageJ software to further validate

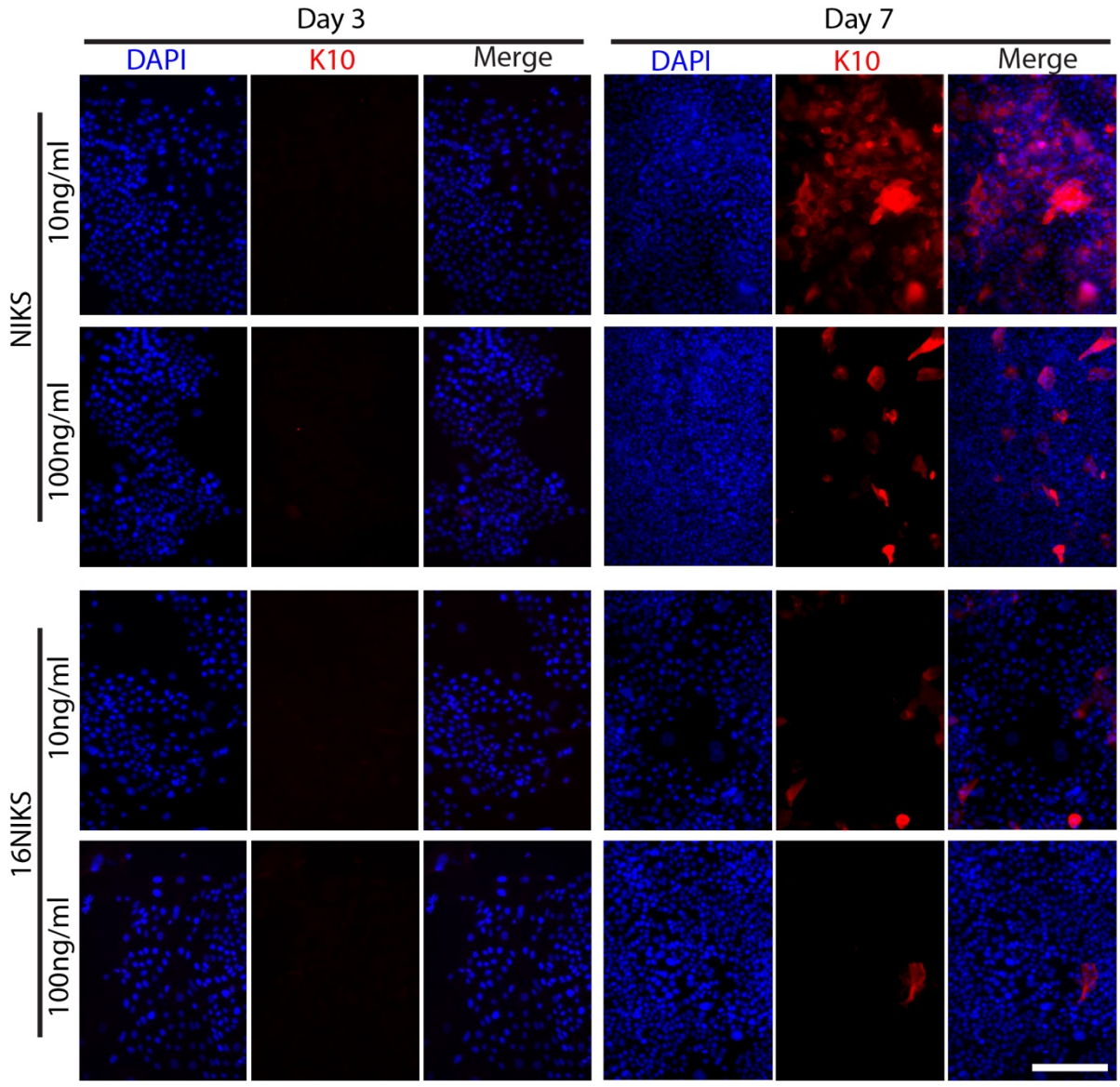

Figure 5.4 A delay in differentiation is observed in cells cultured in media with a higher concentration of EGF, which is more pronounced in cells containing HPV16 genomes
Panels show IF detection of K10 (red) at day three and day seven. Nuclei were counterstained with DAPI to show host DNA. Images show DAPI and K10 stains separately, and then merged. NIKS are shown in the upper panels, while 16NIKS are shown in the lower panels. Scale bar: 100 μm.

these conclusions, as shown below in Figure 5.5. The intensity of K10 staining in NIKS cultured in FC10 media was significantly higher than all three other groups (****$p \leq 0.0001$). Intensity of K10 staining in the NIKS cells cultured in FC100 media was significantly higher than both 16NIKS groups, and the 16NIKS FC10 media group also had significantly higher intensity of K10 staining than the 16NIKS FC100 media group (***$p \leq 0.001$). These results confirmed that cells were differentiating normally in the standard culture model, and that the presence of HPV16 genomes resulted in a decrease in the number of K10 positive cells observed, separate to the decrease in cell differentiation seen in response to increased EGF concentration. As an increase in concentration of EGF in culture media had been shown to have an effect on the genome copy number, the cell growth, and the differentiation status of 16NIKS cells, a third experiment was carried out to look at the effect of a higher concentration of EGF on genome copy number.

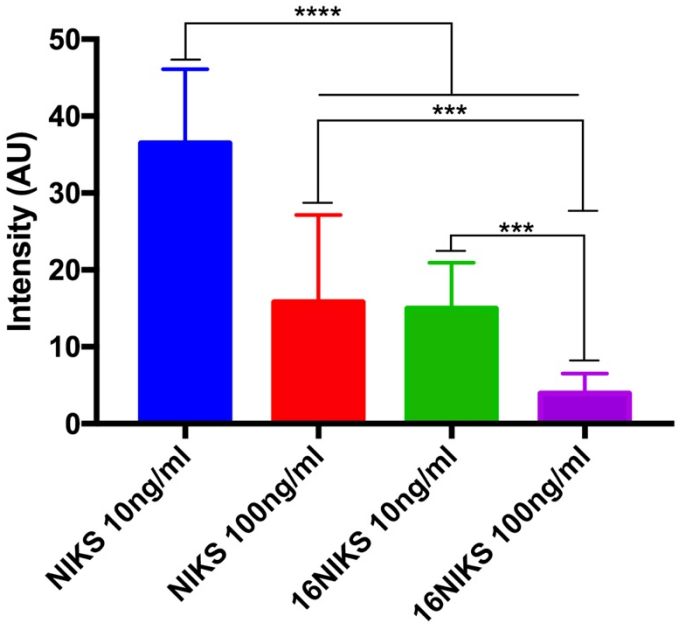

Figure 5.5 Higher concentration of EGF delays differentiation in NIKS and 16NIKS
Graph indicates intensity of K10 fluorescence in arbitrary units. All values were normalised by subtraction of background intensity. One independent experiment, n=18. P-values were calculated with a one-way ANOVA with Tukey's correction; **** = $P \leq 0.0001$, *** = $P \leq 0.001$.

5.2.5 Post-confluent effect of EGF on genome copy number and gene expression in 16NIKS

Experiments to investigate the effect of increasing EGF concentration on genome copy number were repeated, and an extra experimental group of cells cultured in FC media with a higher concentration of 500 ng/ml of EGF was added (termed FC500 within the text). Results are shown below in Figure 5.6. Prior to confluence, no significant difference in genome copy number per cell was observed between any of the experimental groups. However, genomes of 16NIKS cells cultured in FC500 media reached a significantly higher genome copy number than both other groups at day ten (****$p \leq 0.0001$), and the genome copy number per cell of 16NIKS cultured in FC500 media was also significantly higher than cells cultured in FC10 media at day eight (**$p \leq 0.005$). To try to understand the effect of EGF concentration on genome copy number in more detail, an investigation into the post-confluent effect of FC500 media versus FC10 media on RNA expression was carried out. A previous publication has demonstrated that changes to EGF concentration can affect splicing of HPV16 E6, therefore we expected to see some effect on gene expression in this experiment (Rosenberger, De-Castro Arce et al. 2010). RNA had been extracted from the cell samples at the same time as DNA was extracted, so these RNA samples could be interpreted in relation to the observed change in genome copy number.

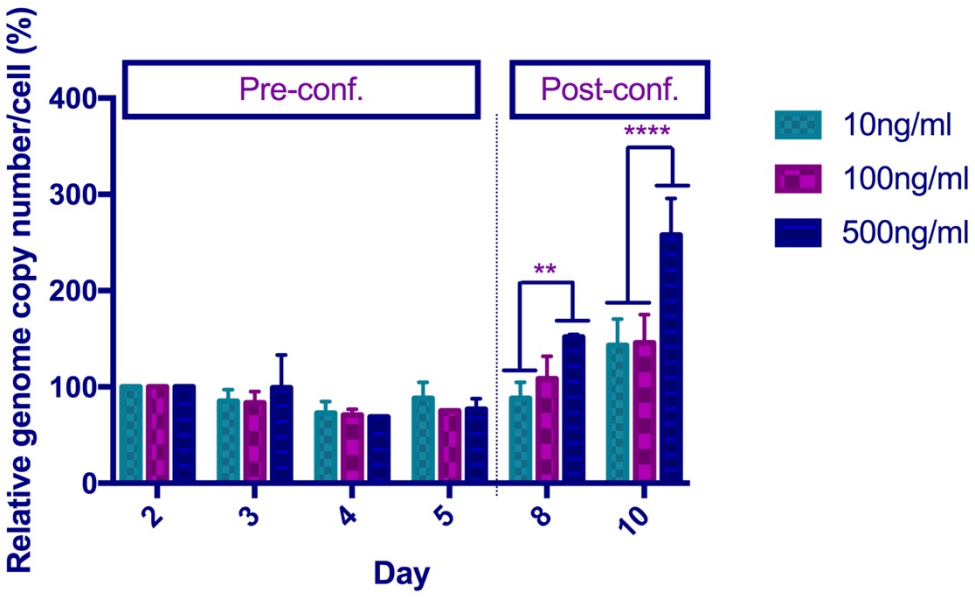

Figure 5.6 The effect of 500 ng/ml EGF concentration on 16NIKS genome copy number per cell
Graph shows genome copy number of cells collected cultured in three different concentrations of EGF: 10 ng/ml, 100 ng/ml, and 500 ng/ml. Cell samples were collected on days one to five, seven and nine (day one not shown). The bars show the average and the standard deviations are shown with error bars. Three independent experiments, n=3. P-values were calculated with a two-way ANOVA with Tukey's correction; **** = $P \leq 0.0001$, ** = $P \leq 0.01$.

Analysis of RNA by cDNA synthesis and qPCR (Figure 5.7) showed that while no significant difference was seen in levels of expression of any of the transcripts investigated at day five or day eight, at day ten there was a significantly higher level of expression of all transcripts examined in 16NIKS cells cultured in FC500 media when compared to those cultured in FC10 media. Expression of target genes was normalised to levels of GAPDH within each sample, to allow for control of experimental variation between the samples. E1 was chosen because it is a DNA helicase, and therefore a likely candidate in mediating an effect on genome copy number. Similarly, E5, E6, and E7 were chosen because these three proteins are often referred to in the field as oncoproteins, and were therefore also considered as likely candidates for involvement in the increase in genome copy number and cell density observed (Roden and Stern 2018).

All primers used in this section were designed by Dr Heather Griffin. For E6, primers that could distinguish between the total level of E6 transcript (E6T) and primers specific to full-length E6 only (E6FL) were used. The HPV16 E6 intron contains one 5' splice site, as well as a further three 3' splice sites. If this intron is not spliced, full length E6 is expressed by the resulting E6E7 mRNA. However, if E6E7 pre-mRNAs are spliced using one of the alternative 3' splice sites, E6 splice variants are produced (Zheng and Baker 2006). Data shows expression of E6FL relative to E6T, which indicated a shift in splicing preference from around 8% to 17% of E6FL relative to total E6 transcripts expressed at day ten. Overall the results show a significant increase in viral RNA transcript expression in 16NIKS cells cultured in FC500 media as opposed to those cultured in FC10 media.

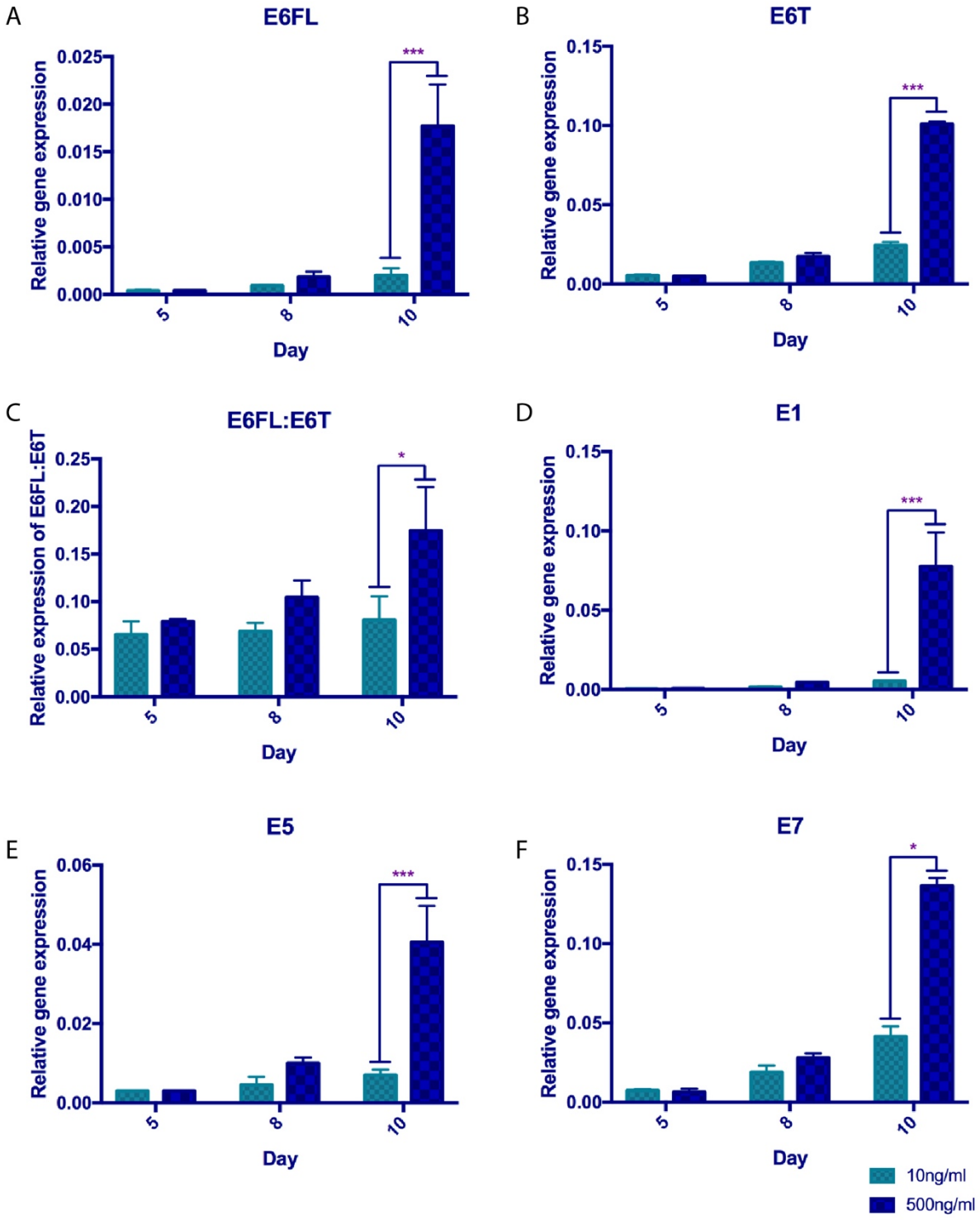

Figure 5.7 Effect of EGF on HPV16 RNA transcription in post-confluent cells
Expression of RNA transcripts in HPV16 genome-containing cells cultured two different concentrations of EGF: 10 ng/ml and 500 ng/ml. A; relative expression levels of E6 full length (FL) transcript. B; relative expression levels of total E6 transcripts (E6FL plus all splice variants). C; expression levels of E6FL transcripts relative to total E6 transcripts. D; relative expression levels of E1 transcript. E; relative expression levels of E5 transcript. F; relative expression levels of E7 transcript. Three independent experiments, n=3. P-values were calculated with two-way ANOVAs with Tukey's correction; *** = $P \leq 0.001$, * = $P \leq 0.05$.

5.3 Discussion

The propagation of cells containing high-risk PV genomes is a well-established technique in the PV field (Doorbar 2016), therefore generation of NIKS cells containing MmuPV1 genomes was a reasonable investigation to pursue. Unfortunately, it was not possible to maintain the MmuPV1 genome or the HPV11 genome in NIKS cell culture, with or without culture in media with a higher concentration of EGF. Although a previous publication from our lab did manage to maintain the HPV11 genome in NIKS cells during pre-confluent growth (Murakami, Egawa et al. 2019), few other studies have successfully propagated cells containing low-risk HPVs, and maintenance of these genomes proved difficult due to the lack of any conferred growth advantage (Thomas, Oh et al. 2001, Oh, Longworth et al. 2004). Another paper did demonstrate maintenance of HPV11 genomes in N-Tert cells, and described induction of a productive life cycle in organotypic rafts of these cells, however this work has not since been reproduced (Fang, Meyers et al. 2006). Therefore, the difficulties in establishing NIKS cells that could stably maintain the MmuPV1 or HPV11 genomes were understandable. It may be that MmuPV1 and HPV11 promoter activity is not high enough to sustain the viral life cycle in NIKS; as shown in Figure 4.2, expression levels from the MmuPV1 genome were much lower than that of the LXSN-based vectors. In contrast, the genomes in the HPV16 NIKS cell line were successfully maintained and amplified post confluence as expected. Attempts to improve genome maintenance in the cell lines by increasing the concentration of EGF present in the culture media demonstrated a mild effect of EGF on genome copy number, as well as statistically significant effects on growth and differentiation status of the cells. All of these effects were observed at post-confluent time points.

Physiological relevance of the use of FC10, FC100 and FC500 was considered. Standard methods for the culture of keratinocytes use media with a concentration of 10 ng/ml of EGF (Davy & Doorbar, 2005). However, little is known for certain about physiological levels of EGF, either in normal skin or in a wounded site. One study employing radiolabelling of EGF found that in adult male mice, levels of EGF in the submaxillary glands (the major EGF production site in mice) rose to around 1000 ng/ml (Byyny, Orth et al. 1972) whilst the skin was shown to contain around 0.06 ng/ml. In humans, wet tissue has been shown to contain around 1.3-5.5 ng/g of EGF (Hirata and Orth 1979). Hauner and colleagues postulated that as serum concentration of EGF in human blood has been found to be in the range of 0.5-2 ng/ml, this may at least reflect a level at which physiological effects might occur (Hauner, Rohrig et al. 1995). Although the actual physiological levels of EGF in the skin of humans or mice

remain unclear, it is likely that the medias used in these experiments provide experimental conditions of EGF that are higher than what is present *in vivo*. EGF is known to inhibit terminal differentiation and stimulate cell proliferation (Blumenberg 2013). The growth factor is present in high concentrations at the basal layer, which then decreases as cells move towards the epidermal surface whilst differentiating (Fuchs 2008). EGFR and its ligands are also known to increase during wound healing, to improve the migratory potential and proliferative capabilities of keratinocytes in the wound area (Werner and Grose 2003). In our model, pre-confluent culture of PV genome-containing NIKS is representative of wound healing and the establishment phase of HPV infection.

Data collected from the growth assays carried out in parallel to the first genome copy number experiments clearly showed that there was little difference between cell growth in FC10 media and FC100 media up to confluence. However, post-confluence, cells cultured in FC100 had a slight growth advantage over their counterparts grown in FC10 media. Similar general pro-proliferative effects of EGF on keratinocytes have been shown in other research (Hebert, Wu et al. 2009, Puccinelli, Bertics et al. 2010). However, recent computational modelling of the effect of local high EGF concentration on the migration of keratinocytes found a negative correlation between high EGF and the distances keratinocytes had migrated across, suggesting a more complex and potentially biphasic role for EGF in keratinocyte migration (Andasari, Lu et al. 2018). Whilst migratory phenotypes were not important for the phenotypes of cells examined post-confluence, it is something to bear in mind for future work that may investigate pre-confluent samples in greater detail.

Post-confluence, 16NIKS cultured in FC100 media had a notable growth advantage over 16NIKS grown in FC10 media, as well as all other cell types cultured, which was shown to be statistically significant at day nine (****$p \leq 0.0001$). MmuPV1 NIKS cultured in FC100 media also showed a significant increase in cell density at day nine when compared to normal NIKS cultured in FC100 media (**$p \leq 0.01$) and MmuPV1 NIKS cultured in FC10 media (****$p \leq 0.0001$). More in-depth analysis considering the effect of increased EGF concentration on the rate of cell growth pre-confluence and post-confluence indicated that the actual rate of growth in cells between day five and nine was statistically significantly higher in response to the EGF concentration in 16NIKS cells and MmuPV1 NIKS cells only. This analysis also allowed more detailed examination of growth rates in all groups. For example, although the cell counts of 16NIKS and NIKS shown at day nine are statistically different, 16NIKS cultured in FC10 did not increase in density from day five to day nine at a greater

rate than that of normal NIKS. Overall, these data suggests that HPV16 and MmuPV1 may be able to respond to density-dependent micro-environmental changes in EGF concentration in a manner that affords the infected cell a competitive advantage over normal keratinocyte cells. Unfortunately, as MmuPV1 and HPV11 genomes were not maintained day by day, these data are somewhat difficult to interpret. With successful genome maintenance, the growth advantage of MmuPV1 cells cultured in FC100 might be even more significant, and HPV11 may in fact show a significant response to changes in EGF concentration.

K10 staining was employed to investigate the differentiation status of the 16NIKS cells and the effect of culture in media with a higher concentration of EGF on differentiation of the cells. Culture in FC100 media resulted in a statistically significant decrease in K10 staining intensity in NIKS, whereas in 16NIKS cultured in FC100 media the K10 signal was almost entirely absent. The effect of HPV16 on differentiation has long been known, with studies on whole genomes and expression of individual proteins also demonstrating that differentiation is delayed by HPV16 proteins (McCance, Kopan et al. 1988) (Woodworth, Mcmullin et al. 1995). It has previously been shown that E6 can inhibit differentiation and keeps cells in cycle by directing degradation of p53 (Thomas, Hubert et al. 1999). Further, research in our lab suggests that E6 may mediate continued cell proliferation by inactivation of Notch signalling as well as p53, allowing avoidance of normal differentiation (Kranjec, Holleywood et al. 2017). Studies have shown that the activation of the Notch pathway acts as a definitive switch in keratinocyte cell status from proliferative to differentiating (Kolly, Suter et al. 2005). Taken together with the data collected, it is evident that increased EGF concentration delays the differentiation of keratinocytes, whilst presence of HPV16 genomes leads to inhibition of differentiation to a greater extent. This more significant delay in differentiation observed could be the result of inactivation of Notch signalling, which could also be responsible for the additional cell growth advantage observed in 16NIKS. Recent studies in lung cancer cell lines have suggested that crosstalk between Notch and EGFR pathways can occur, so changes in EGF concentration may even be influencing Notch directly, although this would have to be further investigated for confirmation (Giannopoulou, Nikolakopoulos et al. 2015).

Taking this decrease in K10 positive cells into account along with the significant increase in cell number shown at day nine for 16NIKS cultured in FC100 media, it was interesting to consider how these cells were physically growing beyond confluence; general interpretation of K10 staining patterns in normal NIKS suggested that cells piling up into the upper layers

would be positive for K10, however in 16NIKS, little to no K10 was seen despite the greater density of cells. One potential mechanism by which HPV16 could form lesions in infection may be by overcoming normal cell density restrictions and growing to greater densities beyond confluence. A recent study into growth of keratinocytes divulged two distinct and interconvertible growth modes in human keratinocytes, and found that the switch between these two was regulated by confluence (Roshan, Murai et al. 2016). Control of this switch could possibly be modified in PV infected cells, and overcoming the control of these modes of growth through an EGF related mechanism may be involved in cell growth to higher densities in 16NIKS and also in MmuPV1 NIKS post-confluence.

Further investigation into the effect of a higher concentration of EGF in 16NIKS revealed a significant increase in genome copy number at day 9 between the cells cultured in FC10 media and those cultured in FC500 media. Comparative RNA analysis between these post-confluent time points was carried out. Previous studies have confirmed that changing the EGF concentration can influence splicing of HPV16 E6 transcripts in immortalised keratinocyte cell lines (Rosenberger, De-Castro Arce et al. 2010). Rosenberger and colleagues showed that an increase in EGF concentration led to a shift in splicing patterns towards increased expression of full length E6. However, this experiment was only carried out over 9 hours whereas the above experiments were carried out over 10 days, which makes any direct comparison difficult. At day five and day eight, there was no significant difference in RNA expression between the FC10 and FC500 groups. However, at day 10 there was a significantly higher level of RNA expression in all transcripts examined in the FC500 group compared with the FC10 group. Although abundance of mRNA is not always predictive of protein level (Payne 2015) (Maier, Guell et al. 2009), increased transcription of genes could result in a subsequent increase in the protein levels within the cells. The oncogenic potential of the E6 and E7 proteins has been thoroughly described in Chapter 1 (Section 1.8), and an increase in these proteins within the cell could contribute to the post-confluent growth advantages observed in the 16NIKS cells cultured in FC100 media. HPV16 E5 protein could similarly be expressed at higher levels as a result of increased levels of E5 viral transcripts. HPV16 E5 protein has been shown to alter the endocytic trafficking of EGF molecules (Suprynowicz, Krawczyk et al. 2010) and also possibly plays a role in upregulation of EGFR-mediated signal transduction by interfering with normal ubiquitination of EGFR (Zhang, Srirangam et al. 2005). Increased levels of E5 protein could therefore amplify the existing EGF-mediated effects on cell growth and differentiation, which could contribute to the growth advantage observed in the cells cultured in higher concentrations of EGF. However,

increased expression of E5 transcript is difficult to interpret; all early HPV16 mRNA products contain the E5 sequence, which therefore means an increase in detected expression of E5 transcript does not necessarily equate to an increase in E5 transcript expression alone (transcript map can be accessed at https://pave.niaid.nih.gov/).

E1 is the HPV DNA helicase (Hughes and Romanos 1993), therefore a rise in transcription of E1 mRNA could result in an increase in protein levels, which could in turn lead to an increase in genome replication and consequent higher copy numbers per cell. Studies carried out by Egawa and colleagues suggested that E1 was required for both initial establishment of infection and the final productive stage of the life cycle, but was dispensable for the maintenance phase (Egawa, Nakahara et al. 2012). These results indicate two different ways in which HPV genomes can be replicated, an E1-dependent and an E1-independent method of replication. Further evidence for two methods of genome replication was shown in experimentation with HPV31 and HPV16 DNA replication. Results indicated that both HPV types were capable of replicating once per cell cycle at S phase along with the cell replication, as well as being able to replicate independently of the cell cycle at random (Hoffmann, Hirt et al. 2006). Considering these results, it is plausible that a higher concentration of EGF could be stimulating replication of genomes to occur through both mechanisms. In cells cultured in FC10 media post-confluence, genomes must be replicating in an E1-dependent manner; this is required for the amplification stage of the virus life cycle to occur (Egawa, Nakahara et al. 2012). Additionally, research has shown that HPV16 E1-dependent replication requires E6; expression an HPV16 E6 binding deficient mutant in HPV16 genome-containing cells meant that E1-dependent genome amplification was not supported post-confluence. HPV16 E7 was also shown to modulate the cellular environment to facilitate E1-dependent replication (Murakami, Egawa et al. 2019). Therefore, the observed increase in E6 and E7 mRNA expression and possible resulting increase in protein levels could also be making the cellular environment more favourable for E1-dependent replication to take place.

Previous studies have established that phosphorylation events can influence E1 protein intracellular localisation. HPV 11 E1 was shown to shuttle in and out of the nucleus via nuclear import and export signals located within the E1 protein, with overall regulation being controlled by phosphorylation. Nuclear import was stimulated by phosphorylation events triggered by signalling from the MAPK signalling cascade (Yu, Lin et al. 2007). Further, phosphorylation of key residues by Cdk2 was shown to promote HPV 11 E1 accumulation in the nucleus, by inhibition of nuclear export (Deng, Lin et al. 2004). In this way,

phosphorylation and subsequent inactivation of the NES by CDKs allows E1 to build up in the nucleus, which in turn would support replication of viral DNA. Further research has shown that mutation of the HPV16 E1 protein within its MAPK phosphorylation sites resulted in inhibition of E1 nuclear accumulation, which again demonstrates the importance of phosphorylation in localisation of E1 to the nucleus (Egawa, Wang et al. 2017). As current understanding shows phosphorylation events as crucial in localisation of E1, it is plausible that increased EGF concentration could stimulate MAPK or Cdk2 signalling via the EGFR, resulting in prolonged localisation of E1 in the nucleus. This could be a mechanism by which higher EGF concentration leads to an increased genome copy number during the post-confluent phase of the cell culture model.

Culture of 16NIKS in media with a higher concentration of EGF led to a two-fold increased splice preference for E6FL. Splice variants of high-risk HPV16 E6 have been shown to have many different oncogenic effects in cell culture, including induction of DNA damage as a result of increased ROS (Williams, Filippova et al. 2014), directing the degradation of cellular adhesion proteins (Pim, Tomaic et al. 2009), and stabilising the oncoproteins E6 and E7 (Ajiro and Zheng 2015). Such research suggests that splice variants have pro-oncogenic effects that are beneficial to the virus in infection. However, *in vivo* analysis of splice variants showed that overexpression of the small splice variant of E6 (E6*) led to a decrease in tumour growth in a nude mouse model (Filippova, Evans et al. 2014). Research has also shown that E6* may lack the ability to immortalise keratinocyte cells in culture, or at least is not required for the immortalisation of the cell to be successful (Sedman, Barbosa et al. 1991). Therefore, the impact of the splice preference shift observed is somewhat difficult to interpret. However, coupling of the splicing preference shift towards E6FL with the post-confluent increased genome copy number and cell growth in 16NIKS cells cultured in higher concentrations of EGF suggests that, within the context of this assay, the effect of increased levels of E6FL expression relative to the amount of total E6 expression is beneficial to the virus.

As HPV needs to first infect basal cells to establish an infection, the virus may need to tightly regulate gene expression in response to external factors of the microenvironment such as EGF. Whilst the changes observed may appear small, current interpretation in the lab suggests that in normal conditions, careful regulation of E6 is required to allow a precise response to the surrounding environment; slight changes in E6 expression are believed to have significant effects. It is also important to bear in mind that the changes observed occur in a heterogeneous population. As shown previously in Section 3.2.10, there is a heterogeneity of

expression of E6/E7 RNA *in vivo* which is likely to be represented in cell culture. The presence of a heterogeneous population in cell culture is further demonstrated by the K10 staining analysis shown in both Chapter 4 and Chapter 5; not all cells in a post-confluent culture stained positive for K10, indicating that cells within a population are heterogeneous. Heterogeneity is further emphasised by the confocal analysis shown in Figure 4.4, showing that cell states can also differ depending on the layer in which the cells are present. Therefore, even slight shifts in total expression levels and splice preferences overall can represent a significant change in the status of cells within the population. A different effect or mechanism than splicing preference change would be expected in low-risk or mouse mRNA expression analysis if the experiments had been carried out; HPV11 and MmuPV1 lack an internal splice site in E6 (Sedman, Barbosa et al. 1991, Xue, Majerciak et al. 2017). Based on data shown in the previous two chapters, it is reasonable to postulate that MmuPV1 may also be able to delay differentiation by interference with the Notch signalling pathway through MAML1 binding. Future studies could attempt to confirm this if issues around maintenance of the genome are overcome.

In conclusion, the data presented in this chapter demonstrates a role for EGF in delaying differentiation in NIKS in agreement with previously published data. A role for high level EGF concentration in mediation of HPV16 RNA transcript expression levels was also shown, suggesting that HPV16 can respond to external stimuli of the microenvironment in a density-dependent manner. The precise mechanisms by which this effect on transcript expression might be involved in the increase in genome copy number and growth advantage are not fully understood, although several potential interactions were discussed. While it was not possible to maintain the MmuPV1 genome, which was the primary goal of this experiment, preliminary data suggest that the MmuPV1 genome could afford a post-confluent EGF-dependent growth advantage on NIKS cells even at relatively low copy numbers within the population. This is in agreement with data from the previous chapter that showed that exogenous expression of MmuPV1 E6 protein in NIKS cells modulated cell density post-confluence.

6.0 Final Discussion

6.1 Summary of work

In this thesis, the mouse model of PV infection has been utilised alongside cell culture techniques to elucidate a role for MmuPV1 E6 in establishing infectious lesions. Improvements to the model have been made by consideration of wounding techniques, and a more thorough understanding of the timing and mechanisms of wound healing. Stages of early lesion formation were characterised, and an increase in cell density unique to these earlier stages was observed. This could not be properly explained by increased mitosis or cell cycle entry in infected cells alone, therefore the differentiation status of the cells was investigated.

6.1.1 Differentiation delay in MmuPV1 E6/E7 expressing cells in vivo

A delay in differentiation was observed in tandem with a surprising HES1 RNA expression pattern. Although differentiation was delayed in infected cells, HES1 RNA expression appeared to be elevated in the infected cells relative to uninfected cells. This gave further credence to the idea that while HES1 expression is commonly understood to be downstream of the Notch signalling pathway, it's presence does not mean that those cells have begun to differentiate. As MmuPV1 E6 is expected to interfere with Notch signalling by binding to MAML1 to disrupt formation of the ternary complex required for downstream signalling, it was surprising that HES1 RNA expression was relatively high in infected tissue. Previous data showed that MmuPV1 E6 expression in human cells led to a decrease in expression of HES1 RNA (Meyers, Uberoi et al. 2017). However, we observed a relative increase in levels of HES1 RNA expression in MmuPV1 E6/E7 expressing cells. This suggested that the interaction of MmuPV1E6 with MAML1 *in vivo* is not able to fully disrupt signalling downstream of the ternary complex. Alternatively, it could be possible for Notch signalling to progress in the absence of MAML1 in certain conditions. Previous research has suggested that other isoforms of MAML could compensate for the loss of MAML1, which could also explain the expression patterns described above (Oyama, Harigaya et al. 2011). Although commonly associated with Notch signalling, expression of HES1 can be upregulated by other pathways, such as Hedgehog and Wnt pathways (Liu, Dai et al. 2015). Therefore, signalling through these pathways could be having a Notch-independent effect on HES1 expression and should be investigated in future experiments. Irrespective of the relatively high HES1 expression levels, differentiation was delayed in E6/E7 expressing cells. Future work can

examine this phenotype in greater detail. Excitingly, productive microlesions were located in a small subset of infections of fully immunocompetent mice. Although evidence of infection has been visualised in some immunocompetent mice previously (Uberoi, Yoshida et al. 2018, Spurgeon, Uberoi et al. 2019), this was the first time that microlesions had been observed *in situ* in C57BL/6J mice. Both the delay in differentiation and the relative increase in HES1 RNA expression were also observed in immunocompetent mice.

6.1.2 Heterogeneous E6/E7 expression could correlate with basal layer exit

Mathematical modelling of the expression levels of MmuPV1 E6/E7 RNA in collaboration with Dr Alberto Giaretta suggested a potential bimodality of expression in cells. Expression of E6/E7 RNA was significantly higher in a sub-group of basal cells with cell morphology indicative of basal exit when compared to the remainder of the cell population. This suggested that expression of MmuPV1 E6/E7 may occur at two levels: one larger subgroup of cells expressing E6/E7 RNA at a lower level may be modulating maintenance of viral genomes in the basal layer, and a second smaller sub-group with higher levels of E6/E7 RNA expression could be those cells exiting the basal layer. Whether increased E6/E7 expression within these selected cells is triggered by initiation of the exit from the basal layer, or whether the increased expression of E6/E7 RNA itself is in some way causative of basal exit is not clear, and would have to be further considered with future experiments.

6.1.3 Exogenous expression of viral proteins in vitro suggests that differentiation delay and cell density regulation is mediated by MmuPV1 E6 interacting with MAML1

From the various phenotypes observed using the mouse model of PV infection, it was clear that MmuPV1 was able to affect differentiation status, cell growth, and cell density *in vivo*. To further understand the mechanisms and proteins involved in these phenotypes, cell lines exogenously expressing MmuPV1 E6 and E7 were established. Experimentation with these cell lines revealed that MmuPV1 E6 was involved in an increase in cell density and delay in differentiation in post-confluent NIKS cells. Further, investigation into the layers of the cell culture system by using EGFP/mCherry expressing cell lines showed that cells expressing MmuPV1 E6 were able to persist in the lower layer of culture, whilst control NIKS/LXSN cells were located mostly in the upper layer after a period of ten days. In comparison, cells expressing MmuPV1 E7, control LXSN-expressing cells, and an E6 MAML1 binding mutant, demonstrated a random distribution of experimental cells and control cells between the lower and upper layers. This phenotype was also observed in 3D organotypic raft culture, giving

further evidence in support of the suggested growth advantage afforded by MmuPV1 E6. Repetition of cell culture experiments with the mutant $E6^{R130A}$ suggested that the effects that expression of MmuPV1 E6 protein had on cell growth, differentiation delay and lower layer persistence in post-confluent NIKS cells were dependent on E6 interaction with MAML1 protein; abrogation of E6 binding to MAML1 led to a loss of these phenotypes in NIKS cells.

6.1.4 Cell lines stably expressing PV genomes

While establishment of NIKS that could stably maintain MmuPV1 genomes or HPV11 genomes during pre-confluent growth was not possible within this thesis, a role for HPV16 genomes in relation to changing concentrations of EGF was examined. Culture of cells in FC100 media resulted in a delay in differentiation of NIKS cells post-confluence, which was further exaggerated by the presence of HPV16 genomes. These data suggested that 16NIKS cells can respond to changes in micro-environmental EGF in a density-dependent manner. Post-confluent transcription of key early RNA transcripts was higher in cells cultured in FC500 media as opposed to those cultured in FC10 media, and a significant post-confluence increase in genome copy number per cell was also quantified in cells cultured in FC500 media. Mechanisms were suggested to explain how 16NIKS could respond to external microenvironment changes to increase expression of viral genes and genome copy number. A potential response to increased EGF concentration post-confluence was also demonstrated with MmuPV1 genome-containing cells, despite the relatively low copy number. Future experiments with HPV11 and MmuPV1 genomes could uncover similar mechanisms for these PV types.

6.2 Future directions

6.2.1 MmuPV1 and the immunocompetent mouse

One aspect of the research that could not be more thoroughly pursued during the course of this PhD was the immunocompetent mouse. Discovery of the microlesions in tail tissue was exciting, and demonstrated the suitability of the C57BL/6J mouse for use in studying PV infection, given accurate and thorough analysis of a large enough sample size of infection sites. It is generally understood that the immune response plays a large role in whether an infection will persist, or be cleared from infected individuals. Some HPV types have been shown to modulate the immune response in a variety of ways, such as interference with IFN signalling pathways, induction of regulatory T cell infiltration, and low level expression of

class I MHCs, which impedes the function of cytotoxic T cells (Song, Li et al. 2015). In particular, some beta papillomaviruses have been shown to interfere with expression of toll-like receptors to impact upon the innate immune response and possibly deregulate the cell cycle (Pacini, Savini et al. 2015). In addition, HPV 8 E7 has been shown to impede the recruitment of Langerhans cells to the site of infection through sequestration of C/EBPβ, preventing it from binding to the promoter of the chemoattractant CCL20, which is necessary for successful recruitment (Sperling, Oldak et al. 2012). Further research using this model will allow detailed analysis of the immune system in relation to MmuPV1 infection. Analysis of infection in a fully immunocompetent mouse may glean important new information as to how MmuPV1, a pi papillomavirus, interacts with the innate immune response. Given previously discussed similarities between MmuPV1 and beta genus papillomaviruses, mechanisms divulged in the mouse model may be applicable to these other papillomavirus types.

6.2.2 Furthering the use of EGFP/mCherry expressing cell lines

Examination of high density cell culture using confocal microscopy revealed that cells can behave differently in discrete layers of cells. For example, cells in the upper layer of a high-density culture of NIKS predominantly stained positive for K10, whereas few cells in the lower layer were K10 positive. This suggested that high density monolayer culture can somewhat mimic the basal and parabasal layers of the epithelium. Generation of cell lines exogenously expressing EGFP and mCherry allowed establishment of a method by which to observe the effect of viral protein expression on growth within these layers. Combination of EGFP/mCherry expressing cells with precise confocal analysis revealed that MmuPV1 E6 could impact upon relative occupancy of the layers through a mechanism involving E6 binding to MAML1.

The scope for future experimentation with this high-density competition assay system is vast due to the different aspects that can be manipulated. Other virus proteins can be exogenously expressed in the fluorescent cell lines, including any mutants generated. This will allow rigorous investigation of any effect of other PV proteins on layer occupancy when competing against LXSN control cells. It would also be possible to ‘compete’ cells expressing virus proteins with cells expressing other virus proteins, to ascertain whether cells expressing one protein might have a competitive advantage over cells expressing another. Furthermore, one could generate NIKS cell lines exogenously expressing a fluorescent marker that can only be

visualised in the 'far red' channel (λ_{em} ~ 600–700 nm), and compete three different cell lines within one experiment. In addition to this, the medium in which cells are cultured can be altered. In this way, this culture system can be used to investigate the effect of various factors on observed phenotypes, to mimic naturally occurring changes in the basal and parabasal layers of infected cells. This system can also be used to test different drug candidates on the persistence phenotype, to establish whether any experimental molecules can disrupt the observed competitive advantage. A more ambitious project would be the generation of EGFP/mCherry cell lines to introduce into a mouse. Transplantation of human cells into immunocompromised mice has been described previously (Paquet-Fifield, Redvers et al. 2005) (Kolodka, Garlick et al. 1998). Therefore, EGFP/mCherry-expressing keratinocytes could be transduced to express viral proteins or control vectors, and then be implanted into immunocompetent mice. The cell fates over time could then be observed by fluorescent microscopy following sample collection. For example, it would be possible to investigate whether cells exogenously expressing MmuPV1 E6 protein would persist preferentially in the basal layer of mouse epidermis following repopulation of the experimental site with a mixed population of MmuPV1 E6 expressing cells and control cells.

6.3 Concluding remarks

In conclusion, this work provides strong evidence of a role for MmuPV1 E6 protein in competitive persistence of infected cells at a greater density in the lower layer of high-density monolayer culture, likely mimicking the dynamics of cells *in vivo*. I expect that MmuPV1 E6 plays a key role in the ability of single infected cells to persist in the basal layer of the epithelium over time to allow establishment of a productive lesion. These alterations of the cell status by the virus keep cells in a state that may be optimal for the virus life cycle to continue into the parabasal layers, whilst maintaining infected cells in the basal layer. It is likely that MmuPV1 has other complex interactions within the microenvironment that allow the successful establishment of a lesion. For example, recent research has demonstrated that some PVs can alter cell adhesion (Woo, Kim et al. 2015), and it is reasonable to consider that similar mechanisms may also be involved in the persistence phenotype observed in this thesis. It is also important to note that keratinocytes have been shown to contribute to the formation of the basement membrane itself, and that the basement membrane and underlying dermis can also regulate the growth and terminal differentiation of keratinocytes (Smola, Stark et al. 1998).

Based on observations made both *in vivo* and *in vitro*, I postulate the following for a life cycle model of MmuPV1 infection (a schematic to show this proposed model of the MmuPV1 life cycle is shown in Figure 6.1). MmuPV1 genomes persist in the basal layer of the epithelium. The relatively high concentration of EGF in the basal layer could give cells containing the MmuPV1 genome a growth advantage over uninfected cells in the confluent cell state of the basal layer. MmuPV1 interferes with normal Notch pathway signalling through E6 protein interaction with MAML1 protein to affect downstream transcription. As a result, MmuPV1 infected cells persist in the basal layer competitively over the surrounding uninfected cells, which are forced to exit and begin the process of terminal differentiation. Cells expressing MmuPV1 E6 are also able to overcome normal cell density homeostasis, leading to an increase in basal cell density. In these ways, infected cells further populate the basal layer, providing a larger reservoir of infection by overcoming the normal modulation of basal layer homeostasis.

When MmuPV1 cells do exit the basal layer, a delay in differentiation of the infected cell is observed, keeping cells in a state similar to that of the basal cells. The amplification stage of the MmuPV1 life cycle could begin from the parabasal layer. This is unlike the general high-risk PV life cycle. However, patterns of expression investigated in an HPV1 wart were shown to also have amplification of viral DNA occurring in the parabasal layers (Egawa, Iftner et al. 2000). Therefore, rapid entry into genome amplification could be a life cycle strategy shared by some PVs. A model of high-risk infection is currently developing in our lab based on observations from other group members, wherein high-risk HPV gene expression is absent in the first few layers of the epithelium, followed by a 're-entry' supported by E5 protein in the upper layers. This presents another novel life cycle mechanism, demonstrating that PVs employ a wide variety of strategies to persist and develop in their niches. MmuPV1 E4 protein is also expressed from the parabasal layer upwards, while L1 and L2 proteins are expressed near the surface of the skin. This is based on observations in immunodeficient mouse samples, however it is important to note that in C57BL/6J mice, expression of E6/E7 RNA appeared more restricted to the lower layers, with higher levels of expression in the cytoplasm. Lower quantities of E4 protein were similarly observed. This could be due to microlesions observed being at an early stage of development, similar to lesions categorised between stages 2 and 3 (discussed in 3.2.7). Conversely, this low-level expression may reflect immune modulation at the site of infection, and limited expression of E6/E7 RNA and E4 could indicate a 'controlled' or regressing infection.

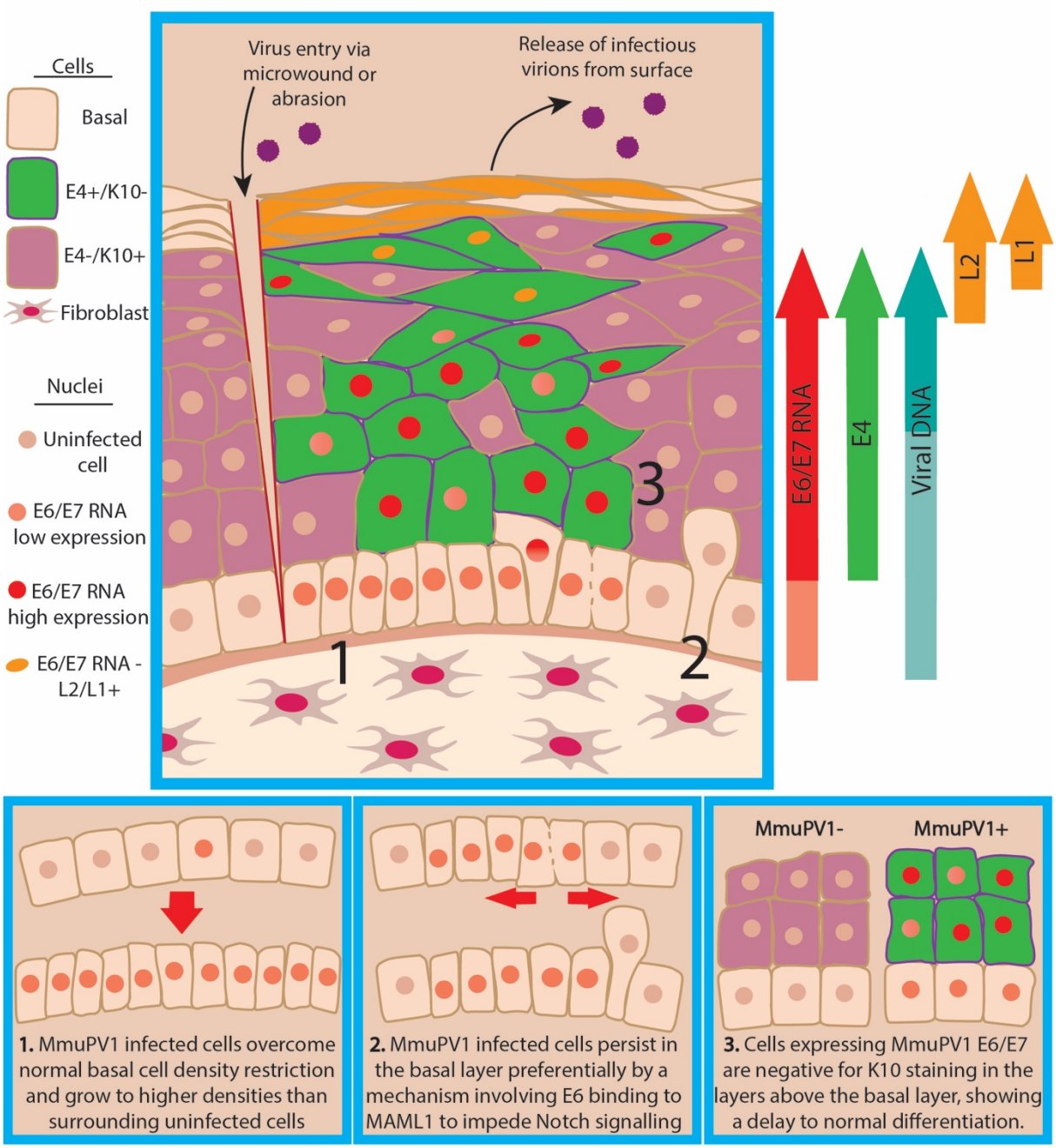

Figure 6.1 The life cycle strategies of MmuPV1
Virus initially infects basal cells and expresses E6/E7 RNA at relatively low levels. Normal basal cell density restrictions are overcome, leading to an increase in cell density in infected cells. Expression of E6 allows infected cells to preferentially persist in the basal layer, whereas uninfected cells are forced to leave. When infected cells do exit the basal layer, a delay in differentiation occurs, which results in an absence of K10 in E6/E7 expressing cells. BrdU analysis suggests that cells remain in cycle in the first 1-2 parabasal layers, after which viral genome amplification must occur. Infectious virus particles are then shed from the surface of the epithelium.

Cells expressing MmuPV1 E6 can outcompete their neighbours to persist in the lower layer of a high-density competition assay, which is likely indicative of mechanisms that occur *in vivo*. While it is expected that multiple MmuPV1 interactions with various pathways together result in the observed phenotypes, it is clear that E6 interaction with MAML1 is an important one. Disruption of this competitive advantage of lower layer persistence could stimulate the detachment, differentiation and subsequent loss of the infected reservoir of cells, providing a mechanism by which such low-level infection could be treated. If similar mechanisms of persistence are present in papillomaviruses that can cause human disease, therapeutics targeting this pathway could be utilised in tandem with established treatment methods aiming to surgically remove infected cells. Total removal of the reservoir of infected cells in papillomavirus infection is the only way in which infection can be fully eradicated, therefore targeting persistent cells is an important avenue to consider in future research.

7.0 References

Ajiro, M. and Z. M. Zheng (2015). "E6^E7, a novel splice isoform protein of human papillomavirus 16, stabilizes viral E6 and E7 oncoproteins via HSP90 and GRP78." MBio **6**(1): e02068-02014.

Alazawi, W., M. Pett, B. Arch, L. Scott, T. Freeman, M. A. Stanley and N. Coleman (2002). "Changes in Cervical Keratinocyte Gene Expression Associated with Integration of Human Papillomavirus 16." Cancer Research **62**: pp6959-6965.

Alcolea, M. P., P. Greulich, A. Wabik, J. Frede, B. D. Simons and P. H. Jones (2014). "Differentiation imbalance in single oesophageal progenitor cells causes clonal immortalization and field change." Nat Cell Biol **16**(6): pp615-622.

Alcolea, M. P. and P. H. Jones (2015). "Cell competition: winning out by losing notch." Cell Cycle **14**(1): pp9-17.

Alizon, S., C. L. Murall and I. G. Bravo (2017). "Why Human Papillomavirus Acute Infections Matter." Viruses **9**(10).

Allen-Hoffmann, B. L., S. J. Schlosser, C. A. Ivarie, C. A. Sattler, L. F. Meisner and S. L. O'Connor (2000). "Normal growth and differentiation in a spontaneously immortalized near-diploid human keratinocyte cell line, NIKS." J Invest Dermatol **114**(3): pp444-455.

Amella, C. A., L. A. Lofgren, A. M. Ronn, M. Nouri, M. J. Shikowitz and B. M. Steinberg (1994). "Latent infection induced with cottontail rabbit papillomavirus. A model for human papillomavirus latency." american Journal of Pathology **144**(6): pp1167-1171.

Amoyel, M. and E. A. Bach (2014). "Cell competition: how to eliminate your neighbours." Development **141**(5): pp988-1000.

An, X., Y. Hao and P. I. Meneses (2017). "Host cell transcriptome modification upon exogenous HPV16 L2 protein expression." Oncotarget **8**(53): pp90730-90747.

Anacker, D. and C. Moody (2012). "Generation of organotypic raft cultures from primary human keratinocytes." J Vis Exp(60).

Andasari, V., D. Lu, M. Swat, S. Feng, F. Spill, L. Chen, X. Luo, M. Zaman and M. Long (2018). "Computational model of wound healing: EGF secreted by fibroblasts promotes delayed re-epithelialization of epithelial keratinocytes." Integr Biol (Camb) **10**(10): pp605-634.

Aubin, F., J. L. Pretet, A. C. Jacquard, M. Saunier, X. Carcopino, F. Jaroud, P. Pradat, B. Soubeyrand, Y. Leocmach, C. Mougin, D. Riethmuller and E. D. S. Group (2008). "Human papillomavirus genotype distribution in external acuminata condylomata: a Large French National Study (EDiTH IV)." Clin Infect Dis **47**(5): pp610-615.

Ball, S. L., D. M. Winder, K. Vaughan, N. Hanna, J. Levy, J. C. Sterling, M. A. Stanley and P. K. Goon (2011). "Analyses of human papillomavirus genotypes and viral loads in anogenital warts." J Med Virol **83**(8): pp1345-1350.

Bandeira, V. S., H. A. Tomas, E. Alici, M. J. Carrondo and A. S. Coroadinha (2017). "Disclosing the Parameters Leading to High Productivity of Retroviral Producer Cells Lines: Evaluating Random Versus Targeted Integration." Hum Gene Ther Methods **28**(2): pp78-90.

Bedell, M. A., J. B. Hudson, T. R. Golub, M. E. Turyk, M. Hosken, G. D. Wilbanks and L. A. Laimins (1991). "Amplification of Human Papillomavirus Genomes In Vitro Is Dependent on Epithelial Differentiation." Journal of Virology **65**(5): pp2254-2260.

Bedell, M. A., K. H. Jones and L. A. Laimins (1987). "The E6-E7 Region of Human Papillomavirus Type 18 Is Sufficient forTransformationofNIH 3T3andRat-1Cells." Journal of Virology **61**(11): pp3635-3640.

Bell, J. A., J. P. Sundberg, S. Ghim, J. Newsome, A. B. Jenson and R. Schlegel (1994). "A Formalin-Inactivated Vaccine Protects against Mucosal Papillomavirus Infection: A Canine Model." Pathobiology **62**: pp194-198.

Berg, M. and A. Stenlund (1997). "Functional Interactions between Papillomavirus E1 and E2 Proteins." Journal of Virology **71**(5): pp3853-3863.

Bergner, S., G. Halec, M. Schmitt, F. Aubin, A. Alonso and E. Auvinen (2016). "Individual and Complementary Effects of Human Papillomavirus Oncogenes on Epithelial Cell Proliferation and Differentiation." Cells Tissues Organs **201**(2): pp97-108.

Bernard, H. U., R. D. Burk, Z. Chen, K. van Doorslaer, H. zur Hausen and E. M. de Villiers (2010). "Classification of papillomaviruses (PVs) based on 189 PV types and proposal of taxonomic amendments." Virology **401**(1): pp70-79.

Bernard, H. U., S.-Y. Chan, M. M. Manos, C.-K. Ong, L. L. Villa, H. Delius, C. L. Peyton, H. M. Bauer and C. M. Wheeler (1994). "Identification and Assessment of Known and Novel Human Papillomaviruses by Polymerase Chain Reaction Amplification, Restriction Fragment Length Polymorphisms, Nucleotide Sequence, and Phylogenetic Algorithms." the Journal of Infectious Diseases **170**: pp1077-1085.

Bian, X. L., G. Rosas-Acosta, Y. C. Wu and V. G. Wilson (2007). "Nuclear import of bovine papillomavirus type 1 E1 protein is mediated by multiple alpha importins and is negatively regulated by phosphorylation near a nuclear localization signal." J Virol **81**(6): pp2899-2908.

Bienkowska-Haba, M., W. Luszczek, J. E. Myers, T. R. Keiffer, S. DiGiuseppe, P. Polk, J. M. Bodily, R. S. Scott and M. Sapp (2018). "A new cell culture model to genetically dissect the complete human papillomavirus life cycle." PLoS Pathog **14**(3): e1006846.

Blanpain, C., W. E. Lowry, H. A. Pasolli and E. Fuchs (2006). "Canonical notch signaling functions as a commitment switch in the epidermal lineage." Genes Dev **20**(21): pp3022-3035.

Blumenberg, M. (2013). "Profiling and metaanalysis of epidermal keratinocytes responses to epidermal growth factor." BMC Genomics **14**: 85.

Bodily, J. and L. A. Laimins (2011). "Persistence of human papillomavirus infection: keys to malignant progression." Trends Microbiol **19**(1): pp33-39.

Borgogna, C., C. Olivero, S. Lanfredini, F. Calati, M. De Andrea, E. Zavattaro, P. Savoia, E. Trisolini, R. Boldorini, G. K. Patel and M. Gariglio (2018). "beta-HPV Infection Correlates with Early Stages of Carcinogenesis in Skin Tumors and Patient-Derived Xenografts from a Kidney Transplant Recipient Cohort." Front Microbiol **9**.

Bouvard, V., R. Baan, K. Straif, Y. Grosse, B. Secretan, F. El Ghissassi, L. Benbrahim-Tallaa, N. Guha, C. Freeman, L. Galichet and V. Cogliano (2009). "A review of human carcinogens—Part B: biological agents." Lancet Oncology **10**(4): pp321-322.

Bowling, S., K. Lawlor and T. A. Rodríguez (2019). "Cell competition: the winners and losers of fitness selection." Development **146**(13): dev167486.

Brandsma, J. and W. Xiao (1993). "Infectious virus replication in papillomas induced by molecularly cloned cottontail rabbit papillomavirus DNA." Journal of Virology **67**(1): pp567-571.

Bray, F., J. Ferlay, I. Soerjomataram, R. L. Siegel, L. A. Torre and A. Jemal (2018). "Global cancer statistics 2018: GLOBOCAN estimates of incidence and mortality worldwide for 36 cancers in 185 countries." CA Cancer J Clin **68**(6): pp394-424.

Bray, S. J. (2006). "Notch signalling: a simple pathway becomes complex." Nat Rev Mol Cell Biol **7**(9): pp678-689.

Brimer, N., C. M. Drews and S. B. Vande Pol (2017). "Association of papillomavirus E6 proteins with either MAML1 or E6AP clusters E6 proteins by structure, function, and evolutionary relatedness." PLoS Pathog **13**(12): e1006781.

Brimer, N., C. Lyons, A. E. Wallberg and S. B. Vande Pol (2012). "Cutaneous papillomavirus E6 oncoproteins associate with MAML1 to repress transactivation and NOTCH signaling." Oncogene **31**(43): pp4639-4646.

Brooks, D. R. and A. L. Ferrao (2005). "The historical biogeography of co-evolution: emerging infectious diseases are evolutionary accidents waiting to happen." Journal of Biogeography **32**(8): pp1291-1299.

Bruni, L., G. Albero, B. Serrano, M. Mena, D. Gómez, J. Muñoz, F. X. Bosch and S. de Sanjosé (2019). "Human Papillomavirus and Related Diseases in the World. Summary Report June 2019." ICO/IARC Information Centre on HPV and Cancer (HPV Information Centre).

Bryan, J. T. and D. R. Brown (2000). "Association of the human papillomavirus type 11 E1()E4 protein with cornified cell envelopes derived from infected genital epithelium." Virology **277**(2): pp262-269.

Bryan, J. T. and D. R. Brown (2001). "Transmission of human papillomavirus type 11 infection by desquamated cornified cells." Virology **281**(1): pp35-42.

Buck, C. B., C. D. Thompson, Y. Y. Pang, D. R. Lowy and J. T. Schiller (2005). "Maturation of papillomavirus capsids." J Virol **79**(5): pp2839-2846.

Bushara, O., D. Miller, A. Giubellino, M. Schomaker, B. Thyagarajan and A. C. Nelson (2019). "Diagnosis of epidermodysplasia verruciformis: Two cases highlighting the role of direct HPV L1 gene sequencing." J Cutan Pathol **46**(6): pp436-441.

Byyny, R. L., D. N. Orth and S. Cohen (1972). "Radioimmunoassay of Epidermal Growth Factor." Endocrinology **90**(5): pp1261-1266.

Campo, M. S. (2002). "Animal models of papillomavirus pathogenesis." Virus Research **89**: pp249-261.

Campo, M. S. and L. W. Coggins (1982). "Molecular Cloning of Bovine Papillomavirus Genomes and Comparison of Their Sequence Homologies by Heteroduplex Mapping." Journal of General Virology **63**(2): pp255-264.

Campo, M. S. and W. F. H. Jarrett (1986). "Papillomavirus infection in cattle: viral and chemical cofactors in naturally occurring and experimentally induced tumours." Ciba Found Symp **120**: pp117-135.

Canuti, M., H. J. Munro, G. J. Robertson, A. N. K. Kroyer, S. Roul, D. Ojkic, H. G. Whitney and A. S. Lang (2019). "New Insight Into Avian Papillomavirus Ecology and Evolution From Characterization of Novel Wild Bird Papillomaviruses." Front Microbiol **10**.

Carroll, D. K., J. S. Carroll, C. O. Leong, F. Cheng, M. Brown, A. A. Mills, J. S. Brugge and L. W. Ellisen (2006). "p63 regulates an adhesion programme and cell survival in epithelial cells." Nat Cell Biol **8**(6): pp551-561.

Chambers, V. C., C. A. Evans and R. S. Weiser (1960). " Canine Oral Papillomatosis

II. Immunologie Aspects of the Disease." Cancer Research **20**(7): pp1083-1093.

Chang, Y. E. and L. A. Laimins (2000). "Microarray Analysis Identifies Interferon-Inducible Genes and
Stat-1 as Major Transcriptional Targets of Human
Papillomavirus Type 31." Journal of Virology **74**(9): pp4174-4182.

Chaturvedi, V., J. Z. Qin, M. F. Denning, D. Choubey and M. O. N. Diaz, B. J. (1999). "Apoptosis in Proliferating, Senescent, and Immortalized Keratinocytes." The Journal of Biological Chemistry **274**(33): pp23358-23367.

Chen, A. C., N. A. McMillan and A. Antonsson (2008). "Human papillomavirus type spectrum in normal skin of individuals with or without a history of frequent sun exposure." J Gen Virol **89**(Pt 11): pp2891-2897.

Chen, E. Y., P. M. Howley, A. D. Levinson and P. H. Seeburg (1982). "The primary structure and genetic organization of the bovine papillomavirus type 1 genome." Nature **299**(5883): pp529-534.

Chen, J., Y. Xue, M. Poidinger, T. Lim, S. H. Chew, C. L. Pang, J. P. Abastado and F. Thierry (2014). "Mapping of HPV transcripts in four human cervical lesions using RNAseq suggests quantitative rearrangements during carcinogenic progression." Virology **462-463**: pp14-24.

Chesters, P. M. and D. J. McCance (1989). "Human Papillomavirus Types 6 and 16 in Cooperation with Ha-ras Transform Secondary Rat Embryo Fibroblasts." Journal of General Virology **70**(pt2): pp252-265.

Cheville, N. F. and C. Olson (1964). "Epithelial and fibroblastic proliferation in bovine cutaneous papillomatosis." Vet Pathol **1**: pp248-257.

Chow, L. T., T. R. Broker and B. M. Steinberg (2010). "The natural history of human papillomavirus infections of the mucosal epithelia." APMIS **118**(6-7): 422-449.

Chow, L. T., A. A. Duffy, H. K. Wang and T. R. Broker (2009). "A highly efficient system to produce infectious human papillomavirus: Elucidation of natural virus-host interactions." Cell Cycle **8**(9): pp1319-1323.

Christensen, N., C. A. Reed, N. M. Cladel, R. Han and J. W. Kreider (1996). "Immunization with Viruslike Particles Induces Long-Term Protection of Rabbits against Challenge with Cottontail Rabbit Papillomavirus." Journal of Virology **70**(2): pp960-965.

Cicchini, L., R. Z. Blumhagen, J. A. Westrich, M. E. Myers, C. J. Warren, C. Siska, D. Raben, K. J. Kechris and D. Pyeon (2017). "High-Risk Human Papillomavirus E7 Alters Host DNA Methylome and Represses HLA-E Expression in Human Keratinocytes." Sci Rep **7**(1).

Cladel, N. M., L. R. Budgeon, K. K. Balogh, T. K. Cooper, S. A. Brendle, N. D. Christensen, T. D. Schell and J. Hu (2017). "Mouse papillomavirus infection persists in mucosal tissues of an immunocompetent mouse strain and progresses to cancer." Sci Rep **7**(1).

Cladel, N. M., L. R. Budgeon, K. K. Balogh, T. K. Cooper, J. Hu and N. D. Christensen (2015). "A novel pre-clinical murine model to study the life cycle and progression of cervical and anal papillomavirus infections." PLoS One **10**(3): e0120128.

Cladel, N. M., L. R. Budgeon, K. K. Balogh, T. K. Cooper, J. Hu and N. D. Christensen (2016). "Mouse papillomavirus MmuPV1 infects oral mucosa and preferentially targets the base of the tongue." Virology **488**: pp73-80.

Cladel, N. M., L. R. Budgeon, T. K. Cooper, K. K. Balogh, J. Hu and N. D. Christensen (2013). "Secondary infections, expanded tissue tropism, and evidence for malignant potential in immunocompromised mice infected with Mus musculus papillomavirus 1 DNA and virus." J Virol **87**(16): pp9391-9395.

Clayton, E., D. P. Doupe, A. M. Klein, D. J. Winton, B. D. Simons and P. H. Jones (2007). "A single type of progenitor cell maintains normal epidermis." Nature **446**(7132): pp185-189.

Collier, B., L. Goobar-Larsson, M. Sokolowski and S. Schwartz (1998). "Translational Inhibition in Vitro of Human Papillomavirus Type 16 L2 mRNA Mediated through Interaction with Heterogenous Ribonucleoprotein K and Poly(rC)-binding Proteins 1 and 2*." The Journal of Biological Chemistry **273**(35): pp22648-22656.

Contreras-Cornejo, H., G. Saucedo-Correa, J. Oviedo-Boyso, J. J. Valdez-Alarcon, V. M. Baizabal-Aguirre, M. Cajero-Juarez and A. Bravo-Patino (2016). "The CSL proteins, versatile transcription factors and context dependent corepressors of the notch signaling pathway." Cell Div **11**: 12.

Crawford, L. V. and E. M. Crawford (1963). "A Comparative Study of Polyoma and Papilloma Viruses." Virology **21**: pp258-263.

Culp, T. D., L. R. Budgeon and N. D. Christensen (2006). "Human papillomaviruses bind a basal extracellular matrix component secreted by keratinocytes which is distinct from a membrane-associated receptor." Virology **347**(1): pp147-159.

de Freitas, A. C., T. H. A. de Oliveira, M. R. Barros, Jr. and A. Venuti (2017). "hrHPV E5 oncoprotein: immune evasion and related immunotherapies." J Exp Clin Cancer Res **36**(1).

De Geest, K., M. E. Turyk, M. I. Hosken, J. B. Hudson, L. A. Laimins and G. D. Wilbanks (1993). "Growth and Differentiation of Human Papillomavirus Type 31b Positive Human Cervical Cell Lines." Gynecologic Oncology **49**: pp303-310.

de Villiers, E. M., C. Fauquet, T. R. Broker, H. U. Bernard and H. zur Hausen (2004). "Classification of papillomaviruses." Virology **324**(1): pp17-27.

Demers, G. W., C. L. Halbert and D. A. Galloway (1994). "Elevated Wild-Type p53 Protein Levels in Human Epithelial Cell Lines Immortalized by the Human Papillomavirus Type 16 E7 Gene." Virology **198**
(1): pp169-174.

Deng, W., B. Y. Lin, G. Jin, C. G. Wheeler, T. Ma, J. W. Harper, T. R. Broker and L. T. Chow (2004). "Cyclin/CDK regulates the nucleocytoplasmic localization of the human papillomavirus E1 DNA helicase." J Virol **78**(24): pp13954-13965.

Derkay, C. S. and B. Wiatrak (2008). "Recurrent Respiratory Papillomatosis: A Review." The Laryngoscope **118**(7): pp1236-1247.

Dickson, M. A., W. C. Hahn, Y. Ino, V. Ronfard, J. Y. Wu, R. A. Weinberg, D. N. Louis, F. P. Li and J. G. Rheinwald (2000). "Human Keratinocytes That Express hTERT and Also Bypass a p16INK4a-Enforced Mechanism That Limits Life Span
Become Immortal yet Retain Normal Growth
and Differentiation Characteristics." Molecular and Cellular Biology **20**(4): pp1436-1447.

Doorbar, J. (2005). "The papillomavirus life cycle." J Clin Virol **32 Suppl 1**: S7-15.

Doorbar, J. (2007). "Papillomavirus life cycle organization and biomarker selection." Disease Markers **23**: pp297-313.

Doorbar, J. (2013). "The E4 protein; structure, function and patterns of expression." Virology **445**(1-2): pp80-98.

Doorbar, J. (2016). "Model systems of human papillomavirus-associated disease." J Pathol **238**(2): pp166-179.

Doorbar, J., N. Egawa, H. Griffin, C. Kranjec and I. Murakami (2015). "Human papillomavirus molecular biology and disease association." Rev Med Virol **25 Suppl 1**: pp2-23.

Doorbar, J., W. Quint, L. Banks, I. G. Bravo, M. Stoler, T. R. Broker and M. A. Stanley (2012). "The biology and life-cycle of human papillomaviruses." Vaccine **30 Suppl 5**: F55-70.

Doupe, D. P., A. M. Klein, B. D. Simons and P. H. Jones (2010). "The ordered architecture of murine ear epidermis is maintained by progenitor cells with random fate." Dev Cell **18**(2): pp317-323.

Drolet, M., É. Bénard, M. C. Boily, H. Ali, L. Baandrup, H. Bauer, S. Beddows, J. Brisson, J. M. L. Brotherton, T. Cummings, B. Donovan, C. K. Fairley, E. W. Flagg, A. M. Johnson, J. A. Kahn, K. Kavanagh, S. K. Kjaer, E. V. Kliewer, P. Lemieux-Mellouki, L. Markowitz, A. Mboup, D.

Mesher, L. Niccolai, J. Oliphant, K. G. Pollock, K. Soldan, P. Sonnenberg, S. N. Tabrizi, C. Tanton and M. Brisson (2015). "Population-level impact and herd effects following human papillomavirus vaccination programmes: a systematic review and meta-analysis." The Lancet Infectious Diseases **15**(5): pp565-580.

Dunne, E. F. and L. E. Markowitz (2006). "Genital Human Papillomavirus Infection." Clinical Infectious Diseases **43**(5): pp624–629.

Durzynska, J., J. Pacholska-Bogalska, M. Kaczmarek, T. Hanc, M. Durda, M. Skrzypczak and A. Gozdzicka-Jozefiak (2011). "HPV genotypes in the oral cavity/oropharynx of children and adolescents: cross-sectional survey in Poland." Eur J Pediatr **170**(6): pp757-761.

Dyson, N. (1998). "The regulation of E2F by pRB-family proteins." Genes and Development **12**: pp2245-2262.

Dyson, N., P. M. Howley, K. Munger and E. Harlow (1989). "The Human PapillomaVirus-16 E7 OncoproteinIs Able to Bind to the Retinoblastoma Gene Product." Science **243**(4893): pp934-937.

Egawa, K., A. Iftner, J. Doorbar, Y. Honda and T. Iftner (2000). "Synthesis of viral DNA and late capsid protein L1 in parabasal spinous cell layers of naturally occurring benign warts infected with human papillomavirus type 1." Virology **268**(2): pp281-293.

Egawa, N. and J. Doorbar (2017). "The low-risk papillomaviruses." Virus Res **231**: pp119-127.

Egawa, N., K. Egawa, H. Griffin and J. Doorbar (2015). "Human Papillomaviruses; Epithelial Tropisms, and the Development of Neoplasia." Viruses **7**(7): pp3863-3890.

Egawa, N., T. Nakahara, S. Ohno, M. Narisawa-Saito, T. Yugawa, M. Fujita, K. Yamato, Y. Natori and T. Kiyono (2012). "The E1 protein of human papillomavirus type 16 is dispensable for maintenance replication of the viral genome." J Virol **86**(6): pp3276-3283.

Egawa, N., Q. Wang, H. M. Griffin, I. Murakami, D. Jackson, R. Mahmood and J. Doorbar (2017). "HPV16 and 18 genome amplification show different E4-dependence, with 16E4 enhancing E1 nuclear accumulation and replicative efficiency via its cell cycle arrest and kinase activation functions." PLoS Pathog **13**(3): e1006282.

Eichner, R. S., T.; Aebi, U (1986). "The Role of Keratin Subfamilies and Keratin Pairs in the Formation of Human Epidermal Intermediate Filaments." The Journal of Cell Biology **102**: pp1767-1777.

Eldakhakhny, S., Q. Zhou, E. J. Crosbie and B. S. Sayan (2018). "Human papillomavirus E7 induces p63 expression to modulate DNA damage response." Cell Death Dis **9**(2).

Elfaki, M. G. (2014). "Immunosuppression Induced by HIV Infection." Biology and Medicine **06**(03).

Facciuto, F., M. Bugnon Valdano, F. Marziali, P. Massimi, L. Banks, A. L. Cavatorta and D. Gardiol (2014). "Human papillomavirus (HPV)-18 E6 oncoprotein interferes with the epithelial cell polarity Par3 protein." Mol Oncol **8**(3): pp533-543.

Fang, L., C. Meyers, L. R. Budgeon and M. K. Howett (2006). "Induction of productive human papillomavirus type 11 life cycle in epithelial cells grown in organotypic raft cultures." Virology **347**(1): pp28-35.

Fehrmann, F. and L. A. Laimins (2003). "Human papillomaviruses: targeting differentiating epithelial cells for malignant transformation." Oncogene **22**(33): pp5201-5207.

Ferry-Galow, K. V. and A. P. Chen (2019). "The use of research biopsies in oncology trials: challenges and controversies." J Hosp Manag Health Policy **3**.

Filippova, M., W. Evans, R. Aragon, V. Filippov, V. M. Williams, L. Hong, M. E. Reeves and P. Duerksen-Hughes (2014). "The small splice variant of HPV16 E6, E6, reduces tumor formation in cervical carcinoma xenografts." Virology **pp450-451**: 153-164.

Fiorio, F. V., V. A. Hajivassiliou and P. C. B. Phillips (2010). "Bimodal t-ratios: the impact of thick tails on inference." Econometrics Journal **13**: pp271-289.

Flores, E. R., B. L. Allen-Hoffmann, D. Lee and P. Lambert (2000). "The Human Papillomavirus Type 16 E7 Oncogene Is Required for the Productive Stage of the Viral Life Cycle." Journal of Virology **74**(14): pp6622-6631.

Flores, E. R., B. L. Allen-Hoffmann, D. Lee, C. A. Sattler and P. F. Lambert (1999). "Establishment of the Human Papillomavirus Type 16 (HPV-16) Life Cycle in an Immortalized Human Foreskin Keratinocyte Cell Line." Virology **262**: pp344-354.

Flores, E. R. and P. F. Lambert (1997). "Evidence for a Switch in the Mode of Human Papillomavirus Type 16 DNA Replication during the Viral Life Cycle." Journal of Virology **71**(10): pp7167-7179.

Florin, L., C. Sapp, R. E. Streeck and M. Sapp (2002). "Assembly and translocation of papillomavirus capsid proteins." J Virol **76**(19): pp10009-10014.

Francis, D. A., S. I. Schmid and P. M. Howley (2000). "Repression of the Integrated Papillomavirus E6/E7 Promoter Is Required for Growth Suppression of Cervical Cancer Cells." Journal of Virology **74**(6): pp2679-2686.

Frattini, M. G., H. B. Lim and L. A. Laimins (1996). "*In vitro* synthesis of oncogenic human papillomaviruses requires episomal genomes for differentiation-dependent late expression." Proc Natl Acad Sci U S A **93**(7): pp3062-3067.

Frazer, I. H. (2004). "Prevention of cervical cancer through papillomavirus vaccination." Nat Rev Immunol **4**(1): pp46-54.

Friedman, J. M. and P. J. Fialkow (1976). "Viral "Tumorigenesis" in man: Cell markers incondylomata acuminata." International Journal of Cancer **17**(1): pp57–61.

Fu, X., L. Tao, A. Jin and X. Zhang (2016). "Identification of Human Papillomavirus Entry Receptors with CRISPR-Cas9 Library." Molecular Therapy **24**: S52.

Fuchs, E. (2008). "Skin stem cells: rising to the surface." J Cell Biol **180**(2): pp273-284.

Fuchs, E. and H. Green (1980). "Changes in Keratin Gene Expression during Terminal Differentiation of the Keratinocyte." Cell **19**(4): pp1033-1042.

Fusenig, N. E., S. M. Amer, P. Boukamp and P. K. M. Worst (1978). "Characteristics of chemically transformed mouse epidermal cells in vitro and in vivo." Bulletins du Cancer **65**(3): pp271-279.

Gao, H., Y. Lin, J. He, S. Zhou, M. Liang, C. Huang, X. Li, C. Liu and P. Zhang (2019). "Role of heparan sulfate in the Zika virus entry, replication, and cell death." Virology **529**: pp91-100.

Garland, S. M., P. Pitisuttithum, H. Y. S. Ngan, C. H. Cho, C. Y. Lee, C. A. Chen, Y. C. Yang, T. Y. Chu, N. F. Twu, R. Samakoses, Y. Takeuchi, T. H. Cheung, S. C. Kim, L. M. Huang, B. G. Kim, Y. T. Kim, K. H. Kim, Y. S. Song, S. Lalwani, J. H. Kang, M. Sakamoto, H. S. Ryu, N. Bhatla, H. Yoshikawa, M. C. Ellison, S. R. Han, E. Moeller, S. Murata, M. Ritter, M. Sawata, C. Shields, A. Walia, G. Perez and A. Luxembourg (2018). "Efficacy, Immunogenicity, and Safety of a 9-Valent Human Papillomavirus Vaccine: Subgroup Analysis of Participants From Asian Countries." J Infect Dis **218**(1): pp95-108.

Gaynor, A. M., S. Fish, R. S. Duerr, F. N. Cruz, Jr. and P. A. Pesavento (2015). "Identification of a novel papillomavirus in a Northern Fulmar (Fulmarus glacialis) with viral production in cartilage." Vet Pathol **52**(3): pp553-561.

Genther, S. M., S. Sterling, S. Duensing, K. Munger, C. Sattler and P. F. Lambert (2003). "Quantitative role of the human papillomavirus type 16 E5 gene during the productive stage of the viral life cycle." J Virol **77**(5): pp2832-2842.

Gheit, T. (2019). "Mucosal and Cutaneous Human Papillomavirus Infections and Cancer Biology." Front Oncol **9**.

Giannopoulou, E., A. Nikolakopoulos, D. Kotsirilou, A. Lampropoulou, S. Raftopoulou, E. Papadimitriou, A. D. Theocharis, T. Makatsoris, K. Fasseas and H. P. Kalofonos (2015). "Epidermal growth factor receptor status and Notch inhibition in non-small cell lung cancer cells." J Biomed Sci **22**.

Gillison, M. L., A. K. Chaturvedi and D. R. Lowy (2008). "HPV prophylactic vaccines and the potential prevention of noncervical cancers in both men and women." Cancer **113**(10 Suppl): pp3036-3046.

Giroglou, T., L. Florin, F. Schäfer, R. E. Streeck and M. E. Sapp (2001). "Human Papillomavirus Infection Requires Cell Surface Heparan Sulfate." Journal of Virology **75**(3): pp1565-1570.

Gissmann, L., H. Pfister and H. zur Hausen (1977). "Human Papilloma Viruses (HPV): Characterization of Four Different Isolates." Virology **76**: pp569-580.

Gottschling, M., A. Stamatakis, I. Nindl, E. Stockfleth, A. Alonso and I. G. Bravo (2007). "Multiple evolutionary mechanisms drive papillomavirus diversification." Mol Biol Evol **24**(5): pp1242-1258.

Grace, M. and K. Munger (2017). "Proteomic analysis of the gamma human papillomavirus type 197 E6 and E7 associated cellular proteins." Virology **500**: pp71-81.

Griffin, L. M., L. Cicchini, T. Xu and D. Pyeon (2014). "Human keratinocyte cultures in the investigation of early steps of human papillomavirus infection." Methods Mol Biol **1195**: pp219-238.

Grose, R., C. Hutter, W. Bloch, I. Thorey, F. M. Watt, R. Fässler, C. Brakebusch and S. Werner (2002). "A crucial role of β1 integrins for keratinocyte migration in vitro and during cutaneous wound repair." Development **129**(9): pp2303-2315.

Gyöngyösi, E., A. Szalmás, A. Ferenczi, S. Póliska, J. Kónya and G. Veress (2015). "Transcriptional regulation of genes involved in keratinocyte differentiation by human papillomavirus 16 oncoproteins." Arch Virol **160**(2): pp389-398.

Habig, M., H. Smola, V. S. Dole, R. Derynck, H. Pfister and S. Smola-Hess (2006). "E7 proteins from high- and low-risk human papillomaviruses bind to TGF-beta-regulated Smad proteins and inhibit their transcriptional activity." Arch Virol **151**(10): pp1961-1972.

Halbert, C. L., G. W. Demers and D. A. Galloway (1991). "The E7 Gene of Human Papillomavirus Type 16 Is Sufficient for Immortalization of Human Epithelial Cells." Journal of Virology **65**(1): pp473-478.

Hall, C., A. and W. W. Meyer (1976). "Optimal error bounds for cubic spline interpolation." Journal of Approximation Theory **16**(2): pp105-122.

Hampras, S. S., A. R. Giuliano, H. Y. Lin, K. J. Fisher, M. E. Abrahamsen, B. A. Sirak, M. R. Iannacone, T. Gheit, M. Tommasino and D. E. Rollison (2014). "Natural history of cutaneous human papillomavirus (HPV) infection in men: the HIM study." PLoS One **9**(9): e104843.

Handisurya, A., P. M. Day, C. D. Thompson, M. Bonelli, D. R. Lowy and J. T. Schiller (2014). "Strain-specific properties and T cells regulate the susceptibility to papilloma induction by Mus musculus papillomavirus 1." PLoS Pathog **10**(8): e1004314.

Handisurya, A., P. M. Day, C. D. Thompson, C. B. Buck, Y. Y. Pang, D. R. Lowy and J. T. Schiller (2013). "Characterization of Mus musculus papillomavirus 1 infection in situ reveals an unusual pattern of late gene expression and capsid protein localization." J Virol **87**(24): pp13214-13225.

Harper, D. M., E. L. Franco, C. Wheeler, D. G. J. Ferris, D. Schuind, A. Zahaf, T., B. Innis, P. Naud, N. S. De Carvalho, C. M. Roteli-Martins, J. Teixeira, M. M. Blatter, A. P. Korn, W. Quint, G. Dubin and G. H. V. S. Group. (2004). "Efficacy of a bivalent L1 virus-like particle vaccine in prevention of infection with human papillomavirus types 16 and 18 in young women: a randomised controlled trial." The Lancet **364**(9447): pp1757-1765.

Hartley, K. A. and K. A. Alexander (2002). "Human TATA binding protein inhibits human papillomavirus type 11 DNA replication by antagonizing E1-E2 protein complex formation on the viral origin of replication." J Virol **76**(10): pp5014-5023.

Hatterschide, J., A. E. Bohidar, M. Grace, T. J. Nulton, H. W. Kim, B. Windle, I. M. Morgan, K. Munger and E. A. White (2019). "PTPN14 degradation by high-risk human papillomavirus E7 limits keratinocyte differentiation and contributes to HPV-mediated oncogenesis." Proc Natl Acad Sci U S A **116**(14): pp7033-7042.

Hauner, H., K. Rohrig and T. Petruschke (1995). "Effects of epidermal growth factor (EGF), platelet- derived growth factor (PDGF) and fibroblast growth factor (FGF) on human adipocyte development and function." European Journal of Clinical Investigation **25**(2): pp90-96.

Haupt, S., M. Berger, Z. Goldberg and Y. Haupt (2003). "Apoptosis - the p53 network." J Cell Sci **116**(Pt 20): pp4077-4085.

Hebert, T. L., X. Wu, G. Yu, B. C. Goh, Y. D. Halvorsen, Z. Wang, C. Moro and J. M. Gimble (2009). "Culture effects of epidermal growth factor (EGF) and basic fibroblast growth factor (bFGF) on cryopreserved human adipose-derived stromal/stem cell proliferation and adipogenesis." J Tissue Eng Regen Med **3**(7): pp553-561.

Hennings, H. G., A. B., D. T. Lowry, L. S. Krsmanovi, L. M. Sly and S. H. Yuspa (1993). "FVB/N mice: an inbred strain sensitive to the chemical induction of squamous cell carcinomas in the skin." Carcinogenesis **14**(11): pp2353-2358.

Herbst, L. H., J. Lenz, K. Van Doorslaer, Z. Chen, B. A. Stacy, J. F. Wellehan, Jr., C. A. Manire and R. D. Burk (2009). "Genomic characterization of two novel reptilian papillomaviruses, Chelonia mydas papillomavirus 1 and Caretta caretta papillomavirus 1." Virology **383**(1): pp131-135.

Hirata, Y. and D. N. Orth (1979). "Epidermal Growth Factor (Urogastrone) in Human Tissues." Journal of Clinical Endocrinology and Metabolism **48**(4): pp667-672.

Hoffmann, R., B. Hirt, V. Bechtold, P. Beard and K. Raj (2006). "Different modes of human papillomavirus DNA replication during maintenance." J Virol **80**(9): pp4431-4439.

Howie, H. L., J. I. Koop, J. Weese, K. Robinson, G. Wipf, L. Kim and D. A. Galloway (2011). "Beta-HPV 5 and 8 E6 promote p300 degradation by blocking AKT/p300 association." PLoS Pathog **7**(8): e1002211.

Hsu, C. Y., F. Mechali and C. Bonne-Andrea (2007). "Nucleocytoplasmic shuttling of bovine papillomavirus E1 helicase downregulates viral DNA replication in S phase." J Virol **81**(1): pp384-394.

Hu, J., L. R. Budgeon, N. M. Cladel, K. Balogh, R. Myers, T. K. Cooper and N. D. Christensen (2015). "Tracking vaginal, anal and oral infection in a mouse papillomavirus infection model." J Gen Virol **96**(12): pp3554-3565.

Hu, J., N. M. Cladel, L. R. Budgeon, K. K. Balogh and N. D. Christensen (2017). "The Mouse Papillomavirus Infection Model." Viruses **9**(9).

Huang, S. M. and D. J. McCance (2002). "Down regulation of the interleukin-8 promoter by human papillomavirus type 16 E6 and E7 through effects on CREB binding protein/p300 and P/CAF." J Virol **76**(17): pp8710-8721.

Hudson, J. B., M. A. Bedell, D. J. McCance and L. A. Laimins (1990). "Immortalization and Altered Differentiation of Human Keratinocytes In Vitro by the E6 and E7 Open Reading Frames of Human

Papillomavirus Type 18." Journal of Virology **64**(2): pp519-526.

Hughes, F. J. and M. A. Romanos (1993). "E1 protein of human papillomavirus is a DNA helicase/ATPase." Nucleic Acids Research **21**(25): pp5817-5823.

Huibregtse, J. M., M. Scheffner and P. M. Howley (1993). "Localization of the E6-AP Regions That Direct Human Papillomavirus E6 Binding, Association with p53, and Ubiquitination of Associated Proteins." Molecular and Cellular Biology **13**(8): pp4918-4927.

Hummel, M., J. B. Hudson and L. A. Laimins (1992). "Differentiation-Induced and Constitutive Transcription of Human Papillomavirus Type 31b in Cell Lines Containing Viral Episomes." Journal ogf Virology **66**(10): pp6070-6080.

Ilagan, M. X. and R. Kopan (2007). "SnapShot: notch signaling pathway." Cell **128**(6): 1246.

Incassati, A., D. Patel and D. J. McCance (2006). "Induction of tetraploidy through loss of p53 and upregulation of Plk1 by human papillomavirus type-16 E6." Oncogene **25**(17): pp2444-2451.

Ingle, A., S. Ghim, J. Joh, I. Chepkoech, A. Bennett Jenson and J. P. Sundberg (2011). "Novel laboratory mouse papillomavirus (MusPV) infection." Vet Pathol **48**(2): pp500-505.

Isaacson Wechsler, E., Q. Wang, I. Roberts, E. Pagliarulo, D. Jackson, C. Untersperger, N. Coleman, H. Griffin and J. Doorbar (2012). "Reconstruction of human papillomavirus type 16-mediated early-stage neoplasia implicates E6/E7 deregulation and the loss of contact inhibition in neoplastic progression." J Virol **86**(11): pp6358-6364.

Ivancic, R., H. Iqbal, B. deSilva, Q. Pan and L. Matrka (2018). "Current and future management of recurrent respiratory papillomatosis." Laryngoscope Investig Otolaryngol **3**(1): pp22-34.

Iwasaki, T., H. Maeda, Y. Kameyama, M. Moriyama, S. Kanai and T. Kurata (1997). "Presence of a novel hamster oral papillomavirus in dysplastic lesions of hamster lingual mucosa induced by application of dimethylbenzanthracene and excisional wounding: molecular cloning and complete nucleotide sequence." Journal of Virology **78**(pt 5): pp1087-1093.

Jablonska, S., J. Dabrowski and K. Jakubowicz (1972). "Epidermodysplasia Verruciformis as a Model in Studies on the Role of Papovaviruses in Oncogenesis." Cancer Research **32**: pp583-589.

Jackson, P. R., G. T. Tucker and H. F. Woods (1989). "Testing for bimodality in frequency distributions of data suggesting polymorphisms of drug metabolism - hypothesis testing." British Journal of Clinical Pharmacology **28**: pp655-662.

Jareborg, N., A. Alderborn and S. Burnett (1992). "Identification and genetic definition of a bovine papillomavirus type 1 E7 protein and absence of a low-copy-number phenotype exhibited by E5, E6, or E7 viral mutants." Journal of Virology **66**(8): pp4957-4965.

Jarrett, W. F. H., P. E. McNeil, W. T. R. Grimshaw, I. E. Selman and W. I. M. McIntyre (1978). "High incidence area of cattle cancer with a possible interaction between an environmental carcinogen and a papilloma virus." Nature **274**: pp215-217.

Jiang, R. T., J. W. Wang, S. Peng, T. C. Huang, C. Wang, F. Cannella and R. Roden (2017). "Spontaneous and Vaccine-Induced Clearance of Mus Musculus Papillomavirus 1 Infection." Journal of Virology **91**(15): e00699-00617.

Joh, J., S. J. Ghim, P. M. Chilton, J. P. Sundberg, J. Park, S. A. Wilcher, M. L. Proctor and A. Bennett Jenson (2016). "MmuPV1 infection and tumor development of T cell-deficient mice is prevented by passively transferred hyperimmune sera from normal congenic mice immunized with MmuPV1 virus-like particles (VLPs)." Exp Mol Pathol **100**(1): pp212-219.

Joh, J., A. B. Jenson, W. King, M. Proctor, A. Ingle, J. P. Sundberg and S. J. Ghim (2011). "Genomic analysis of the first laboratory-mouse papillomavirus." J Gen Virol **92**(Pt 3): pp692-698.

Jones, D. L., R. M. Alani and K. Munger (1997). "The human papillomavirus E7 oncoprotein can uncouple cellular differentiation and proliferation in human keratinocytes by abrogating p21Cip1-mediated inhibition of cdk2." Genes Dev **11**(16): pp2101-2111.

Jones, P. H., B. D. Simons and F. M. Watt (2007). "Sic transit gloria: farewell to the epidermal transit amplifying cell?" Cell Stem Cell **1**(4): pp371-381.

Kim, K. and P. F. Lambert (2002). "E1 protein of bovine papillomavirus 1 is not required for the maintenance of viral plasmid DNA replication." Virology **293**(1): pp10-14.

Kirby, T. (2012). "Australia to be first country to vaccinate boys against HPV." The Lancet Oncology **13**(8): e333.

Kiyono, T., A. Hiraiwa, M. Fujita, Y. Hayashi, T. Akiyama and M. Ishibashi (1997). "Binding of high-risk human papillomavirus E6 oncoproteins to the human homologue of the Drosophila discs large tumor
suppressor protein." Proc Natl Acad Sci U S A **94**(1): pp11612-11616.

Kmietowicz, Z. (2018). "Boys in England to get HPV vaccine from next year." BMJ **362**: k3237.

Kocjan, B. J., L. Hosnjak, J. Racnik, M. Zadravec and M. Poljak (2014). "Complete Genome Sequence of Phodopus sungorus Papillomavirus Type 1 (PsPV1), a Novel Member of the Pipapillomavirus Genus, Isolated from a Siberian Hamster." Genome Announc **2**(2).

Koh, S. B., P. Mascalchi, E. Rodriguez, Y. Lin, D. I. Jodrell, F. M. Richards and S. K. Lyons (2017). "A quantitative FastFUCCI assay defines cell cycle dynamics at a single-cell level." J Cell Sci **130**(2): pp512-520.

Kolly, C., M. M. Suter and E. J. Muller (2005). "Proliferation, cell cycle exit, and onset of terminal differentiation in cultured keratinocytes: pre-programmed pathways in control of C-Myc and Notch1 prevail over extracellular calcium signals." J Invest Dermatol **124**(5): pp1014-1025.

Kolodka, T. M., J. A. Garlick and L. B. Taichman (1998). "Evidence for keratinocyte stem cells in vitro: long term engraftment and persistence of transgene expression from retrovirus-transduced keratinocytes." Proc Natl Acad Sci U S A **95**(8): pp4356-4361.

Konishi, S., H. Tokita and H. Ogata (1972). "Studies on canine oral papillomatosis: I. Transmission and characterization of the virus." The Japanese Journal of Veterinary Science **34**(5): pp263-268.

Kopan, R. and M. X. Ilagan (2009). "The canonical Notch signaling pathway: unfolding the activation mechanism." Cell **137**(2): pp216-233.

Kranjec, C. and L. Banks (2011). "A systematic analysis of human papillomavirus (HPV) E6 PDZ substrates identifies MAGI-1 as a major target of HPV type 16 (HPV-16) and HPV-18 whose loss accompanies disruption of tight junctions." J Virol **85**(4): pp1757-1764.

Kranjec, C., C. Holleywood, D. Libert, H. Griffin, R. Mahmood, E. Isaacson and J. Doorbar (2017). "Modulation of Basal Cell Fate During Productive and Transforming HPV16 Infection is Mediated by Progressive E6-Driven Depletion of Notch." J Pathol.

Kranjec, C., P. Massimi and L. Banks (2014). "Restoration of MAGI-1 expression in human papillomavirus-positive tumor cells induces cell growth arrest and apoptosis." J Virol **88**(13): pp7155-7169.

Kurian, K. M., C. J. Watson and A. H. Wyllie (2000). "Retroviral vectors." Journal of Clinical Pathology: Molecular Pathology **53**: pp173-176.

Kyo, S., D. J. Klumpp, M. Inoue, T. Kanaya and L. A. Laimins (1997). "Expression of AP1 during cellular differentiation determines human papillomavirus E6/E7 expression in stratified epithelial cells." J Gen Virol **78 (Pt 2)**: pp401-411.

Lambert, P. F., M. A. Ozbun, A. Collins, S. Holmgren, D. Lee and T. Nakahara (2005). "ing an Immortalized Cell Line to Study the HPV Life Cycle in Organotypic “Raft” Cultures." Methods in Molecular Medicine **119**: pp141-155.

Lambert, P. F., B. A. Spalholz and P. M. Howley (1987). " A Transcriptional Repressor Encoded by BPV-1 Shares a Common Carboxy=Terminal Domain with the E2 Transactivator." Cell **50**: pp69-78.

Lan, R., H. Geng, Y. Hwang, P. Mishra, W. L. Skloss, E. A. Sprague, P. Saikumar and M. Venkatachalam (2010). "A novel wounding device suitable for quantitative biochemical analysis of wound healing and regeneration of cultured epithelium." Wound Repair Regen **18**(2): pp159-167.

Lathion, S., J. Schaper, P. Beard and K. Raj (2003). "Notch1 Can Contribute to Viral-Induced Transformation of Primary
Human Keratinocytes." Cancer Research **63**(24): pp8687-8694.

Lechner, M. S. and L. A. Laimins (1994). "Inhibition of p53 DNA Binding by Human Papillomavirus E6 Proteins." Journal of Virology **68**(7): pp4262-4273.

Lee, C. and L. A. Laimins (2004). "Role of the PDZ domain-binding motif of the oncoprotein E6 in the pathogenesis of human papillomavirus type 31." J Virol **78**(22): pp12366-12377.

Lee, D. K., B. C. Kim, I. Y. Kim, E. A. Cho, D. J. Satterwhite and S. J. Kim (2002). "The human papilloma virus E7 oncoprotein inhibits transforming growth factor-beta signaling by blocking binding of the Smad complex to its target sequence." J Biol Chem **277**(41): pp38557-38564.

Lee, K. Y., T. R. Broker and L. T. Chow (1998). "Transcription Factor YY1 Represses Cell-Free Replication from Human Papillomavirus Origins." Journal of Virology **72**(6): pp4911-4917.

Lee, S. S., R. S. Weiss and R. T. Javier (1997). "Binding of human virus oncoproteins to hDlg/SAP97, a mammalian homolog of the Drosophila discs large tumor suppressor protein." Proc Natl Acad Sci U S A **94**(13): pp6670-6675.

Lehman, C. W. and M. R. Botchan (1998). "Segregation of viral plasmids depends on tethering to chromosomes and is regulated by phosphorylation." Proc Natl Acad Sci U S A **95**: pp4338-4343.

Lentz, M. R., D. Pak, I. Mohr and M. R. Botchan (1993). "The E1 replication protein of bovine papillomavirus type 1 contains an extended nuclear localization signal that includes a p34cdc2 phosphorylation site." Journal of Virology **67**(3): pp1414-1423.

Li, N., S. Franceschi, R. Howell-Jones, P. J. Snijders and G. M. Clifford (2011). "Human papillomavirus type distribution in 30,848 invasive cervical cancers worldwide: Variation by geographical region, histological type and year of publication." Int J Cancer **128**(4): pp927-935.

Lin, H. Y., C. H. Kao, K. M. Lin, V. Kaartinen and L. T. Yang (2011). "Notch signaling regulates late-stage epidermal differentiation and maintains postnatal hair cycle homeostasis." PLoS One **6**(1): e15842.

Lipke, M. M. (2006). "An Armamentarium of Wart Treatments." Clinical Medicine & Research **4**(4): 273-293.

Liu, Z. H., X. M. Dai and B. Du (2015). "Hes1: a key role in stemness, metastasis and multidrug resistance." Cancer Biol Ther **16**(3): 353-359.

Logeat, F., C. Bessia, C. Brou, O. LeBail, S. Jarriault, N. G. Seidah and A. Israël (1998). "The Notch1 receptor is cleaved constitutively by a furin-like convertase." Proc Natl Acad Sci U S A **95**(14): pp8108-8112.

Lopez, D. and R. Kolter (2010). "Extracellular signals that define distinct and coexisting cell fates in Bacillus subtilis." FEMS Microbiol Rev **34**(2): pp134-149.

Lopez-Bueno, A., C. Mavian, A. M. Labella, D. Castro, J. J. Borrego, A. Alcami and A. Alejo (2016). "Concurrence of Iridovirus, Polyomavirus, and a Unique Member of a New Group of Fish Papillomaviruses in Lymphocystis Disease-Affected Gilthead Sea Bream." J Virol **90**(19): pp8768-8779.

Lorenz, L. D., J. Rivera Cardona and P. F. Lambert (2013). "Inactivation of p53 rescues the maintenance of high risk HPV DNA genomes deficient in expression of E6." PLoS Pathog **9**(10): e1003717.

Maglennon, G. A., P. McIntosh and J. Doorbar (2011). "Persistence of viral DNA in the epithelial basal layer suggests a model for papillomavirus latency following immune regression." Virology **414**(2): 153-163.

Maier, T., M. Guell and L. Serrano (2009). "Correlation of mRNA and protein in complex biological samples." FEBS Lett **583**(24): 3966-3973.

Mariani, L. and A. Venuti (2010). "HPV vaccine: an overview of immune response, clinical protection, and new approaches for the future." J Transl Med **8**: 105.

Massimi, P., A. Shai, P. Lambert and L. Banks (2008). "HPV E6 degradation of p53 and PDZ containing substrates in an E6AP null background." Oncogene **27**(12): 1800-1804.

McBride, A. A. (2013). "The papillomavirus E2 proteins." Virology **445**(1-2): 57-79.

McBride, A. A. (2017). "Mechanisms and strategies of papillomavirus replication." Biol Chem **398**(8): 919-927.

McBride, A. A. and A. Warburton (2017). "The role of integration in oncogenic progression of HPV-associated cancers." PLoS Pathog **13**(4): e1006211.

McCance, D., R. Kopan, E. Fuchs and L. Laimins (1988). "Human papillomavirus type 16 alters human epithelial cell differentiation in vitro." Proceedings of the National Academy of Sciences of the United States of America **85**: pp7169-7173.

McElhinny, A. S., J. L. Li and L. Wu (2008). "Mastermind-like transcriptional co-activators: emerging roles in regulating cross talk among multiple signaling pathways." Oncogene **27**(38): 5138-5147.

McGowan, K. C., PA (1998). "Onset of Keratin 17 Expression Coincides with the Definition of Major Epithelial Lineages during Skin Development." The Journal of Cell Biology **143**(2): p469-486.

McLemore, M. R. (2006). "Gardasil: Introducing the new human papillomavirus vaccine." Clin J Oncol Nurs **10**(5): 559-560.

Meiring, T. L., Z. Z. A. Mbulawa, M. Lesosky, D. Coetzee and A. L. Williamson (2017). "High diversity of alpha, beta and gamma human papillomaviruses in genital samples from HIV-negative and HIV-positive heterosexual South African men." Papillomavirus Res **3**: 160-167.

Mendelsohn, A. H., C. K. Lai, I. P. Shintaku, D. A. Elashoff, S. M. Dubinett, E. Abemayor and M. A. St John (2010). "Histopathologic findings of HPV and p16 positive HNSCC." Laryngoscope **120**(9): 1788-1794.

Mengual-Chulia, B., L. Domenis, S. Robetto and I. G. Bravo (2014). "A novel papillomavirus isolated from a nasal neoplasia in an Italian free-ranging chamois (Rupicapra r. rupicapra)." Vet Microbiol **172**(1-2): pp108-119.

Merino, M. M., C. Rhiner, J. M. Lopez-Gay, D. Buechel, B. Hauert and E. Moreno (2015). "Elimination of unfit cells maintains tissue health and prolongs lifespan." Cell **160**(3): pp461-476.

Meyer, T., R. Arndt, I. Nindl, C. Ulrich, E. Christophers and E. Stockfleth (2003). "Association of human papillomavirus infections with cutaneous tumors in immunosuppressed patients." Transplant International **16**(3): pp146-153.

Meyers, C., M. G. Frattini, J. B. Hudson and L. A. Laimins (1992). "Biosynthesis of Human Papillomavirus from a
Continuous Cell Line Upon Epithelial Differentiation." Science **257**(5072): pp971-973.

Meyers, J. M., A. Uberoi, M. Grace, P. F. Lambert and K. Munger (2017). "Cutaneous HPV8 and MmuPV1 E6 Proteins Target the NOTCH and TGF-beta Tumor Suppressors to Inhibit Differentiation and Sustain Keratinocyte Proliferation." PLoS Pathog **13**(1): e1006171.

Middleton, K., W. Peh, S. Southern, H. Griffin, K. Sotlar, T. Nakahara, A. El-Sherif, L. Morris, R. Seth, M. Hibma, D. Jenkins, P. Lambert, N. Coleman and J. Doorbar (2003). "Organization of human papillomavirus productive cycle during neoplastic progression provides a basis for selection of diagnostic markers." J Virol **77**(19): 10186-10201.

Midwood, K. S. and G. Orend (2009). "The role of tenascin-C in tissue injury and tumorigenesis." J Cell Commun Signal **3**(3-4): 287-310.

Miller, A. D. (1992). "Retroviral Vectors." Current Topics in Microbiology and Immunology **158**: pp1-24.

Miller, A. K., K. Munger and F. R. Adler (2017). "A Mathematical Model of Cell Cycle Dysregulation Due to Human Papillomavirus Infection." Bull Math Biol **79**(7): 1564-1585.

Mishra, A. (2010). "Implementing HPV vaccines: public knowledge, attitudes, and the need for education." Int Q Community Health Educ **31**(1): 71-98.

Modis, Y., B. L. Trus and S. C. Harrison (2002). "Atomic model of the papillomavirus capsid." The EMBO Journal **21**(18): pp4754-4762.

Molijn, A., B. Kleter, W. Quint and L. J. van Doorn (2005). "Molecular diagnosis of human papillomavirus (HPV) infections." J Clin Virol **32 Suppl 1**: S43-51.

Moriyama, M., A. D. Durham, H. Moriyama, K. Hasegawa, S. Nishikawa, F. Radtke and M. Osawa (2008). "Multiple roles of Notch signaling in the regulation of epidermal development." Dev Cell **14**(4): 594-604.

Mumm, J. S. and R. Kopan (2000). "Notch signaling: from the outside in." Dev Biol **228**(2): 151-165.

Munday, J. S. (2014). "Bovine and human papillomaviruses: a comparative review." Vet Pathol **51**(6): 1063-1075.

Munger, K., W. C. Phelps, V. Bubb, P. M. Howley and R. Schlegel (1989). "The E6 and E7 genes of the human papillomavirus type 16 together are necessary and sufficient for transformation of primary human keratinocytes." J Virol **63**(10): 4417-4421.

Münger, K., B. Werness, N. Dyson, W. Phelps, E. Harlow and P. Howley (1989). "Complex formation of human papillomavirus E7 proteins
with the retinoblastoma tumor suppressor gene product." EMBO Journal **8**(13): pp4099-4105.

Muñoz, N., F. Bosch, S. de Sanjosé, R. Herrero, X. Castellsagué, K. Shah, P. Snijders and C. Meijer (2003). "Epidemiologic Classification of Human Papillomavirus Types Associated with Cervical Cancer
." New England Journal of Medicine **348**(6): pp518-527.

Murakami, I., N. Egawa, H. Griffin, W. Yin, C. Kranjec, T. Nakahara, T. Kiyono and J. Doorbar (2019). "Roles for E1-independent replication and E6-mediated p53 degradation during low-

risk and high-risk human papillomavirus genome maintenance." PLoS Pathog **15**(5): e1007755.

Murray, R. F., J. Hobbs and B. Payne (1971). "Possible Clonal Origin of Common Warts (Verruca vulgaris)." Nature **232**: pp51-52.

Nakagawa, S. and J. Huibregtse (2000). "Human Scribble (Vartul) Is Targeted for Ubiquitin-Mediated
Degradation by the High-Risk Papillomavirus E6 Proteins
and the E6AP Ubiquitin-Protein Ligase." Molecular and Cellular Biology **20**(21): pp8244-8253.

Nandagopal, N., L. A. Santat, L. LeBon, D. Sprinzak, M. E. Bronner and M. B. Elowitz (2018). "Dynamic Ligand Discrimination in the Notch Signaling Pathway." Cell **172**(4): 869-880.e819.

Naviaux, R. K., E. Costanzi, M. Haas and I. Verma (1996). "The pCL Vector System: Rapid Production of Helper-Free, High-Titer, Recombinant Retroviruses." Journal of Virology **70**(8): p5701-5705.

Nees, M., J. M. Geoghegan, T. Hyman, S. Frank, L. Miller and C. D. Woodworth (2001). "Papillomavirus type 16 oncogenes downregulate expression of interferon-responsive genes and upregulate proliferation-associated and NF-kappaB-responsive genes in cervical keratinocytes." J Virol **75**(9): 4283-4296.

Nees, M., J. M. Geoghegan, P. Munson, V. Prabhu, Y. Liu, E. Androphy and C. D. Woodworth (2000). "Human Papillomavirus Type 16 E6 and E7 Proteins Inhibit Differentiation-dependent Expression of Transforming Growth Factor-β2 in Cervical Keratinocytes." Cancer Research **60**: pp4289-4298.

Nguyen, B. C., K. Lefort, A. Mandinova, D. Antonini, V. Devgan, G. Della Gatta, M. I. Koster, Z. Zhang, J. Wang, A. Tommasi di Vignano, J. Kitajewski, G. Chiorino, D. R. Roop, C. Missero and G. P. Dotto (2006). "Cross-regulation between Notch and p63 in keratinocyte commitment to differentiation." Genes and Development **20**(8): pp1028-1042.

Nicholls, P. K., J. Doorbar, R. A. Moore, W. Peh, D. M. Anderson and M. A. Stanley (2001). "Detection of viral DNA and E4 protein in basal keratinocytes of experimental canine oral papillomavirus lesions." Virology **284**(1): 82-98.

Nicholls, P. K. and M. A. Stanley (1999). "Canine papillomavirus - A centenary review." J Comp Pathol **120**(3): pp219-233.

Norman, M., K. A. Wisniewska, K. Lawrenson, P. Garcia-Miranda, M. Tada, M. Kajita, H. Mano, S. Ishikawa, M. Ikegawa, T. Shimada and Y. Fujita (2012). "Loss of Scribble causes cell competition in mammalian cells." J Cell Sci **125**(Pt 1): pp59-66.

Noske, K., H. J. Stark, L. Nevaril, M. Berning, L. Langbein, A. Goyal, S. Diederichs and P. Boukamp (2016). "Mitotic Diversity in Homeostatic Human Interfollicular Epidermis." Int J Mol Sci **17**(2).

Noya, F., W. M. Chien, T. R. Broker and L. T. Chow (2001). "p21cip1 Degradation in differentiated keratinocytes is abrogated by costabilization with cyclin E induced by human papillomavirus E7." J Virol **75**(13): 6121-6134.

Oh, S. T., M. S. Longworth and L. A. Laimins (2004). "Roles of the E6 and E7 Proteins in the Life Cycle of Low-Risk Human Papillomavirus Type 11." Journal of Virology **78**(5): 2620-2626.

Omland, T., K. A. Lie, H. Akre, L. E. Sandlie, P. Jebsen, L. Sandvik, D. A. Nymoen, D. Bzhalava, J. Dillner and K. Brondbo (2014). "Recurrent respiratory papillomatosis: HPV genotypes and risk of high-grade laryngeal neoplasia." PLoS One **9**(6): e99114.

Orlando, P. A., J. S. Brown, R. A. Gatenby and A. R. Guliano (2013). "The ecology of human papillomavirus-induced epithelial lesions and the role of somatic evolution in their progression." J Infect Dis **208**(3): 394-402.

Oyama, T., K. Harigaya, N. Sasaki, Y. Okamura, H. Kokubo, Y. Saga, K. Hozumi, A. Suganami, Y. Tamura, T. Nagase, H. Koga, M. Nishimura, R. Sakamoto, M. Sato, N. Yoshida and M. Kitagawa (2011). "Mastermind-like 1 (MamL1) and mastermind-like 3 (MamL3) are essential for Notch signaling in vivo." Development **138**(23): 5235-5246.

Ozbun, M. A. (2019). "Extracellular events impacting human papillomavirus infections: Epithelial wounding to cell signaling involved in virus entry." Papillomavirus Res **7**: 188-192.

Ozbun, M. A. and C. Meyers (1998). "Human Papillomavirus Type 31b E1 and E2 Transcript Expression Correlates with Vegetative Viral Genome Amplification." Virology **248**(2): pp218-230.

Ozbun, M. A. and C. Meyers (1998). "Temporal Usage of Multiple Promoters during the Life Cycle of Human Papillomavirus Type 31b." Journal of Virology **72**(4): pp2715-2722.

Pacini, L., C. Savini, R. Ghittoni, D. Saidj, J. Lamartine, U. A. Hasan, R. Accardi, M. Tommasino and R. M. Sandri-Goldin (2015). "Downregulation of Toll-Like Receptor 9 Expression by Beta Human Papillomavirus 38 and Implications for Cell Cycle Control." Journal of Virology **89**(22): pp11396-11405.

Paladini, R. D., K. Takahashi, N. S. Bravo and P. A. Coulombe (1996). "Onset of re-epithelialization after skin injury correlates with a reorganization of keratin filaments in wound edge keratinocytes: defining a potential role for keratin 16." The Journal of Cell Biology **132**(3): pp381-397.

Paquet-Fifield, S., R. Redvers, N. Pouliot and P. Kaur (2005). "A Transplant Model for Human Epidermal Skin Regeneration. In: Turksen K. (eds) Epidermal Cells. Methods in Molecular Biology (Methods and Protocols)." Springer Protocols **585**(pp369-382).

Park, Y. J., J. M. Kim, B. R. Lee, T. H. Kim and E. G. Lee (2018). "Annual prevalence and economic burden of genital warts in Korea: Health Insurance Review and Assessment (HIRA) service data from 2007 to 2015." Epidemiol Infect **146**(2): 177-186.

Parsons, R. J. and J. G. Kidd (1943). "Oral papillomatosis of rabbits: a virus disease." Journal of Experimental Medicine **772**(3): pp33–250.

Pasparakis, M., I. Haase and F. O. Nestle (2014). "Mechanisms regulating skin immunity and inflammation." Nat Rev Immunol **14**(5): 289-301.

Pastar, I., O. Stojadinovic, N. C. Yin, H. Ramirez, A. G. Nusbaum, A. Sawaya, S. B. Patel, L. Khalid, R. R. Isseroff and M. Tomic-Canic (2014). "Epithelialization in Wound Healing: A Comprehensive Review." Adv Wound Care (New Rochelle) **3**(7): 445-464.

Patel, C., J. M. Brotherton, A. Pillsbury, S. Jayasinghe, B. Donovan, K. Macartney and H. Marshall (2018). "The impact of 10 years of human papillomavirus (HPV) vaccination in Australia: what additional disease burden will a nonavalent vaccine prevent?" Euro Surveill **23**(41).

Payne, S. H. (2015). "The utility of protein and mRNA correlation." Trends Biochem Sci **40**(1): 1-3.

Peh, W. L., K. Middleton, N. Christensen, P. Nicholls, K. Egawa, K. Sotlar, J. Brandsma, A. Percival, J. Lewis, W. J. Liu and J. Doorbar (2002). "Life cycle heterogeneity in animal models of human papillomavirus-associated disease." J Virol **76**(20): 10401-10416.

Penberthy, J. (1898). "Contagious Warty Tumours in Dogs." Journal of Comparative Pathology and Therapeutics **11**: 363-365.

Pett, M. R., W. O. F. Alazawi, I. Roberts, S. Dowen, D. I. Smith, M. A. Stanley and N. Coleman (2004). "Acquisition of High-Level Chromosomal Instability Is Associated with Integration of Human Papillomavirus Type 16 in Cervical Keratinocytes." Cancer Research **64**(4): pp1359-1368.

Pillai, S., D. Bikle, M. Mancianti, P. Cline and M. Hincenbergs (1990). "Calcium regulation of growth and differentiation of normal human keratinocytes: modulation of differentiation competence by stages of growth and extracellular calcium." Journal of Cellular Physiology **143**(2): pp294-302.

Pim, D., M. Bergant, S. S. Boon, K. Ganti, C. Kranjec, P. Massimi, V. K. Subbaiah, M. Thomas, V. Tomaic and L. Banks (2012). "Human papillomaviruses and the specificity of PDZ domain targeting." FEBS J **279**(19): 3530-3537.

Pim, D., M. Thomas and L. Banks (2002). "Chimaeric HPV E6 proteins allow dissection of the proteolytic pathways regulating different E6 cellular target proteins." Oncogene **21**(53): pp8140-8148.

Pim, D., V. Tomaic and L. Banks (2009). "The human papillomavirus (HPV) E6* proteins from high-risk, mucosal HPVs can direct degradation of cellular proteins in the absence of full-length E6 protein." J Virol **83**(19): 9863-9874.

Porter, R. M. and E. B. Lane (2003). "Phenotypes, genotypes and their contribution to understanding keratin function." Trends in Genetics **19**(5): pp278-285.

Ports, K. A., D. M. Reddy and A. Rameshbabu (2013). "Barriers and facilitators to HPV vaccination: perspectives from Malawian women." Women Health **53**(6): 630-645.

Potocki, L., A. Lewinska, J. Klukowska-Rotzler, M. Bugno-Poniewierska, C. Koch, K. Mahlmann, J. Janda and M. Wnuk (2012). "DNA hypomethylation and oxidative stress-mediated increase in genomic instability in equine sarcoid-derived fibroblasts." Biochimie **94**(9): 2013-2024.

Poumay, Y. and M. R. Pittelkow (1995). "Cell density and culture factors regulate keratinocyte commitment to differentiation and expression of suprabasal K1/K10 keratins." J Invest Dermatol **104**(2): pp271-276.

Prue, G., P. Baker, D. Graham, C. Nutting, P. Greenhouse and M. Lawler (2018). "It is time for universal HPV vaccination." The Lancet **392**(10151): pp913-914.

Puccinelli, T. J., P. J. Bertics and K. S. Masters (2010). "Regulation of keratinocyte signaling and function via changes in epidermal growth factor presentation." Acta Biomater **6**(9): pp3415-3425.

Pyeon, D., M. A. Newton, P. F. Lambert, J. A. den Boon, S. Sengupta, C. J. Marsit, C. D. Woodworth, J. P. Connor, T. H. Haugen, E. M. Smith, K. T. Kelsey, L. P. Turek and P. Ahlquist (2007). "Fundamental differences in cell cycle deregulation in human papillomavirus-positive and human papillomavirus-negative head/neck and cervical cancers." Cancer Res **67**(10): pp4605-4619.

Pyeon, D., S. M. Pearce, S. M. Lank, P. Ahlquist and P. F. Lambert (2009). "Establishment of human papillomavirus infection requires cell cycle progression." PLoS Pathog **5**(2): e1000318.

Qin, J. Y., L. Zhang, K. L. Clift, I. Hulur, A. P. Xiang, B. Z. Ren and B. T. Lahn (2010). "Systematic comparison of constitutive promoters and the doxycycline-inducible promoter." PLoS One **5**(5): e10611.

Quigley, D. A., E. Kandyba, P. Huang, K. D. Halliwill, J. Sjolund, F. Pelorosso, C. E. Wong, G. L. Hirst, D. Wu, R. Delrosario, A. Kumar and A. Balmain (2016). "Gene Expression Architecture of Mouse Dorsal and Tail Skin Reveals Functional Differences in Inflammation and Cancer." Cell Rep **16**(4): pp1153-1165.

Rangamani, P., A. Lipshtat, E. U. Azeloglu, R. C. Calizo, M. Hu, S. Ghassemi, J. Hone, S. Scarlata, S. R. Neves and R. Iyengar (2013). "Decoding information in cell shape." Cell **154**(6): pp1356-1369.

Ranganathan, P., K. L. Weaver and A. J. Capobianco (2011). "Notch signalling in solid tumours: a little bit of everything but not all the time." Nat Rev Cancer **11**(5): pp338-351.

Rangarajan, A., C. Talora, R. Okuyama, M. Nicolas, C. Mammucari, H. Oh, J. C. Aster, S. Krishna, D. Metzger, P. Chambon, L. Miele, M. Aguet, F. Radtke and G. P. Dotto (2001). "Notch signaling is a direct determinant of keratinocyte growth arrest and entry into differentiation." EMBO Journal **20**(13): pp3427-3436.

Raymakers, A. J. N., M. Sadatsafavi, F. Marra and C. A. Marra (2012). "Economic and Humanistic Burden of External Genital Warts." Pharmacoeconomics **30**(1): pp1-16.

Rector, A. and M. Van Ranst (2013). "Animal papillomaviruses." Virology **445**(1-2): pp213-223.

Reed, L. J. and H. Muench (1938). "A simple method of estimating fifty per cent endpoints." American Journal of Hygiene **27**: pp493–497.

Reuter, J. D., D. Gomez, J. L. Brandsma, J. K. Rose and A. Roberts (2001). "Optimization of cottontail rabbit papilloma virus challenge technique." Journal of Virological Methods **98**: pp127-134.

Rheinwald, J. G. and H. Green (1975). "Serial cultivation of strains of human epidermal keratinocytes: the formation of keratinizing colonies from single cells." Cell **6**(3): pp331-343.

Rheinwald, J. G., W. C. Hahn, M. R. Ramsey, J. Y. Wu, Z. Guo, H. Tsao, M. De Luca, C. Catricala and K. M. O'Toole (2002). "A two-stage, p16(INK4A)- and p53-dependent keratinocyte senescence mechanism that limits replicative potential independent of telomere status." Mol Cell Biol **22**(14): pp5157-5172.

Roberts, J. N., C. B. Buck, C. D. Thompson, R. Kines, M. Bernardo, P. L. Choyke, D. R. Lowy and J. T. Schiller (2007). "Genital transmission of HPV in a mouse model is potentiated by nonoxynol-9 and inhibited by carrageenan." Nat Med **13**(7): pp857-861.
Roden, R. B. S. and P. L. Stern (2018). "Opportunities and challenges for human papillomavirus vaccination in cancer." Nat Rev Cancer **18**(4): pp240-254.
Roman, A. and K. Munger (2013). "The papillomavirus E7 proteins." Virology **445**(1-2): pp138-168.
Rosenberger, S., J. De-Castro Arce, L. Langbein, R. D. Steenbergen and F. Rosl (2010). "Alternative splicing of human papillomavirus type-16 E6/E6* early mRNA is coupled to EGF signaling via Erk1/2 activation." Proc Natl Acad Sci U S A **107**(15): 7006-7011.
Roshan, A., K. Murai, J. Fowler, B. D. Simons, V. Nikolaidou-Neokosmidou and P. H. Jones (2016). "Human keratinocytes have two interconvertible modes of proliferation." Nat Cell Biol **18**(2): pp145-156.
Rozenblatt-Rosen, O., R. C. Deo, M. Padi, G. Adelmant, M. A. Calderwood, T. Rolland, M. Grace, A. Dricot, M. Askenazi, M. Tavares, S. J. Pevzner, F. Abderazzaq, D. Byrdsong, A. R. Carvunis, A. A. Chen, J. Cheng, M. Correll, M. Duarte, C. Fan, M. C. Feltkamp, S. B. Ficarro, R. Franchi, B. K. Garg, N. Gulbahce, T. Hao, A. M. Holthaus, R. James, A. Korkhin, L. Litovchick, J. C. Mar, T. R. Pak, S. Rabello, R. Rubio, Y. Shen, S. Singh, J. M. Spangle, M. Tasan, S. Wanamaker, J. T. Webber, J. Roecklein-Canfield, E. Johannsen, A. L. Barabasi, R. Beroukhim, E. Kieff, M. E. Cusick, D. E. Hill, K. Munger, J. A. Marto, J. Quackenbush, F. P. Roth, J. A. DeCaprio and M. Vidal (2012). "Interpreting cancer genomes using systematic host network perturbations by tumour virus proteins." Nature **487**(7408): pp491-495.
Ryser, M. D., E. R. Myers and R. Durrett (2015). "HPV clearance and the neglected role of stochasticity." PLoS Comput Biol **11**(3): e1004113.
Sakaue-Sawano, A., H. Kurokawa, T. Morimura, A. Hanyu, H. Hama, H. Osawa, S. Kashiwagi, K. Fukami, T. Miyata, H. Miyoshi, T. Imamura, M. Ogawa, H. Masai and A. Miyawaki (2008). "Visualizing spatiotemporal dynamics of multicellular cell-cycle progression." Cell **132**(3): pp487-498.
Scase, T., S. Brandt, C. Kainzbauer, S. Sykora, S. Bijmholt, K. Hughes, S. Sharpe and A. Foote (2010). "Equus caballus papillomavirus-2 (EcPV-2): an infectious cause for equine genital cancer?" Equine Vet J **42**(8): pp738-745.

Scheffner, M., B. A. Werness, J. M. Huibregtse, A. J. Levine and P. M. Howley (1990). "The E6 oncoprotein encoded by human papillomavirus types 16 and 18 promotes the degradation of p53." Cell
63(6): pp1129-1136.
Schelhaas, M., H. Ewers, M. L. Rajamaki, P. M. Day, J. T. Schiller and A. Helenius (2008). "Human papillomavirus type 16 entry: retrograde cell surface transport along actin-rich protrusions." PLoS Pathog **4**(9): e1000148.
Schmitt, M., V. Fiedler and M. Muller (2010). "Prevalence of BPV genotypes in a German cowshed determined by a novel multiplex BPV genotyping assay." J Virol Methods **170**(1-2): pp67-72.
Schulz, E., M. Gottschling, R. G. Ulrich, D. Richter, E. Stockfleth and I. Nindl (2012). "Isolation of three novel rat and mouse papillomaviruses and their genomic characterization." PLoS One **7**(10): e47164.
Schutze, D. M., P. J. Snijders, L. Bosch, D. Kramer, C. J. Meijer and R. D. Steenbergen (2014). "Differential in vitro immortalization capacity of eleven (probable) [corrected] high-risk human papillomavirus types." J Virol **88**(3): pp1714-1724.
Schweizner, J. and H. Winter (1983). "Keratin Biosynthesis in Norma Mouse Epithelia and in Squamous Cell Carcinomas." The Journal of Biological Chemistry **258**(21): pp13268-13272.
Sedman, S. A., M. S. Barbosa, W. C. Vass, N. L. Hubbert, J. A. Haas, D. R. Lowy and J. T. Schiller (1991). "The Full-Length E6 Protein of Human Papillomavirus Type-16 Has Transforming and Trans-Activating Activities and Cooperates with E7 to Immortalize Keratinocytes in Culture." Journal of Virology **65**(9): pp4860-4866.
Sedman, T., J. Sedman and A. Stenlund (1997). "Binding of the E1 and E2 Proteins to the Origin of Replication of Bovine Papillomavirus." Journal of Virology **71**(4): pp2887-2896.
Shope, R. (1933). "Infectious Papillomatosis of Rabbits." Journal of Experimental Medicine **58**(5): pp607–624.
Sichero, L., D. E. Rollison, R. P. Amorrortu and M. Tommasino (2019). "Beta Human Papillomavirus and Associated Diseases." Acta Cytol **63**(2): pp100-108.
Siegsmund, M., K. Wayss and A. Eberhard (1991). "Activation of latent papillomavirus genomes by chronic mechanical irritation." Journal of General Virology **72**(pt 11): pp2787-2789.
Skiadopoulos, M. H. and A. A. McBride (1998). "Bovine Papillomavirus Type 1 Genomes and the E2

Transactivator Protein Are Closely Associated
with Mitotic Chromatin." Journal of Virology **72**(3): pp2079-2088.
Smelov, V., R. Muwonge, O. Sokolova, S. McKay-Chopin, C. Eklund, B. Komyakov and T. Gheit (2018). "Beta and gamma human papillomaviruses in anal and genital sites among men: prevalence and determinants." Sci Rep **8**(1): 8241.
Smith, J. S., L. Lindsay, B. Hoots, J. Keys, S. Franceschi, R. Winer and G. M. Clifford (2007). "Human papillomavirus type distribution in invasive cervical cancer and high-grade cervical lesions: a meta-analysis update." Int J Cancer **121**(3): pp621-632.
Smola, H., H.-J. Stark, G. Thiekötter, N. Mirancea, T. ThomasKrieg and N. E. Fusenig (1998). "Dynamics of Basement Membrane Formation by Keratinocyte–Fibroblast Interactions in Organotypic Skin Culture." Experimental Cell Research **239**(2): pp399-410.
Song, D., H. Li, H. Li and J. Dai (2015). "Effect of human papillomavirus infection on the immune system and its role in the course of cervical cancer." Oncol Lett **10**(2): pp600-606.
Song, H. K. and D. Y. Hwang (2017). "Use of C57BL/6N mice on the variety of immunological researches." Lab Anim Res **33**(2): pp119-123.
Sperling, T., M. Oldak, B. Walch-Ruckheim, C. Wickenhauser, J. Doorbar, H. Pfister, M. Malejczyk, S. Majewski, A. C. Keates and S. Smola (2012). "Human papillomavirus type 8 interferes with a novel C/EBPbeta-mediated mechanism of keratinocyte CCL20 chemokine expression and Langerhans cell migration." PLoS Pathog **8**(7): e1002833.
Spurgeon, M. E., A. Uberoi, S. M. McGregor, T. Wei, E. Ward-Shaw and P. F. Lambert (2019). "A Novel In Vivo Infection Model To Study Papillomavirus-Mediated Disease of the Female Reproductive Tract." MBio **10**(2).
Stanley, M. A. (2012). "Epithelial cell responses to infection with human papillomavirus." Clin Microbiol Rev **25**(2): 215-222.
Stanley, M. A., H. M. Browne, M. Appleby and A. C. Minson (1989). "Properties of a non-tumorigenic human cervical keratinocyte cell line." International Journal of Cancer **43**: pp672-676.
Stanley, M. A. and P. K. Nicholls (1997). "In vitro and animal models for antiviral therapy in papillomavirus infections." Antiviral Chemistry & Chemotherapy **8**(5): pp381-400.
Sterling, J., M. Stanley, G. Gatward and T. Minson (1990). "Production of Human Papillomavirus Type 16 Virions in a Keratinocyte Cell Line." journal of Virology **64**(12): pp6305-6307.

Storrs, C. H. and S. J. Silverstein (2007). "PATJ, a tight junction-associated PDZ protein, is a novel degradation target of high-risk human papillomavirus E6 and the alternatively spliced isoform 18 E6." J Virol **81**(8): pp4080-4090.

Stubenrauch, F. and L. A. Laimins (1999). "Human papillomavirus life cycle: active and latent phases." Seminars in Cancer Biology **9**(6): pp379-386.

Sundberg, J. P., M. K. O'Banion, A. Shima, C. Knupp and M. E. Reichmann (1988). "Papillomas and Carcinomas Associated with a Papillomavirus in European Harvest Mice (Micromys minutus)." Vet Pathol **25**: pp356-361.

Sundberg, J. P., T. M. Stearns, J. Joh, M. Proctor, A. Ingle, K. A. Silva, S. S. Dadras, A. B. Jenson and S. J. Ghim (2014). "Immune status, strain background, and anatomic site of inoculation affect mouse papillomavirus (MmuPV1) induction of exophytic papillomas or endophytic trichoblastomas." PLoS One **9**(12): e113582.

Suprynowicz, F. A., E. Krawczyk, J. D. Hebert, S. R. Sudarshan, V. Simic, C. M. Kamonjoh and R. Schlegel (2010). "The human papillomavirus type 16 E5 oncoprotein inhibits epidermal growth factor trafficking independently of endosome acidification." J Virol **84**(20): pp10619-10629.

Suzich, J. A., S. J. Ghim, F. J. Palmer-Hill, W. I. White, J. K. Tamura, J. A. Bell, J. A. Newsome, A. B. Jenson and R. Schlegel (1995). "Systemic immunization with papillomavirus L1 protein completely prevents the development of viral mucosal papillomas." Proc Natl Acad Sci U S A **92**: pp11553-11557.

Syverton, J. T. (1952). "The pathogenesis of the rabbit papilloma-to-carcinoma sequence." Ann N Y Acad Sci. **54**(6): pp1126-1140.

Tachezy, R., A. Rector, M. Havelkova, E. Wollants, P. Fiten, G. Opdenakker, A. B. Jenson, J. Sundberg and M. Van Ranst (2002). "Avian papillomaviruses: the parrot Psittacus erithacus papillomavirus (PePV) genome has a unique organization of the early protein region and is phylogenetically related to the chaffinch papillomavirus." BMC Microbiology **2**(19).

Takagi, S., M. L. McFadden, R. E. Humphreys, B. A. Woda and T. Sairenji (1993). "Detection of 5-bromo-2-deoxyuridine (BrdUrd) incorporation with monoclonal anti-brdurd antibody after deoxyribonuclease treatment." Cytometry **14**: pp640-648.

Tan, M. J., E. A. White, M. E. Sowa, J. W. Harper, J. C. Aster and P. M. Howley (2012). "Cutaneous β-human papillomavirus E6 proteins bind Mastermind-like coactivators and repress Notch signaling." Proc Natl Acad Sci U S A **109**(23): E1473-1480.

Tang, S., M. Tao, J. P. McCoy, Jr. and Z. M. Zheng (2006). "The E7 oncoprotein is translated from spliced E6*I transcripts in high-risk human papillomavirus type 16- or type 18-positive cervical cancer cell lines via translation reinitiation." J Virol **80**(9): pp4249-4263.

Terai, M., R. DeSalle and R. D. Burk (2002). "Lack of canonical E6 and E7 open reading frames in bird papillomaviruses: Fringilla coelebs papillomavirus and Psittacus erithacus timneh papillomavirus." J Virol **76**(19): pp10020-10023.

Thaiwong, T., D. G. Sledge, A. G. Wise, K. Olstad, R. K. Maes and M. Kiupel (2018). "Malignant transformation of canine oral papillomavirus (CPV1)-associated papillomas in dogs: An emerging concern?" Papillomavirus Res **6**: pp83-89.

Thomas, J. T., W. G. Hubert, M. N. Ruesch and L. A. Laimins (1999). "Human papillomavirus type 31 oncoproteins E6 and E7 are required for the maintenance of episomes during the viral life cycle in normal human keratinocytes." Proc Natl Acad Sci U S A **96**(15): pp8449-8454.

Thomas, J. T. and L. A. Laimins (1998). "Human Papillomavirus Oncoproteins E6 and E7 Independently Abrogate the Mitotic Spindle Checkpoint." Journal of Virology **72**(2): pp1131-1137.

Thomas, J. T., S. T. Oh, S. S. Terhune and L. A. Laimins (2001). "Cellular changes induced by low-risk human papillomavirus type 11 in keratinocytes that stably maintain viral episomes." J Virol **75**(16): pp7564-7571.

Thompson, D. A., G. Belinksky, T. H. T. Chang, D. L. Jones, R. Schlegel and K. Munger (1997). "The human papillomavirus-16 E6 oncoprotein decreases the vigilance of mitotic checkpoints." Oncogene **15**: pp3025-3035.

Todara, G. J. G., H. (1963). "Quantitative Studies of the Growth of Mouse Embryo Cells in Culture and Their Development into Established Lines." The Journal of Cell Biology **17**: pp299-313.

Truong, A. B., M. Kretz, T. W. Ridky, R. Kimmel and P. A. Khavari (2006). "p63 regulates proliferation and differentiation of developmentally mature keratinocytes." Genes Dev **20**(22): pp3185-3197.

Tummers, B., R. Goedemans, L. P. Pelascini, E. S. Jordanova, E. M. van Esch, C. Meyers, C. J. Melief, J. M. Boer and S. H. van der Burg (2015). "The interferon-related developmental regulator 1 is used by human papillomavirus to suppress NFkappaB activation." Nat Commun **6**: 6537.

Uberoi, A. and P. F. Lambert (2017). "Rodent Papillomaviruses." Viruses **9**(12).

Uberoi, A., S. Yoshida, I. H. Frazer, H. C. Pitot and P. F. Lambert (2016). "Role of Ultraviolet Radiation in Papillomavirus-Induced Disease." PLoS Pathog **12**(5): e1005664.

Uberoi, A., S. Yoshida and P. F. Lambert (2018). "Development of an in vivo infection model to study Mouse papillomavirus-1 (MmuPV1)." J Virol Methods **253**: pp11-17.

Ueno, T., K. Sasaki, S. Yoshida, N. Kajitani, A. Satsuka, H. Nakamura and H. Sakai (2006). "Molecular mechanisms of hyperplasia induction by human papillomavirus E7." Oncogene **25**(30): pp4155-4164.

Ustav, M. and A. Stenlund (1991). "Transient replication of BPV-1 requires two viral polypeptides encoded by the E1 and E2 open reading frames." The EMBO Journal **10**(2): pp449-457.

Ustav, M., E. Ustav, P. Szymanski and A. Stenlund (1991). "Identification of the origin of replication of bovine papillomavirus and characterization of the viral origin recognition factor E1." The EMBO Journal **10**(13): pp4321-4329.

Utada, M., P. Chernyavskiy, W. J. Lee, S. Franceschi, C. Sauvaget, A. B. de Gonzalez and D. R. Withrow (2019). "Increasing risk of uterine cervical cancer among young Japanese women: Comparison of incidence trends in Japan, South Korea and Japanese-Americans between 1985 and 2012." Int J Cancer **144**(9): pp2144-2152.

Vaccarella, S., M. Laversanne, J. Ferlay and F. Bray (2017). "Cervical cancer in Africa, Latin America and the Caribbean and Asia: Regional inequalities and changing trends." Int J Cancer **141**(10): pp1997-2001.

van der Burg, S. H. and J. M. Palefsky (2009). "Human Immunodeficiency Virus and Human Papilloma Virus - why HPV-induced lesions do not spontaneously resolve and why therapeutic vaccination can be successful." J Transl Med **7**: 108.

Van Doorslaer, K. (2013). "Evolution of the papillomaviridae." Virology **445**(1-2): pp11-20.

Van Doorslaer, K., Z. Chen, H. U. Bernard, P. K. S. Chan, R. DeSalle, J. Dillner, O. Forslund, T. Haga, A. A. McBride, L. L. Villa and R. D. Burk (2018). "ICTV Virus Taxonomy Profile: Papillomaviridae." Journal of General Virology **99**(8): pp989-990.

Van Doorslaer, K. and J. Dillner (2019). "The Launch of an International Animal Papillomavirus Reference Center." Viruses **11**(1).

Van Doorslaer, K., Z. Li, S. Xirasagar, P. Maes, D. Kaminsky, D. Liou, Q. Sun, R. Kaur, Y. Huyen and A. A. McBride (2017). "The Papillomavirus Episteme: a major update to the papillomavirus sequence database." Nucleic Acids Res **45**(D1): D499-D506.

Van Doorslaer, K. and A. A. McBride (2016). "Molecular archeological evidence in support of the repeated loss of a papillomavirus gene." Sci Rep **6**: 33028.
Van Doorslaer, K., A. Rector, A. B. Jenson, J. P. Sundberg, M. Van Ranst and S. J. Ghim (2007). "Complete genomic characterization of a murine papillomavirus isolated from papillomatous lesions of a European harvest mouse (Micromys minutus)." J Gen Virol **88**(Pt 5): pp1484-1488.
Vande Pol, S. B. and A. J. Klingelhutz (2013). "Papillomavirus E6 oncoproteins." Virology **445**(1-2): pp115-137.
Varsani, A., S. Kraberger, S. Jennings, E. L. Porzig, L. Julian, M. Massaro, A. Pollard, G. Ballard and D. G. Ainley (2014). "A novel papillomavirus in Adelie penguin (Pygoscelis adeliae) faeces sampled at the Cape Crozier colony, Antarctica." J Gen Virol **95**(Pt 6): pp1352-1365.
Veras, E., A. Malpica, M. T. Deavers and E. G. Silva (2009). "Mitosis-specific marker phospho-histone H3 in the assessment of mitotic index in uterine smooth muscle tumors: a pilot study." Int J Gynecol Pathol **28**(4): pp316-321.
Vinzón, S. E., I. Braspenning-Wesch, M. Müller, E. K. Geissler, I. Nindl, H. J. Gröne, K. Schäfer and F. Rösl (2014). "Protective Vaccination against Papillomavirus-Induced Skin Tumors under Immunocompetent and Immunosuppressive Conditions: A Preclinical Study Using a Natural Outbred Animal Model." PLOS Pathogens **10**(2): e1003924.
Walboomers, J. M. M., M. V. Jacobs, M. M. Manos, F. X. Bosch, J. A. Kummer, K. V. Shah, P. J. F. Snijders, J. Peto, C. J. L. M. Meijer and N. Muñoz (1999). "Human Papillomavirus is a necessary cause of invasive cervical cancer worldwide." Journal of Pathology **189**: pp12-19.
Wang, H. K., A. A. Duffy, T. R. Broker and L. T. Chow (2009). "Robust production and passaging of infectious HPV in squamous epithelium of primary human keratinocytes." Genes Dev **23**(2): pp181-194.
Wang, J. W., R. Jiang, S. Peng, Y. N. Chang, C. F. Hung and R. B. Roden (2015). "Immunologic Control of Mus musculus Papillomavirus Type 1." PLoS Pathog **11**(10): e1005243.
Wang, X., H. Liu, H. Ge, M. Ajiro, N. R. Sharma, C. Meyers, P. Morozov, T. Tuschl, A. Klar, D. Court and Z. M. Zheng (2017). "Viral DNA Replication Orientation and hnRNPs Regulate Transcription of the Human Papillomavirus 18 Late Promoter." MBio **8**(3): e00713-00717.
Watanabe, H., K. Ishibashi, H. Mano, S. Kitamoto, N. Sato, K. Hoshiba, M. Kato, F. Matsuzawa, Y. Takeuchi, T. Shirai, S. Ishikawa, Y. Morioka, T. Imagawa, K. Sakaguchi, S. Yonezawa, S. Kon and Y. Fujita (2018). "Mutant p53-Expressing Cells Undergo Necroptosis

via Cell Competition with the Neighboring Normal Epithelial Cells." Cell Rep **23**(13): pp3721-3729.

Watt, F. M., S. Estrach and C. A. Ambler (2008). "Epidermal Notch signalling: differentiation, cancer and adhesion." Curr Opin Cell Biol **20**(2): pp171-179.

Watt, F. M., C. Lo Celso and V. Silva-Vargas (2006). "Epidermal stem cells: an update." Curr Opin Genet Dev **16**(5): pp518-524.

Watt, F. M. and D. Phil (1983). "Involucrin and other markers of keratinocyte terminal differentiation." J Invest Dermatol **81**(1 Suppl): 100s-103s.

Werner, S. and R. Grose (2003). "Regulation of wound healing by growth factors and cytokines." Physiol Rev **83**(3): pp835-870.

White, E. A., R. E. Kramer, M. J. Tan, S. D. Hayes, J. W. Harper and P. M. Howley (2012). "Comprehensive analysis of host cellular interactions with human papillomavirus E6 proteins identifies new E6 binding partners and reflects viral diversity." J Virol **86**(24): pp13174-13186.

White, E. A., J. Walther, H. Javanbakht and P. M. Howley (2014). "Genus Beta Human Papillomavirus E6 Proteins Vary in Their Effects on the Transactivation of p53 Target Genes." Journal of Virology **88**(15): pp8201-8212.

Willemsen, A. and I. G. Bravo (2019). "Origin and evolution of papillomavirus (onco)genes and genomes." Philos Trans R Soc Lond B Biol Sci **374**(1773): 20180303.

Williams, V. M., M. Filippova, V. Filippov, K. J. Payne and P. Duerksen-Hughes (2014). "Human papillomavirus type 16 E6* induces oxidative stress and DNA damage." J Virol **88**(12): pp6751-6761.

Wilson, V. G., M. West, K. Woytek and D. Rangasamy (2002). "Papillomavirus E1 Proteins: Form, Function, and Features." Virus Genes **24**(3): pp275-290.

Wohlschlegel, J. A., B. T. Dwyer, S. K. Dhar, C. Cvetic and J. C. D. Walter, A. (2000). "Inhibition of Eukaryotic DNA Replication by Geminin

Binding to Cdt1." Science **290**(5500): pp2309-2312.

Woo, H. J., S. J. Kim, K. J. Song, S. S. Kim, C. H. Yoon, B. S. Choi and J. E. Rhee (2015). "Hypermethylation of the tumor-suppressor cell adhesion molecule 1 in human papillomavirus-transformed cervical carcinoma cells." Int J Oncol **46**(6): pp2656-2662.

Woodworth, C. D., E. Mcmullin, M. Iglesias and G. D. Plowman (1995). "Interleukin-1-Alpha and Tumor-Necrosis-Factor-Alpha Stimulate Autocrine Amphiregulin Expression and Proliferation of Human Papillomavirus-Immortalized and Carcinoma-Derived Cervical

Epithelial-Cells." Proceedings of the National Academy of Sciences of the United States of America **92**(7): 2840-2844.

Woolford, L., A. Rector, M. Van Ranst, A. Ducki, M. D. Bennett, P. K. Nicholls, K. S. Warren, R. A. Swan, G. E. Wilcox and A. J. O'Hara (2007). "A novel virus detected in papillomas and carcinomas of the endangered western barred bandicoot (Perameles bougainville) exhibits genomic features of both the Papillomaviridae and Polyomaviridae." J Virol **81**(24): 13280-13290.

Wu, L., J. C. Aster, S. C. Blacklow, R. Lake, S. Artavanis-Tsakonas and J. D. Griffin (2000). "MAML1, a human homologue of Drosophila Mastermind, is a transcriptional co-activator for NOTCH receptors." 26 **4**(pp484-489).

Xue, X. Y., V. Majerciak, A. Uberoi, B. H. Kim, D. Gotte, X. Chen, M. Cam, P. F. Lambert and Z. M. Zheng (2017). "The full transcription map of mouse papillomavirus type 1 (MmuPV1) in mouse wart tissues." PLoS Pathog **13**(11): e1006715.

Yu, J. H., B. Y. Lin, W. Deng, T. R. Broker and L. T. Chow (2007). "Mitogen-activated protein kinases activate the nuclear localization sequence of human papillomavirus type 11 E1 DNA helicase to promote efficient nuclear import." J Virol **81**(10): pp5066-5078.

Zerfass-Thome, K., W. Zwerschke, B. Mannhardt, R. Tindle, J. W. Botz and P. Jansen-Dürr (1996). "Inactivation of the cdk inhibitor p27KIP1 by the human papillomavirus type 16 E7 oncoprotein." Oncogene **13**(11): pp2323-2330.

Zhang, B., W. Chen and A. Roman (2006). "The E7 proteins of low- and high-risk human papillomaviruses share the ability to target the pRB family member p130 for degradation." Proc Natl Acad Sci U S A **103**(2): pp437-442.

Zhang, B., A. Srirangam, D. A. Potter and A. Roman (2005). "HPV16 E5 protein disrupts the c-Cbl-EGFR interaction and EGFR ubiquitination in human foreskin keratinocytes." Oncogene **24**(15): pp2585-2588.

Zhang, W., J. Li, S. Kanginakudru, W. Zhao, X. Yu and J. J. Chen (2010). "The human papillomavirus type 58 E7 oncoprotein modulates cell cycle regulatory proteins and abrogates cell cycle checkpoints." Virology **397**(1): pp139-144.

Zhang, Z., S. Schwartz, L. Wagner and W. Miller (2000). "A Greedy Algorithm for Aligning DNA Sequences." Journal of Computational Biology **7**(1/2): pp203-214.

Zheng, Z. M. and C. C. Baker (2006). "Papillomavirus genome structure, expression, and post-transcriptional regulation." Front Biosci **11**: pp2286-2303.

Zhu, S., H. S. Oh, M. Shim, E. Sterneck, P. F. Johnson and R. C. Smart (1999). "C/EBPβ Modulates the Early Events of Keratinocyte Differentiation Involving Growth Arrest and Keratin 1 and Keratin 10 Expression." Molecular and Cellular Biology **19**(10): pp7181-7190.

Zimmermann, H., R. Degenkolbe, H. U. Bernard and M. J. O'Connor (1999). "The Human Papillomavirus Type 16 E6 Oncoprotein Can Down-Regulate p53 Activity by Targeting the Transcriptional Coactivator CBP/p300." Journal of Virology **73**(8): pp6209-6219.

Zomer, H. D. and A. G. Trentin (2018). "Skin wound healing in humans and mice: Challenges in translational research." J Dermatol Sci **90**(1): pp3-12.

zur Hausen, H. (2009). "Papillomaviruses in the causation of human cancers - a brief historical account." Virology **384**(2): pp260-265.

zur Hausen, H., E. M. de Villiers and L. Gissmann (1981). "Papillomavirus infections and human genital cancer." Gynecologic Oncology **12**(2pt2): pps124-s128.

8.0 Appendix

8.1 PLASMIDS

8.1.1 pQCXIN (CLONTECH LABORATORIES, US)

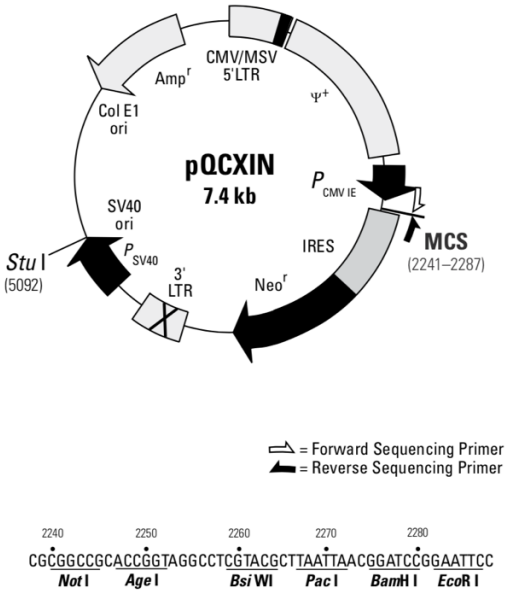

Source/vendor: Clontech Cat. No. 631514

8.1.2. pLXSN (CLONTECH LABORATORIES, US)

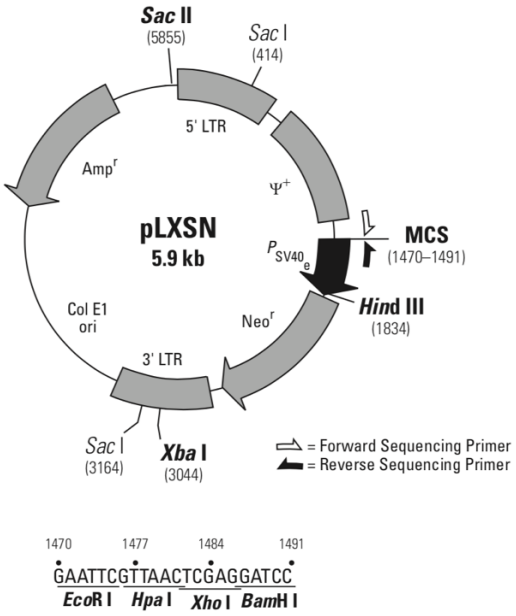

Source/vendor: Clontech Cat. No. 631509

8.1.3 pBOB-EF1-FastFUCCI-Puro

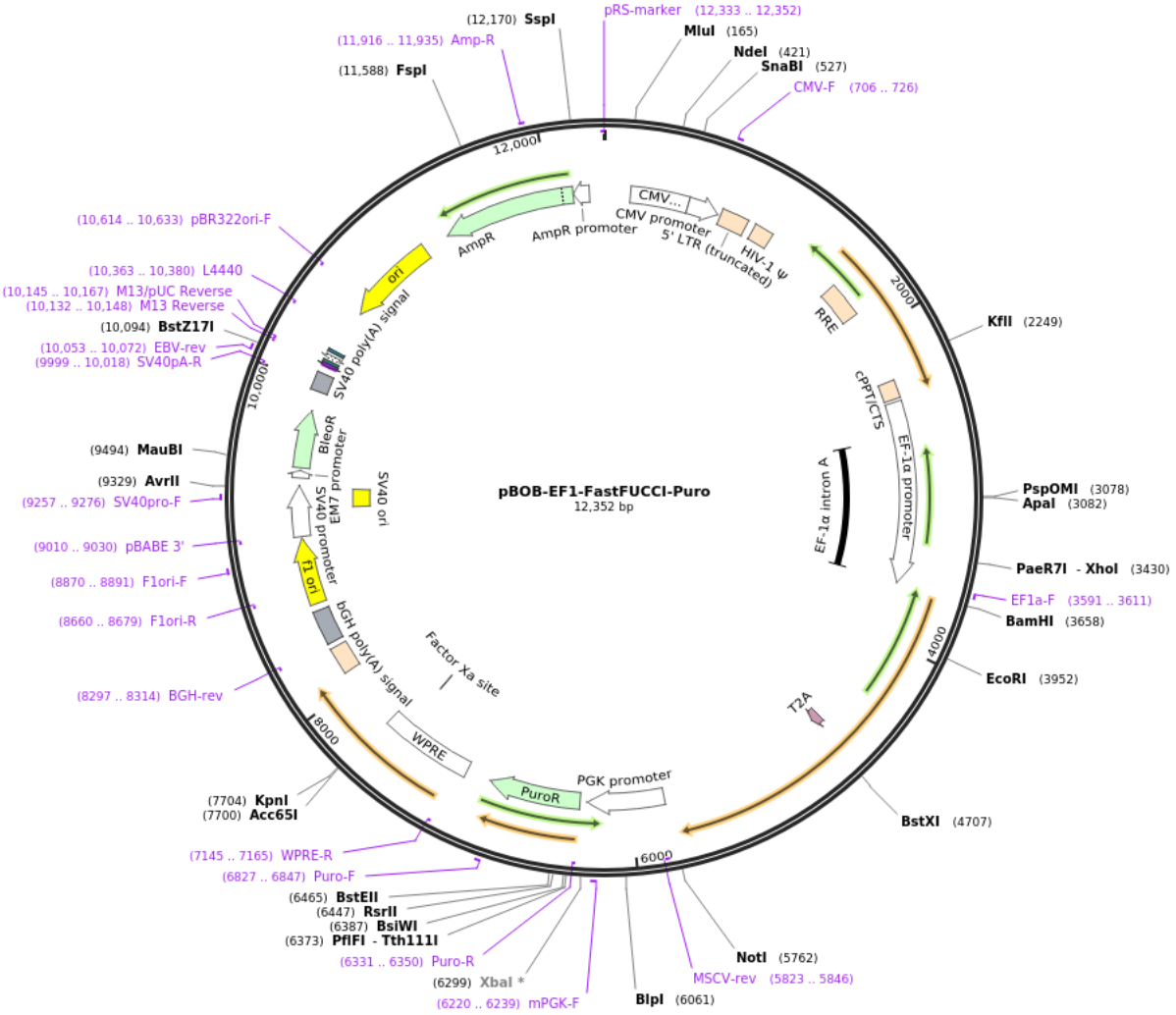

Source/vendor: addgene Cat. No. 86849

More information available in the following paper:

Quantitative FastFUCCI assay defines cell cycle dynamics at single-cell level. Koh SB, Mascalchi P, Rodriguez E, Lin Y, Jodrell DI, Richards FM, Lyons SK. *J Cell Sci. 2016 Nov 25. pii: jcs.195164*. 10.1242/jcs.195164 PubMed 27888217